The University of Manchester

PHARMACOLOGICAL INHIBITION OF THE HIPPO PATHWAY IN THE CARDIOVASCULAR SYSTEM

A thesis submitted to the University of Manchester for the degree of Doctor of Philosophy in the Faculty of Biology, Medicine and Health

Efta Triastuti

2021

School of Medical Sciences

Division of Cardiovascular Sciences

TABLE OF CONTENTS

Word count: 56,867

LIST OF FIGURES

LIST OF TABLES

ABBREVIATIONS

α-MHC	:	α-myosin heavy chain
ACE	:	Angiotensin-converting enzyme
Akt	:	A serine/threonine kinase
ALT	:	Alanine transaminase
AMOT	:	Angiomotin
AMPK	:	AMP-activated protein kinase
ANP	:	Atrial natriuretic peptide
AREG	:	Amphiregulin
ASPA	:	Animal Scientific Procedure Act
AURKA	:	Aurora kinase A
AURKB	:	Aurora kinase B
BA	:	Border area
Bak	:	Bcl-2 homologous antagonist/killer
Bax	:	Bcl-2-associated X protein
BCA	:	Bicinchoninic acid assay
Bcl-2	:	B-cell lymphoma 2
BNP	:	Brain natriuretic peptide
BrdU	:	Bromodeoxyuridine
BSA	:	Bovine serum albumin
CaMKII	:	Calmodulin-dependent protein kinase II
cIAP	:	Cellular inhibitor of apoptosis protein-1
cKO	:	Cardiomyocyte-specific knockout
CO	:	Cardiac output
Crbs	:	Crumbs
cTG	:	Cardiac transgenic
CTGF	:	Connective tissue growth factor
cTnI	:	Cardiac Troponin I
CVD	:	Cardiovascular disease
Cyr61	:	Cysteine-rich 61
DAPI	:	4', 6'-diamidino-2-phenylindole
DCM	:	Dilated cardiomyopathy
dIVS	:	Diastolic intraventricular septum
dLVID	:	Diastolic left ventricular internal diameter
DMEM	:	Dulbecco's modified eagle's medium
DMSO	:	Dimethyl sulfoxide

DNA	:	Deoxyribonucleic acid
DPBS	:	Dulbecco's phosphate-buffered saline
dPW	:	Diastolic posterior wall
Dronc	:	Death regulator Nedd2-like caspase
Drp1	:	Dynamin-related protein 1
Ds	:	Dachsous
ECG	:	Electrocardiogram
ECL	:	Enhanced chemiluminescence
ECM	:	Extracellular matrix
EF	:	Ejection fraction
ELISA	:	Enzyme-linked immunosorbent assay
eNO	:	Endothelial nitric oxide
EPC	:	Endothelial progenitor cell
ERK	:	Extracellular-signal-regulated kinase
ERM	:	Ezrin-radixin-moesin
FADD	:	Fas-associated via death domain
FAK	:	Focal adhesion kinase
FAST-MI	:	French Registry of Acute ST-Elevation or Non-ST Elevation Myocardial Infarction
FBS	:	Foetal bovine serum
FGF1	:	Fibroblast growth factor 1
Fj	:	Four-jointed
Fox01	:	Forkhead box protein 01
FRMD6	:	FERM domain containing 6
FS	:	Fractional shortening
GAPDH	:	Glyceraldehyde-3-Phosphate Dehydrogenase
GATA4	:	GATA binding protein 4
GFP	:	Green fluorescent protein
GPCR	:	G-protein coupled receptor
GSK3	:	Glycogen synthase kinase 3
H&E	:	Haematoxylin and eosin
HCM	:	Hypertrophic cardiomyopathy
HDFs	:	Human dermal fibroblasts
HF	:	Heart failure
HIF-1	:	Hypoxia-inducible factor 1
HMG-CoA	:	3-hydroxy-3-methyl-glutaryl-coenzyme A
HO-1	:	Heme oxygenase-1
HR	:	Heart rate

HRP	:	Horseradish peroxide
HUVEC	:	Human umbilical vein endothelial cell
HW	:	Heart weight
IC50	:	Half maximal inhibitory concentration
ICH	:	Intracerebral haemorrhage
IF	:	Immunofluorescence
IMS	:	Industrial methylated spirit
iPS	:	Induced pluripotent stem
IVS	:	Interventricular septal thickness
JAK1	:	Janus kinase 1
JNK	:	Jun amino-terminal kinases
KBR	:	Kibra
LAD	:	Left anterior descending artery
Lats1/2	:	Large tumour suppressor kinase 1/2
LC3	:	Light chain 3
LIMD1	:	LIM domains containing 1
LPA	:	Lysophosphatidic acid
LV	:	Left ventricle
LVID	:	Left ventricular internal diameter
LVM	:	Left Ventricular Mass
LVPW	:	Left ventricular posterior wall thickness
MAP	:	Mitogen-activated protein
MAP3K	:	Mitogen-activated protein kinase kinase kinase
MAPK	:	Mitogen-activated protein kinase
Mats	:	Mob as tumour suppressor
MEK	:	Mitogen-activated protein kinase
Mer	:	Merlin
mg/kgBW	:	Milligram per kilogram body weight
MI	:	Myocardial infarction
MLKL	:	Mixed-lineage kinase domain-like
MLP	:	Muscle LIM protein
MOB1	:	Mps1 binding protein
MPTP	:	Mitochondrial permeability transition pore
Mst1/2	:	Mammalian STE20-like protein kinase 1/2
mTOR	:	Mechanistic target of rapamycin
MTT	:	Thiazoyl blue tetrazodium bromide
NF2	:	Neurofibromin type 2
NFAT	:	Nuclear factor of activated T cells

NF-κB	:	Nuclear Factor Kappa B
NLK	:	Nemo-like kinase
NRCMs	:	Neonatal rat cardiomyocytes
Pax3	:	Paired box gene 3
PBS	:	Phosphate-buffered saline
PCR	:	Polymerase chain reaction
PE	:	Phenylephrine
PFA	:	Paraformaldehyde
pH-H3	:	Phospho Histone H3
PI3K	:	Phosphoinositide-3-kinase
PIK3CG	:	Phosphatidylinositol-4,5-biphosphate 3-kinase catalytic subunit gamma
PMFS	:	Phenylmethylsulfonyl fluoride
PPARγ	:	Peroxisome proliferator-activated receptor gamma
PPCI	:	Primary percutaneous coronary intervention
PPIX	:	Protoporphyrin IX
PPXY	:	Proline-proline-X–tyrosine
PR38	:	Peptide regulator 39
PUFA	:	Polyunsaturated fatty acids
PVDF	:	Polyvinylidene fluoride
PW	:	Posterior wall
qPCR	:	Quantitative polymerase chain reaction
RA	:	Remote area
Raf	:	Rapidly accelerated fibrosarcoma
Ras	:	Rat sarcoma
RASSF1A	:	Ras association domain family 1 isoform A
RIP	:	Receptor-Interacting Proteins
RNA	:	Ribonucleic acid
ROK	:	Rho-kinase
ROS	:	Reactive oxygen species
rpm	:	Revolutions per minute
RTK	:	Receptor tyrosine kinase
RT-qPCR	:	Real-time quantitative polymerase chain reaction
RUNX	:	Runt-related transcription factor
RWT	:	Relative wall thickness
S1P	:	Sphingosine-1-phosphate
Sav	:	Salvador
Sd	:	Scalloped

SDS	:	Sodium dodecyl sulfate
SEM	:	Standard error of means
siRNA	:	Small interfering RNA
sIVS	:	Systolic intraventricular septum
sLVID	:	Systolic left ventricular internal diameter
sPW	:	Systolic posterior wall
TAC	:	Transverse aortic constriction
TAOK	:	Serine/threonine-protein kinase
TAZ	:	Transcriptional coactivator with PDZ-binding motif
TBST	:	Tris-buffered saline with 0.05% Tween-20
TBX5	:	T-Box Transcription Factor 5
TEAD	:	Transcriptional enhanced associate domain
TEF	:	Transcriptional enhancer factor
TFs	:	Transcription factors
TL	:	Tibia length
TLR	:	Toll-like receptor
TMB	:	Tetramethylbenzidine
TNF	:	Tumour necrosis factors
TRADD	:	TNF RI-associated Death Domain
TRAF	:	Tumour necrosis factor receptor associated factor
Treg	:	Regulatory T
TTF-1	:	Thyroid transcription factor-1
TUNEL	:	Terminal deoxynucleotidyl transferase mediated nick end labelling
VEGF	:	Vascular endothelial growth factor
VEGFR	:	Vascular endothelial growth factor receptor
VGLL4	:	Vestigial-like family member 4
VP	:	Verteporfin
YAP	:	Yes-associated protein
Yki	:	Yorkie

ABSTRACT

A thesis submitted to the University of Manchester by Efta Triastuti for the degree of Doctor of Philosophy entitled

"Pharmacological inhibition of the Hippo pathway in the cardiovascular system"

March 2021

The Hippo pathway plays an important role in the regulation of cell proliferation, apoptosis, and differentiation, making it a potential therapeutic target for many diseases. Inhibition of the Hippo pathway may lead to the induction of cell proliferation and tissue regeneration, which could be beneficial in several pathological conditions, including cardiovascular diseases. Mst1 and Mst2 are two major components of the Hippo pathway that can potentially be targeted pharmacologically since they can interact with many ligands, including chemical compounds. Genetic inhibition of Mst1 and Mst2 is associated with improvement of cardiac remodelling following pathological stimuli. However, studies on evaluating the effects of Mst1/2 pharmacological inhibition in treating cardiovascular diseases are limited. This study aimed to investigate the effects of Mst1/2 pharmacological inhibition in the cardiovascular system in pathological settings.

This study comprises *in vitro* studies using neonatal rat cardiomyocytes (NRCMs) and human umbilical vein endothelial cells (HUVECs) and *in vivo* experiments using mouse models of pressure overload hypertrophy and myocardial infarction. The effects of the Mst1/2 inhibitor (XMU-MP-1) were examined in both *in vitro* and *in vivo* systems. In addition, analysis of a novel Mst2-specific inhibitor (MRT137) was conducted in an *in vitro* model using NRCMs.

XMU-MP-1 significantly increased YAP activity in NRCM and HUVEC cultures. In NRCM, XMU-MP-1 was found to protect against phenylephrine-induced hypertrophy and peroxide-induced apoptosis. Additionally, XMU-MP-1 was able to induce NRCM proliferation. However, XMU-MP-1 appeared to reduce cell viability and angiogenesis in HUVECs.

The *in vivo* experiments using C57Bl/6 mice showed that XMU-MP-1 treatment preserved cardiac function, prevented cardiac hypertrophy and reduced fibrosis following transverse aortic constriction (TAC). However, XMU-MP-1 treatment did not show any significant effects in terms of survival, cardiac function and remodelling in mouse models of acute and sub-acute myocardial infarction (MI).

In addition, *in vitro* experiments using NRCM culture to study the effects of a novel Mst2 inhibitor, MRT137, revealed that YAP activity was augmented, accompanied by increased proliferation and reductions in NRCM apoptosis and hypertrophy.

In conclusion, inhibition of Mst1 and Mst2 using pharmacological compounds is protective against pressure overload cardiac remodelling, possibly via protection against cardiomyocyte hypertrophy and apoptosis. However, Mst1/2 inhibition does not affect the cardiac phenotype following MI. This study provides new insights into the possibility of targeting Mst1/2 for pharmacological treatment of pathological cardiac hypertrophy in the future.

DECLARATION

I declare that no portion of the work referred to in this thesis has been submitted in support of an application for another degree or qualification at this or any other university or other institute of learning.

Efta Triastuti

Division of Cardiovascular Sciences

School of Medical Sciences

Faculty of Biology, Medicine and Health

COPYRIGHT STATEMENT

LIST OF PUBLICATIONS

i. Triastuti, E., Nugroho, A. B., Zi, M., Prehar, S., Kohar, Y. S., Bui, T. A., Stafford, N., Cartwright, E. J., Abraham, S., & Oceandy, D. (2019). Pharmacological inhibition of Hippo pathway, with the novel kinase inhibitor XMU-MP-1, protects the heart against adverse effects during pressure overload. British journal of pharmacology, 176(20), 3956-3971.

ii. Faizah, Z., Amanda, B., Ashari, F. Y., Triastuti, E., Oxtoby, R., Rahaju, A. S., Aziz, M. A., Lusida, M. I., & Oceandy, D. (2020). Treatment with Mammalian Ste-20-like Kinase 1/2 (MST1/2) Inhibitor XMU-MP-1 Improves Glucose Tolerance in Streptozotocin-Induced Diabetes Mice. Molecules, 25(19), 4381.

ACKNOWLEDGEMENTS

I would like to express my utmost gratitude to my supervisor Dr. Delvac Oceandy for his support and guidance throughout my PhD, especially since the spring of 2020 during the COVID-19 pandemic. His calm insights and sage advice have been invaluable in helping me navigate a challenging year.

I greatly value my co-supervisor, Dr. Sabu Abraham, for his valuable advice. Great appreciation to Dr. Elizabeth Cartwright, Dr. Min Zi, Mr. Sukhpal Prehar, Dr. Nicholas Stafford, Dr. Thuy Anh Bui and Mrs. Florence Boudoin for their support and presence whenever I asked for help regarding the *in vitro* and *in vivo* experiments.

I would like to extend my immense gratitude to Dr. Angel Armesilla and Mr. Suhail Ahmed from the University of Wolverhampton for their kind support with the organotypic co-culture assay.

I would also like to thank Farrah, the two Bayus, Yulia, Rinal, Alex and all other Cartwright/Oceandy lab members who have supplied me with encouragement and support, not to mention good food. Your friendship and professionalism are invaluable.

I am massively indebted to my family, my mother and my sisters, who have kept two pieces of my soul, Antania and Regina, in their arms since I left Indonesia to pursue my PhD. I also would like to pay tribute to my late father, who instilled the virtue of hard work.

Manchester has been very kind to me. This city has given me my dear husband, Jaydin, who pours his eternal love, and our precious baby daughter, Fatima.

Finally, this PhD would not be achieved without valuable support from the Indonesia Endowment Fund for Education (LPDP) and the Indonesian Ministry of Finance. Hence, I dedicate this thesis to my motherland, Indonesia.

CHAPTER 1

INTRODUCTION

1.1 Cardiovascular disease

The frame of cardiovascular disease (CVD) encompasses all disorders in the heart and circulatory systems that are initiated by multifactorial risk factors. CVD also includes cardiac remodelling, cardiac hypertrophy and heart failure, which take place just before the end-stage of heart disease in the cardiovascular disease continuum (Dzau et al., 2006).

1.1.1 Epidemiology of CVD

As CVD is responsible for around 30% of death globally, it is one of the leading causes of mortality in the world (Jagannathan et al., 2019; Mahmood et al., 2014). CVD mortality rate is relatively affected by economic status, which is proven by the trends of declining CVD mortality rates in high-income countries and the plateau mortality rates in middle and lower-income countries (Jagannathan et al., 2019). Even though there was a trend of declining total mortality caused by CVD in the United Kingdom (UK) by 68% between 1980 and 2013, CVD was still the second biggest contributor to death in the UK in 2014 (Bhatnagar et al., 2016). Additionally, CVD yearly costs in the UK reach around 19 billion pounds sterling (GBP), thus supporting the argument that CVD is a financial burden (Meininger and Hill, 2020).

At a certain developmental stage, CVD can cause clinical syndromes called heart failure (HF). HF contributes to a high number of hospitalisations of approximately 26 million cases per year worldwide. Hence, the role of HF in morbidity related to CVD cannot be diminished (Ambrosy et al., 2014).

1.1.2 Risk factors for CVD

Based on the Framingham Heart Study and other epidemiological cohort studies, metabolic syndromes such as hypertension, hyperlipidaemia, diabetes mellitus are some of the many conditions identified as CVD risk factors. The probability of someone developing CVD can be estimated using the calculation of risk factor scores. Risk factors of CVD are multifactorial. The calculation of risk factor scores needs to consider both physiological abnormality and lifestyle, which can exaggerate the likelihood of CVD development. (Mahmood et al., 2014)

Age is an unmodifiable risk factor that has a significant impact on the risk of CVD development. Gender should also be considered in assessing risk factor scores because men are more susceptible to developing CVD than women in the younger population. Physiological abnormalities, including high blood pressure, high cholesterol level and

electrocardiogram (ECG) abnormality, are categorised as a high risk of CVD. Additionally, smoking is an important risk factor that can be modified by changing lifestyle (Truett et al., 1967; Wilson et al., 1998). The prediction of CVD risk factors should also include a family history of CVD, physical activity and obesity. Risk factor estimation is not a pre-determined value, but it can be used to find appropriate approaches to reduce the risks of CVD development (Wilson et al., 1998).

Interestingly, there was a new method introduced in 2019 to predict CVD risk using automated machine learning. Predictions using this new method were applied to the data of participants without CVD in the UK Biobank. Interestingly, this new method could determine the relative prediction of CVD events between men and women. Some parameters such as smoking-related variables, self-reported health rating and long-standing illness or disability are more predictive of CVD events for women than for men (Alaa et al., 2019). On the other hand, ECG-related variables are more predictive for men (See Figure 1.1).

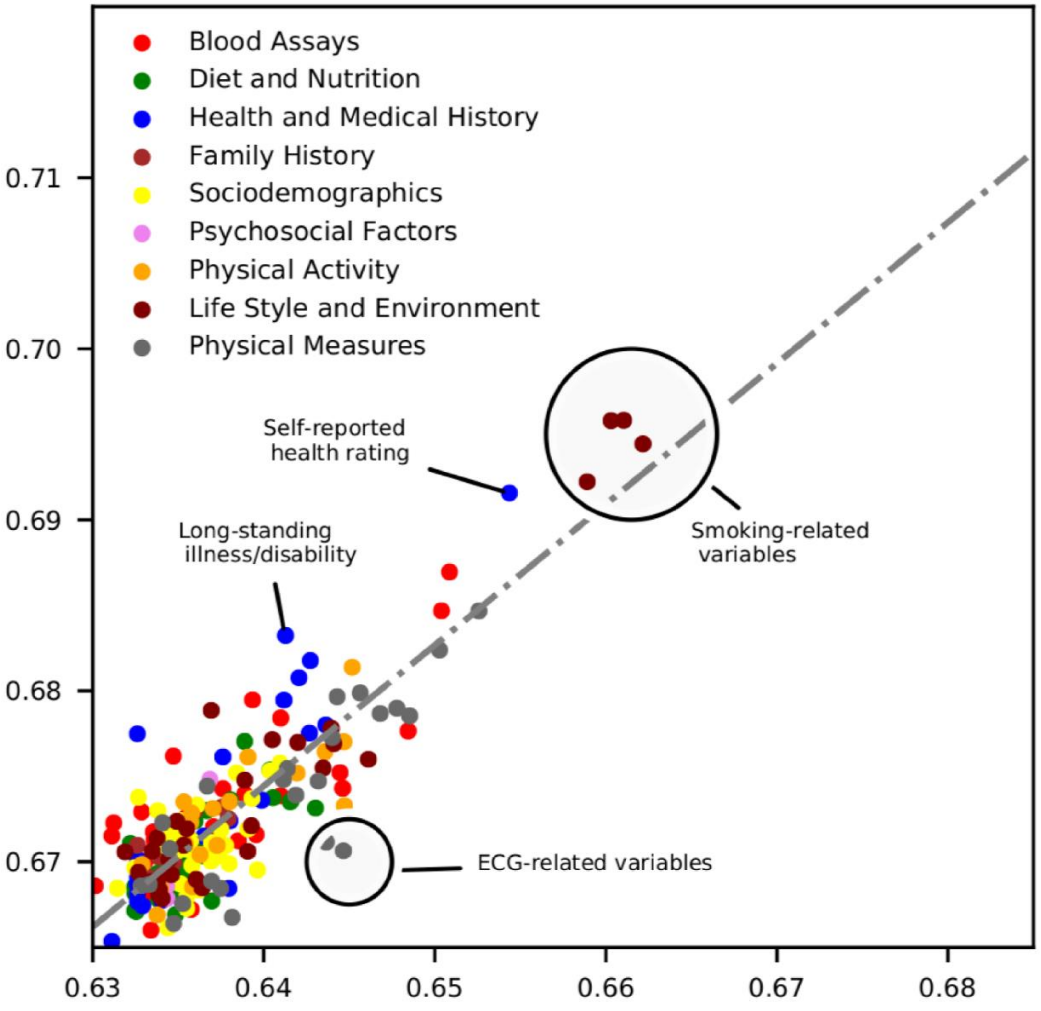

Figure 1.1 CVD risk prediction using automated machine learning on UK Biobank. Data represent the predictive ability of listed parameters for men and women of the same age. The vertical line depicts predictive performance in female participants, whereas the horizontal line portrays predictive performance in male participants. The image was taken from Alaa et al. (2019).

1.2 Adverse cardiac remodelling

Adverse cardiac remodelling is the term given to the changes in the shape, size, structure and function of the heart as the manifestations of underlying pathological molecular and cellular processes that prompt HF (Bernardo et al., 2010). Cardiac remodelling initially occurs as an adaptive response to haemodynamic and neurohormonal determinants that involve various cells and tissues. Prolonged adverse cardiac remodelling causes impairment in cardiac function and other HF symptoms through several processes such as cardiomyocyte death and fibrosis development (Cohn et al., 2000).

1.2.1 Adverse cardiac remodelling features

Heart enlargement, also known as cardiac hypertrophy, is one of the characteristics of cardiac remodelling that can occur either physiologically or pathologically (Bernardo et al., 2010). The disparity between the two different forms of cardiac hypertrophy starts from the initiation process. The stress stimuli in physiological cardiac hypertrophy are usually temporary and the hypertrophic condition is reversible. In contrast, persistent stress stimulation results in adverse cardiac remodelling (Nakamura and Sadoshima, 2018).

Morphological changes in cardiac hypertrophy are distinct between physiological and pathological hypertrophy (Bernardo et al., 2010). Physiological hypertrophy manifests in increasing wall thickness accompanied by enlargement of cardiac chambers (eccentric hypertrophy). The dimension of cardiomyocytes in physiological hypertrophy appears to be growing in width and length (Heineke and Molkentin, 2006). In contrast, eccentric hypertrophy in adverse cardiac remodelling is characterised by dilatation of the ventricle and thinning of the cardiac wall associated with decreasing contractility. On the other hand, concentric hypertrophy happens when the cardiac wall is thickened and stiffened, followed by reduced stroke volume. Increasing wall thickness in concentric hypertrophy is initially followed by shrinking cardiac chambers. Concentric hypertrophy accompanied by mitochondrial dysfunction and cardiomyocyte death can lead to eccentric hypertrophy in a prolonged remodelling process (Nakamura and Sadoshima, 2018). Figure 1.2 describes the discrepancy between physiological and pathological cardiac hypertrophy.

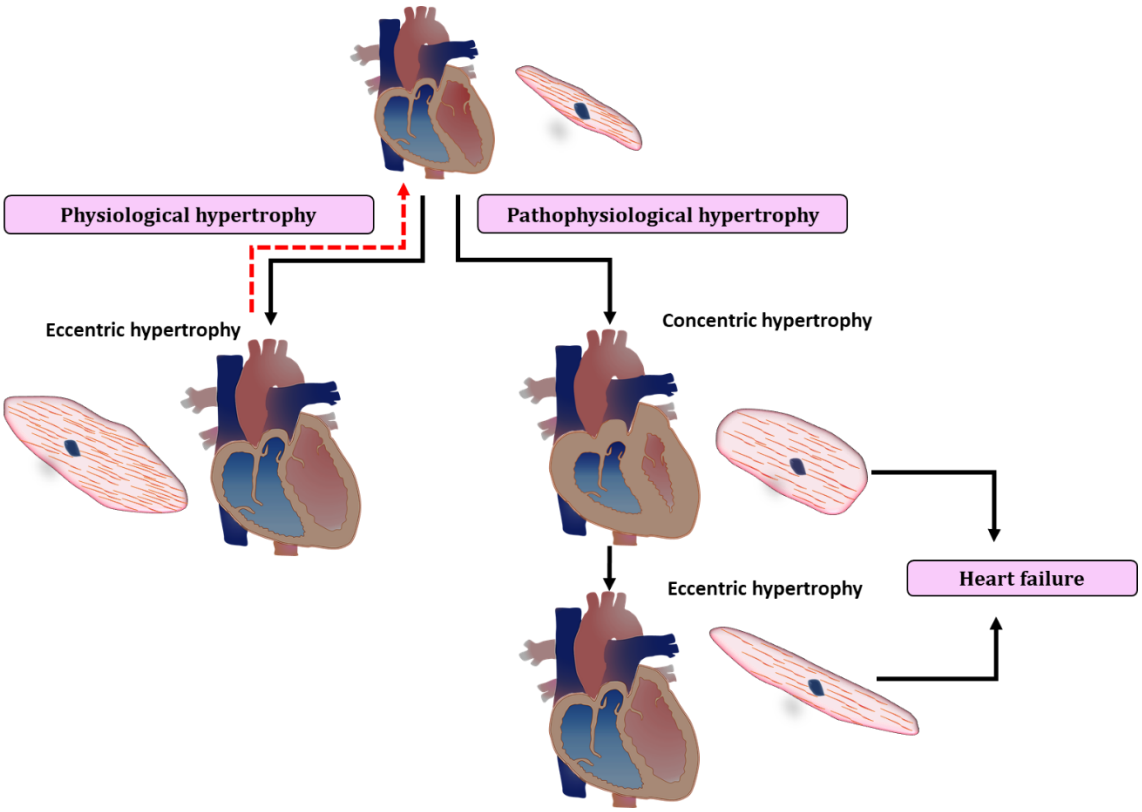

Figure 1.2 The features of physiological and pathological hypertrophy of the heart. The enlargement of the heart in physiological hypertrophy usually does not affect or slightly augments cardiac function. In pathological conditions, both concentric and eccentric hypertrophy can develop heart failure with either preserved or reduced cardiac contractility. Adapted from Nakamura and Sadoshima (2018)

1.2.2 Adverse cardiac remodelling pathophysiology

Adverse cardiac remodelling usually develops in response to various types of pathological conditions such as hypertension, aortic stenosis and myocardial infarction (Nakamura and Sadoshima, 2018). Depending on the stimuli, cardiac remodelling can be adaptive or maladaptive. Hypertension and aortic stenosis usually cause adaptive remodelling because they induce increased afterload leading to concentric hypertrophy development. Myocardial infarction is a type of stress stimulation that can trigger a maladaptive response and develop eccentric hypertrophy (Samak et al., 2016).

Cardiomyocytes undergo significant changes during adverse cardiac remodelling. Individual cardiomyocytes expand in response to hypertrophic gene expression induced by neurotransmitter signals from norepinephrine, angiotensin and endothelin. This cardiomyocyte growth initially improves cardiac contractility (Cohn et al., 2000). However, this process is followed by mitochondrial dysfunction, cardiomyocyte apoptosis and calcium handling impairment that ultimately deteriorate cardiac function (Nakamura and Sadoshima, 2018).

The remodelling process also affects the contractile unit of cardiomyocytes, sarcomeres, following contractile-protein synthesis. During pressure overload, the sarcomeres were added in parallel, which increases cardiomyocyte thickness. On the other hand, the assembly of the sarcomeres following myocardial infarction is in series and results in cardiomyocyte elongation (Bernardo et al., 2010). The alteration of sarcomere assembly leads to an increase of stress on the cardiac wall that induces energy imbalance and ischaemia. Prolonged insufficient oxygen supply causes the deterioration of the contractile activity (Cohn et al., 2000). Figure 1.3 summarises the effects of adverse cardiac remodelling in cardiomyocytes.

Furthermore, mechanical stress and pressure overload can induce collagen synthesis, which ends up as cardiac fibrosis. Cardiac fibrosis development ultimately increases cardiac stiffness and reduces cardiac function(Cohn et al., 2000). HF, which ensues from prolonged adverse cardiac remodelling, reveals some symptoms such as fatigue, breathlessness, fluid retention and swollen legs due to the imbalance between systemic demands and cardiac function in pumping the blood (Ambrosy et al., 2014; Heineke and Molkentin, 2006).

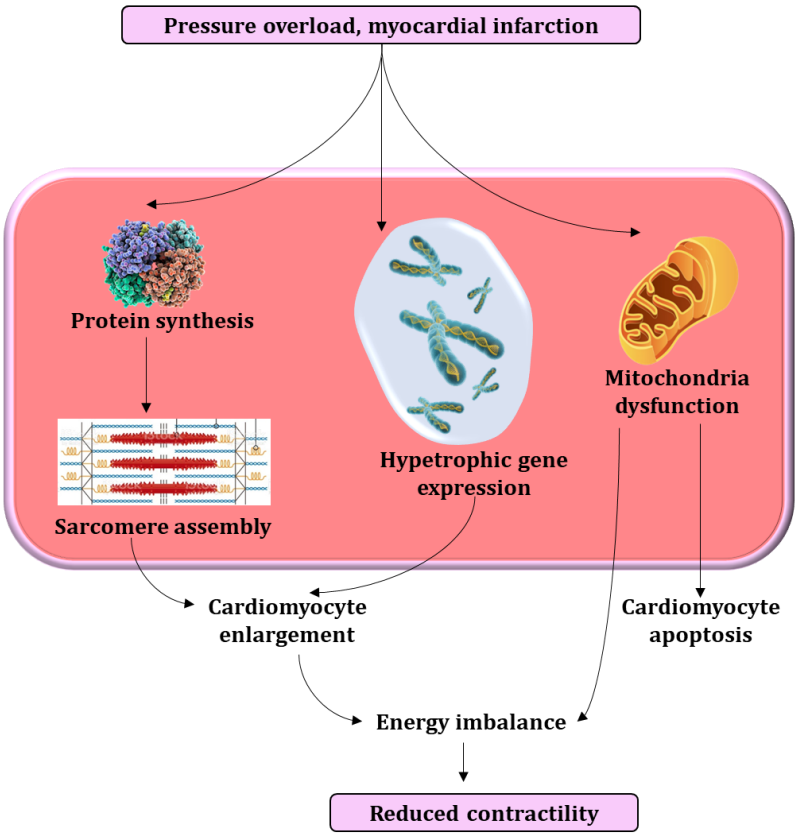

Figure 1.3 Cardiomyocyte changes during pathological remodelling Stress signals from pathological conditions stimulate the synthesis of proteins required for sarcomere assembly in the hypertrophy process. Together with the upregulation of hypertrophic genes, sarcomere assembly results in cardiomyocyte enlargement. Besides, sustained stress stimuli induce mitochondrial dysfunction, which causes the failure of energy supply and apoptosis. Adapted from Bernardo et al. (2010) and Cohn et al. (2000).

1.2.3 Current treatments

Diuretics and digoxin were standard conventional therapies of HF in the past. The medical treatment aiming at HF has now evolved with a new focus on inhibiting adverse cardiac remodelling progression. Based on the clinical studies in HF patients, ACE (angiotensin-converting enzyme) inhibitors such as captopril and enalapril enhanced ejection fraction (EF) and reduced left ventricular (LV) dilation. Pharmacological therapies targeting the renin-angiotensin-aldosterone and sympathetic nervous systems, which are recommended for HF patients, also show beneficial effects in improving morbidity and mortality rates. However, HF treatments mostly address symptom relief rather than the fundamental remodelling process. Isosorbide dinitrate is a vasodilator that was proven to improve cardiac function and decrease mortality (Cohn et al., 2000). Beta-blockers such as bisoprolol, carvedilol and metoprolol showed beneficial effects on HF patients. Polyunsaturated fatty acids (PUFA) as anti-inflammatory agents that have anti-inflammatory activity also effectively reduce the hospitalisation rate associated with cardiovascular events (Krum and Teerlink, 2011).

HF standard therapies such as diuretics and vasodilators are usually given in combination. Diuretics have been demonstrated to control fluid retention and decrease cardiac pre-load (Ellison and Felker, 2017). Vasodilators also work on cardiac pre-load by reducing vascular tension. Nitrate is an example of a vasodilator that showed improvement in HF patients because it can modulate ventricular size (Cohn et al., 2000). Other HF treatments, ACE inhibitors, have been reported to prevent ventricular dilatation by improving hemodynamic capacity. The inhibition of the renin-angiotensin-aldosterone system by ACE inhibitors prompts vasodilation to attenuate mechanical stress into the cardiac wall (Greenberg et al., 1995; Konstam et al., 1992). On the other hand, beta-blockers can provide long-term relief of HF symptoms by reducing heart rate (HR) and blocking sympathetic catecholamines. HR reduction can give the heart a prolonged period to complete the blood filling and emptying phases in all cardiac chambers. The inhibition of the sympathetic nervous system is useful because this system is activated in HF conditions (Packer et al., 1996).

The current standard therapies mostly focus on resolving extra-cardiac issues, mainly haemodynamic abnormalities. The intra-cardiac issues remain untreated by the current standard therapies, making myocardium problems unresolved. Given that the prognosis of HF remains poor, the identification of new treatment modalities is needed.

1.2.4 Treatment innovations

New therapeutic agents are required in addressing a distinct gap between available HF treatments and the underlying problem, which is adverse cardiac remodelling. Many recent studies have elaborated on new pharmacological approaches reversing cardiac remodelling. However, only a few drugs can be translated into clinical settings due to safety or efficacy concerns. The following are some drugs that have been tested clinically:

- Statins

  Statins that have been used to treat hypercholesterolemia are now projected to treat HF patients. Statins exert improvement on cardiac function and structural remodelling through their effects in augmenting endothelial nitric oxide (eNO) production and attenuating eNO degradation. Increased eNO levels promote vascular dilatation and neovascularisation, which might be beneficial in reversing cardiac remodelling (Landmesser et al., 2005). Other mechanisms of statins associated with their potency in reversing cardiac remodelling are improving endothelial function, reducing oxidative stress and enhancing endothelial progenitor cell (EPC) function (Landmesser et al., 2004).

- Oxidant stress inhibitors

  Reactive oxygen species (ROS) production is augmented in HF patients. Xanthine oxidase inhibitors, such as allopurinol and febuxostat, have been tested to reduce ROS production in HF patients (Stull et al., 2004). Both allopurinol and febuxostat are usually used as medications in hyperuricemic conditions. The administration of allopurinol in HF conditions showed beneficial effects, such as inhibiting LV remodelling and improving LV function in the experimental models (Engberding et al., 2004). However, febuxostat effects exceeded allopurinol in improving survival rates when they were given to HF patients (Cicero et al., 2019).

- Vasopressin-receptor antagonists

  Vasopressin, an antidiuretic hormone that acts by increasing water reabsorption, is also known as a potent vasoconstrictor. Some agents such as tolvaptan and conivaptan that work as vasopressin-receptor antagonists have been translated into clinical trials for treating HF patients. Tolvaptan was reported to reduce body weight and improve volume management in acute HF patients, but with no significant change in symptom relief (Felker et al., 2017). On the other hand, a single dose of conivaptan infusion increased cardiac output (CO) in advance HF patients during exercise. The increase in CO during exercise was significant compared to the placebo (Balling et al., 2016).

- Calcium sensitising agent

  It is common knowledge that calcium handling is impaired in HF conditions. Levosimendan acts as an inducer of myofilament sensitisation to calcium. The effects of levosimendan in HF patients were evaluated in the LION-HEART multicentre randomised trial. This trial reported that levosimendan could decrease hospitalisation rates and increase the quality of life in chronic HF patients (Comín-Colet et al., 2018).

- Cell therapy

  The heart consists of terminally differentiated cardiomyocytes with minimum regeneration capability. Mending a damaged heart using cell therapy has been reported to have favourable effects. The evaluation of bone-marrow cells, EPC and other stem cells in HF patients showed cardiac improvement due to their cytokine paracrine effects (Wollert and Drexler, 2005). Experimental studies reported that induced pluripotent stem (iPS) cells derived from cardiomyocytes exhibited both paracrine effects and cardiomyocyte renewal (Miyagawa and Sawa, 2018).

1.3 Biological mechanisms underlying the development of adverse cardiac remodelling

Adverse cardiac remodelling is a complex process involving biochemical and neuro-humoral signals. There is an alteration of gene expression and protein synthesis in cardiomyocytes, fibroblasts and endothelial cells following pernicious stimuli sensed by the heart. Various ligands, including hormones, cytokines and chemokines, are responsible for mediating the remodelling process from adaptive compensatory response to decompensation. A maladaptive heart occurs when cardiomyocyte growth is accompanied by apoptosis, fibrosis and calcium-handling dysregulation (Heusch et al., 2014).

1.3.1 Stress injury associated with cardiac hypertrophy

Once the heart senses any mechanical stress, fetal genes and hypertrophic pathways are upregulated. Signal transduction of mechanical stress in cardiomyocytes is mediated by mechano-sensors called integrins and muscle LIM protein (MLP) (Heineke and Molkentin, 2006). Integrins are transmembrane receptors that were initially identified as regulators of cellular and extracellular matrix (ECM) integrity. Later, the ability of integrins was identified to transduce both physiological and pathological signals. Integrins do not have enzymatic activities, and they can transduce signals by activating downstream molecules.

Thus, mechanical stress signal transduction mediated by integrins ensues from the activation of tyrosine kinases or small GTPases that will activate phosphoinositide 3-kinase (PI3K) and Ras pathways. Ras activation results in the upregulation of hypertrophic protein, extracellular-signal-regulated kinase (ERK1/2) (Ross and Borg, 2001).

An additional mechanical stress sensor is MLP, that is one of the Z disc proteins. The deficiency of MLP in the heart is associated with the progression of dilated cardiomyopathy (DCM) (Knöll et al., 2002). MLP is necessary to pass on stress signals to the hypertrophic pathway, particularly the calcineurin-nuclear factor of the activated T-cells (NFAT) signalling pathway. The absence of MLP in cardiomyocytes results in cardiomyocyte elongation and less thickened cardiomyocytes (Heineke et al., 2005). The summary of stress-induced cardiomyocyte hypertrophy is shown in Figure 1.4.

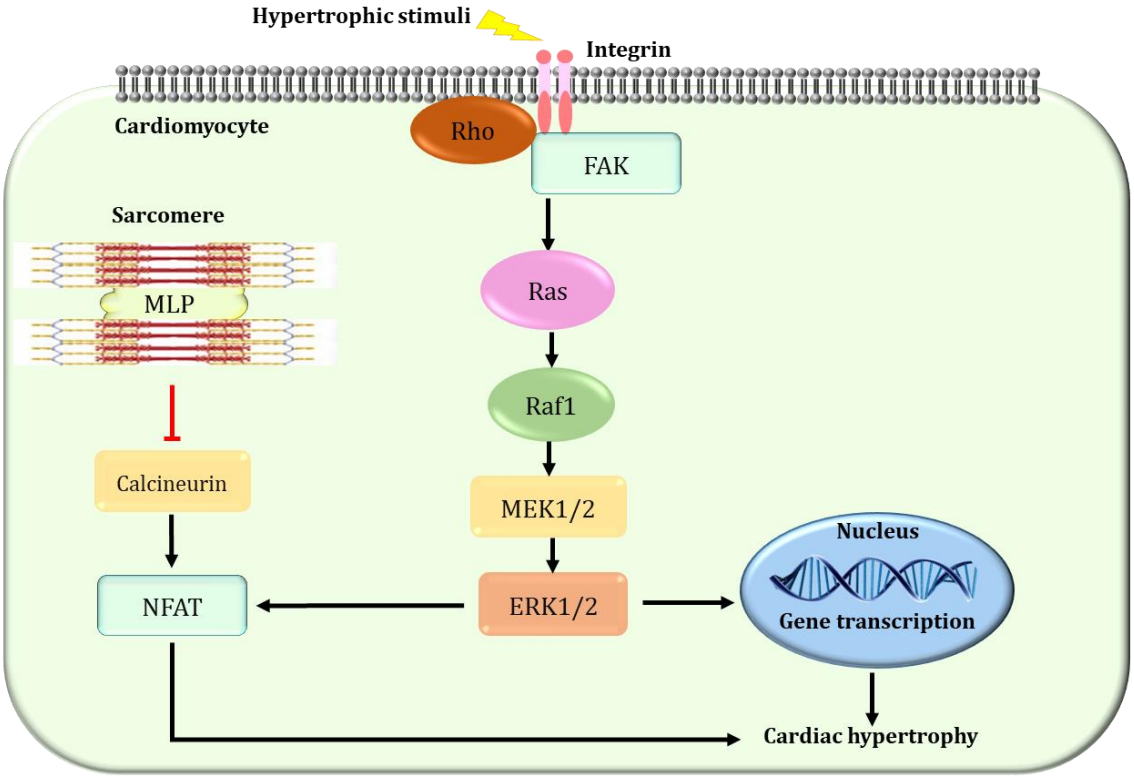

Figure 1.4 Mechanisms of stress-induced hypertrophy in the cardiomyocyte. Mechanical stress sensors such as integrins and MLP are essential in hypertrophic signal transduction. The MLP regulates signal transmission for adaptive hypertrophy. The ablation of the MLP augments NFAT signalling to induce pathological hypertrophy. Stress transduction mediated by integrins results in cardiomyocyte hypertrophy through Ras-ERK1/2 pathway activation mediated by Rho-FAK activation. Adapted from Ross and Borg (2001) and Knöll et al. (2002). FAK: Focal adhesion kinase; Raf: rapidly accelerated fibrosarcoma; MEK1/2: MAP (Mitogen-Activated Protein) Kinase/ERK (Extracellular Signal-Regulated Kinase) Kinase 1/2; ERK1/2: extracellular signal-regulated kinases 1/2.

1.3.2 Cell death in adverse cardiac remodelling

The remodelling process is inevitably associated with cardiomyocyte death. The mechanism in which dysregulated apoptosis, necrosis and autophagy are involved. The upregulation of

reactive oxygen species (ROS) and G protein-coupled receptor (GPCR) signalling contributes to promoting cytokine releases, such as chemokines, interleukins, lymphokines, interferons and tumour necrosis factors (TNF), which induce cell death. Increased ROS production due to mitochondrial dysfunction in adverse cardiac remodelling provokes matrix metalloproteinase activation and causes LV dilatation. Although ROS is produced in physiological conditions, ROS level rises in adverse cardiac remodelling because there are imbalance levels between oxidants and antioxidants (Xu et al., 2019). Abundant ROS is the initiator of many different pathways that end up in cell death. ROS can induce the intrinsic apoptosis pathway by increasing mitochondrial membrane permeability by activating the Bcl-2 pro-apoptotic protein. ROS might also provoke the extrinsic apoptosis pathways that involve death receptors, such as the TNF receptor family (Biala and Kirshenbaum, 2014).

Post-MI reperfusion might promote the opening of the mitochondrial permeability transition pore (MPTP) by inducing ROS. ROS-induced mitochondrial permeability can augment necrosis through the mitochondrial necrosis pathway (Nakagawa et al., 2005). Necrosis is a type of cell death where the cells leak and release their contents. A new term called necroptosis is used for an event associated with programmed-cell necrosis, which shares some features with apoptosis (Zhe-Wei et al., 2018).

There is a cascade involving the serine/threonine kinases-Receptor-Interacting Proteins (RIP1 and RIP3), which are responsible for necroptosis and apoptosis during adverse cardiac remodelling. The RIP1 protein can make complex I with the TNF receptor family, TNF RI-associated Death Domain (TRADD), Tumour Necrosis Factor Receptor Associated Factor 2 (TRAF2) and cellular inhibitor of apoptosis protein-1 (cIAPs) to drive Nuclear Factor Kappa B (NF-κB) activation and induce cell survival. When the complex I detaches from the TNF receptor family, RIP1 undergoes deubiquitination. RIP1 will then form another complex with caspase-8 and Fas-associated protein with death domain (FADD) named complex II. Under the conditions when caspase-8 is activated through phosphorylation, complex II will promote the intrinsic apoptosis pathway by recruiting Bax-Bak proteins to the mitochondrial outer membrane. The attachment of Bax-Bak proteins to the mitochondrial outer membrane results in increased mitochondrial membrane permeability that stimulates the release of cytochrome C and pro-apoptotic protein (Biala and Kirshenbaum, 2014). On the other hand, inactive caspase-8 provokes complex III formation consisting of caspase-8, phosphorylated RIP1, phosphorylated RIP3, mixed-lineage kinase domain-like (MLKL) and FADD. Complex III can either activate Calmodulin-dependent protein kinase II (CaMKII) to induce the opening of MPTP or translocate into the cell membrane to increase cell permeability, which then causes necroptosis (Zhe-Wei et al., 2018).

Autophagy has a unique role in protecting the heart during pathological conditions. Short-term upregulation of autophagy during cardiovascular pathologies is beneficial, but prolonged stimulation can be harmful. The autophagy process removes or recycles damaged or unnecessary cell components to keep cellular homeostasis. In the autophagy process, the lysosome acts as a digestion apparatus with some help from autophagosomes to deliver unwanted cell components (Levine and Kroemer, 2008). The regulation of the autophagy process depends on either external or internal stimuli. The nutrient and oxygen deficiency that occurs after a myocardial infarction can trigger the autophagy process that turns over proteins and mitochondrial constituents for the nutrient provision and energy supply (Matsui et al., 2007). This adaptive function of autophagy occurs in ischaemia conditions. A reperfusion post-myocardial infarction (MI) attack can switch the autophagy's adaptive function into maladaptive because of impaired autophagosome clearance (Ma et al., 2012). It was also found that the inhibition of the autophagy process through Beclin-1 deletion attenuates cardiac remodelling both in MI and pressure overload conditions. The suppression of autophagy through Beclin-1 omission is attributed to less apoptotic cell death (Zhu et al., 2007).

There is an interplay between autophagy and apoptosis that is mediated by Mst1 kinase of the Hippo pathway. Mst1 phosphorylates Beclin-1 after oxidative stress stimuli. Phosphorylated Beclin-1 disrupts the Bcl2 and Bax complex, followed by the formation of a new complex between Beclin-1 and Bcl2. The Beclin-1-Bcl2 complex will induce cell apoptosis and also prevent the formation of the Beclin-1–Vps34–Atg14L complex. By obviating the Beclin-1–Vps34–Atg14L complex formation, Mst1 inhibits the autophagy process (Biala and Kirshenbaum, 2014). Figure 1.5 illustrates the interplay in cell death signalling pathways.

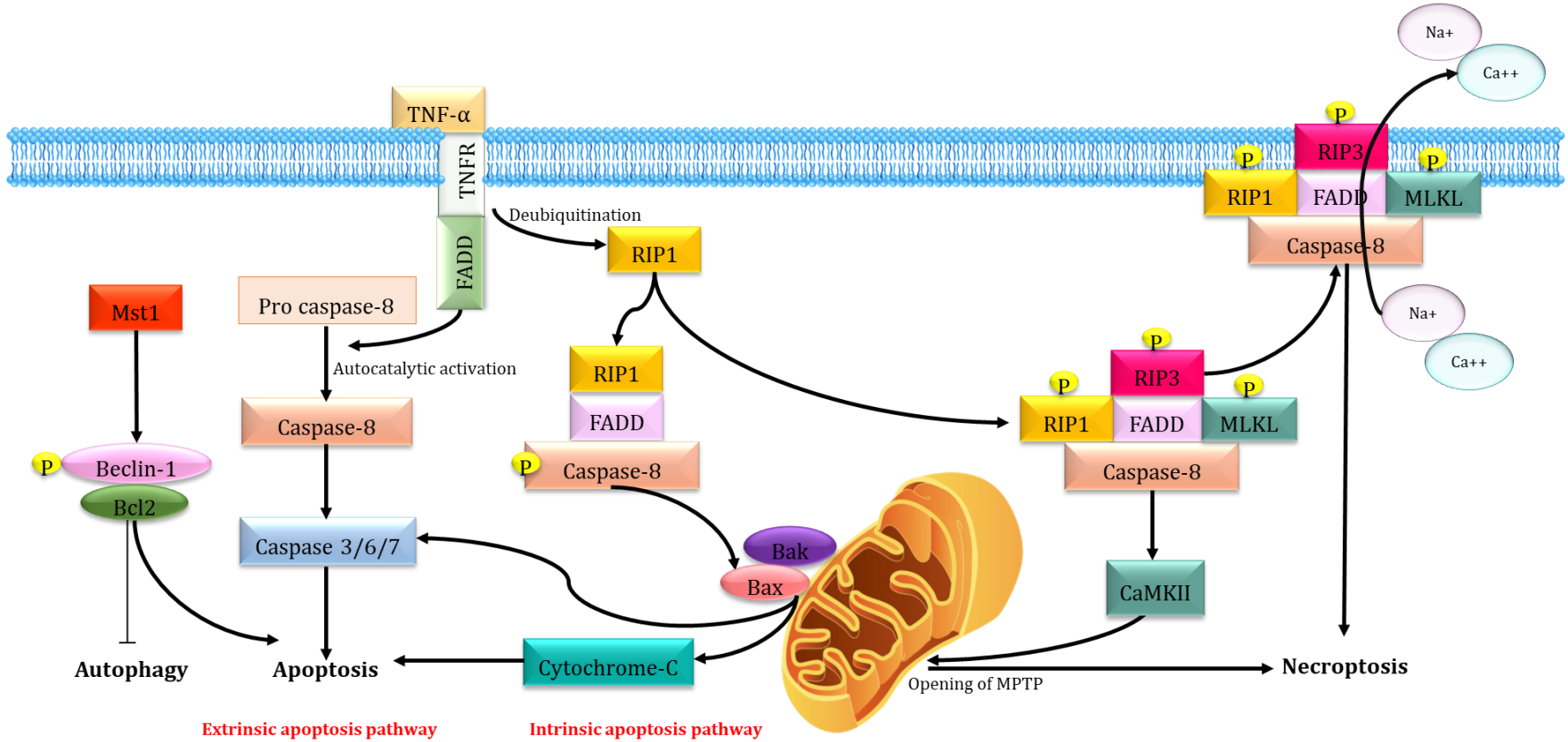

Figure 1.5 The interplay between death signalling pathways in adverse cardiac remodelling. Excess ROS in the adverse cardiac remodelling process can induce cell death through several mechanisms, such as apoptosis, necroptosis and autophagy. These mechanisms share some interplays in their operations. Cytokines stimulation on the death receptors can induce caspase-8 formation from pro-caspase to cause apoptosis (the intrinsic apoptosis pathway). On the other hand, phosphorylated caspase-8 stimulates Bax-Bak protein recruitment on the mitochondrial membrane to increase membrane permeability. Inactive caspase-8 forms a complex with FADD, RIP1, RIP3 and MLKL to induce necroptosis. Mst1 contributes to the switch control between autophagy and the apoptosis pathway through Beclin-1 phosphorylation. Adapted from Biala and Kirshenbaum (2014) and Zhe-Wei et al. (2018).

1.3.3 The association between angiogenesis and cardiac remodelling

In response to either physiological or pathological cues, endothelial cells undergo cellular mechanisms that affect their performance in angiogenesis. Angiogenesis is increased markedly during physiological cardiac hypertrophy to compensate for the additional oxygen demand. On the other hand, maladaptive remodelling of the heart is not accompanied by sufficient microvasculature development (Talman and Kivelä, 2018). In certain conditions, cardiomyocytes generate proteins and peptides that can affect endothelial cells as a part of cell-cell communication. Atrial natriuretic peptide (ANP) and brain natriuretic peptide (BNP) are examples of peptides produced by cardiomyocytes during stress stimuli. ANP has been found to have the ability to dilate vessels and increase vascular permeability (Kuhn, 2012).

There are contradictory findings from the studies evaluating the effects of ANP and BNP in endothelial cell regeneration and neovascularisation. In 2008 Chen et al. reported that ANP showed pro-angiogenesis effects in bovine aortic endothelial cells (Chen et al., 2008). However, other studies by Pedram et al. and Lara-Castillo et al. revealed the opposite effects of ANP in angiogenesis using human umbilical vein endothelial cells (HUVECs), bovine aortic endothelial cells (Pedram et al., 2001) and human retinal endothelial cells (Lara-Castillo et al., 2009), respectively. Another study by Shmilovich et al. in 2009 reported the pro-angiogenic effects of BNP based on increased proliferation, adhesion and migration of endothelial progenitor cells accompanied by augmented vascular regeneration in the ischaemic limb (Shmilovich et al., 2009).

The crosstalk between cardiomyocytes and endothelial cells occurs through paracrine signalling, which can be mediated by vascular endothelial growth factor (VEGF). VEGF is responsible for activating VEGF receptor-2 and inducing angiogenesis (Talman and Kivelä, 2018). Kivelä et al. in 2014 reported that VEGF-B contributes to the development of physiological cardiac hypertrophy via the ERK1/2 pathway. Although VEGF-B has a significant role in angiogenesis during cardiac hypertrophy development, the deletion of this protein does not affect the vasculature of the heart (Kivelä et al., 2014). Another angiogenic factor, peptide regulator 39 (PR39), can also activate VEGF and increase vasculature mass (Tirziu et al., 2007). Interestingly, angiogenesis can become an independent determinant inducing cardiac hypertrophy. Thus, the characteristic of signal transduction between angiogenesis and cardiac hypertrophy is reciprocal. The initiation of signal transduction can come either from endothelial cells or cardiomyocytes and the crosstalk between those cells will stop when vascular density is balanced with the heart size (Walsh and Shiojima, 2007). Figure 1.6 illustrates the crosstalk between endothelial cells and cardiomyocytes in the hypertrophy process.

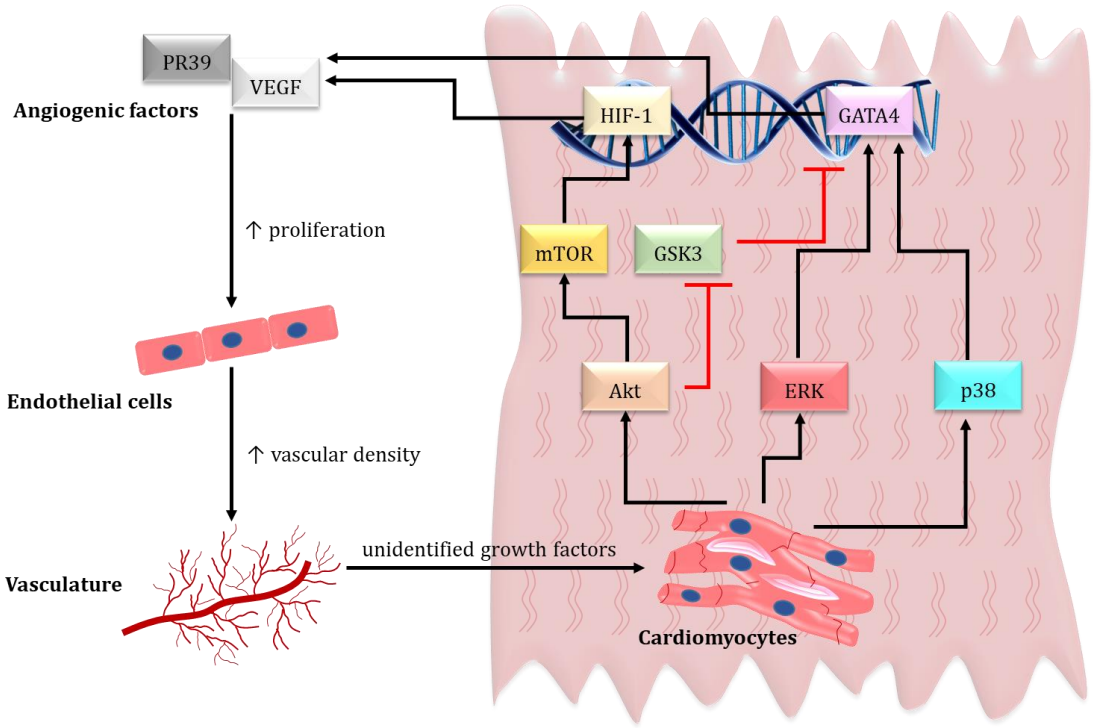

Figure 1.6 The crosstalk between endothelial cells and cardiomyocytes in the hypertrophy process. An increase of angiogenic factors (PR39 and VEGF) sends angiogenic signals to endothelial cells and promotes angiogenesis. Angiogenesis stimulation results in more dense vasculature that transduces hypertrophic signals to cardiomyocytes. Cardiomyocytes then stimulate Akt, ERK and P38 pathways that eventually activate hypertrophic genes. Increased hypertrophic genes in cardiomyocytes can be a signal to induce angiogenic factor production reciprocally. PR39: peptide regulator 39; VEGF: vascular endothelial growth factor; Akt: a serine/threonine kinase; Erk: Extracellular signal-regulated kinases; p38: mitogen-activated protein kinase p38; mTOR: mechanistic target of rapamycin; GSK3: glycogen synthase kinase 3. HIF-1: hypoxia-inducible factor 1. Adapted from Walsh and Shiojima (2007) and Tirziu et al. (2007).

1.4 Overview of the Hippo pathway

The Hippo pathway is a growth-limiting system that was first revealed in 1995 when Warts was identified in *Drosophila* (Kim and Jho, 2018). The Hippo pathway consists of tumour-suppressor kinases and scaffold proteins that inhibit mammalian transcriptional co-activators Yes-associated protein (YAP) and Transcriptional coactivator with PDZ-binding motif (TAZ) or Yorkie (Yki) in *Drosophila*. Taking into consideration that the Hippo pathway has a pivotal role in organ size control and tissue homeostasis, any impairment affecting the Hippo pathway might result in either degenerative or malignancy disease (Ma et al., 2019).

The core kinase cascade of the Hippo pathway in mammalian cells consists of mammalian STE20-like protein kinase 1/2 (Mst1/2) and large tumour suppressor kinase 1/2 (Lats1/2). Those kinases share similar functions as tumour suppressor proteins to their homologues Hpo and Warts in *Drosophila*. The activation of the Hippo pathway leads to the phosphorylation of Mst1/2 mediated by a scaffold protein, MOB kinase activator (MOB1 in

mammals or Mob as tumour suppressor (Mats) in *Drosophila*). The interaction between Salvador (Sav1 in mammals or sav in *Drosophila*) and phosphorylated Mst1/2 subsequently promote the phosphorylation of Lats1/2. Phosphorylated Lats1/2 then bind with Mob and induce the phosphorylation of YAP at Ser127 and TAZ at Ser311. YAP/TAZ phosphorylation results in their proteasomal degradation and cytoplasmic retention through 14-3-3 binding (Ma et al., 2019). The inactivation phosphorylation of YAP and TAZ prevents their translocation into the nucleus and interaction with transcriptional enhanced associate domain (TEAD) family members or the proline-proline-X–tyrosine (PPXY) transcription factors, which limits organ growth. In reverse, Hippo pathway inhibition makes YAP and TAZ active to interact with transcription factors in the nucleus (Fu et al., 2017).

Apart from the TEADs family, YAP is known to interact with other transcription factors, such as Smad1, Smad 2/3, runt-related transcription factor (RUNX), ErbB4 and p73. Meanwhile, other transcription factors that interact with TAZ are Smad 2/3, RUNX, peroxisome proliferator-activated receptor gamma (PPARγ), paired box gene 3 (Pax3), T-box transcription factor 5 (TBX5) and thyroid transcription factor-1 (TTF-1) (Zhao et al., 2011). The interaction between YAP/TAZ and their transcription factors turns on the expression of connective tissue growth factor (*Ctgf*), cysteine-rich 61 (*Cyr61*), fibroblast growth factor 1 (*Fgf1*) and amphiregulin (*Areg*) genes in mouse. *Ctgf* and *Areg* are protein-coding genes that regulate cell proliferation. The *Cyr61* gene has a pro-angiogenic function on endothelial cells. Meanwhile, the *Fgf1* gene is important for cell mitosis, cell survival and endothelial cell migration (Ma et al., 2019). An illustration of the Hippo pathway in mammals is shown in Figure 1.7.

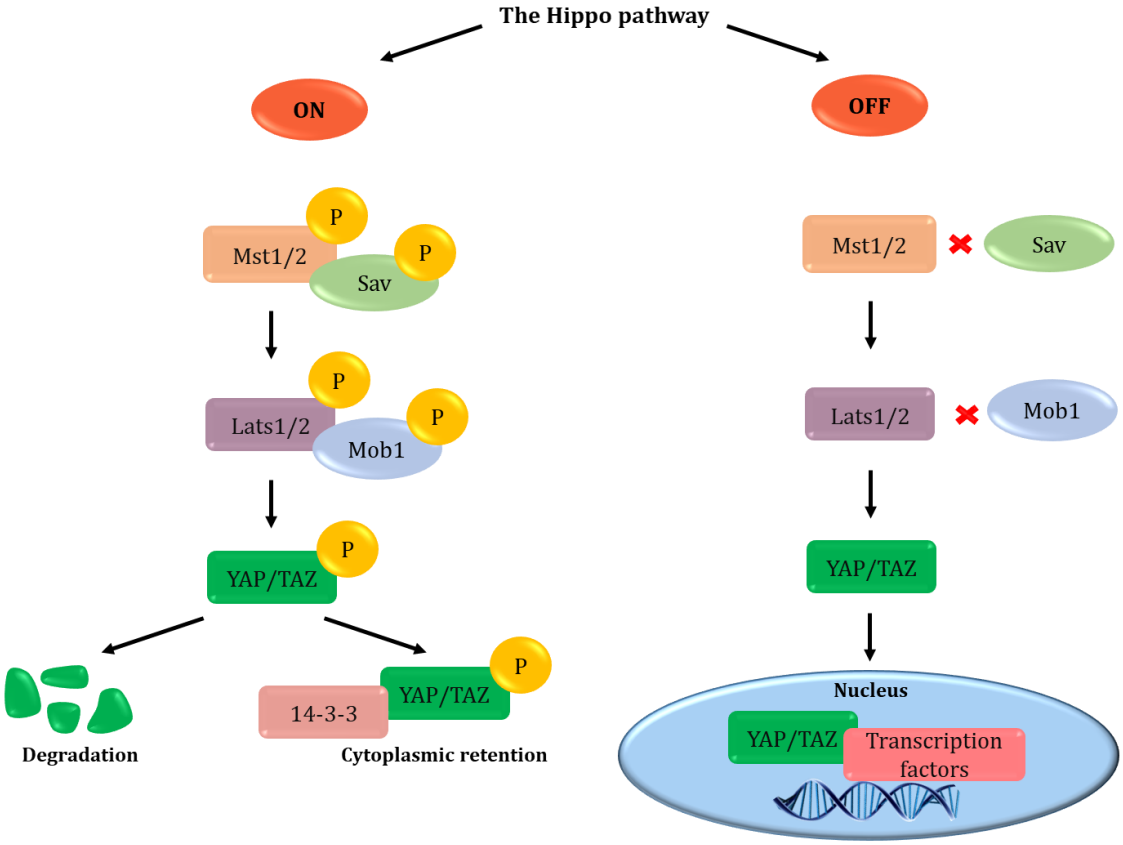

Figure 1.7 Illustration of the Hippo pathway in mammals. When the Hippo pathway is active, the Hippo kinases are phosphorylated and YAP/TAZ are in the cytoplasm. When the Hippo pathway is inactive, Mst1/2 and Lats1/2 are not phosphorylated, whereas scaffold proteins Sav and MOB1 are prevented from their interaction with those kinases. Dephosphorylated Lats1/2 cannot induce YAP/TAZ phosphorylation. Hence, YAP/TAZ are accumulated in the nucleus and interact with transcription factors, such as TEADs, to promote organ growth. Adapted from Fu et al. (2017) and Ma et al. (2019).

Apart from its core components, the Hippo pathway can be extended into a broader system with robust connectivity. In mammals, vestigial-like family member 4 (VGLL4) is another transcription cofactor that competes with YAP in its binding with TEAD, making YAP less active. The role of Rassf in Hippo pathway regulation in mammals is to help the interaction between Mst1 and sav1. Neurofibromatosis type 2 (NF2), kibra (KBR) and FERM domain containing 6 (FRMD6) form a complex that induces Mst1/2 phosphorylation. Other proteins that work on the cell junction are angiomotin (AMOT) and FAT1-4, which promote Lats1/activation (Ma et al., 2019). The following table matches the Hippo components in *Drosophila* and mammals:

Table 1.1 The Hippo components in *Drosophila* and mammals. data were taken from Zhou et al. (2015)

Drosophila		**Mammals**	
Scalloped	Sd	TEA domain family member 1/2/3/4	TEAD
Yorkie	Yki	Yes-associated protein	YAP
		Transcriptional coactivator with PDZ-binding motif	TAZ
Tondu-domain–containing growth inhibitor	Tgi	Transcription cofactor vestigial-like protein 4	VGLL4
Warts	Wts	Large tumour suppressor kinase 1/2	LATS1/2
Mob as tumour suppressor	Mats	Mps one binder kinase activator-like 1A/1B	MOB
Hippo	Hpo	serine/threonine kinase 4/3	MST1/2
Salvador	Sav	Salvador	SAV1
Ras association family member	Rassf	Ras association domain-containing protein 1–6	RASSF1-6
Merlin	Mer	Neurofibromin 2	NF2
Expanded	Ex	FERM domain-containing protein 6	FRMD6
Kibra	Kibra	Kibra	KBR
Fat	Fat	Protocadherin Fat1-4	FAT1-4
		Angiomotin	AMOT

1.4.1 The Hippo pathway and tissue homeostasis

The Hippo pathway keeps the balance between the proliferation of the cells and cell death to maintain tissue homeostasis. Hippo pathway activation comes from intrinsic cues, including cell polarity, cell-cell contact, cell junction and mechanotransduction, or extrinsic cues that consist of soluble factors, extracellular matrix and environmental conditions. Ablation of the Hippo kinases Mst1/2 and Lats1/2 or scaffold protein Sav results in abnormal organ growth due to over-stimulation of cell proliferation and cell death restriction. The regulation of organ growth by the Hippo pathway mostly relies on YAP activity. When the Hippo pathway is suppressed, YAP/TAZ move into the nucleus and bind with their cofactors, either TEADs or the proline-proline-X–tyrosine (PPXY). Those YAP/TAZ target transcription factors are important for gene transcription because both YAP and TAZ have limited ability to bind with DNA. TEADs and PPXY help YAP/TAZ to bind with DNA. The interaction between YAP/TAZ and TEADs will induce the expression of genes that promote cell proliferation and inhibit cell apoptosis (Mao et al., 2015).

The activation of the Hippo pathway leads to YAP/TAZ inactivation. One of the consequences of YAP/TAZ inactivation is the downregulation of YAP target genes (Mao et al., 2015). Another mechanism that limits YAP activity is through YAP competition with VGLL4, which can disturb the interaction between YAP and TEADs. Limited YAP/TAZ activity causes the inhibition of cell regeneration and the upregulation of cell apoptosis. Overstimulation of the Hippo pathway kinases can lead to impaired cell regeneration, organ dysfunction, or premature death (Wu and Guan, 2020).

Together with other biochemical mechanisms, the Hippo pathway regulates organ development and regeneration. During organ growth, the Hippo pathway is less active and YAP/TAZ are more functional to induce cell proliferation and inhibit cell death mediated by their conjugation with TEADs or PPXY. After organs reach the appropriate size, the Hippo pathway becomes active and shows its function of controlling organ growth and preventing hyperplasia. The Hippo pathway also controls cell differentiation, which is important in organ function maintenance and tissue homeostasis. If YAP is more likely attributed to immature cells, the Hippo pathway activation can induce cell differentiation and promote cell maturity (Yu and Guan, 2013). The role of the Hippo components in organ development and tissue homeostasis is listed in Table 1.2.

Table 1.2 The impact of the Hippo pathway on tissue homeostasis. Adapted from Fu et al. (2017), Mao et al. (2015) and Ardestani et al. (2018).

Organs/Tissues	The Hippo components	Roles	References
Neuron	Hippo and Warts activation	Preserve dendritic tiling	(Parrish et al., 2007)
	YAP-TEAD activation	Promote neural progenitor cell proliferation and reduce differentiation of neuron	(Cao et al., 2008)
Heart	Mst1/2, Sav1 and Lats2 inactivation	Enhance cardiomyocyte proliferation	(Yamamoto et al., 2003)
	MST1 and Lats2 activation	Induce cardiac dysfunction and reduced heart size	(Matsui et al., 2008)
	Fetal YAP inactivation	Induce cardiac hypoplasia and decrease cardiomyocyte proliferation	(von Gise et al., 2012)
	YAP activation	Induce cardiac hypertrophy	(Wang et al., 2014)
Liver	YAP activation	Induce liver hyperplasia and enhance hepatocyte proliferation	(Camargo et al., 2007)
	YAP activation	Induce progenitor-phenotype hepatocytes	(Lee et al., 2010)
Skin	YAP activation	Induce progenitor-phenotype epidermis, increase epidermal proliferation and inhibit epidermal differentiation	(Beverdam et al., 2013)
	Mst1/2 or Lats1/2 inactivation	No abnormalities in skin	(Schlegelmilch et al., 2011)
Lung	TAZ inactivation	Induce airspace enlargement	(Mitani et al., 2009)
	Mst1/2 inactivation	Induce respiratory failure	(Chung et al., 2013)
Kidney	TAZ inactivation	Induce renal cyst phenotype	(Makita et al., 2008)
	YAP inactivation	Reduce nephrogenesis	(Reginensi et al., 2013)
Adipose tissue	TAZ activation	Reduce adipogenic differentiation	(Hong et al., 2005)
	Hpo inactivation	Induce fat accumulation and weight gain	(Huang et al., 2013)
	Yki activation	Increase fat cell number	(Huang et al., 2013)
	Lats2 activation	Reduce fat cell proliferation and induce differentiation	(An et al., 2013)
Muscle	Mst1 activation	Induce muscle atrophy	(Wei et al., 2013)
	YAP/TAZ activation	Induce myoblast differentiation	(Chen et al., 2017)

1.4.2 Upstream and control mechanisms of the Hippo pathway

The Hippo pathway can be upregulated by diverse signals both from intrinsic and extrinsic cues. The intrinsic cues that regulate the Hippo pathway include cell polarity, cell-cell contact, cell junction and mechanotransduction, whereas the extrinsic cues are oxygen and nutrient availability, cellular stress and soluble factors (Kim and Jho, 2018).

The fact that cell density in mammals can activate the Hippo pathway explains how cell-cell contact is an important mechanism in regulating the Hippo pathway. Angiomotin (AMOT) and neurofibromin 2 (NF2) complex at the tight junction can activate Lats2. AMOT can also interact with YAP and inactivate YAP by preventing YAP from nucleus translocation (Li et al., 2015). Conversely, cell-cell contact can also be mediated by E-cadherin at the adherens junction through an α/β-catenin, Kibra, and NF2 complex, which promotes Mst1/2 phosphorylation (Kim et al., 2011).

Additionally, Hippo pathway regulation in *Drosophila* was found to be affected by cell polarity, which is mediated by several factors, such as the apical transmembrane protein Crumbs (Crb) and the Fat–Dachsous complex. Cell polarity defect activates the Mer–Ex–Kibra complex located in the apical domain of epithelial cells to directly bind with Hpo and sav and activate the Hippo pathway (Yu et al., 2010). Otherwise, Dachsous (Ds) cadherin and four-jointed (Fj) are ligands expressed for cell-cell communication purposes. If there is a discrepancy in Ds and Fj levels among cells, Ds and Fj will interact with Fat and upregulate Hippo target gene expression (Willecke et al., 2008).

High cell density triggers mechanotransduction signals of the cells to decrease the adhesive area and inactivate Rho GTPases. Rho GTPase inactivation prevents actin cytoskeleton action, thus stimulating Lats1/2 phosphorylation and inhibiting YAP/TAZ activity (Wada et al., 2011). On the contrary, increased adhesion of cells to the extracellular matrix (ECM) is a mechanotransduction factor that inhibits the Hippo pathway through the c-Jun N-terminal kinase (JNK)-dependent mechanism associated with LIM domains containing 1 (LIMD1) activation. LIMD1 acts as a Lats1 inhibitor that subsequently stimulates YAP/TAZ activity (Codelia et al., 2014).

Cellular stress, for instance, changes in liquid flow force, can affect Hippo pathway regulation. YAP activity is influenced by shear stress through mechanisms that are either dependent or independent of the canonical Hippo regulation. In the Hippo pathway-dependent mechanism, shear stress stimulates integrin–$G\alpha_{13}$ interaction, which subsequently inhibits RhoA action, promotes Lats1 phosphorylation and inhibits YAP activity (L. Wang et al., 2016). In the Hippo pathway-independent mechanism, YAP activity is mediated via the actin cytoskeleton and AMOT (Nakajima et al., 2017).

Soluble factors, such as lysophosphatidic acid (LPA) and sphingosine-1-phosphate (S1P), have been reported to inhibit Lats and stimulate YAP/TAZ activity through their interaction with $G\alpha_{12}$ of G protein-coupled receptors (GPCRs). Conversely, the activation of $G\alpha_s$, another GPCR, by other ligands, such as glucagon and epinephrine, inhibits YAP/TAZ activity. Rho GTPases and actin cytoskeleton are revealed to facilitate the mechanisms of how GPCRs affect the Hippo pathway (Yu et al., 2012). Another ligand that can upregulate the Hippo pathway is TGFβ through Ser/Thr kinase receptor binding and SMAD activation (Massagué, 2012). A summary of the Hippo pathway regulation is shown in Figure 1.8.

The regulation of the Hippo pathway is also affected by Wnt and Notch signalling pathways. Wnt signaling inhibits the Hippo pathway in the regulation of cell proliferation and apoptosis, whereas, Notch signalling activates the Hippo pathway during cell differentiation and proliferation. Interestingly, the Hippo pathway can also affect the regulation of the Notch and Wnt signalling pathways. The Hippo pathway inactivation can send feedback signals to stimulate the Notch and Wnt signalling pathways (W. Kim et al., 2017).

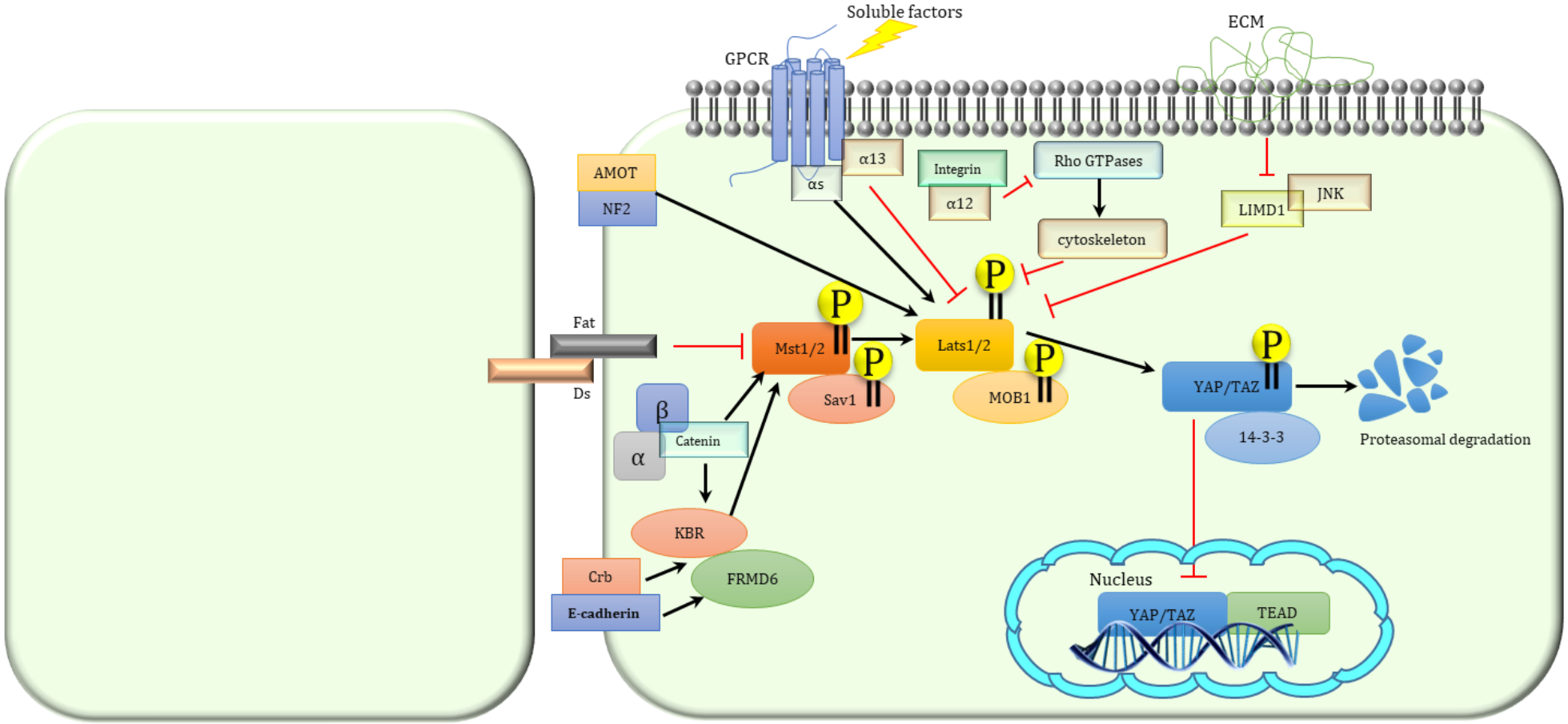

Figure 1.8 The regulation of the Hippo pathway. There are intrinsic and extrinsic factors that regulate the Hippo pathway. Each factor has components that mediate the mechanisms, whether upregulating or downregulating the Hippo pathway. The NF2-KBR-FRMD6 complex, the AMOT-NF2 complex and GPCR Gαs are upstream regulators of the Hippo pathway. The downstream regulation of the Hippo pathway is facilitated by the Dachs and Fat complex, Gα13, Rho GTPases and LIMD1. Adapted from Ma et al. (2019) and Wu and Guan (2020).

1.4.3 Targets and outputs of the Hippo pathway

Some studies have identified the targets and outputs of the Hippo pathway. The scalloped (Sd) protein of the TEAD/transcriptional enhancer factor (TEF) family was found to interact directly with Yorkie (Yki), the YAP homologue in *Drosophila*. Sd-Yki binding is important for promoting the expression of the diap1 gene that induces clone growth in *Drosophila* (Wu et al., 2008). Yki activation facilitates cycE transcription, which further induces cell proliferation and inhibits apoptosis (Huang et al., 2005). Other genes that are targeted by Yki are *Bantam* microRNA (Nolo et al., 2006) and *Myc* (Neto-Silva et al., 2010). Both genes regulate cell proliferation and tissue growth. Moreover, *Ctgf1* is identified as a gene-targeted by YAP that regulates cell growth during organ development (Zhao et al., 2008).

The role of Yki in regulating apoptosis was associated with its capability to suppress the transcription of death regulator Nedd2-like caspase (Dronc) (Verghese et al., 2012). Another piece of evidence showing the importance of the Hippo pathway in apoptosis and autophagy regulation was reported by Maejima et al. in 2016, revealing the interaction between Mst1 and Beclin1 (Maejima et al., 2016). Additionally, Mst1 can regulate the autophagy process through its interaction with light chain 3 (LC3). Mst1 induces LC3 phosphorylation, which facilitates the fusion between autophagosomes and lysosomes (Wilkinson and Hansen, 2015).

The Hippo pathway also has a pivotal role in controlling cell differentiation. The inhibition of the Hippo pathway is associated with less differentiated and more proliferative cell phenotypes. The suppression in cell differentiation is primarily mediated by YAP activity. For instance, in the nervous system, YAP inhibits the NeuroM expression and stops the differentiation process (Cao et al., 2008). Additionally, another study reported that inactivation of the Hippo components, such as Hpo, Salvador and Warts, disturbs follicle cell differentiation. The regulation of cell differentiation by the Hippo pathway is associated with its interaction with the Notch signalling (Yu et al., 2008).

1.4.4 Dysregulation of the Hippo pathway in diseases

Impairment in the regulation of the Hippo pathway can lead to either malignancy or degenerative diseases. Prolonged downregulation of the Hippo kinases or protein adaptors is associated with hyperplasias, such as lethal histiocytic sarcomas in Mst1 ablation and mammary tumours in Mst2 deletion. Meanwhile, the inactivation of both Mst1/2 results in hepatocellular carcinoma, cholangiocarcinoma and colon cancer (Zhou et al., 2009). Protein adaptor Sav deletion was reported to develop hepatocellular carcinoma and cholangiocarcinoma (Lee et al., 2010). The omission of another protein adaptor of the Hippo

pathway, MOB1, also has consequences of causing malignancy diseases, such as skin tumour, osteosarcoma, breast, lung and liver cancers (Nishio et al., 2012). Lats1 kinase knockout is associated with soft-tissue sarcoma and ovarian stromal cell tumour (St John et al., 1999). Furthermore, the over-expression of the Hippo pathway downstream, YAP, results in hepatocellular carcinoma and squamous cell carcinoma-like tumours (Dong et al., 2007).

Downregulation of the Hippo pathway can be beneficial in alleviating degenerative diseases. Sav depletion was reported to show better vascularisation, fibrosis inhibition and cardiac function post-myocardial infarction (Heallen et al., 2011). The inhibition of Mst1/2 using a small molecule called XMU-MP-1 has been reported to improve liver tissue regeneration (Fan et al., 2016).

Furthermore, some studies have reported the association between Hippo pathway upregulation and pathological conditions. Several studies reported the association between the Hippo kinases and metabolic syndromes, such as increased Mst1 in diabetic conditions (Ardestani et al., 2014), excessive fat accumulation (Kawano et al., 2012) and atherosclerosis plaque formation (Wang et al., 2016). Moreover, the inactivation of YAP, a downstream effector of the Hippo pathway, drives into a reduction of the progenitor cell pool due to high differentiation activity in the airway epithelium. The airway epithelium more likely forms a columnar shape in uncontrolled cell differentiation (Zhao et al., 2014). Meanwhile, TAZ deletion in the kidney is associated with polycystic kidney disease (Makita et al., 2008). Additionally, YAP inactivation causes impairment in nephron morphogenesis (Reginensi et al., 2013) and focal segmental glomerulosclerosis (Schwartzman et al., 2016).

1.5 The role of the Hippo pathway in CVDs

The Hippo pathway has a conserved control in regulating heart development, both in physiological and pathological conditions. The Hippo effector, YAP, is highly expressed in fetal heart growth to induce cardiomyocyte proliferation. YAP expression is reduced remarkably after birth and the Hippo pathway is activated to control heart development, making cardiomyocytes lack renewal capacity (Wang et al., 2018). The limitation in cardiomyocyte regeneration is a significant threat to human life because any disease damaging the heart will be challenging to treat. Interestingly, a previous study proved that cardiomyocytes do have the capacity to renew but only in a small portion. Human cardiomyocyte turnover is at around 0.5% in the elderly and about 1% at a younger age (Lázár et al., 2017). The evidence of human cardiomyocyte turnover drives therapeutic strategies that increase cardiomyocyte renewal capacity.

The Hippo pathway has emerged as a potential therapeutic target in increasing cardiac renewal capacity since its inhibition was reported to induce cardiac enlargement during development (Yamamoto et al., 2003). Moreover, recent studies found that Hippo pathway downregulation can improve cardiomyocyte renewal capacity (Heallen et al., 2013; Heallen et al., 2011). This fact indicates a potency in improving cardiac function after aberrant exposure by modulating the Hippo pathway.

YAP deletion using Nkx2.5-Cre promotor in cardiac progenitor cells was found to be embryonic lethal at E10.5 with about a 50% reduction in cardiomyocyte numbers. Cardiomyocyte proliferation was significantly reduced when compared to the wild-type group (Xin et al., 2011). Notably, Del Re et al. in 2013 reported that postnatal cardiomyocyte-specific Yap1 ablation using α-MHC-Cre caused cardiac defects. Dilated cardiomyopathy-induced premature death with high cardiomyocyte apoptosis and fibrosis levels was observed in Yap1 cardiomyocyte-specific knockout (cKO) mice (Del Re et al., 2013). On the other hand, YAP over-expression significantly increased cardiomyocyte proliferation in mice (von Gise et al., 2012; Xin et al., 2013; Xin et al., 2011).

Other studies supported the role of the Hippo pathway in cardiac development, regeneration and diseases. TAZ cKO did not show any defects in the heart, but in combination with YAP cKO, the heart developed dilated cardiomyopathy with less proliferation and more apoptosis (Xin et al., 2013). Lats1 inducible-cKO was reported to increase cardiomyocyte renewal capacity after apex-resection (Heallen et al., 2013). Cardiomyocyte-specific knockout of sav1 and Mst1/2 results in cardiomegaly phenotypes with increased cardiomyocyte proliferation (Heallen et al., 2011). Together with increased cardiomyocyte apoptosis and dilated cardiomyopathy, premature death was found in Mst1

cardiac transgenic (cTG) mice (Yamamoto et al., 2003). Table 1.3 summarises the results of some studies on how the Hippo pathway affects cardiac phenotypes.

Table 1.3 The association between cardiac phenotypes and the Hippo pathway Adapted from Zhou et al. (2015).

Gene	Mouse Models	Promoter	Phenotypes	References
Yap	cKO	Nkx2.5-Cre	Embryonic lethal with low cardiomyocyte proliferation	(Xin et al., 2011b)
		α-MHC-Cre	Premature death accompanied by high apoptosis and fibrosis level with dilated cardiomyopathy	(Del Re et al., 2013)
	cTG	α-MHC	Cardiac enlargement with high cardiomyocyte proliferation	(Xin et al., 2013)
		β-MHC	High proliferation rate in embryonic phase with thick myocardium	(Xin et al., 2011b)
	Inducible cTG	Tnnt2-Cre	Prenatal induction is embryonic lethal with cardiomegaly. Increased heart weight and proliferation without hypertrophy in postnatal induction	(von Gise et al., 2012)
Taz	cKO	α-MHC-Cre	No defect in the heart unless when combined with Yap1 cKO	(Xin et al., 2013)
Lats1/2	Inducible cKO	Myh6-CreERT2	Increased cardiomyocyte renewal capacity post-apex resection	(Heallen et al., 2013)
Sav1	cKO	Nkx2.5-Cre	Cardiomegaly and increased proliferation rate	(Heallen et al., 2011)
Mst1	cTG	α-MHC	Premature death with dilated cardiomyopathy and increased cardiomyocyte apoptosis	(Yamamoto et al., 2003)
Mst1/2	cKO	Nkx2.5-Cre	Cardiac enlargement	(Heallen et al., 2011)

cTG: cardiac transgenic; cKO: cardiac-specific knockout; α-MHC: α-myosin heavy chain

1.5.1 The Hippo pathway in myocardial infarction and heart failure

Myocardial infarction (MI) is one of the leading causes of death worldwide. Saving life after a MI attack is the main target of the treatment. Rapid reperfusion becomes the standard treatment given to reduce the mortality rate. Evidence taken from the French Registry of Acute ST-Elevation or Non-ST Elevation Myocardial Infarction (FAST-MI) in 2005 showed that reperfusion therapy could increase the post-myocardial infarction survival rate. Additionally, reperfusion therapy significantly reduces infarct size and protects the remaining cardiomyocytes from further damage due to ischaemia (Danchin et al., 2014). Figure 1.9 shows 5-year survival in MI patients based on the use of reperfusion methods.

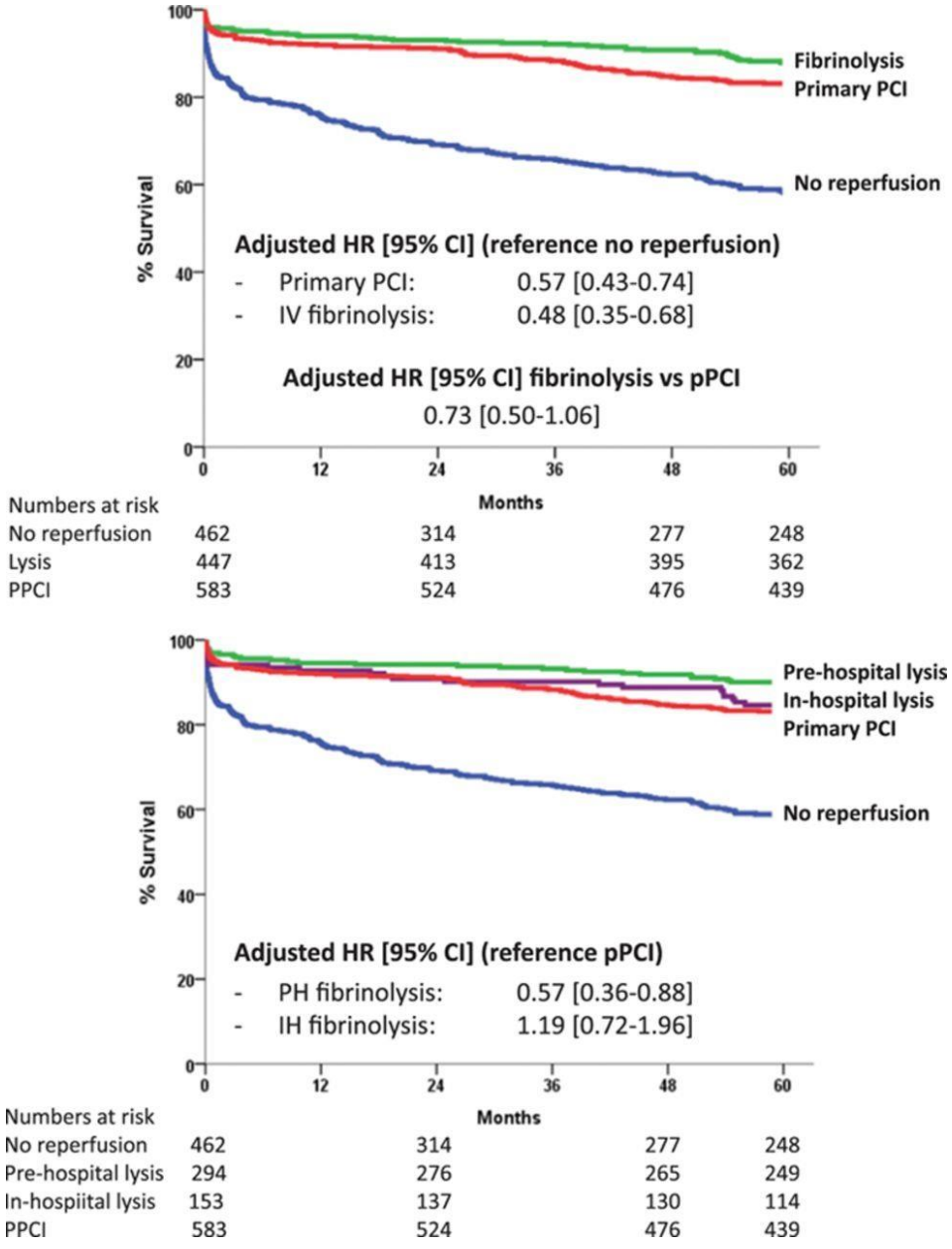

Figure 1.9 5-year survival rate of MI patients based on the use of reperfusion methods. Reperfusion treatments increase the 5-year survival rate by 30% in the FAST-MI 2005 patients compared to MI patients who did not receive reperfusion treatment. The image was taken from Danchin et al. (2014). PPCI: primary percutaneous coronary intervention.

Despite the beneficial effects of reperfusion therapy, there is a paradoxical phenomenon that is caused by reperfusion therapy called reperfusion injury. Soon after a myocardial infarction attack, the opening of the coronary artery can drive cardiomyocyte damage because of oxidative stress. Hence, MI/reperfusion still has a risk of heart failure development. There is a requirement for additional therapy to inhibit heart failure progression following MI/reperfusion. Figure 1.10 illustrates the association between MI/reperfusion and infarct size.

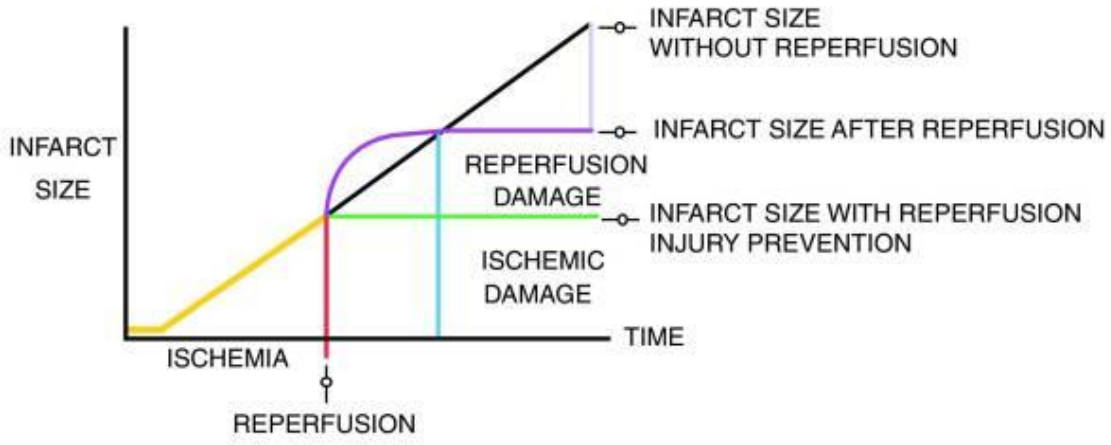

Figure 1.10 The estimation of infarct size based on the use of reperfusion therapy. There is a gap between cardiac damage caused by reperfusion injury and an ischaemic attack that can be reduced with reperfusion injury prevention. The image was taken from Farah and Barbagelata (2017).

The Hippo pathway is a potential therapeutic target to minimise reperfusion injury because this pathway is upregulated in reperfusion injury. MI/reperfusion induces the activation of the Hippo kinases Mst1 and Lats2, which then stimulate the apoptosis cascade. The inhibition of the Hippo pathway might stop progressive cardiomyocyte damage that is induced by MI/reperfusion (Singh and Mia, 2019). Some preclinical studies revealed the beneficial effects of the Hippo pathway inhibition in cardiac diseases. Sav depletion in the MI mouse model is associated with cardiac function improvement and fibrosis reduction (Leach et al., 2017). The inactivation of NF2, an upstream regulator of Mst1, results in cardiac protection against reperfusion injury (Matsuda et al., 2016). Furthermore, the Hippo pathway was known to engage regulatory T (Treg) cells in the infarct area. Treg is important in suppressing inflammatory responses and can thus reduce fibrosis and the immune response (Ramjee et al., 2017). Figure 1.11 summarises the effects of the Hippo pathway modulation in MI, cardiac remodelling and heart failure.

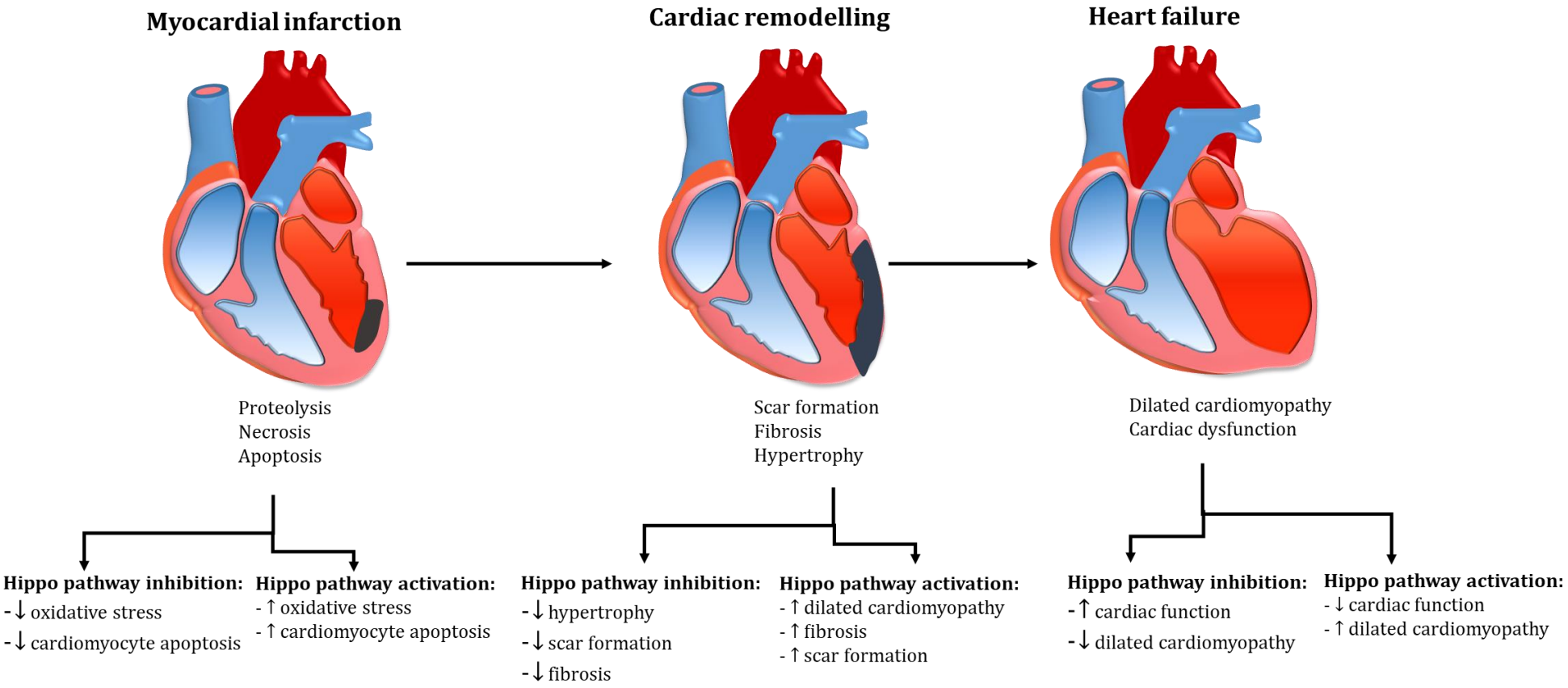

Figure 1.11 The effects of the Hippo pathway modulation in myocardial infarction, cardiac remodelling and heart failure. Hippo pathway inhibition might be beneficial in preventing the progression of cardiac remodelling and heart failure post-myocardial infarction. Adapted from Singh and Mia (2019).

1.5.2 The Hippo pathway in pathological cardiac hypertrophy

The role of YAP in cardiac hypertrophy is debatable. Some studies reported that YAP activation significantly induces cardiomyocyte proliferation without changing their size (Lin et al., 2014; von Gise et al., 2012; Xin et al., 2011a). Another study stated that YAP action in improving cardiac function is related to increased cardiomyocyte proliferation and hypertrophy (Del Re et al., 2013). YAP-induced cardiomyocyte hypertrophy is attributed to its action in activating miR-206, a hypertrophy promoter (Yang et al., 2015). Interestingly, a previous clinical study found that YAP is activated in hypertrophic cardiomyopathy (HCM) patients. YAP upregulation was also observed in pressure overload in the murine model (Wang et al., 2014).

Mst1 is known to contribute to the development of cardiac hypertrophy. Nonetheless, cardiac hypertrophy is not affected solely by Mst1 action. Rassf1, the upstream regulator of Mst1, has a strong association with cardiac hypertrophy. Rassf1 is upregulated in the first week of transverse aortic constriction (TAC) model mice, but it is decreased after 12 weeks (Oceandy et al., 2009). Rassf1 action in cardiac hypertrophy is attributed to its function in inhibiting the interaction between Raf1 and Ras. The inhibition of Raf1 and Ras interaction eventually downregulates extracellular regulated kinase 1/2 (ERK1/2) hypertrophic action (Oceandy et al., 2009). Intriguingly, Rassf1 involvement during adverse cardiac remodelling depends on the cell type. Activation of Rassf1 and Mst1 signalling cascade during pressure overload promotes cardiomyocyte apoptosis whilst also inhibiting cardiac fibroblast proliferation and cardiac hypertrophy (Del Re et al., 2010).

Another Hippo kinase, Mst2, has been reported to regulate cardiac hypertrophy. Mst2 global knockout in mice was found to protect the heart against pressure overload-induced cardiac hypertrophy. The interaction between Mst2 and Raf1 eventually activates ERK1/2 to induce hypertrophy (Zi et al., 2014). The regulation of cardiac hypertrophy by Rassf1 and Mst2 is illustrated in Figure 1.12.

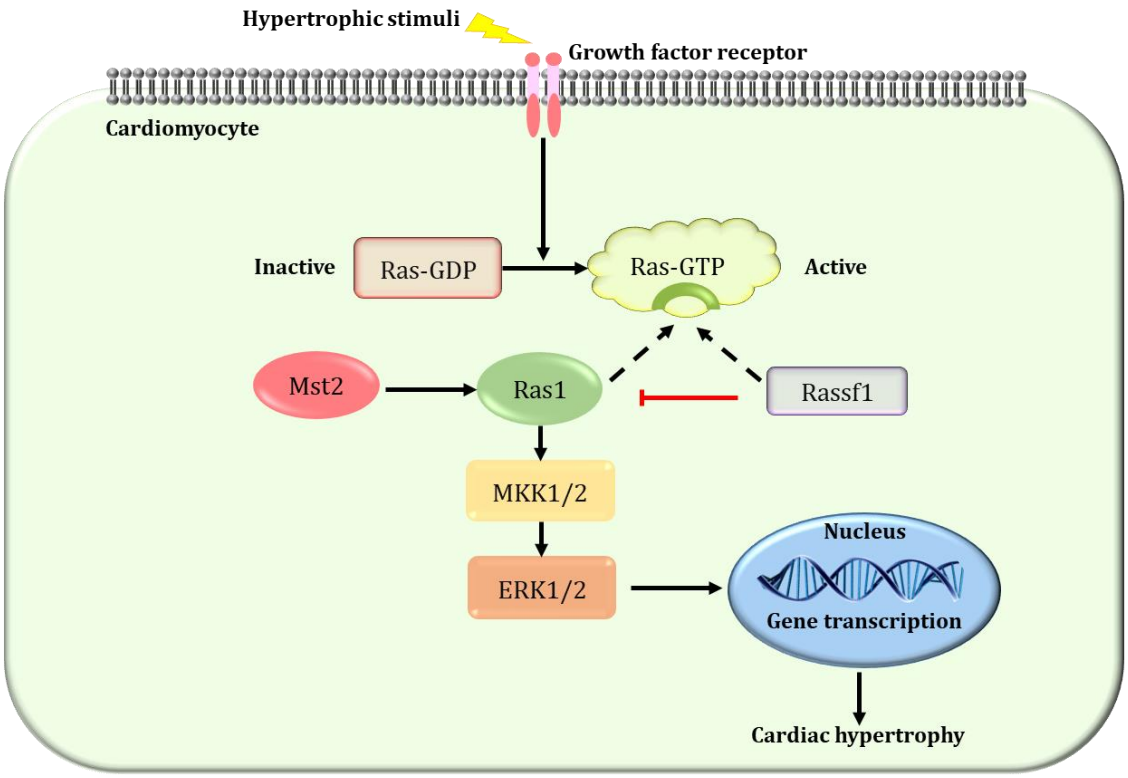

Figure 1.12 Cardiac hypertrophy regulation by the Hippo pathway. Mst2 is a Hippo kinase that has a pro-hypertrophic effect. The mechanism of hypertrophy stimulation by Mst2 is mediated by Ras1 activity, which eventually promotes ERK1/2 action. Rassf1 is an upstream regulator of Mst1 that has an anti-hypertrophy effect through its inhibition on Ras1. Adapted from Oceandy et al. (2009) and Zi et al. (2014).

1.5.3 The Hippo pathway and atherosclerosis

Despite the beneficial effects of YAP in degenerative diseases due to its regenerative function, YAP was identified as one of the atherogenic factors. Endothelial cell-specific overexpression of YAP remarkably increases plaque formation in mice and YAP inhibition significantly reduces atherosclerotic plaque size (L. Wang et al., 2016). YAP is involved in endothelial cell activation that initiates the atherosclerotic process (K.-C. Wang et al., 2016). Activated endothelial cells recruit monocytes which infiltrate the arterial wall and subsequently transform into macrophages (Gibbons, 1997). Following macrophage accumulation in the arterial wall, the immune response is activated to initiate plaque formation (He et al., 2018). Disturbed blood-flow and increased shear-stress can promote the interaction between ECM and endothelial cells and subsequently deactivate integrin and Gα13 (Heo et al., 2014). The inactivation of integrin and Gα13 subsequently increase Rho activity. Rho is important to block YAP phosphorylation. Rho activation will eventually accelerate YAP translocation into the nucleus and its binding to transcription factors (L. Wang et al., 2016). Figure 1.13 illustrates the Hippo pathway control in atherosclerosis.

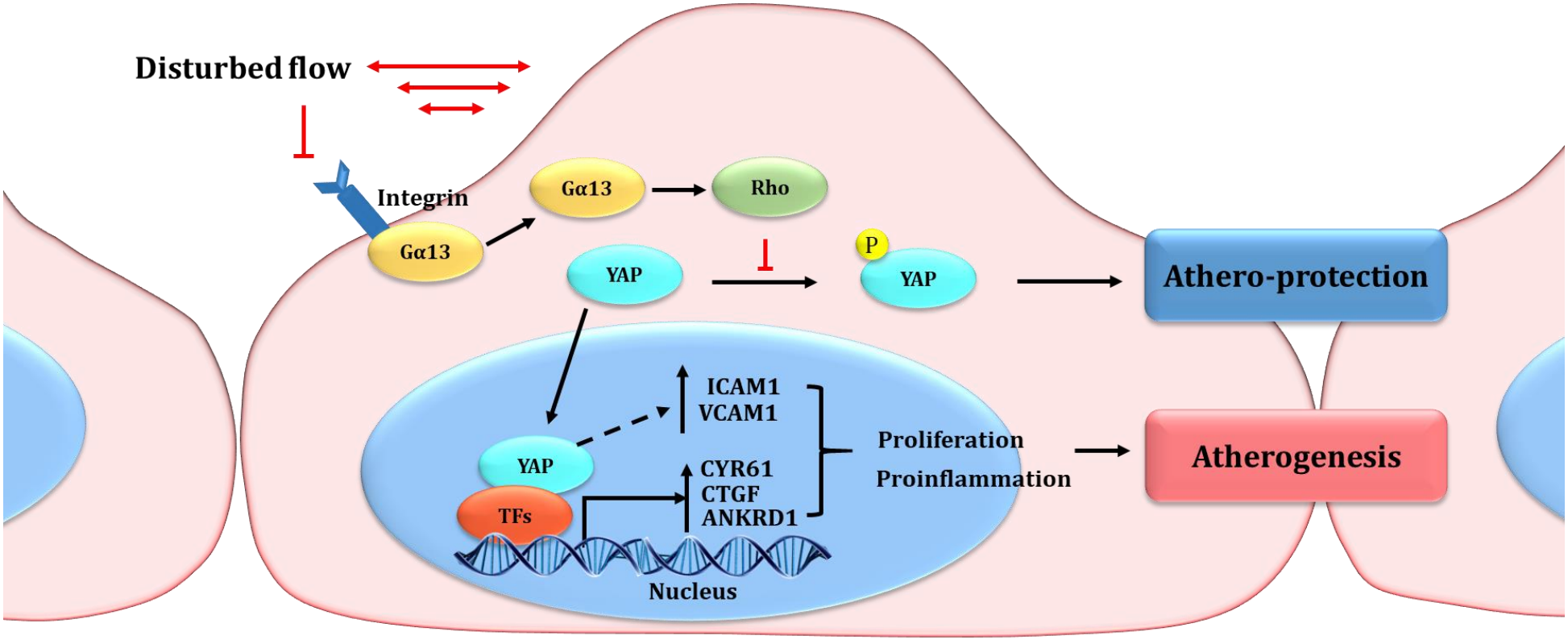

Figure 1.13 The Hippo pathway control in atherosclerosis. Disturbance in blood flow and increased shear stress inhibits integrin and Gα13 interaction that subsequently activates Rho. Rho activation drives YAP translocation into the nucleus to bind with transcription factors, which eventually increases YAP target gene expression. These genes have pro-inflammatory effects that can induce atherogenesis. Adapted from He et al. (2018), Heo et al. (2014) and Wang et al. (2016). TFs: Transcription factors

1.6 Therapeutic strategies targeting the Hippo pathway

Since the Hippo pathway exerts important roles in regulating cell regeneration and apoptosis, it becomes a potential therapeutic target. Many studies have been conducted which focus on Hippo pathway modulation, either inhibiting or activating the Hippo pathway in diverse disease models. Therapeutic strategies based on the target diseases of the Hippo pathway modulation are listed as follows:

1.6.1 Therapeutic strategies against malignancy

YAP/TAZ binding to TEAD is responsible for tumour development. Disrupting the interaction between YAP/TAZ and TEAD can be used to treat malignancy diseases. Verteporfin is an inhibitor of YAP/TAZ binding that showed substantial inhibition of excessive liver growth. However, verteporfin has limitations, such as aberrant impacts in non-malignant cells and difficulty to dissolve in water (Liu-Chittenden et al., 2012). Another compound that disrupts YAP/TAZ interaction is flufenamic acid, which obstructs the YAP binding site at the hydrophobic core of TEAD (Pobbati et al., 2015). Peptides similar to YAP residues 86-100 or VGLL4 potentially decrease YAP affinity to TEAD through competition. For instance, Super TDU is a hybrid of VGLL4 and YAP AAs 74-99 that exerts anti-oncogenic properties. However, the development of peptide-based therapy is challenging in terms of production cost and delivery systems (Juan and Hong, 2016).

The binding of AMOT family proteins inhibits YAP/TAZ activity through direct and indirect mechanisms. Direct interaction between AMOT and YAP/TAZ will prevent YAP/TAZ from migration into the nucleus inhibiting the YAP target gene transcription. The indirect mechanism is mediated by Lats1/2 activity, which is promoted by AMOT (Wang et al., 2015). The upregulation of Lats1/2 will increase YAP/TAZ phosphorylation and promote their proteasomal degradation. Some compounds are available to enhance AMOT action by inhibiting its tankyrase-induced degradation, such as XAV939 and IWR-1. Those compounds are suggested as potential treatments for cancers (Lehtiö et al., 2013).

YAP target genes can be antagonised to block tumour development. Monoclonal antibodies, such as FG-3019 (Neesse et al., 2013) and 093G9 (Lin et al., 2012), were reported to target *Ctgf* and *Cyr61*. The preclinical studies for those antibodies demonstrated that both effectively inhibit tumour growth in mouse models. An antiapoptosis gene, *Birc5*, is also one of the YAP target genes. *Birc5* transcription is activated by a complex that consists of phosphorylated YAP, β-catenin and TBX5. This complex formation is mediated by tyrosine kinase, which induces YAP phosphorylation. Some compounds, such as dasatinib, foretinib

and sunitinib, which exert inhibition on tyrosine kinases, may reduce tumour growth (Rosenbluh et al., 2012).

Hippo kinases were identified as therapeutic targets because they can easily interact with many ligands. In pre-translation studies, okadaic acid and C19 (Mst activators) were found to inhibit malignancy through YAP inactivation (Basu et al., 2014). Indirect targeting of the Hippo pathway kinases also could be a therapeutic strategy. Statins are compounds that have been used widely as lipid-lowering agents. However, the inhibition of 3-hydroxy-3-methyl-glutaryl-coenzyme A reductase (HMG-CoA reductase) by statins could alter Lats1/2 activity through RhoA activation, which subsequently reduces YAP/TAZ activity that is potentially beneficial to prevent tissue overgrowth (Sorrentino et al., 2014).

1.6.2 Therapeutic strategies for regenerative medicine

Targeting GPCR is an alternative choice to modulate the Hippo pathway. The activation of $G\alpha_{13}$ will subsequently dephosphorylate YAP/TAZ by inhibiting Lats1/2 phosphorylation. Thus, YAP target gene expression is upregulated and cell regeneration is enhanced (Yu et al., 2012).

Cell and *in vivo* works suggest activation of Mst might offer a route to treat cancer while inactivation might induce cell regeneration (Johnson and Halder, 2014). 9E1 is a kinase inhibitor that has a remarkable inhibition towards Mst1 with IC_{50} (half maximal inhibitory concentration) = 45 nM based on kinase assays. Even though 9E1 highly inhibits Mst1, its effects on YAP/TAZ activity have not been determined (Anand et al., 2009).

Fan et al. in 2016 discovered a potent inhibitor that selectively inhibits Mst1/2 and Mst2, that is called 4-((5,10-dimethyl-6-oxo-6,10-dihydro-5H-pyrimido [5,4-b] thieno[3,2-e][1,4] diazepin-2-yl)amino) benzenesulfonamide or is known as XMU-MP-1 (shown in Figure 1.14). The selection of kinase inhibitors, which was performed using an enzyme-linked immunosorbent assay (ELISA)–based high-throughput screen of a kinase-directed compound library, exhibited a molecular basis for selectivity. Based on kinase assays, XMU-MP-1 exerts more inhibition on Mst2 (IC_{50} value = 38.1±6.9 nM) compared to Mst1 (IC_{50} value = 71.1±12.9 nM). Mechanistically, XMU-MP-1 inhibits Mst1/2 through ATP-competitive inhibition. Even though XMU-MP-1 has a high affinity to Mst1/2, it can also inhibit other kinases. Therefore, the effects of this compound are not solely based on Mst1/2 inhibition. Most importantly, *in vivo* experiments in this study suggested that the administration of XMU-MP-1 at the dose of 1 to 3 mg/kgBW (milligram per kilogram body weight) intraperitoneally could enhance intestine and liver tissue repair following injury in mouse models. The healing of intestine and liver tissues was accompanied by increased cell

proliferation showing the regenerative effects of XMU-MP-1 (Fan et al., 2016). Considering the potency of XMU-MP-1 in cell regeneration, this compound will be examined further in this PhD project.

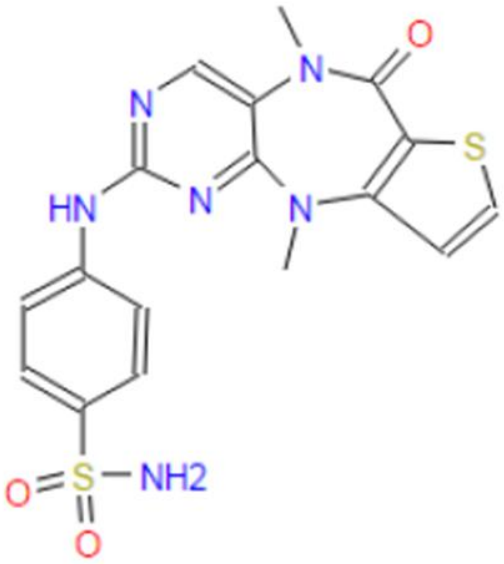

Figure 1.14 Molecular Structure of XMU-MP-1. Image was drawn using an online cheminformatics tool [molinspiration.com].

To summarise therapeutic strategies targeting the Hippo pathway, the table below listed small molecules and their specific targets:

Table 1.4 Small molecules targeting the Hippo pathway

Treating malignancy diseases	
Compounds	**Targets**
Verteporfin	YAP/TAZ - TEAD binding
Flufenamic acid	YAP/TAZ - TEAD binding
Super-TDU	YAP/TAZ - TEAD binding
XAV939	AMOT
IWR-1	AMOT
FG-3019	*Ctgf* and *Cyr61*
093G9	*Ctgf* and *Cyr61*
Dasatinib	Tyrosine kinase
Foretinib	Tyrosine kinase
Sunitinib	Tyrosine kinase
Okadaic acid	Mst1/2 (activator)
C19	Mst1/2 (activator)
Statins	HMG-CoA reductase (target lats indirectly)
Treating degenerative diseases	
Compounds	**Targets**
9E1	Mst1
LPA	$G\alpha_{13}$ - Rho
S1P	$G\alpha_{13}$ - Rho
Thrombin	$G\alpha_{13}$ - Rho
XMU-MP-1	Mst1/2 (inhibitor)

1.7 Hypothesis

The Hippo pathway plays a vital role in regulating cell survival and regeneration. Given that genetic approaches on the Hippo pathway are able to modify cardiomyocyte characteristics, the Hippo components emerge as potential therapeutic targets. The development of therapeutic modalities targeting the Hippo components for treating malignancy diseases has evolved extensively. However, the development of pharmacological approaches targeting the Hippo components in treating degenerative diseases, particularly heart failure, is still limited. Therefore, I hypothesise that pharmacological inhibition of Mst1/2 will prevent the progression of cardiac remodelling to heart failure.

1.8 Aims

This thesis aims to address the following issues:

1. To investigate the effects of pharmacological inhibition of Mst1/2 using XMU-MP-1 in pressure overload-induced cardiac hypertrophy.
2. To examine the effects of Mst1/2 inhibition using XMU-MP-1 in acute and sub-acute myocardial infarction.
3. To study the effects of Mst1/2 pharmacological inhibition using XMU-MP-1 in endothelial cells.
4. To characterise the effects of a novel specific Mst2 inhibitor that was recently identified in modifying cardiomyocyte hypertrophic response.

CHAPTER 2

MATERIALS AND METHODS

2.1 Cell isolation and *in vitro* cell culture

In the *in vitro* experiments, this PhD project examined two types of cells: neonatal rat cardiomyocytes (NRCMs) and human umbilical vein endothelial cells (HUVECs). NRCMs were subjected to cardiomyocyte-hypertrophy analyses, whereas HUVECs were subjected to angiogenesis analyses. Both cells were assessed for cell proliferation and viability analyses. Treatments given to the cells were either dimethyl sulfoxide (DMSO) as a control, XMU-MP-1 (1 μM, 3 μM, 5 μM) or MRT137 (1 μM, 3 μM, 5μM). XMU-MP-1 and MRT137 were dissolved in DMSO to make a 5mM stock solution, which was then diluted in the medium to achieve the chosen concentration.

2.1.1 Neonatal rat cardiomyocyte isolation

The NRCM isolation was performed using enzymatic digestion to 2-3 day old Sprague-Dawley rat hearts (Charles River UK, Ltd. Margate, Kent, UK). The hearts were collected from the neonates following cervical dislocation and chest incision. Subsequently, the hearts were stored in an ice-cold sterile ADS buffer consisting of 116 mM NaCl, 20 mM HEPES, 1 mM NaH_2PO_4, 5.5 mM glucose, 5.5 mM KCl and 1 mM $MgSO_4$ (pH 7.35). The heart tissue digestion was conducted in the class II tissue culture hood, through sequential rounds of 5-minute incubation in 25 U/75 mL Collagenase A (Roche) and 100 mg/mL pancreatin (Sigma) added on the ADS buffer at the 37 °C shaking incubator followed by trituration using a 25 mL pipette. NRCMs were collected by passing the digested tissues into a cell strainer. FBS (Gibco) was added to the digested tissue to stop enzymatic reaction. Once the heart tissues were completely digested, the cell suspension was then centrifuged at 1200 revolutions per minute (rpm) for 5 minutes (room temperature).

The cell pellet was resuspended in 40 mL of pre-plating medium consisting of 68% DMEM (Gibco), 17% medium-199 (Gibco), 10% horse serum (Gibco), 5% FBS (Gibco), 2.5 mg/mL amphotericin B (Gibco) and 1% penicillin-streptomycin (Gibco). Afterwards, the cell suspension was plated into cell culture dishes and subsequently incubated in a humidified incubator at 37 °C with 5% CO_2 for an hour to allow NRCM and fibroblast separation. After the fibroblasts attached to the cell culture dishes, the NRCM suspension was transferred into a flask containing the plating medium (0.1% BrdU (Sigma) added on the pre-plating medium). Subsequently, NRCMs were seeded on the BD Falcon Primaria tissue culture plates at a density of 250,000 cells/mL for 24-well plates or 1,000,000 cells/mL for 6-well plates. NRCMs were allowed to attach to the plates by overnight incubation at 37 °C with 5% CO_2. The following day, after several washes, the plating medium was replaced by the maintenance medium (80% DMEM, 20% medium-199, 1% FBS, 2.5 mg/mL amphotericin B,

1 mM bromodeoxyuridine (BrdU) and 1% penicillin-streptomycin) and was ready for the experiments. The outline of the *in vitro* experiments using NRCMs is shown in Figure 2.1.

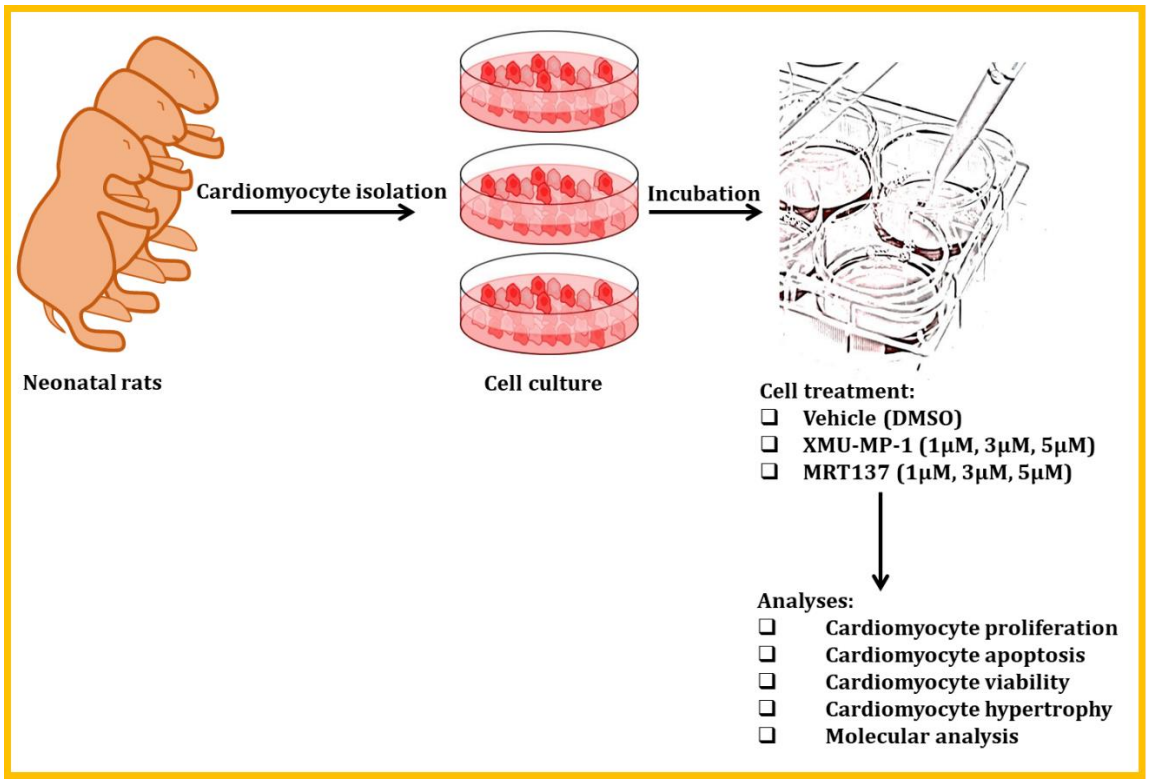

Figure 2.1 The outline of *in vitro* experiments using NRCMs.

2.1.2 HUVEC culture and maintenance

HUVECs obtained from TCS Cellworks were cultured using HUVEC growth medium (TCS Cellworks) plus 2% growth supplement and 0.1% antibiotic supplement (amphotericin B/gentamycin). The cells were kept in a 0.1% gelatin (MilliporeSigma™EmbryoMax™)-coated tissue culture flask at 37 °C with 5% CO_2. HUVECs could be passaged up to seven times when they reached about 80% confluency. During the passaging process, 5 mL of trypsin (Gibco) was used to detached the cells from the flask and Dulbecco's phosphate-buffered saline (DPBS from Gibco) was used to wash the cells. While waiting for cells to reach confluency, the medium was replaced with a fresh medium every two days. HUVECs were seeded onto 24-well plates (150,000 cells per well) for cell viability and proliferation experiments, 6-well plates (300,000 cells per well) for protein extraction, 12-well plates (30,000 cells per well) for organotypic co-culture assay and 96-well plates (30,000-60,000 cells per well) for Matrigel and cell migration assays. All plates were coated with 0.1% gelatin before seeding the cells, except the Matrigel experiment. Figure 2.2 shows the outline of *in vitro* experiments using HUVECs.

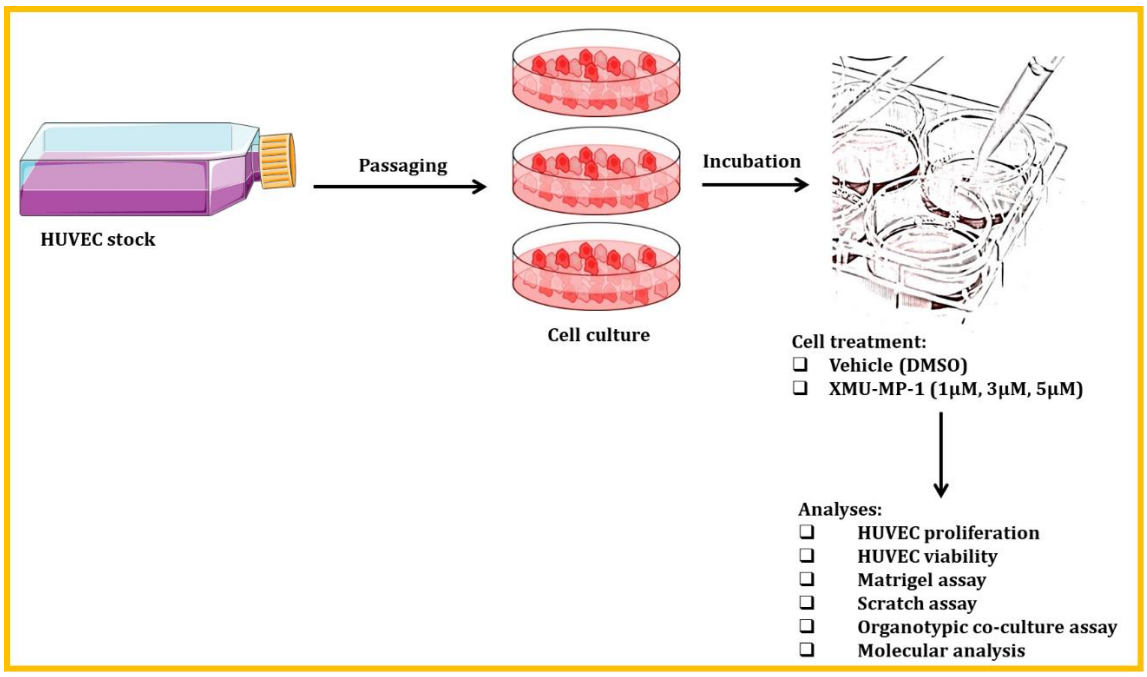

Figure 2.2 The outline of *in vitro* experiments using HUVECs.

2.1.3 Mst1 and Mst2-knockdown using small interfering RNA (siRNA)

NRCMs were subjected to siRNA targeting Mst1 (Sigma # SASI_Rn02_00232395) and Mst2 (Sigma # SASI_Rn01_00056484) for Mst1 and Mst2-knockdown western blotting. NRCMs were seeded onto 6-well plates at a density of 2,000,000 cells per well and allowed to sit at 37 °C with 5% CO_2. The next day, NRCMs were washed with phosphate-buffered saline (PBS) and incubated in serum-free OptiMEM (Gibco) for an hour before transfection. The Mst1 siRNA, Mst2 siRNA or scrambled siRNA was dissolved in the siRNA buffer (Thermo Scientific) to make a 5 μM stock. 10 μL of the stock solution of each siRNA was added to 190 μL of OptiMEM to get a 25 nM final siRNA concentration per well. Meanwhile, 5 μL of DharmaFECT (Dharmacon), added onto 195 μL of OptiMEM, was used as a transfection reagent. Following 5-minute incubation, each siRNA solution was mixed with the same volume of transfection reagent and allowed to sit for 20 minutes at room temperature. 400 μL of total transfection mixture was then added to the allocated cells mixed with 1,600 μL of maintenance medium. After 72-hour incubation, the medium was replaced with a fresh maintenance medium for further treatment. NRCMs were treated with either DMSO, XMU-MP-1 or MRT137 (1 μM, 3 μM or 5 μM) for 24 hours then harvested for protein extraction.

2.2 *In vitro* characterisation of cell proliferation, apoptosis or viability

Cell proliferation analysis was performed in both NRCMs and HUVECs using immunofluorescence stainings, such as Ki-67 and Phospho Histone H3 (pH-H3). Cell

apoptosis analysis in NRCMs treated with XMU-MP-1 was examined using a terminal deoxynucleotidyl transferase-mediated nick end labelling (TUNEL) assay. Meanwhile, cell viability was determined using an MTT assay in NRCMs or MTT and Alamar blue assays in HUVECs.

2.2.1 Cell proliferation analysis

Two methods were used to identify cell proliferation based on cell activities. Ki-67 staining can detect cell cycles at the G1, S, G2 and M phases, whereas pH-H3 can determine only the M phase of the cell cycles.

2.2.1.1 Ki-67 staining

Cell preparation:

NRCMs were seeded at a density of 250,000 cells/well onto sterilised laminin (Sigma) pre-coated coverslips in 24-well plates followed by incubation at 37 °C with 5% CO_2. The following day, the cells were treated with DMSO, XMU-MP-1 or MRT137 for 24 hours. HUVECs followed similar processes to NRCMs, apart from the number of HUVECs seeded, which was 150,000 cells/well, and the coverslips were precoated with 0.1% gelatin.

Immunofluorescence (IF) steps:

The cells were washed with PBS three times and were fixed with 4% paraformaldehyde (PFA) for 20 minutes. Following fixation, the cells were permeabilised with 0.5% Triton-X for 30 minutes. After the permeabilisation process, the cells were incubated with anti-Ki-67 antibody and anti-α-actinin (for NRCMs) or Alexa Fluor™ 680 phalloidin (for HUVECs) (details are in Table 2.6) for at least two hours at room temperature or overnight at 4 °C. The next step was an hour incubation of secondary antibodies (Alexa Fluor®647-conjugated anti-mouse for NRCMs and Alexa Fluor®488-conjugated anti-rabbit IgG for both NRCMs and HUVECs). The cells were then incubated with DAPI (Invitrogen by Thermo Fisher Scientific) for one minute and mounted with Vectashield. Immunofluorescence signals were observed under the snapshot fluorescent microscope (Zeiss). The green fluorescence signal in the nucleus indicates positive Ki-67 cells, whereas the red signal indicates cardiomyocytes and the blue signal indicates the nucleus. Images were taken at 20x magnification and analysed using ImageJ software. At least ten images were taken for each coverslip (three coverslips per group in each independent experiment) for technical replication.

2.2.1.2 pH-H3 staining

Cell preparation:

NRCM and HUVEC treatments followed the same preparation steps that have been written in section 2.2.1.1 of this thesis, except that the XMU-MP-1 treatment was not analysed using the pH-H3 antibody.

Immunofluorescence steps:

Both NRCMs and HUVECs underwent the processes in section 2.2.1.1, but the Ki-67 antibody was replaced with a pH-H3 antibody (detailed information in Table 2.6). The green fluorescence signal in the nucleus under the snapshot fluorescent microscope indicated positive pH-H3 cells, the red signal cardiomyocytes and the blue signal the nucleus.

2.2.2 Cell apoptosis analysis

Cell preparation:

NRCMs were seeded at a density of 250,000 cells/well onto sterilised laminin-precoated coverslips in 24-well plates followed by incubation at 37 °C with 5% CO_2. The next day, the cells were treated with 200μM of H_2O_2 concomitantly with DMSO or XMU-MP-1 (1 μM, 3 μM, 5 μM) for 4 hours.

IF steps:

The cells were fixed with 4% paraformaldehyde (PFA) for 20 minutes and permeabilised with 0.5% Triton-X for 30 minutes. After that, the cells were incubated with TUNEL reagents (Roche) at 37 °C for an hour, followed by anti-α-actinin incubation (see Table 2.6 for details) for two hours and Alexa Fluor®647-conjugated anti-mouse IgG incubation for an hour. The cells were subsequently incubated with 4', 6'-diamidino-2-phenylindole (DAPI) for one minute and mounted with Vectashield. Immunofluorescence signals detection using the snapshot fluorescent microscope showed the green fluorescence signal in the nucleus for positive TUNEL cells, the red signal for cardiomyocytes and the blue signal for the nucleus.

2.2.3 Cell viability analysis

Twenty-four hours after NRCMs and HUVECs seeding, XMU-MP-1 (1 μM, 3 μM, 5 μM), MRT137 (1 μM, 3 μM, 5 μM) and DMSO were given together with 200 μM H_2O_2. The incubation period of H_2O_2 treatment is 4 hours to induce stress oxidative. Thereafter, the cells were incubated for another two hours with 100 μl of filter-sterilised Thiazolyl Blue Tetrazolium Bromide (MTT Sigma, 5mg/mL in DPBS). Viable cells would produce dark

purple crystals, known as formazan, which were dissolved in the solubilisation solution (0.1 N HCl in Isopropanol). The solution absorbance was measured at 570 nm using a Multiskan ascent spectrophotometer (Thermo Labsystem). The absorbance value was considered as a readout of cell viability.

Another cell viability assay using alamarBlue® was performed to determine HUVEC viability over time. HUVECs were plated at a density of 10,000 cells per well of a 24-well plate and incubated for 24 hours to adhere and normalise. The baseline viability was assessed by applying a 1:10 dilution of alamarBlue® (ThermoFisher) to the medium in the plates, followed by 2 hours incubation. Cell culture medium mixed with alamarBlue® was moved to 96-well plates and read under a spectrofluorophotometer, FLUOStar Omega (BMG Labtech) at 540-570 nm (excitation) and 580-610 nm (emission). After measuring the baseline viability, HUVECs were treated with either DMSO or XMU-MP-1 (1 μM, 3 μM or 5 μM) every other day for up to six days and the cell viability was recorded every two days after the treatment.

2.3 Determination of cardiomyocyte hypertrophy

Cardiomyocyte hypertrophy analysis was performed using the measurement of cardiomyocyte circumference and Brain Natriuretic Peptide (BNP) expression. 50 μM of phenylephrine (Sigma) was used to induce cardiomyocyte hypertrophy.

2.3.1 Cardiomyocyte size measurement

Cell preparation:

NRCMs were seeded at a density of 250,000 cells/well onto sterilised laminin-precoated coverslips in 24-well plates. The cells were incubated in a humidified incubator at 37 °C with 5% CO_2. The next day, the cells were treated with 50 μM of phenylephrine together with the treatments (DMSO and 1 μM, 3 μM, 5 μM of XMU-MP-1 or MRT137). Cells were cultured for 72 hours with medium, phenylephrine and treatments changed daily.

IF steps:

After 72 hours of phenylephrine induction together with the treatments, NRCMs were processed in the same immunofluorescence steps as in section 2.2.1.1, but only using anti-α-actinin (as a primary antibody) and Alexa Fluor®647-conjugated anti-mouse (as a secondary antibody). Cardiomyocyte circumference was measured from 20x magnification images using ImageJ software.

2.3.2 Analysis of hypertrophy gene activity

The hypertrophy marker, BNP, was measured using a BNP-luciferase assay. The adenovirus expressing luciferase signal rat BNP promoter was transfected in cardiomyocytes that have been treated with 50 μM phenylephrine (PE) and the treatments (DMSO and 1 μM, 3 μM, 5 μM of XMU-MP-1 or MRT137). After 24 hours of incubation in a humidified incubator, the medium was aspirated and NRCMs were rinsed with PBS three times. NRCMs were then lysed in 1X cell lysis buffer (Promega) with gentle shaking for 20 minutes at room temperature. The luciferase signal was measured by mixing 25 μl of cell lysates and 25 μl of Luciferase Assay Reagent (Promega) and read using Lumat LB9507 Tube Luminometer (Berthold). Three technical replications for each treatment group were performed in each independent experiment.

2.4 Characterisation of endothelial cell angiogenesis and migration

HUVEC migration and angiogenesis were examined following XMU-MP-1 treatment. The Matrigel assay was conducted to determine the angiogenic property of HUVEC based on the tubule-like formation. The purpose of doing the scratch assay was to observe the ability of HUVEC to migrate and cover the scratched area. The organotypic co-culture assay was used to determine the angiogenesis process based on multiple interactions between HUVECs and human dermal fibroblasts (HDFs).

2.4.1 Matrigel assay (tubule-like formation)

Geltrex™ Matrix (Invitrogen) was used to cover the base of 96-well plates before HUVECs were seeded. Once the gel became solid, HUVECs were plated at a density of 30,000 cells/well. DMSO and XMU-MP-1 at the dose of 1 μM, 3 μM and 5 μM were given to the medium prior to the seeding. The plates were then incubated in a humidified incubator at 37 °C with 5% CO_2 for 24 hours. The following day, HUVECs were observed under Leica M165Fc stereomicroscope at 4x magnification. The quantification of tubule-like formation was performed using ImageJ software. Tubule-like shapes were drawn as single lines (Figure 2.3).

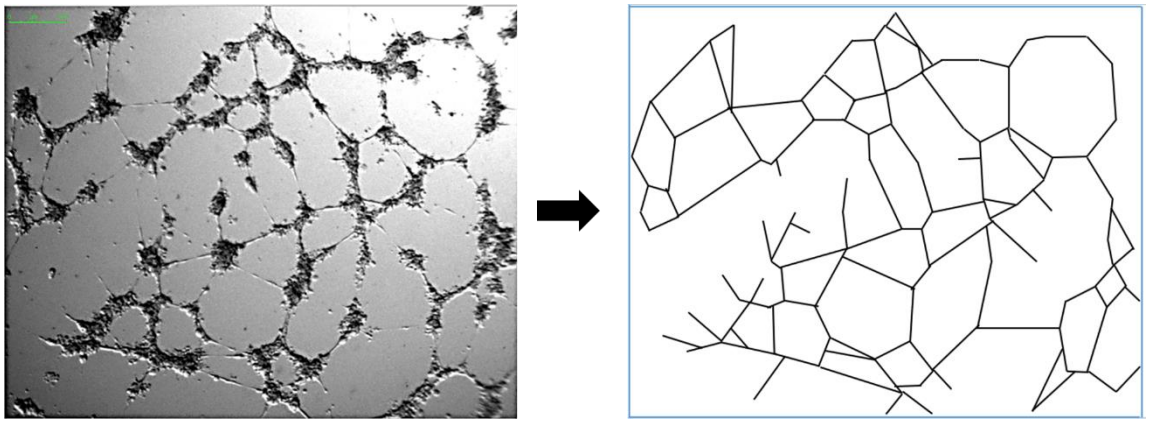

Figure 2.3 The quantification of tubule-like formation of the Matrigel assay. Each line represents a tubule-like shape that connects to other tubule-like shapes at a junction. The number of tubule-like shapes was quantified and the average number of each group was analysed.

2.4.2 Scratch assay (incuCyte)

HUVECs were plated into the IncuCyte ImageLock® (Sartorius) 96-well plates at a density of 30,000 cells per well, then incubated in a humidified incubator at 37 °C with 5% CO_2 for 24 hours. On the next day, the wells were scratched using the WoundMaker™ (Sartorius) to ensure an equal scratch size. After the scratch, the wells were washed using the cell culture medium three times, followed by administering the treatments (DMSO and XMU-MP-1) mixed in the medium. The plate was kept in a standard tissue culture incubator at 37°C with 5% CO_2, which is in line with the Essen InCucyte ZOOM® to monitor the cell kinetics for 24 hours. The images were taken every six hours at 10x magnification. The total migrated area was the parameter that was analysed in this assay (Figure 2.4).

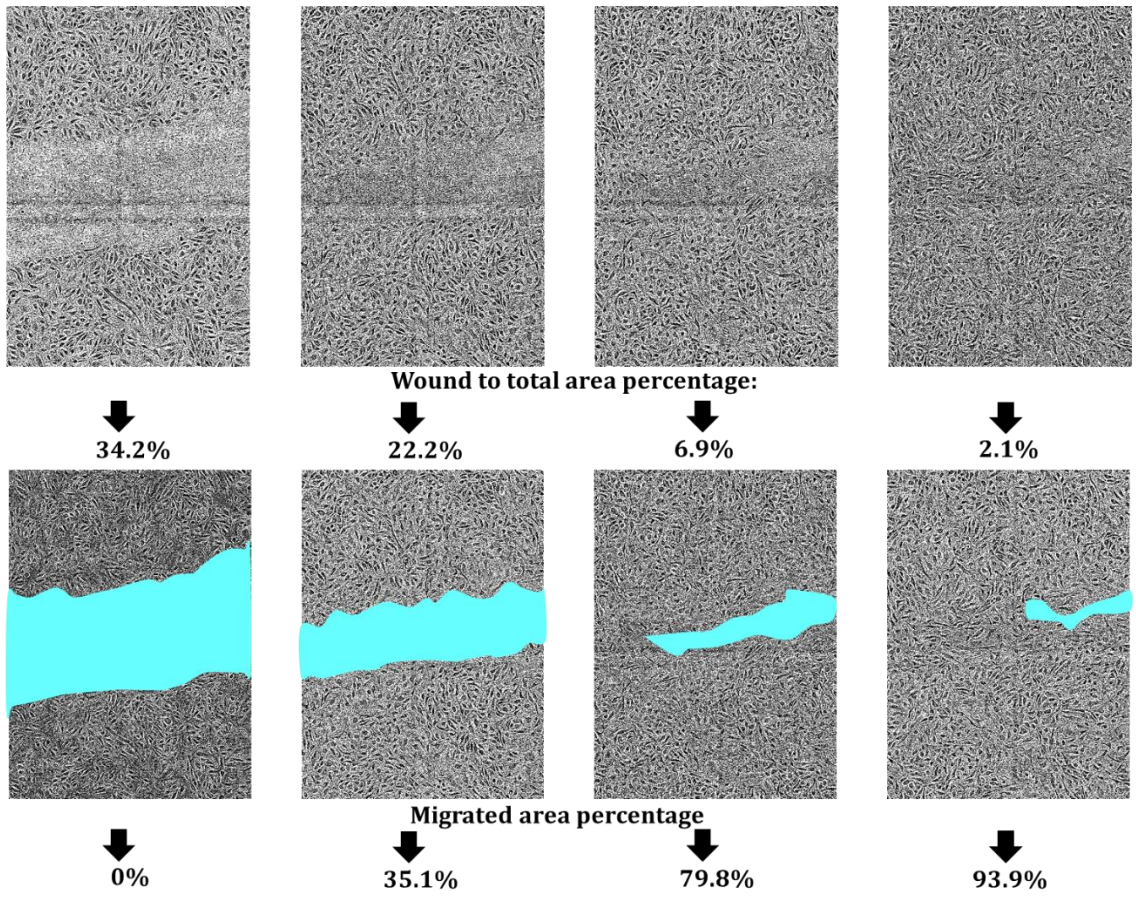

Figure 2.4 The analysis of the scratch assay. The initial wound to total area percentage (t=0) was measured as a baseline level of migration area. The migrated area was calculated from the initial wound size from the same well.

2.4.3 Organotypic co-culture assay

On the first day, HUVECs and HDFs co-culture cells were plated into 24-well plates at a density of 30,000 cells/well using the seeding medium (Cellworks #ZHA-4000). After 24 hours of incubation in a humidified incubator at 37 °C with 5% CO_2, the seeding medium was replaced by the growth medium added with 0.1% vascular endothelial growth factor (VEGF). On the same day, the cells were treated with either DMSO or XMU-MP-1 (1 μM, 3 μM, 5 μM). On day 4, the cells were observed under the microscope, followed by replacing the medium with the fresh growth medium and treatments. The medium and the treatments were replaced every two days for up to 12 days. On day 14, the cells were washed using a wash buffer containing 0.20 g KCl, 0.20 g KH_2PO_4, 8.00 g NaCl, 1.15 g Ha_2HPO_4, then fixed with the fixative solution (70% ethanol). After 30 minutes of incubation, the cells were blocked using the blocking buffer (wash buffer added with 1% BSA) a few times, then incubated with the primary antibody (CD31 1:400 dilution in the blocking buffer) for 60 minutes at 37 °C. Following the incubation, the cells were washed with blocking buffer three times and incubated with secondary antibody (goat anti-mouse IgG AP conjugate 1:500 dilution in the blocking buffer). A permanent insoluble BCIP/NBT chromatogenic substrate

was added to the wells to visualise the cells. After 3-10 minutes of BCIP/NBT incubation, a dark purple colour will be developed and can be observed under the microscope for imaging. All the reagents in the organotypic co-culture assay were obtained from Cellworks (V2a kit #ZHA-4000). Tubule quantification and analysis were performed using ImageJ software. Angiogenesis parameters that were quantified are shown in Figure 2.5.

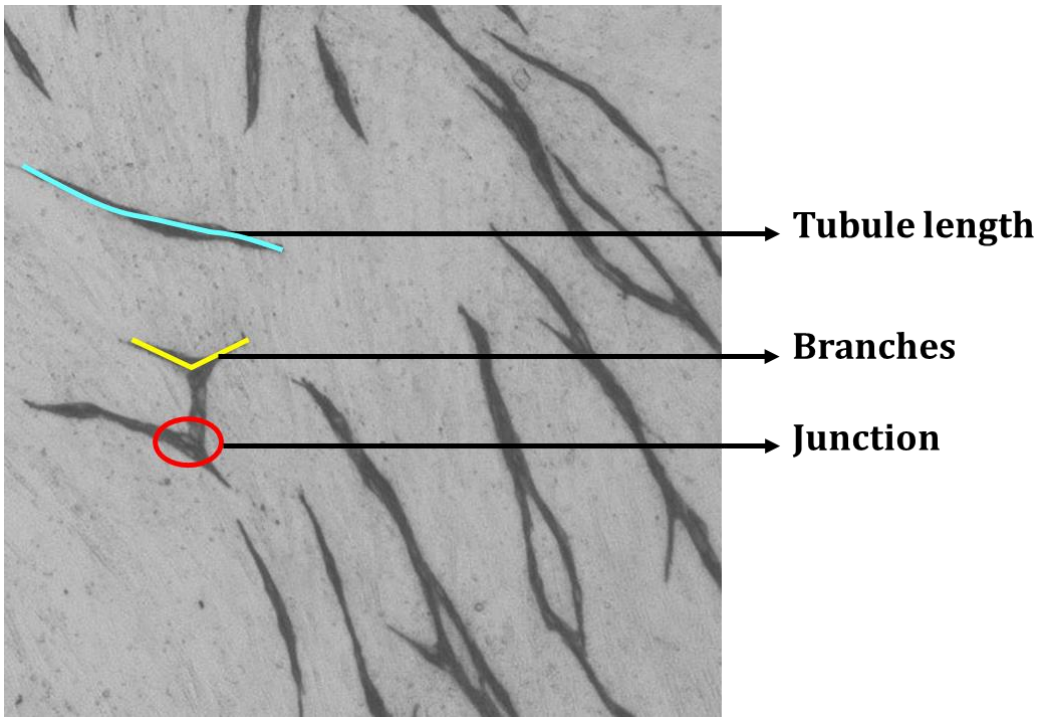

Figure 2.5 The angiogenesis parameters obtained from the organotypic co-culture assay. Using ImageJ software, the quantification of tubule length, numbers of branches and numbers of junctions was performed manually. The average of parameters for each group was compared and analysed.

2.5 Animal studies

All animal experiments in this PhD project were carried out under project license No. P3A97F3D1 granted to Dr. Elizabeth Cartwright of the University of Manchester and the University of Manchester Ethics Committee's approval. The *in vivo* experiments in this PhD project were performed using 8-12 week-old male mice. All mice were kept in standard cages with a 12-hour light/dark cycle in a controlled temperature of 19–22 °C and humidity of 40–65%. A standard chow diet was given to the mice during the experiments. At the end of the experiments, all mice were sacrificed through cervical dislocation following the schedule 1 method. The calculation of sample size in the TAC experiment was based on power calculation analysis of the previous study in our lab using Mst2 global knockout mice. The MI experiments were pilot studies. Hence, I used a smaller sample size.

2.5.1 Transverse aortic constriction model

The Transverse aortic constriction (TAC) surgical procedure causes the heart to undergo hypertrophy through pressure overload. 8-week old wild-type male C57Bl/6 mice were subjected to either TAC or sham surgical procedures after one week of acclimatisation. A simple random sampling was performed to determine the animal grouping. Prior to surgery, the mice were anaesthetised with 1 L/minute inhalation of 5% isoflurane, followed by subcutaneous injection of 0.1 mg/kg buprenorphine as an analgesic. During the surgical procedure, isoflurane was maintained at 3%. In this experiment, Dr. Min Zi performed the surgery, whereas the author did other animal handlings with help from Mr. Sukhpal Prehar. After the chest cavity was opened, a 7-0 silk suture was tied around a 27-Gauge needle that lay across the aortic arch, between the brachiocephalic trunk and the left common carotid artery, to produce a pressure gradient around 25-30 mmHg (as shown in Figure 2.6). After the constriction, the chest was sutured and the mice were allowed to recover by administering an intraperitoneal injection of 0.1 mL/30 gBW saline, then placed in a 30 °C incubator. Sham animals were subjected to the same procedure as the TAC mice, but the suture was passed around the back of the aorta without tying. After the mice recovered, they were moved to normal housing and then followed up the following day.

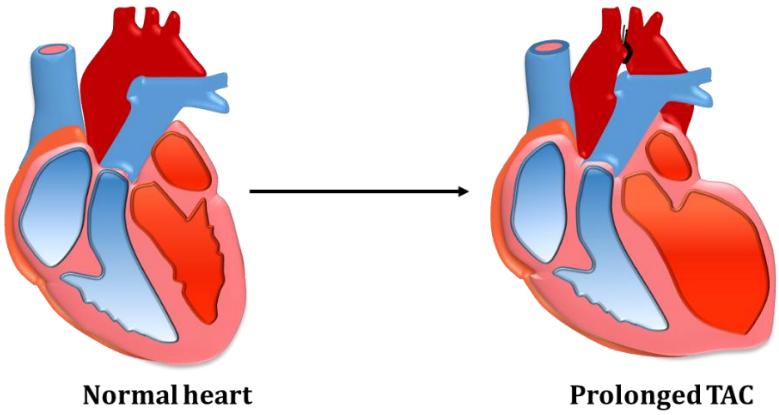

Figure 2.6 Aortic arch constriction in TAC model heart Prolonged constriction in the aortic arch in the TAC model heart results in cardiac hypertrophy or further progression into heart failure.

Twelve out of 32 mice in the TAC groups were excluded from the experiment because they died within two days after the surgery due to surgical complications. Twenty mice from the TAC groups and five mice in the sham group were maintained for three weeks before they started to get the treatments. The TAC mice were assigned to get 1 mg/kgBW of XMU-MP-1 or an equal volume of DMSO (vehicle) through a randomised block design. The treatments were given every two days for ten days following the project license that allows a maximum of five injections per animal. At the end of the experiment, the mice were sacrificed and heart tissues were collected for histological, protein and ribonucleic acid (RNA) analysis. Figure 2.7 shows the timeline of the TAC experiment.

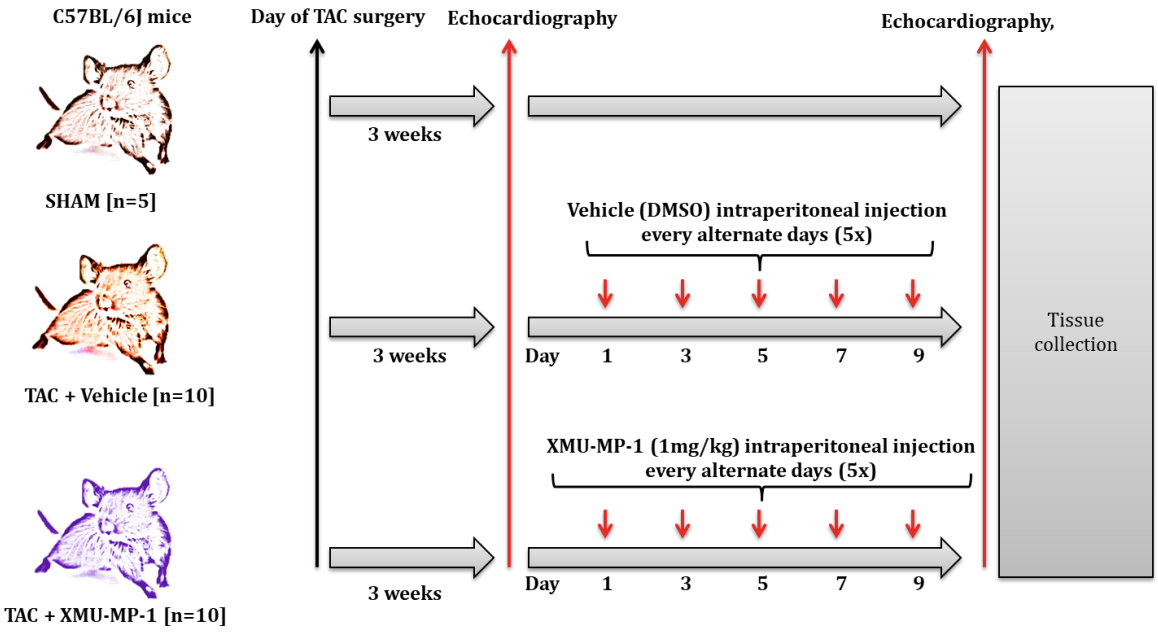

Figure 2.7 The timeline of the TAC experiment.

2.5.2 LAD ligation in mice

Similar to the TAC experiment, the left anterior descending artery (LAD) ligation performed by Dr. Min Zi also used wild-type male C57Bl/6 mice. Twelve-week-old mice were acclimatised in standard cages with a 12-hour light/dark cycle in a controlled temperature and humidity for a week before the surgery. Using the same anaesthetic and analgesic regimentation as the TAC experiment, the mice were then intubated and placed on a Miniventilator 845 (Harvard Apparatus) at 200 breaths per minute and a tidal volume of 0.1 mL. When the chest was opened, the isoflurane dose was reduced to 3%, supplemented with 1 L/min oxygen. A binocular stereomicroscope (Olympus) was used to assist in visualising the procedure of making a 5 mm incision at the left sternal border. A cut was made at the fourth intercostal space to expose the heart and coronary arteries, followed by permanent ligation of the LAD coronary artery using an 8-0 nylon suture (Ethilon) at the level of the left atrial appendage. After the left ventricle wall became pale (an indicator of successful ligation), the chest was closed with 6-0 Prolene® sutures. Subsequently, the mice were injected with 0.1 mL/30 gBW saline and moved to a recovery chamber. Once recovered, the mice were transferred to an incubator at 30 °C and closely monitored every 2 hours, up to 6 hours, then eventually moved to normal housing. Sham animals were subjected to the same procedure without LAD coronary artery ligation.

The effects of XMU-MP-1 in MI model mice were examined at acute and sub-acute phases. In the acute MI model, 1 mg/kgBW of XMU-MP-1 was injected right after the LAD ligation, together with saline injection. The XMU-MP-1 treatment continued to be given every two days for up to 10 days. The mice were sacrificed and the tissues were collected on day 12

after the surgery (Figure 2.8). The second model was sub-acute MI, in which 1 mg/kgBW injection of XMU-MP-1 was started three weeks after the surgical procedure. The experiment was ended 12 days after XMU-MP-1 was first given (Figure 2.9).

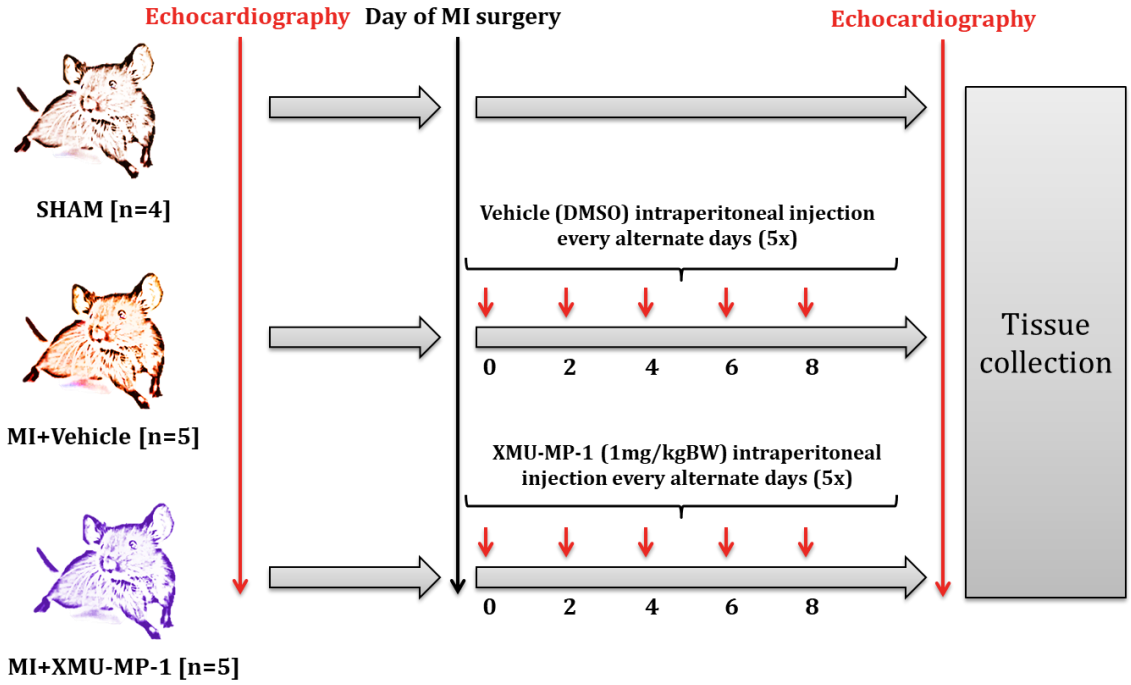

Figure 2.8 The timeline of the acute MI experiment.

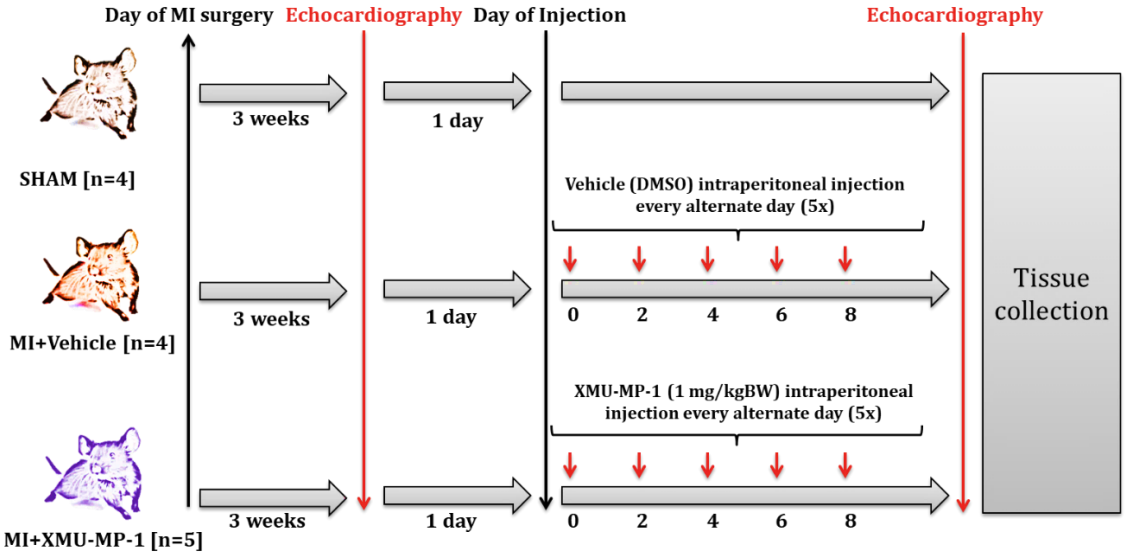

Figure 2.9 The timeline of the sub-acute MI experiment.

2.5.3 Cardiac Troponin I analysis

Blood sampling for cardiac Troponin I (cTnI) analysis was taken 24 hours after the MI surgical procedure. The blood was collected from the lateral tail vein 20 minutes after

applying an anaesthetic cream (EMLA™). About 40 µL of the collected blood was placed in a tube containing 40 µl of 3.2% sodium citrate and soon after that, they were spun at 8000 rpm for 6 minutes at 4 °C. The plasma (supernatant) was examined using a high-sensitivity mouse cTnI ELISA kit (Life Diagnostics). Before the assay was started, the plasma was diluted 1:5 with plasma diluent provided in the kit. Serial dilutions of known cTnI concentration were prepared as the standards. The diluted samples and standards were placed in a 96-well ELISA plate coated with anti-mouse cTnI antibody provided in the kit. The HRP-linked antibody was added to the microtiter wells containing diluted samples and standards, followed by an hour incubation on an orbital shaker at room temperature. After that, the wells were washed using a wash solution supplied from the kit, followed by drying the wells and adding the HRP substrate, Tetramethylbenzidine (TMB). After 20 minutes of incubation on the orbital shaker, the stop solution (1N HCl) was added. The absorbance of yellow colour formed at the end of the reaction was measured at 450nm using a Multiskan ascent spectrophotometer (Thermo Labsystem). The cTnI values were obtained by plotting the absorbance of the samples to the standard curve.

2.5.4 Transthoracic two-dimensional echocardiography

The VisualSonics Vevo770® (VisualSonics, inc.), equipped with a 14 MHz transducer, was used to perform transthoracic echocardiography on mice to evaluate cardiac function and performance. In the TAC and sub-acute MI experiments, echocardiography was conducted three weeks (before the treatment was started) and five weeks (after the last treatment) post-surgical procedure. Meanwhile, in the acute MI experiment, the echocardiography analysis was conducted before the surgical procedure and after the serial treatments were completed. Initially, the chest area was cleaned with hair removal cream and the mice were anaesthetised using 2% isoflurane supplemented with 1mL/min of oxygen. After that, the mice were placed on a warmed pad fitted with an isoflurane tube to maintain the anaesthesia. Ultrasound transmission gel was applied on the chest, in which the transducer was placed to generate either a short-axis or long-axis M-mode image of the heart. The echocardiography parameters measured using M-mode images were left ventricular internal diameter (LVID), the left ventricular posterior wall (PW) thickness and the interventricular septal thickness (IVS) during systole and diastole (Figure 2.10). Other parameters, such as fractional shortening (FS), ejection fraction (EF), left ventricular mass (LVM) and relative wall thickness (RWT), were calculated using the equations listed in Table 2.1. The researcher was blinded to the treatment groups during the echocardiography analysis.

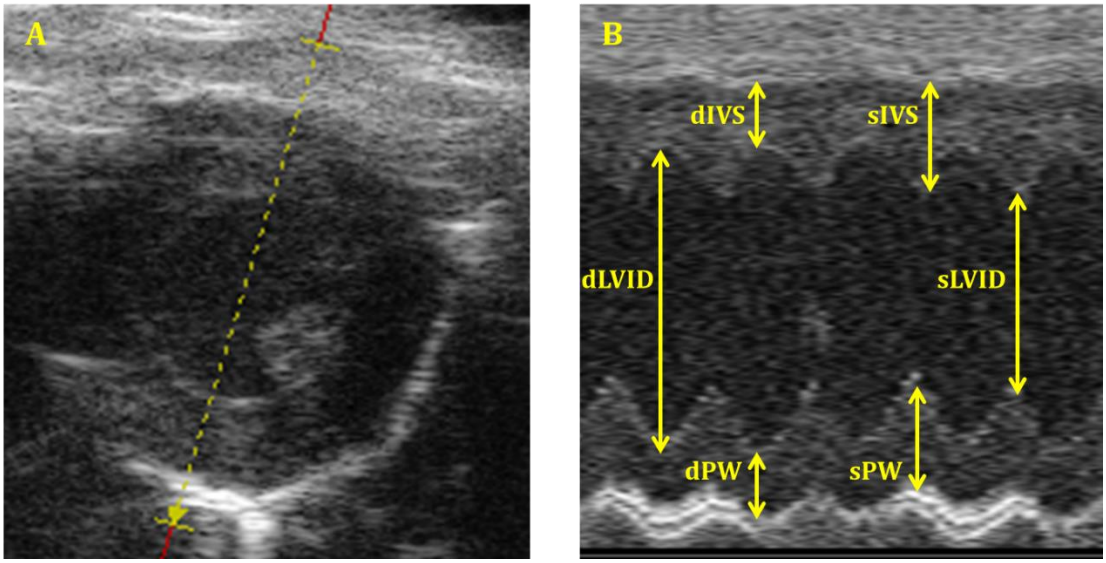

Figure 2.10 A short-axis M-mode image of the left ventricle A. An image taken in the short-axis view. B. Echocardiography parameters measured from the left ventricle in both diastole (d) and systole (s).

Table 2.1 Calculation of cardiac parameters based on echocardiographic measurements.

Parameters	Equations
Fractional Shortening (FS %)	[(dLVID- sLVID/ dLVID)] x 100
Ejection Fraction (EF %)	[(1.05xdLVID^3)- (1.05xsLVID^3)/ (1.05xdLVID^3)] x 100
Left Ventricular Mass (LVM)	1.055 x[(dLVID + dPW + dIVS)^3 – dLVID^3]
Relative Wall Thickness (RWT)	(dIVS + dPW) / dLVID

2.5.5 Serum alanine transaminase analysis

Serum from the mice that underwent surgery was collected at the end of the experiment. 1 mL of blood was taken from the chest and then kept in Eppendorf tubes on an icebox for an hour. After the blood clot appeared, the supernatant was transferred into centrifuge tubes, then spun at 3000 rpm for 5 minutes at 4 °C. Serum (supernatant) was taken and kept at -80 °C. The serum alanine transaminase (ALT) analysis was measured using the Alanine Transaminase Activity Assay kit (Abcam #ab105134). Serial dilutions of pyruvate standard with known concentration were prepared as per manufacturer protocol. Using the same ALT assay buffer as used in the standard dilution, the samples were diluted at 1:5 dilution. All materials and reagents were equilibrated at room temperature before the assay. 20 µL of pyruvate standards or diluted samples were put in a 96-well plate. 100 µL of reaction mix (86 µL of ALT assay buffer, 2 µL of OxiRed Probe, 2 µL of ALT enzyme mix and 10 µL of ALT substrate) was added into each wells containing standards or diluted samples. The absorbance was measured at 570 nm using a Multiskan ascent spectrophotometer (Thermo Labsystem) in a kinetic mode after 10 minutes, then every 2–3 minutes for at least 60

minutes at 37 °C protected from light. The absorbance was taken at two time points (T1 and T2) during the linear range after the initial lag phase. The average absorbance of all standard and sample duplicate measurements was used to calculate the amount of pyruvate during T1 and T2 by plotting the sample absorbance into the standard curve equation. The ALT activity was calculated using the following formula:

$$ALT\ activity\ (nmol/min/mL) = \left(\frac{B}{\Delta T \times V}\right) \times D$$

Where:

B: the amount of pyruvate generated by ALT between T1 and T2.

ΔT: reaction time (minutes).

V: sample volume added into each well.

D: sample dilution factor.

2.5.6 Serum creatinine analysis

Serum collection was performed using the same methods as mentioned in section 2.5.5. Creatinine standard was dissolved in 100 µL ddH_2O to get a 100 mM concentration, then diluted using an assay buffer to obtain 1 nmol/µL. Serial concentrations of creatinine standard were prepared from 1 nmol/µL stock as per manufacturer guidelines. Samples were diluted using an assay buffer with a 1:5 dilution factor. The standards and samples were duplicated to get the average values. 50 µL of standards or diluted samples were placed into each well of a 96-well plate and then added with 50 µL of the reaction mix containing 42 µL of assay buffer, 2 µL of creatinase, 2 µL of creatininase, 2 µL of enzyme mix and 2 µL of creatinine probe. The absorbance value was taken at 570 nm using a Multiskan ascent spectrophotometer (Thermo Labsystem). The absorbance values from the samples were plotted into the standard curve to get the amount of creatinine. The level of creatinine was calculated using the following equation:

$$Creatinine\ level\ = \left(\frac{Sa}{Sv}\right) \times D$$

Sa: creatinine amount of the samples plotted from the standard curve (nmol)

Sv: sample volume put in each well (µL)

D: dilution factor

Creatinine molecular weight: 113.12 g/mol

2.6 Histological analysis

For histological analysis, the heart, liver and kidney tissues harvested at the end of the experiments were fixed with 4% PFA (Sigma) in PBS for 24 hours at 4 °C under agitation. The tissues were then placed in histology cassettes and transferred to 70% ethanol for a further 24 hours before being processed using a Leica ASP300 automated tissue processor. During tissue processing, serial solutions were used to soak the tissues at specific times (outlined in Figure 2.11).

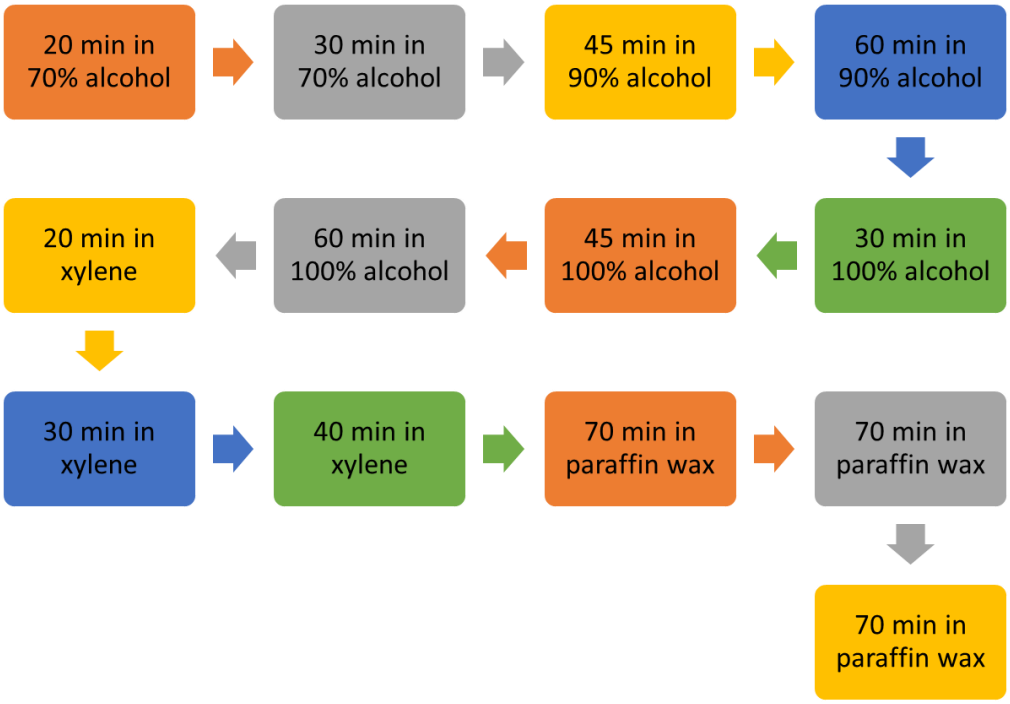

Figure 2.11 Tissue processing protocol using a Leica ASP300 automated tissue processor

Following tissue processing, the tissues were embedded in paraffin wax prior to cutting into 5µm sections using an automated rotary Leica RM2255 microtome. The sections were then flattened in a warm water bath and transferred to poly-L-lysine coated histological slides, which were then left to dry overnight in a 37 °C oven. The heart tissues obtained from the MI experiment were cut into six to eight levels with 500 µm intervals between each level (Figure 2.12). Meanwhile, the middle part of the heart, liver and kidney tissues were collected from the TAC experiment for histological purposes.

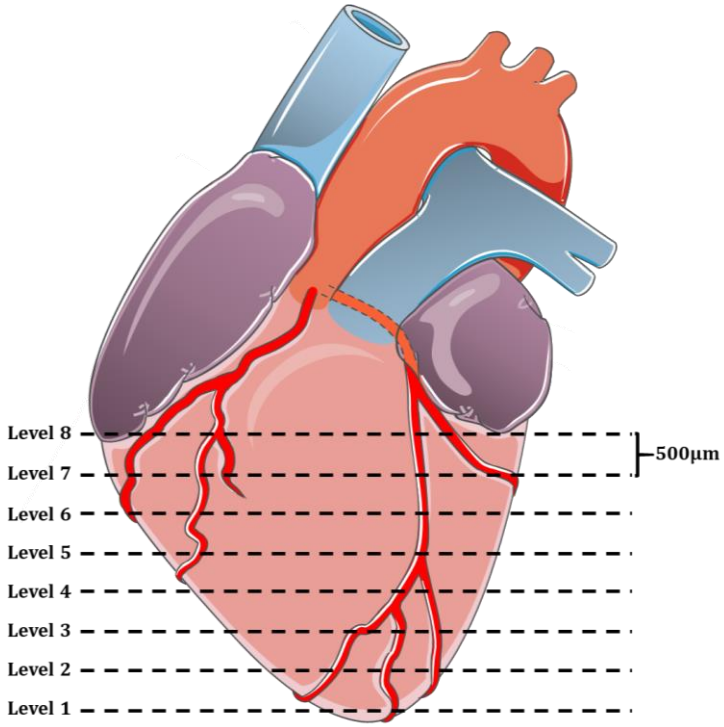

Figure 2.12 The heart tissue sectioning from the MI experiment.

2.6.1 Masson's Trichrome staining

Masson's Trichrome staining was used to visualise any fibrosis on the histological sections. Before staining, histology slides were deparaffinised by immersing them in xylene for 30 minutes after putting them onto a heat block. The histology sections were then rehydrated by soaking the slides in gradual concentrations of industrial methylated spirit (100%, 90% and 70% IMS) and then washing them in water before staining. Afterward, the sections were soaked in Bouin's fixative solution (Sigma) for two hours at room temperature and subsequently rinsed thoroughly in running water until clear. Following fixation, the sections were immersed in Harris' Haematoxylin (Sigma) solution for 3 minutes to stain the nucleus, and then washed in water for 10 minutes. The sections were then differentiated using 1% HCl in 70% ethanol solution for 10 seconds, then washed in warm running tap water for five minutes. The next step was five minutes incubation in the red solution containing 0.9% Biebrich Scarlet (Sigma), 0.1% ponceau Fuschin (Sigma) and 1% acetic acid (Sigma), five minutes washing in water, then differentiation with 2.5% phosphomolybdic acid (Sigma) for 15 minutes. Following another water-wash, the sections were immersed in aniline blue (Sigma, 2.5% aniline blue in 2% acetic acid) for 10 minutes, then washed in water before being differentiated with 1% acetic acid for 1 minute. The next step was sequential dehydration using the increasing concentration of IMS (50%, 75% and 100% five minutes each), followed by 20 minutes of incubation in xylene. The sections were then mounted using DPX mounting media (Sigma) before being sealed with coverslips. Images were

acquired using a 3D Histech Panoramic 250 Flash II slide scanner and were analysed using the Case Viewer software. The fibrosis levels of the heart, kidney and liver tissues from the TAC experiment were presented as the percentage of fibrotic area to the total tissue area. The fibrosis levels of the heart tissues from the MI experiment were presented as an infarct size that was quantified using a midline length measurement.

2.6.2 Haematoxylin and Eosin staining

Deparaffination and rehydration processes (as explained in section 2.6.1) were applied before staining histology sections with haematoxylin and eosin (H&E). Rehydrated histology sections were soaked in haematoxylin (Sigma) for 5 minutes to stain the nucleus. Next, the histology sections were rinsed in running tap water and then differentiated using acid alcohol (1% HCL in 70% ethanol) for 5 seconds. Following another wash in running tap water, 5-minute incubation in eosin (Sigma) was applied to the histology sections to stain the cytoplasm. The histology sections were eventually washed in water for five minutes. The dehydration, mounting and imaging processes were performed using the same procedures outlined in section 2.6.1. The images obtained from H&E staining were used to measure the cell size through circumference measurement using the Case Viewer software.

2.6.3 TUNEL staining

As a sign of cell apoptosis, deoxyribonucleic acid (DNA) fragmentation on the heart tissues was determined using Terminal deoxynucleotidyl transferase-mediated nick end labelling (TUNEL) staining provided by the in situ Cell Death Detection Kit, Fluorescein (Roche). After deparaffination and rehydration of the histological sections, the first process was 15 minutes of incubation in 3% H_2O_2, this was followed by washing three times with PBS for 10 minutes each. The histology sections were then incubated with proteinase K (20 µg/mL in PBS, Invitrogen) for 15min at 37 °C, before permeabilising them in 0.1% Triton X and 0.1% Sodium citrate solution for eight minutes at room temperature. Following permeabilisation, all sections were incubated with a 1:10 dilution of TUNEL mixture containing enzyme solution for an hour at 37 °C. Next, the sections were soaked in a blocking solution containing 1% BSA for 1 hour at room temperature, then incubated with a 1:200 dilution of anti-α-actinin antibody (Sigma) in blocking solution overnight at 4 °C. The next day, all sections were rinsed with PBS and incubated with Alexa®Fluor 647-conjugated anti-mouse IgG antibody (details in Table 2.6) for an hour at room temperature. The histology sections were eventually incubated with DAPI and mounted with Vectashield mounting medium before imaging them using the snapshot fluorescent microscope (Zeiss). The

analysis of TUNEL staining on histology sections was similar to that in NRCMs (section 2.2.2).

2.6.4 Ki-67 staining

Dewaxed and rehydrated histology sections (heart, liver and kidney tissues) were immersed in boiled sodium citrate buffer (10mM sodium citrate, 0.05% Tween 20, adjusted to pH 6.0 with 1 N HCl) for 20 minutes. Once they reached room temperature, they were then washed with water and permeabilised with 0.3% Triton-X in PBS for 30 minutes. Next, all sections were incubated in the blocking solution (10% goat serum diluted with permeabilisation buffer) for an hour, followed by overnight incubation of anti-α-actinin and Ki-67 antibodies (details in Table 2.6) at 4 °C. After several times of washing in PBS on the next day, the sections were incubated for an hour at room temperature with Alexa Fluor®647-conjugated anti-mouse and Alexa Fluor®488-conjugated anti-rabbit (details in Table 2.6). After several washes in PBS, all the sections were subsequently incubated with DAPI and mounted with Vectashield mounting medium, then imaged using the snapshot fluorescent microscope (Zeiss). The identification of fluorescence signals and the analysis of Ki-67 positive cells on histology sections followed the same protocol as that in NRCMs (section 2.2.1.1).

2.7 Molecular analysis

Molecular analysis was performed to estimate the mechanisms of action of the Mst1/2 inhibitors that are attributed to their effects. In this PhD project, the molecular analysis was conducted using immunofluorescence, luciferase system, western blot and the real-time quantitative polymerase chain reaction (RT-QPCR).

2.7.1 GFP-YAP transfection

Transduction of adenovirus expressing green fluorescent protein (GFP)-YAP was used to assess YAP translocation into the nucleus. NRCMs were seeded onto laminin-coated coverslips in a 24-well plate at a density of 250,000 cells/well. The next day, the GFP-YAP construct (pEGFP-C3-hYAP1) generated in Oceandy's lab was transduced into the wells together with DMSO and XMU-MP-1 or MRT137 (1 μM, 3 μM and 5 μM) treatments. The construct was given by Dr. Marius Sudol (Basu et al., 2003). Following overnight incubation in humidified cell culture incubator, NRCMs were washed with PBS and fixed with 4% PFA (15-minute incubation), then counterstained with DAPI (1-minute incubation). NRCMs

were subsequently mounted with Vechtashield mounting medium and imaged using an Olympus BX51 upright microscope at 20x magnification. Green fluorescence signals in the nucleus showed YAP translocation in the nucleus. The percentage of positive nuclear GFP-YAP signal cells amongst treatment groups was analysed.

2.7.2 YAP Luciferase assay

YAP activity was assessed using a luciferase reporter system of GAL4-TEAD and UAS-luciferase adenoviruses generated in Oceadny's lab. The Ad-GAL4-TEAD system was given by Dr. Kunliang Guan, whereas the Ad-UAS-luciferase system was from Dr. Liqun Luo (Tian et al., 2010). One day after NRCMs or HUVECs seeding, the cells were transduced with Ad-GAL4-TEAD and Ad-UAS-luciferase. The treatments of either DMSO, XMU-MP-1 or MRT137 (1 μM, 3 μM and 5 μM) were given together with the adenoviruses. The cells were then incubated in a humidified cell culture incubator for 24 hours. Next, the cells were lysed 1x cell lysis buffer (Promega) for 20 minutes on an orbital shaker after several washes with PBS. After that, 25 μl of cell lysate was mixed with 25 μl of Luciferase Assay Reagent (Promega) and the luciferase signals were read using a Lumat LB9507 Tube Luminometer (Berthold). For technical repetition, each treatment group was read twice. In each independent experiment, at least three wells were allocated for the same treatment group.

2.7.3 Protein extraction

Protein extraction from either cells or tissues was conducted using RIPA buffer (containing 1% IGEPAL CA-630, 0.5% sodium deoxycholate, 0.1% SDS, 0.5 mM phenylmethylsulfonyl fluoride (PMSF), 1 μg/mL Aprotinin, 2.5 μg/mL Pepstatin A, 500 ng/mL Leupeptin and 1x PBS). The cells were scraped after adding 150 μL of RIPA buffer following several washes with PBS. The heart tissue was mixed with 500 μL of RIPA buffer, then crushed using a tissue homogeniser (Dounce homogeniser). The protein lysates were then incubated on an orbital shaker for 30 minutes at 4 °C, followed by 10-minute centrifugation at 3000 rpm. The supernatant was taken for bicinchoninic acid assay (BCA) assay to determine protein concentration and western blotting. Pierce BCA Protein assay kit (Thermo Scientific) was used to measure protein concentration. A set of protein standards with known concentrations was used to determine the concentration of unknown samples. 10 μL of either standards or unknown samples were incubated with 200 μL of the reaction mixture provided in a 96-well plate for 30 minutes at 37 °C. The purple colour developed after the incubation was measured at 562 nm in a Multiscan Ascent microplate reader. The

calculation of protein concentration was performed by plotting against the standard concentration.

2.7.4 Western blotting

Extracted proteins from the cells or tissues were separated using the sodium dodecyl sulfate (SDS) polyacrylamide gel electrophoresis based on the protein size. 20 µg of protein samples mixed with 6x Laemmli buffer (Sigma) were loaded into the 8-15% acrylamide gel after being heated at 90 °C for 5 minutes. A standard of 10-180 kDa (Bio-Rad) was loaded in one well to determine the protein size. The electrophoresis gels were placed in a tank filled with Tris-glycine running buffer, then run at 130 V for 90 minutes. Following the separation, the proteins were transferred onto polyvinylidene fluoride (PVDF) membrane (Millipore) using a TransBlot Turbo system (Bio-Rad) for 7 min at 25 V and 2.5 A. The membranes were then incubated with the blocking solution, either 5% milk or 1-3% bovine serum albumin (BSA) solution, for an hour to block non-specific binding. After three times wash using Tris-buffered saline with 0.05% Tween-20 (TBST), the membranes were incubated either at 4 °C overnight or for 2 hours at room temperature in a 1:1000 dilution of primary antibody in the blocking solution. After that, the membranes were washed with TBST several times, then incubated in a 1:5000 dilution of horseradish peroxide (HRP)-linked secondary antibody in TBST for an hour at room temperature. Details of the antibodies used in the western blot are listed in Table 2.6. Following several washes in TBST, the membranes were incubated in enhanced chemiluminescence (ECL) western blotting detection reagent (Amersham Biosciences) containing 1 µL/mL H_2O_2 to detect bound antibodies. The proteins were imaged using a ChemiDoc XRS+imaging system, whereas band intensities were determined using Image Lab software (BioRad). After the target proteins were determined, the housekeeping proteins were assessed by another incubation in a 1:5000 dilution of a control antibody in TBST for an hour at room temperature. All band intensity was normalised to the housekeeping protein (Glyceraldehyde-3-Phosphate Dehydrogenase (GAPDH), beta-actin or alpha-tubulin) from the same sample.

2.7.5 RNA extraction

Small pieces of heart tissues were added with 500 µL of TRIzol® (Invitrogen), then homogenised using a Dounce homogeniser and incubated for 15 minutes. After that, 200 µL of chloroform was added, then vigorously shaken before being centrifuged at 10,000 rpm for 15 minutes at 4 °C. The aqueous layer was moved to a new Eppendorf tube and added

with 600 µL propan-2-ol (BDH Ltd.), inverted 30 times and incubated for 10 minutes at room temperature. Following the incubation, the samples were spun at 13,000 rpm for 10 minutes at 4 °C. Next, the supernatant was removed and replaced with 1 mL of 70% ethanol, followed by another centrifugation at 13,000 rpm for 10 minutes at 4 °C. The supernatant was then discarded and the pellets were air-dried, then resuspend with 20 µL RNAse free water. Extracted RNA was then quantified using a nanodrop (ND-8000) to get the RNA concentration (ng/µL). Samples that can be used were samples with 260/280 absorbance values of between 1.8 and 2.2. The samples then underwent DNase treatment (Sigma) to remove the remaining DNA in the samples. As per the manufacturer's guidance, 1 µg RNA was added with 1 µL Amplification grade DNase 1, 1 µL DNase 1 reaction buffer and nuclease-free water up to 10 µL, then incubated for 15 minutes at room temperature. Following the incubation, 1 µl of 25 mM EDTA stop solution (Sigma) was added, then heated at 70 °C for 10 minutes. The next step was converting RNA into cDNA using a High capacity RNA-to-cDNA kit (Applied Biosystems). 10 µL of each DNase-treated sample was added with a mixture of reagents, as listed in Table 2.2, in polymerase chain reaction (PCR) tubes. After that, mRNA to cDNA conversion was run using an MJ Research PTC-200 Thermal Cycler (Bio-Rad) through cycles listed in Table 2.3.

Table 2.2 Reagents required for cDNA conversion

Reagents	Volume (µL)
10x RT buffer	2.0
25x dNTP Mix	0.8
10x ST Random Primers	2.0
Multiscribe Reverse Transcriptase	1.0
Nuclease-free water	4.2
Total volume per reaction	10

Table 2.3 cDNA conversion cycles

Step	Temperature (°C)	Time (minutes)
1	25	10
2	37	120
3	85	5
4	4	∞

cDNA samples were stored at -20 °C. Samples without Multiscribe Reverse Transcriptase and RNA were set as controls for the quantitative polymerase chain reaction (qPCR) to detect DNA contamination.

2.7.6 Gene expression analysis using RT-qPCR

All samples were run in triplicate in the RT-qPCR (real-time quantitative polymerase chain reaction) process for gene expression analysis. ANP and BNP genes were determined by adding the Brilliant III Ultra-Fast SYBR® Green qPCR Master Mix (Agilent Technologies) to the cDNA samples as listed in Table 2.4.

The primer sequences of the *Anp* gene (*Mus musculus*) are ATCACCCTGGGCTTCTTCCT (forward) and TGTTGGACACCGCACTGTAC (reverse), whereas the *Bnp* gene (*Mus musculus*) consist of GAGGTCACTCCTATCCTCTGG (forward) and GCCATTTCCTCCGACTTTTCTC (reverse).

Table 2.4 cDNA and SYBR Green mixture

Reagent	Volume (µL)
cDNA	1.0
SYBR Green	5.0
Quantitect primer assay (Qiagen)	1.0
Reference Dye	0.15
Nuclease-free water	2.85

The RT-qPCR process was conducted using the Applied Biosystems® 7500 Fast Real-Time PCR System with the program listed in Table 2.5. The expression of target genes was quantified by measuring the C_T values normalised against the C_T value for the relevant reference gene, then assessing the comparative C_T method (ΔC_T). Data obtained were calculated as $2^{-\Delta\Delta CT}$.

Table 2.5 RT-qPCR cycles for SYBR Green

Stage	Temperature (°C)	Time	No of cycles
Initiation	95	15 minutes	1
Cycling	95	5 seconds	40
	60	25 seconds	
Melt curve	95	15 seconds	1
	60	1 minute	
	95	15 seconds	
	60	15 seconds	
Holding	4		∞

2.8 Antibodies

The antibodies used in the experiments in this PhD project are listed below:

Table 2.6 List of antibodies

Antibodies	Species	Isotype	Source	Epitope	Dilution and use
Anti-α-actinin	Mouse Monoclonal	IgG	Sigma Aldrich (#A7811)	Rabbit skeletal α-actinin 1	1:200 (IF)
Alexa Fluor™ 680 phalloidin	NA	NA	ThermoFisher Scientific (#A22286)	F-actin	1:200 (IF)
Ki-67	Rabbit	IgG	Abcam (#Ab15580)	KLH derived from within residues 1200-1300 of Human Ki67	1:200 (IF)
pH-H3	Rabbit polyclonal	IgG	Invitrogen (#PA5-17869)	Histone H3 only when phosphorylated at Ser10	1:200 (IF)
Alexa Fluor® 647 Anti-mouse	Mouse Polyclonal	IgG	Jackson ImmunoResearch (#115-605-072)	F(ab')2/Fab portion of mouse IgG	1:200 (IF)
Alexa Fluor® 488 Anti-Rabbit	Rabbit Polyclonal	IgG	Jackson ImmunoResearch (#711-545-152)	Whole molecule rabbit IgG	1:200 (IF)
Non-Phospho (Active) YAP (Ser127) (E6U8Z)	Rabbit Monoclonal	IgG	Cell Signaling Technology (#29495)	Endogenous YAP protein only when Ser127 is not phosphorylated (Human, Mouse, Rat, Bovine)	1:1000 Western Blot
YAP Antibody (G-6)	Mouse Monoclonal	IgG	Santa Cruz Biotechnology (#sc-376830)	YAP of mouse, rat and human origin	1:500 Western Blot
Phospho-MOB1 (Thr35)(D2F10)	Rabbit Monoclonal	IgG	Cell Signaling Technology (#8699)	Endogenous levels of MOB1 protein only when phosphorylated at Thr35 (Human, Mouse, Rat, Monkey)	1:1000 Western Blot
MOB1 (E1N9D)	Rabbit Monoclonal	IgG	Cell Signaling Technology (#13730)	Total MOB1 protein (Human, Mouse, Rat, Hamster, Monkey)	1:1000 Western Blot
Phospho-LATS1 (Ser909)	Rabbit Monoclonal	IgG	Cell Signaling Technology (#9157)	Phosphorylated LATS1 at Ser909 (Human, Mouse, Rat)	1:1000 Western Blot
Total LATS1	Rabbit Polyclonal	IgG	Proteintech (#17049-1-AP)	Total LATS1 (Human, Mouse, Rat)	1:1000 Western Blot
Mst1	Rabbit Monoclonal	IgG	Cell Signaling Technology (#3682)	Total Mst1 (Human, Mouse, Rat)	1:1000 Western Blot
Mst2	Rabbit Monoclonal	IgG	Cell Signaling Technology (#3952)	Total Mst2 (Human, Mouse, Rat)	1:1000 Western Blot
Phospho Mst1 (Thr183)/ Mst2 (Thr180)	Rabbit Polyclonal	IgG	Cell Signaling Technology (#49332)	Phosphorylated Mst1 at Thr183 and Mst2 at Thr180 (Human, Mouse, Rat)	1:1000 Western Blot

Table 2.6 List of antibodies (continued)

Antibodies	Species	Isotype	Source	Epitope	Dilution and use
SAV1	Rabbit Monoclonal	IgG	Cell Signaling Technology (#13301)	Total SAV1 (Human, mouse, Rat)	1:1000 Western Blot
ERK1/2	Rabbit Monoclonal	IgG	Cell Signaling Technology (#9102)	Total ERK1/2 (Human, Mouse, Rat)	1:1000 Western Blot
Phospho ERK1/2	Rabbit Polyclonal	IgG	Cell Signaling Technology (#9101)	Phosphorylated ERK1 at Thr202 and ERK2 at Tyr204	1:1000 Western Blot
Caspase 3	Rabbit Monoclonal	IgG	Cell Signaling Technology (#9662)	Total caspase 3 (Human, Mouse, Rat)	1:1000 Western Blot
Cleaved caspase 3	Rabbit Polyclonal	IgG	Cell Signaling Technology (#9661)	Cleaved caspase 3 at Asp175 (Human, Mouse, Rat)	1:1000 Western Blot
FoxO1	Rabbit Polyclonal	IgG	Cell Signaling Technology (#2880)	Total FoxO1(Human, Mouse, Rat)	1:1000 Western Blot
Phospho p-38 MAPK	Rabbit Polyclonal	IgG	Cell Signaling Technology (#9211)	Phosphorylated p-38 MAPK at Thr180 and Tyr182	1:1000 Western Blot
p-38 MAPK	Rabbit Polyclonal	IgG	Cell Signaling Technology (#9212)	p-38 MAPK	1:1000 Western Blot
Anti-mouse IgG, HRP-linked Antibody	Mouse	IgG	Cell Signaling Technology (#7076)	Mouse IgG	1:5000 Western Blot
Anti-rabbit IgG, HRP-linked Antibody	Rabbit	IgG	Cell Signaling Technology (#7074)	Polyclonal and monoclonal rabbit IgG	1:5000 Western Blot
GAPDH HRP-linked	Rabbit	IgG	Cell Signaling Technology (#3683)	GAPDH	1:5000 Western Blot
β-actin HRP linked	Rabbit	IgG	Cell Signaling Technology (#5125)	β-actin	1:5000 Western Blot
α-tubulin HRP linked	Rabbit	IgG	Cell Signaling Technology (#9099)	α-tubulin	1:5000 Western Blot

2.9 Statistical analysis

All data were presented as mean ± standard error of means (SEM) and screened for normality distribution before proceeding to the statistical analysis. The statistical analysis was performed using GraphPad Prism (v7.02). The appropriate statistical tests were chosen based on the data set. The statistical and *post-hoc* tests used are stated on each figure legend. The p-value < 0.05 indicates statistical significance.

CHAPTER 3

INHIBITION OF MST1/2 USING XMU-MP-1 PROTECTS THE HEART AGAINST PRESSURE OVERLOAD INDUCED REMODELLING

Most of the parts in this chapter have been published in the British Journal of Pharmacology: Triastuti, E., Nugroho, A. B., Zi, M., Prehar, S., Kohar, Y. S., Bui, T. A., Stafford, N., Cartwright, E. J., Abraham, S. & Oceandy, D. (2019). Pharmacological inhibition of Hippo pathway, with the novel kinase inhibitor XMU-MP-1, protects the heart against adverse effects during pressure overload. British journal of pharmacology, 176(20), 3956-3971.

3.1 Theoretical overview and conceptual frameworks

The heart undergoes adaptive responses to various stimuli, such as mechanical and neuro-hormonal abnormalities (Rockman et al., 1991). Constriction at the ascending aorta (as a form of mechanical hypertrophic forces) results in hemodynamic, physiological, morphological and genetic changes in the heart, which represent adverse cardiac remodelling (Chen et al., 2011). Adverse cardiac remodelling encompasses cardiomyocyte hypertrophy to compensate for increased ventricular-wall stress due to a persistent spike of preload or afterload. However, prolonged pressure overload in the heart results in compensatory response failure and cardiac dysfunction (Nakamura and Sadoshima, 2018). Adverse cardiac remodelling needs to be inhibited as it is a progress that is determinant of heart failure (HF).

Despite the current pharmacological treatments of HF, which are aimed to reduce preload and improve cardiac emptying, new strategies addressing various pathways involved in underlying processes of cardiac remodelling offer more expectations than relieving symptoms. Among the pharmacological treatments that have been used clinically, ACE (angiotensin-converting enzyme) inhibitors and beta-blockers have positive effects on cardiac remodelling. However, vasodilators and inotropic agents do not affect cardiac remodelling (Cohn et al., 2000). A combination of an angiotensin II receptor antagonist and a neprilysin inhibitor preserves haemodynamic stability by modulating angiotensin II and natriuretic peptide levels. Current treatments have shown evidence of reducing mortality and hospitalisation rates, but they cannot fully reverse cardiac remodelling or protect cardiomyocytes from enlargement, meaning that progression to HF still occurs (Wu et al., 2017).

The cellular pathways involved in adverse cardiac remodelling may ultimately cause cardiomyocyte death and cardiac fibrosis. The Hippo pathway strongly contributes to adverse cardiac remodelling through its regulation in cell apoptosis, autophagy (Nakamura and Sadoshima, 2018) and hypertrophy (Zi et al., 2014). The suppression of the Hippo components (Mst2 and sav) in an animal model subjected to transverse constriction and coronary artery ligation was shown to improve heart function (Leach et al., 2017). Additionally, Mst1 is known to be involved in HF progression following MI. The cardiac-specific inhibition of endogenous Mst1 has been reported to preserve cardiac function post-MI through cardiomyocyte apoptosis inhibition (Odashima et al., 2007). In contrast, Mst1 overexpression is associated with increased caspase-induced apoptosis and dilated cardiomyopathy (Yamamoto et al., 2003). Furthermore, the global knockout of Mst2 in mice is attributed to cardiac protection against pressure overload corresponding to cardiac hypertrophy and fibrosis reduction (Zi et al., 2014).

Inhibition of Mst1/Mst2 using a chemical substance, XMU-MP-1, protects against liver tissue injury and promotes hepatocyte regeneration when administered at the dose of 1 to 3 mg/kg, prompting the chance for its usage in other disease models (Fan et al., 2016). XMU-MP-1 was also found to have beneficial effects in reducing neuronal death following ischaemia (Huang et al., 2020). Additionally, XMU-MP-1 was revealed to antagonise angiotensin II-induced aortic arch aneurysm (Okuyama et al., 2019). Considering the need for new therapeutic approaches targeting remodelling mechanisms, in this chapter, I investigate the effects of the MST1/2 inhibitor, XMU-MP-1, in neonatal rat cardiomyocytes (*in vitro*) and the cardiac pressure-overload model in mice (*in vivo*). I outline the hypothesised effects of XMU-MP-1 in adverse cardiac remodelling in Figure 3.1.

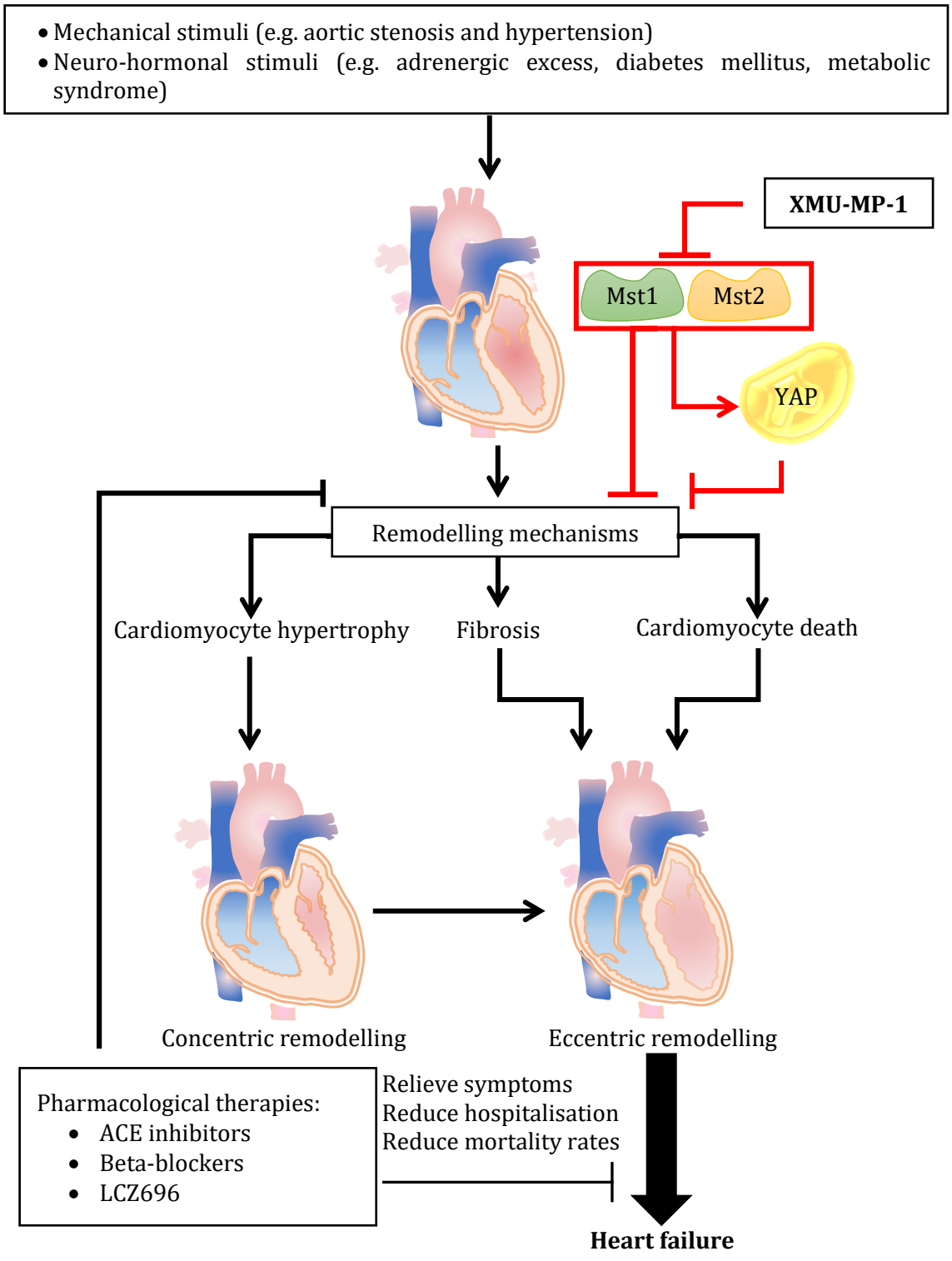

Figure 3.1 Conceptual framework of the estimated role of XMU-MP-1 in the cardiac remodelling process. Adverse cardiac remodelling occurs when pathological stimuli affect the heart and promote the development of cardiomyocyte hypertrophy, fibrosis and cardiomyocyte death. Current pharmacological therapies are mostly symptomatic-focused. The role of the Hippo pathway in modulating cell death is a breakthrough strategy of reversing cardiac remodelling to prevent the progression of heart failure.

3.2 Aims

The main objective of this chapter is to evaluate the effects of XMU-MP-1 treatment in neonatal cardiomyocytes (*in vitro*) and in mouse models of pressure overload hypertrophy using a transverse aortic constriction (TAC) procedure (*in vivo*), this is specified as follows:

- To investigate the effects of XMU-MP-1 in cardiomyocyte proliferation, hypertrophy and apoptosis.
- To assess cardiac function before and after XMU-MP-1 treatment in mice post-TAC surgical procedure.
- To examine if XMU-MP-1 treatment affects some features of hypertrophy, apoptosis and proliferation markers in mice after TAC surgical procedure.
- To determine any possible side effects of XMU-MP-1 treatment, including kidney and liver function, undesirable cell proliferation.

3.3 Hypotheses

I postulate that Mst1/2 inhibition by XMU-MP-1 preserves cardiac function in TAC model mice through its impact on cardiomyocyte physiology, including proliferation, hypertrophy, and apoptosis. Off-target effects could possibly occur after intraperitoneal administration of XMU-MP-1, such as in the kidney and liver. The screening of increasing undesirable cell proliferation worth attempting in non-specific targeted drug delivery.

3.4 Results

This chapter illustrates the role of XMU-MP-1 treatment in neonatal cardiomyocyte physiology and details a further investigation of the XMU-MP-1 treatment in TAC model mice. Three different dosages of XMU-MP-1, i.e., 1 μM, 3 μM and 5 μM, were given to treat NRCMs. An equal volume of DMSO was used in the control group because XMU-MP-1 was dissolved in DMSO. Some parts of this chapter discuss the *in vivo* experiment of transverse aortic arch constriction using a procedure described in Chapter 2. Intraperitoneal injection of XMU-MP-1 at the dose of 1 mg/kgBW every alternate-day and vehicle (50% DMSO + 50% water) were administered 3-weeks after the TAC surgical procedure. Delayed treatment administration was aimed to resemble the real condition because the progression of cardiac remodelling is commonly detected at the advanced stage once cardiac hypertrophy had occurred.

3.4.1 Cardiomyocyte proliferation in response to XMU-MP-1 treatment

Hippo pathway activation has been explicitly shown to inhibit cell proliferation. It is, therefore, necessary to investigate whether Mst1/2 inhibition using XMU-MP-1 can

increase cardiomyocyte proliferation. In determining the cardiomyocyte proliferation, primary culture of neonatal rat cardiomyocytes (NRCMs) was used. NRCMs were treated with three different doses of XMU-MP-1 (1 μM, 3 μM and 5 μM) before being fixed and stained with a specific staining method for cell proliferation. Ki-67 staining was performed to determine the active cell cycle and the anti-α-actinin antibody was used to distinguish cardiomyocytes from non-cardiomyocyte cells. After 24-hour treatment of XMU-MP-1, cardiomyocyte proliferation was enhanced significantly (as shown in Figure 3.2). Interestingly, the highest dose of XMU-MP-1 used (5 μM) showed no significant change in cardiomyocyte proliferation compared to the control (DMSO). This discrepancy will be discussed later in the discussion section.

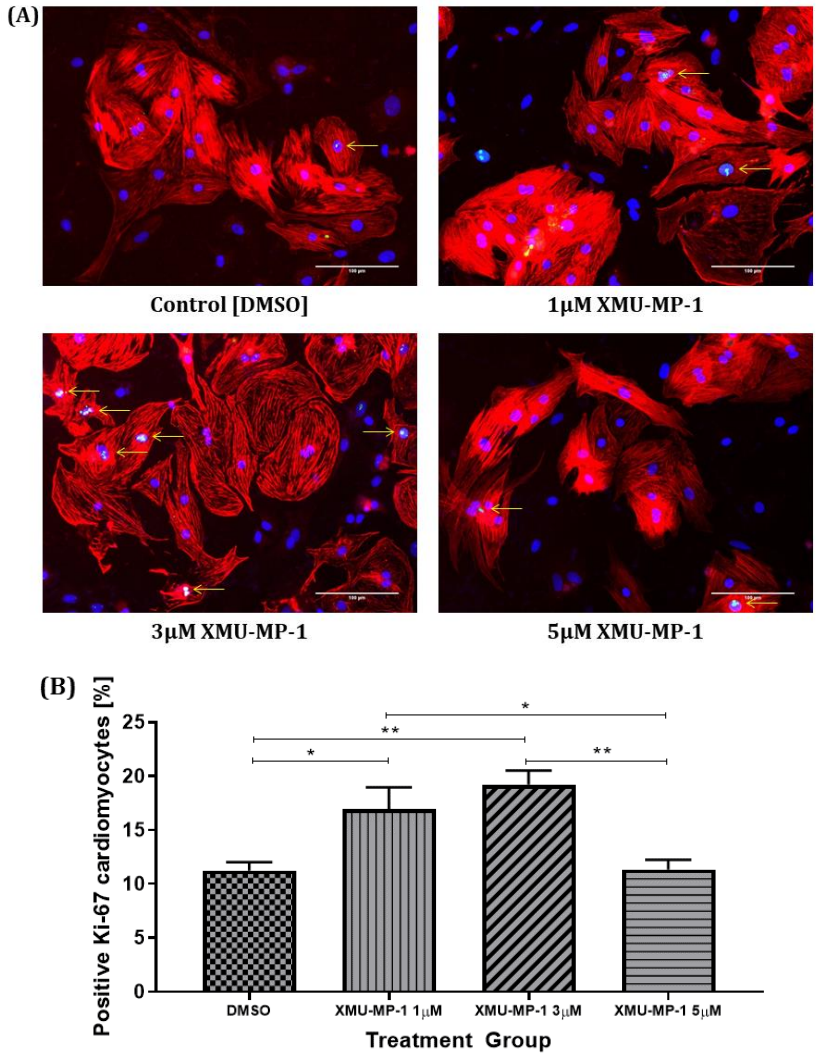

Figure 3.2 Ki-67 staining as an indicator of cell proliferation in neonatal cardiomyocytes. (A) Representative images of Ki-67 staining in neonatal cardiomyocytes. Overlay of green, blue and red fluorescence signals indicates positive Ki-67 cardiomyocytes (shown by yellow arrows). (B) A significant increase in cardiomyocyte proliferation was observed in the XMU-MP-1 treatment at the dose of 1 μM (16.93 ± 2.02 %) and 3 μM (19.22 ± 1.30 %). XMU-MP-1 at the dose of 5 μM (11.35 ± 0.90 %) has no difference in cardiomyocyte proliferation compared to the control group (11.23 ± 0.79 %). Data (shown as mean ± SEM) were analysed using one-way ANOVA with Tukey's *post-hoc* test for multiple comparisons, *p<0.05 and **p<0.01 indicate significant differences in results. The number of independent experiments = 5 (more than 2,000 cardiomyocytes were analysed in each independent experiment). Scale bar = 100 μm.

3.4.2 The effects of XMU-MP-1 treatment in Cardiomyocyte hypertrophy

In 2014, our lab members reported that Mst2 of the Hippo pathway has pro-hypertrophic effects (Zi et al., 2014). As XMU-MP-1 is an inhibitor of Mst1/2, it is essential to elaborate on the effects of XMU-MP-1 in cardiomyocyte hypertrophy. An experiment was designed to investigate cardiomyocyte hypertrophy by inducing cardiomyocytes with 50 μM of phenylephrine (PE). The tests performed were BNP luciferase assay and cardiomyocyte size analysis. The duration of PE exposure in the BNP luciferase assay was 24 hours. For cardiomyocyte size analysis, the duration of PE exposure was 72 hours (the medium and treatments were changed every day), followed by fixing and staining of the cells. In Figure 3.3 and Figure 3.4, we can see that XMU-MP-1 has anti-hypertrophic effects and makes a similar dose-dependent pattern in both experiments.

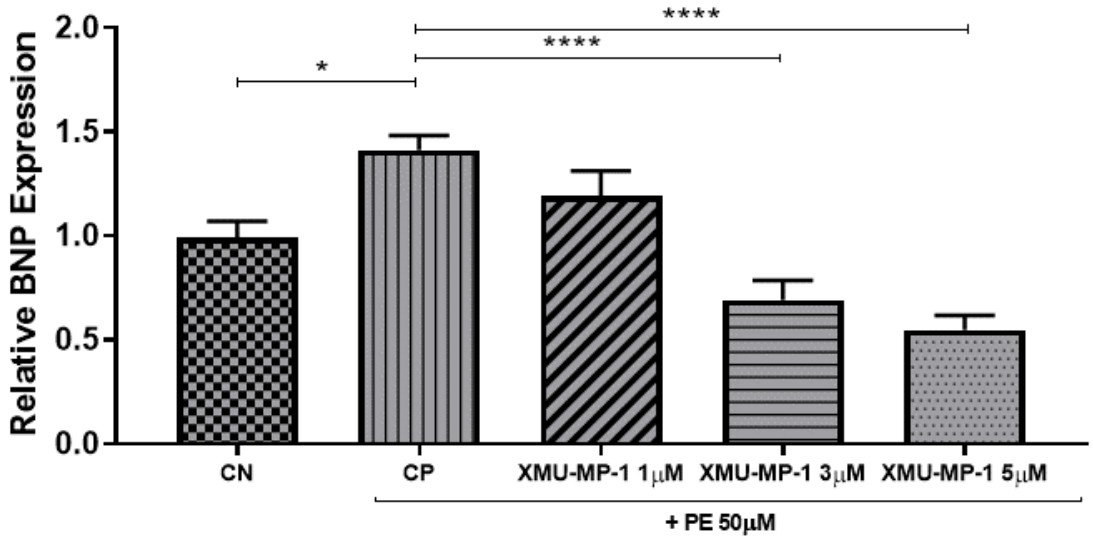

Figure 3.3 Brain Natriuretic Peptide (BNP) luciferase activity in NRCMs in response to phenylephrine treatment. BNP luciferase activity is enhanced by around 50% in the positive control group (1.41 ± 0.07) following 24-hour induction of 50 μM phenylephrine. 1 μM of XMU-MP-1 (1.19 ± 0.11) does not show any effect in reducing BNP expression, whereas 3 μM and 5 μM of XMU-MP-1 (0.69 ± 0.09 and 0.55 ± 0.07, respectively) significantly inhibit the expression of BNP. Data (shown as mean ± SEM) were analysed using one-way ANOVA with Tukey's *post-hoc* test for multiple comparisons, *p<0.05 and ****p<0.0001 indicate significant differences in results. The number of independent experiments = 5. 250,000 cardiomyocytes were seeded on the plate for BNP luciferase assay.

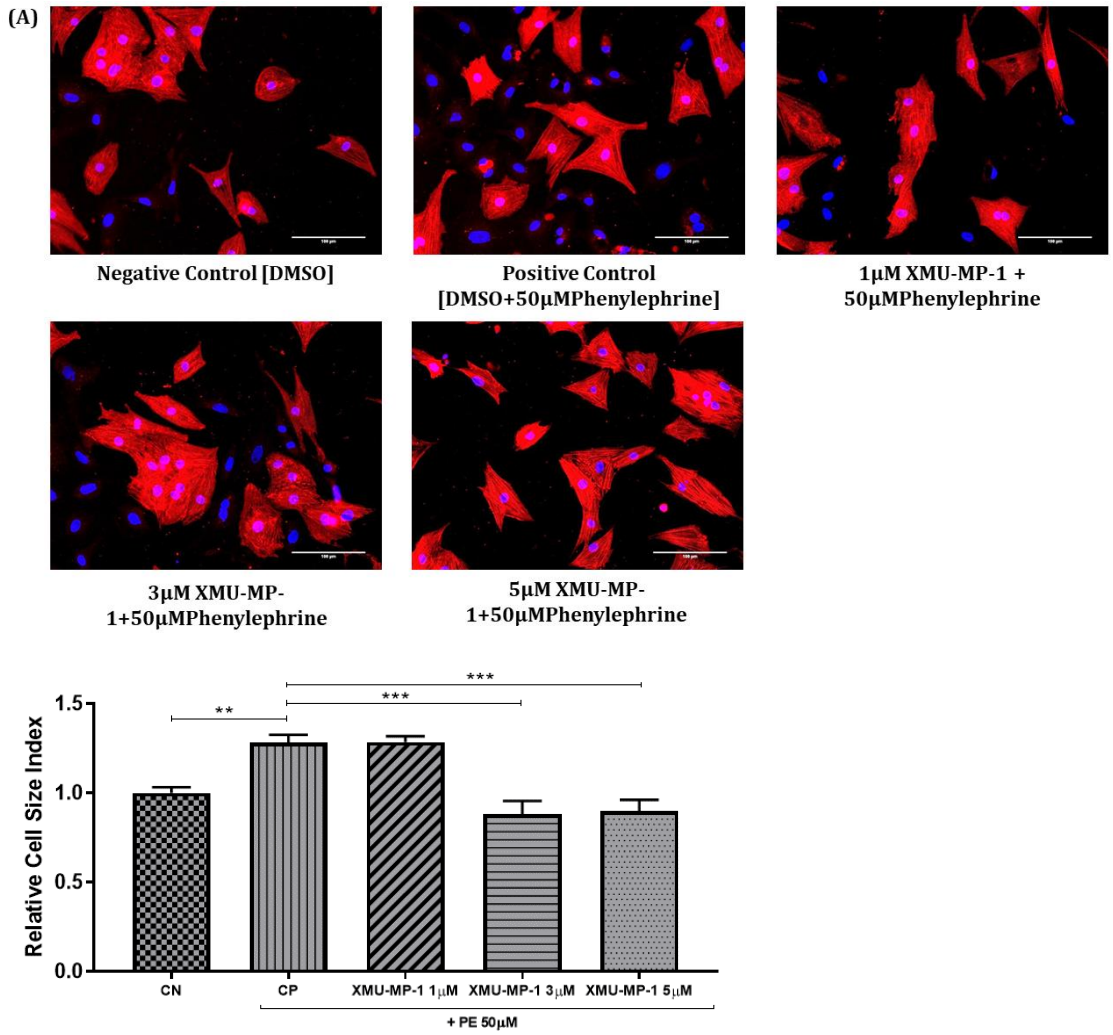

Figure 3.4 Cardiomyocyte size analysis in neonatal rat cardiomyocytes after the induction of 50µM phenylephrine. (A) Representative images of cardiomyocytes stained using an anti-α-actinin antibody. (B) The administration of 50 µM of phenylephrine for 72 hours significantly increases cardiomyocyte cell size by around 25% (1.28 ± 0.04 in the positive control group). There is no change in the size of cardiomyocyte treated with 1 µM of XMU-MP-1 (1.29 ± 0.03). However, at the dose of 3 µM and 5 µM (0.88 ± 0.08 and 0.89 ± 0.06, respectively), XMU-MP-1 significantly prevents cardiomyocytes from phenylephrine-induced hypertrophy. Data (shown as mean ± SEM) were analysed using one-way ANOVA with Tukey's post-hoc test for multiple comparisons, **p<0.01 and ***p<0.001 indicate significant differences in results. The number of independent experiments = 6. More than 100 cardiomyocytes were analysed in each independent experiment for cell size analysis. Scale bar = 100 µm.

3.4.3 Characterisation of cardiomyocyte apoptosis and viability associated with XMU-MP-1 treatment

The Hippo pathway is strongly related to cell apoptosis regulation (Del Re et al., 2014). Thus, I analysed the impacts of XMU-MP-1 treatment in neonatal rat cardiomyocyte apoptosis. An immunofluorescence-based analysis called the TUNEL assay was performed to clarify cardiomyocyte apoptosis. TUNEL assay identifies DNA fragmentation in the cells undergoing apoptosis as a green fluorescence signal in the nucleus. I also conducted an MTT assay to determine the effects of XMU-MP-1 on cardiomyocyte viability. In both experiments, NRCMs were exposed with 200 µM of H_2O_2 to induce oxidative stress for 4

hours and treated the cells with XMU-MP-1 at the same time. Figure 3.5 reveals the results of the TUNEL and MTT assay in neonatal rat cardiomyocytes.

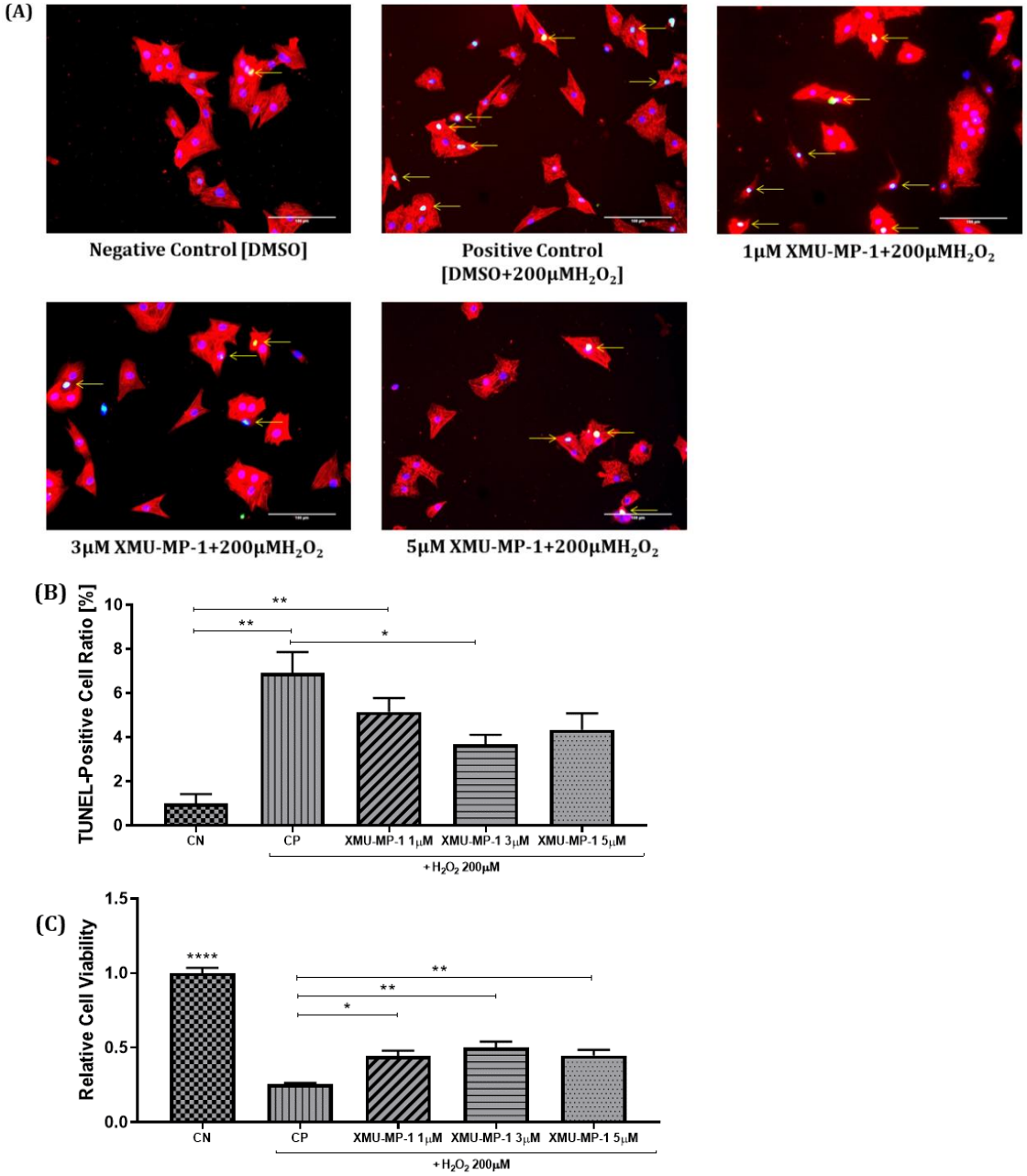

Figure 3.5 TUNEL and MTT assays in neonatal rat cardiomyocytes after 200 μM of H_2O_2 treatment. (A) Representative images of TUNEL assay. Green fluorescence in the nuclei indicates positive TUNEL cells. Positive TUNEL cardiomyocytes are shown in yellow arrows. (B) 3 μM XMU-MP-1 treatment significantly decreases the number of positive TUNEL cardiomyocytes (3.69 ± 0.43 %) when compared to the positive control group (6.91 ± 0.96 %). Both 1 μM and 5 μM of XMU-MP-1 (5.15 ± 0.63 % and 4.33 ± 0.75 %, respectively) are not significantly different from the positive control group. (C) 4-hour treatment of 200 μM of H_2O_2 significantly decreases cell viability (determined using MTT assay) by around 75% (0.26 ± 0.01 in the positive control group). XMU-MP-1 treatments cannot enhance cell viability back to the normal level. However, when compared to the positive control, all XMU-MP-1 doses significantly increase cell viability as follows: 0.44 ± 0.03, 0.51 ± 0.04, 0.45 ± 0.03 at the dose of 1 μM, 3 μM and 5 μM, respectively. Data (shown as mean ± SEM) were analysed using one-way ANOVA with Tukey's post-hoc test for multiple comparisons, *p<0.05, **p<0.01, and ****p<0.0001 indicate significant differences in results. The number of independent experiments = 4. More than 1,000 cardiomyocytes were analysed in each independent experiment for the TUNEL assay. NRCMs were seeded at a density of 250,000 per well for the MTT assay. Scale bar = 100 μm.

3.4.4 Analysis of the Hippo core component activation

One of the consequences of Mst1/2 inhibition is the activation of YAP, the Hippo pathway main effector. Based on canonical Hippo signalling, YAP activation due to Mst inhibition is mediated by inhibition of the MOB1 and LATS phosphorylation. Here I carried out a western blot analysis of the Hippo components to confirm the molecular mechanisms of XMU-MP-1 inhibition in the Hippo/Mst. Based on my western blot analysis of protein from NRCMs, I found that XMU-MP-1 inhibits the phosphorylation of LATS1 and MOB1, which enhances the expression of active YAP (Figure 3.6). The protein extraction from the cells was obtained through enzymatic digestion, as described in Chapter 2, after 24-hour treatment of XMU-MP-1.

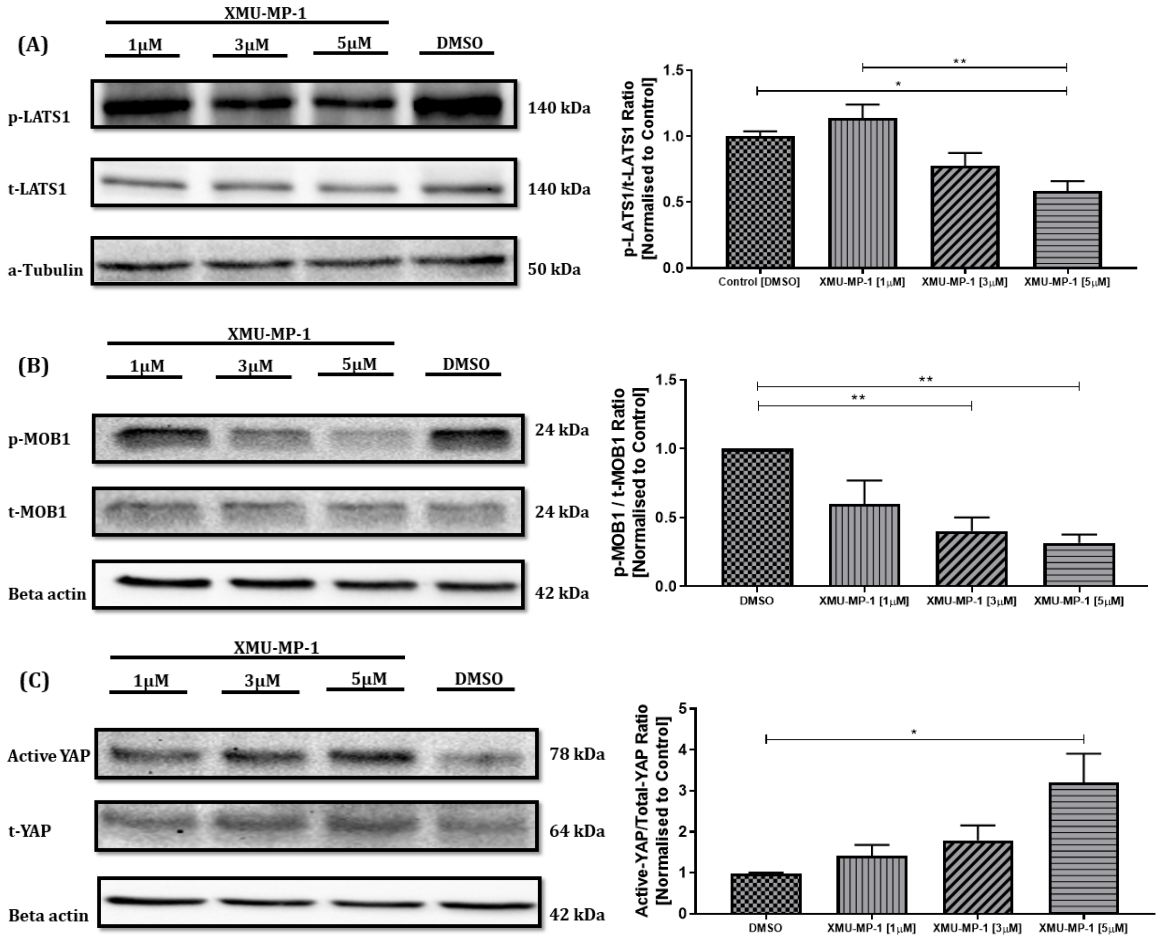

Figure 3.6 Western blotting of the Hippo components from neonatal rat cardiomyocyte protein. (A) Western blot results of phosphorylated-LATS1 and total LATS1 expression. The results show that there is a significant decrease in the ratio of phosphorylated-LATS1 to total LATS1 expression after XMU-MP-1 treatment. (B) The representative images and the quantification of phosphorylated-MOB1 and total MOB1 western blot show that XMU-MP-1 significantly reduces the ratio between phosphorylated-MOB1 and total MOB1 expression. (C) XMU-MP-1 significantly increases active YAP expression relative to total YAP expression. Data were analysed using one-way ANOVA with Tukey's post-hoc test for multiple comparisons, *p<0.05 and **p<0.01, indicate significant differences in results. N = 3 of independent experiments.

SiRNA-mediated knockdown of Mst1 or Mst2 in NRCMs was applied before XMU-MP-1 treatment to check the selectivity of XMU-MP-1 on Mst1 and Mst2. Western blot analysis after Mst1 or Mst2 knockdown shows that XMU-MP-1 can work in inhibiting the phosphorylation of the Hippo components even though Mst1 or Mst2 is diminished (Figure 3.7). I treated the cells with the Mst1 and Mst2 SiRNA for two days and then treated them with XMU-MP-1 for 24 hours before performing protein extraction.

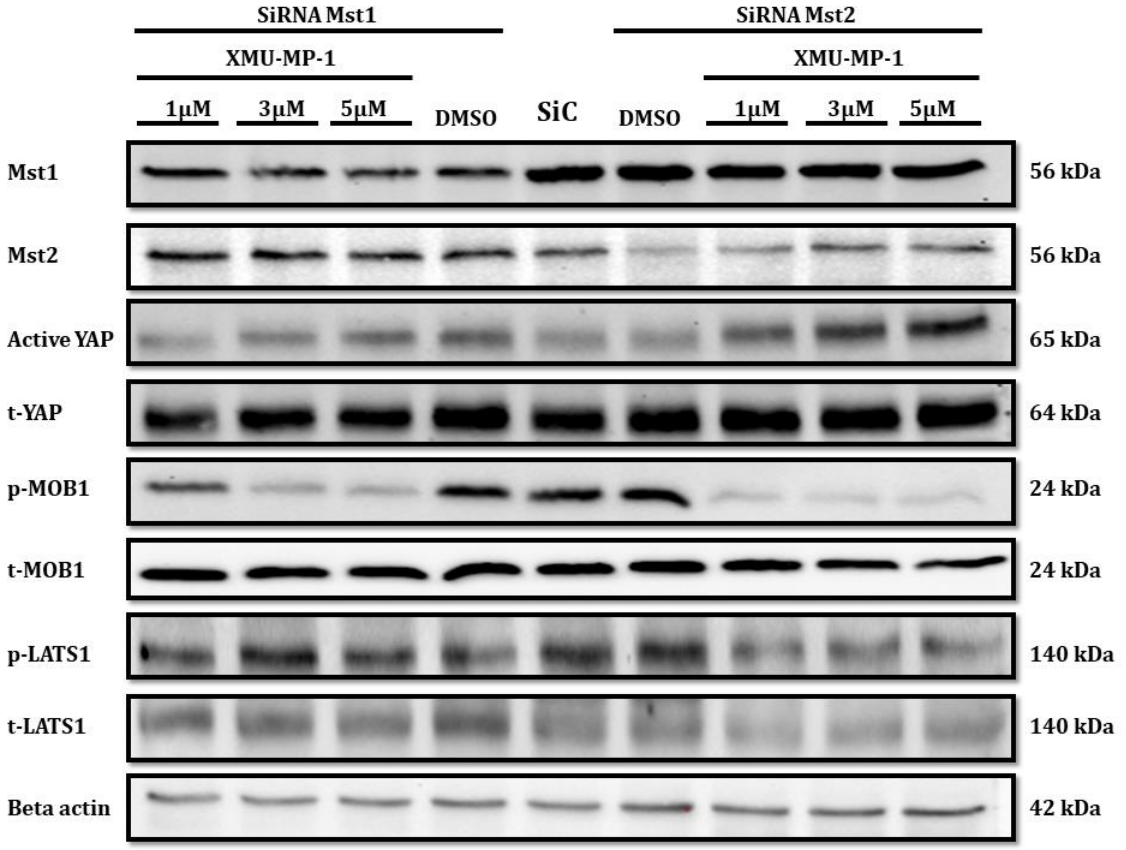

Figure 3.7 XMU-MP-1 effects on the Hippo component expression following siRNA-mediated knockdown of Mst1 and Mst2 in neonatal rat cardiomyocyte. The effects of XMU-MP-1 on the Hippo component expression are not diminished because of Mst1 or Mst2 proteins knockdown. Western blot data suggest that Mst1 and Mst2 expressions are not affected by XMU-MP-1 treatment. The expression of active YAP is increased with XMU-MP-1 even after Mst1 and Mst2 knockdown. The phosphorylation of MOB1 and LATS1 is reduced with XMU-MP-1 treatment following Mst1 or Mst2 knockdown.

An analysis of GAL4-TEAD-luciferase was conducted to confirm YAP activation attributed to XMU-MP-1 effects in NRCMs, whereas the GFP-YAP immunofluorescence experiment was performed to detect nucleus translocation of YAP. The findings of this study demonstrate that XMU-MP-1 enhances YAP activity and YAP translocation into the nuclei based on a dose-dependent manner (Figure 3.8).

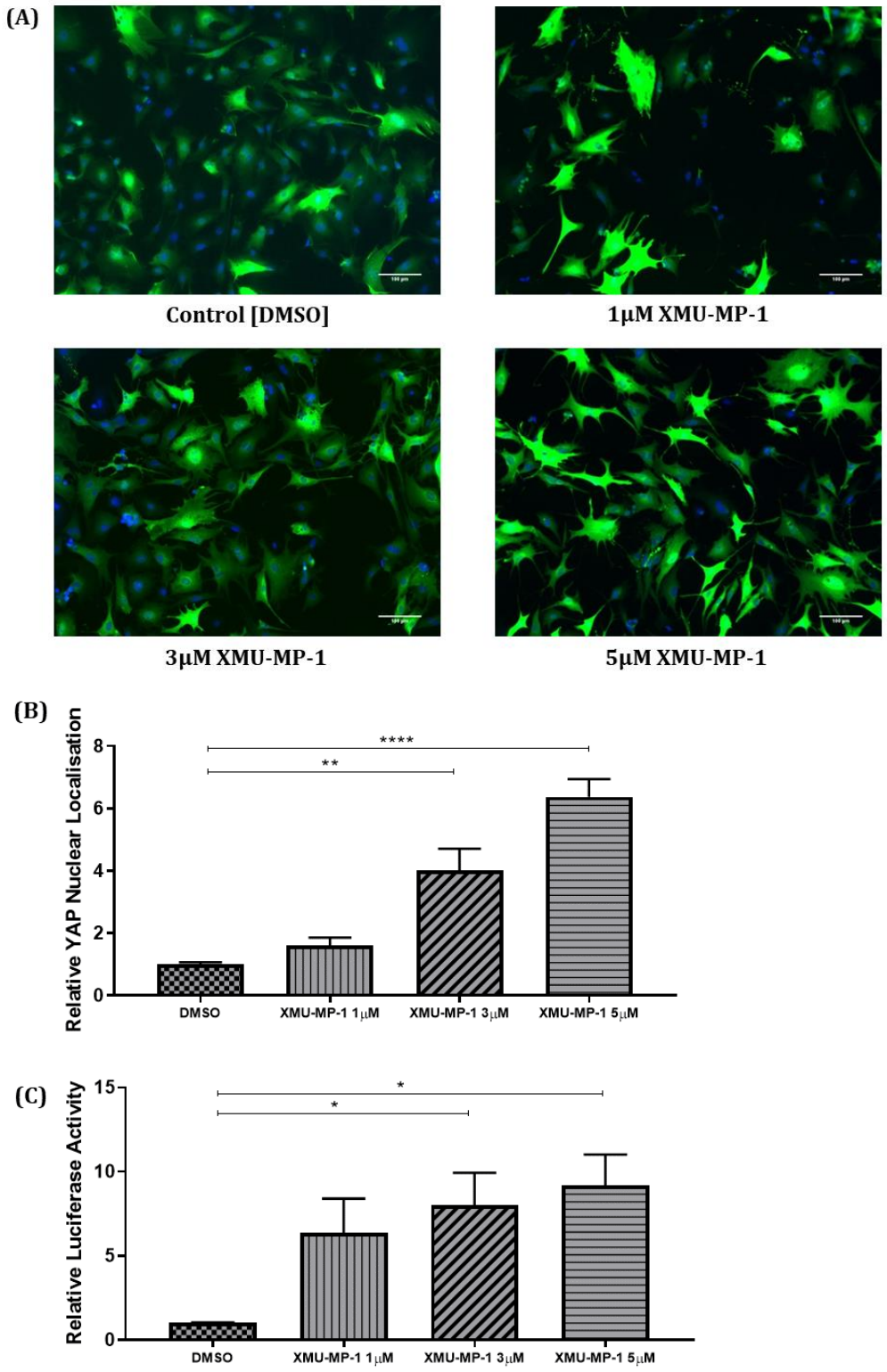

Figure 3.8 Activation of YAP due to XMU-MP-1 treatment in neonatal rat cardiomyocytes. (A) Representative images of GFP-YAP localisation in the neonatal rat cardiomyocytes after 24-hour treatment of XMU-MP-1. Green fluorescence signal co-localised with DAPI (blue fluorescence signal) indicates translocation of YAP into the nuclei. (B) Analysis of GFP-YAP localisation suggests that XMU-MP-1 significantly increases the translocation of YAP into the nuclei. (C) As a confirmation GFP-YAP experiment, YAP activity that was determined using a luciferase transporter system shows a significant increase after XMU-MP-1 treatment for 24 hours at the dose of 3 μM and 5 μM. Data were analysed using one-way ANOVA with Tukey's post-hoc test for multiple comparisons, *$p<0.05$, **$p<0.01$, and ****$p<0.0001$ indicate significant differences in results. N = 6 of independent experiments. More than 1,000 cardiomyocytes were analysed in each independent experiment. Scale bar = 100 μm.

3.4.5 The effects of XMU-MP-1 treatment in the pressure overload-induced cardiac hypertrophy model in mice

Transverse aortic ligation resembles aortic stenosis because it causes left ventricular (LV) hypertrophy as a compensatory response for increased resistance. The hypertrophic heart shows some morphological characteristics such as an increased heart weight (HW) to tibia length (TL) ratio and LV mass to body/weight ratio. Having the HW to TL ratio assessed at the end of the experiment, the TAC group reveals a significantly higher HW to TL ratio than the sham group. As mentioned in section 2.5.1 of Chapter 2 about the TAC experiment, injections of DMSO or 1mg/kgBW XMU-MP-1 were given within ten days (every two days), starting from three weeks after the TAC surgical procedure. The results can be seen in Figure 3.9 (A), showing that both XMU-MP-1 and vehicle treatments in the TAC group do not show statistical significance in the HW to TL ratio. The LV to BW ratio, measured using echocardiography, is significantly higher in the TAC group compared to the sham group. Meanwhile, the difference of LV to BW ratio between pre and post-treatment is relatively persistent (as shown in Figure 3.9 (B)).

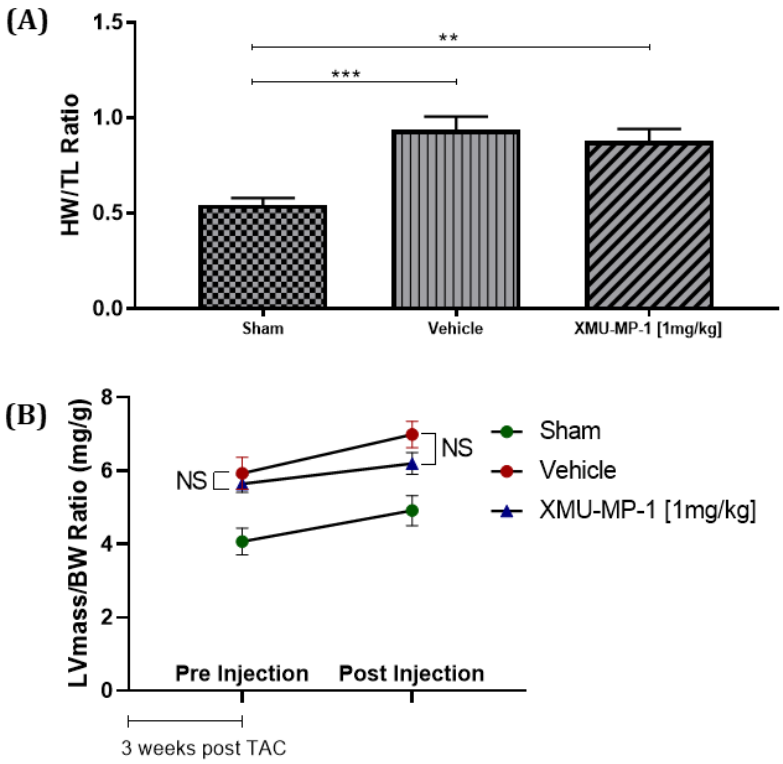

Figure 3.9 Morphological characteristics of TAC model mice treated with XMU-MP-1. Observation of morphological characteristics in TAC model mice exhibits a significant increase in HW/TL ratio and LV/BW ratio but not in between treatment groups in TAC mice. (A) TAC procedure markedly increases HW/TL ratio from 0.67 ± 0.04 in the sham group to 1.07 ± 0.05 in the vehicle group and 1.04 ± 0.08 in the XMU-MP-1 group. (B) There is no significant difference between LV/BW ratio before and after treatment, both in the vehicle and XMU-MP-1 groups. Data are presented as mean ± SEM with statistical analysis as follows: one-way ANOVA with Tukey's post-hoc test for multiple comparisons in (A) and two-way ANOVA for multiple comparisons in (B). **p<0.01 and ***p<0.001 indicate significant differences in results. NS: not significant. Sham n=5, vehicle n=10, XMU-MP-1 n=10.

Standard morphometric measurements assessed after TAC surgery are presented as follows:

Table 3.1 Morphometric measurements of TAC model mice.

Parameters	Treatment groups		
	Sham	Vehicle	XMU-MP-1
Heart weight (mg)	137.10 ± 7.78	224.00 ± 12.22	212.00 ± 13.73
Lung weight (mg)	171.80 ± 7.41	279.90 ± 39.91	210.40 ± 18.53
Body weight (g)	29.44 ± 0.75	28.06 ± 0.47	28.30 ± 0.67

Heart weight and lung weight are morphometric parameters used to indicate abnormal growth in the heart and lung due to the TAC procedure. Body-weight measurement shows the state of well-being of the mice. The outcome of all morphometric parameters, shown in Table 3.1, was obtained at the end of the experiment (five weeks after the TAC procedure).

The cardiac structure was assessed to determine the level of dilation in the heart that can be a predictor of the remodelling stage. Diastolic and systolic diameters were measured before and after treatment as cardiac structure parameters. Measurement was conducted using echocardiography, which was performed by two operators to minimise technical bias. The diastolic diameter in all treatment groups is increased within the treatment duration, but this is not statistically significant (as revealed in Figure 3.10 (A)). Interestingly, the systolic diameter in the XMU-MP-1 group remains stable, whereas it is significantly higher in the vehicle group showing the weaker ability of the heart to contract (Figure 3.10 (B)).

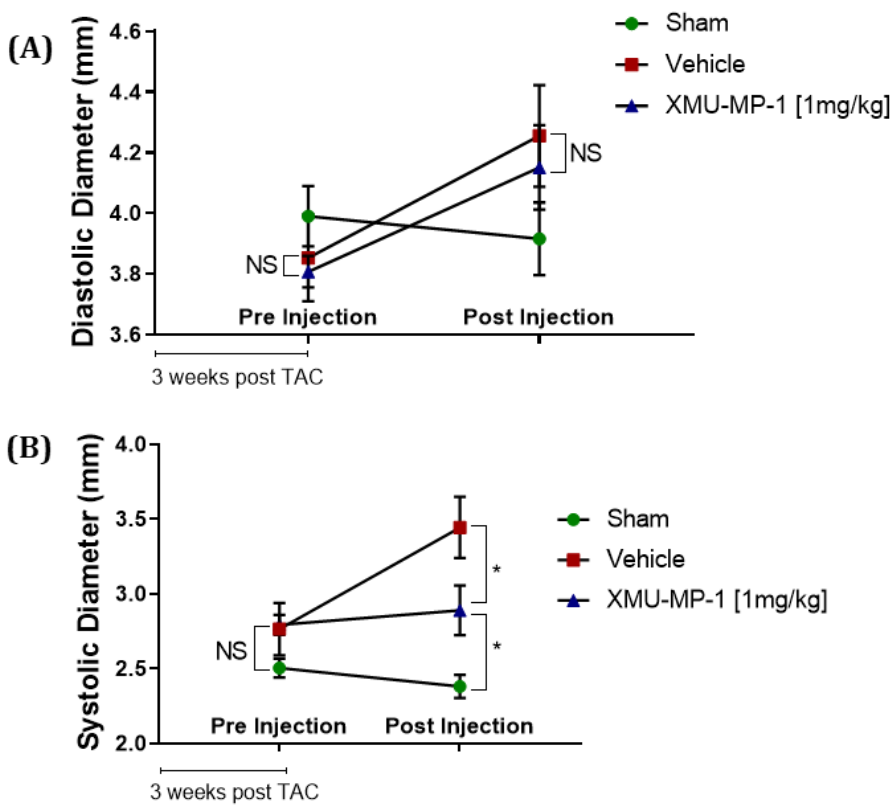

Figure 3.10 Analysis of cardiac structure in TAC model mice within the treatment period. (A) There is no significant difference amongst groups in left ventricular diameter during diastolic phase three weeks after TAC surgery or before treatment (3.99 ± 0.10 mm in the sham group, 3.87 ± 0.15 mm in the vehicle group, 3.81 ± 0.15 mm in XMU-MP-1 group). There is an increase of diastolic diameter in the TAC groups at the end of the treatment period, but the diastolic diameter remains stable in the sham group (3.92 ± 0.12 mm in the sham group, 4.26 ± 0.17 mm in the vehicle group, 4.15 ± 0.14 mm in XMU-MP-1 group). (B) Within-group comparison in the systolic diameter before and after treatment shows that there is a significant increase in the vehicle group but not in other groups (2.50 ± 0.06 mm in the sham group, 2.76 ± 0.18 mm in the vehicle group, 2.79 ± 0.07 mm in XMU-MP-1 group). The comparison of systolic diameter after treatment among groups shows a statistical difference between the sham and the vehicle groups (2.38 ± 0.08 mm in the sham group, 3.44 ± 0.20 mm in the vehicle group, and 2.89 ± 0.17 mm in the XMU-MP-1 group). Data (shown as mean ± SEM) were analysed using two-way ANOVA with Tukey's post-hoc test for multiple comparisons, *$p<0.05$ indicates significant differences in results. NS: not significant. Sham n=5, vehicle n=10, XMU-MP-1 n=10.

Cardiac remodelling, as one of the compensatory mechanisms to the TAC procedure, initially begins with left ventricular hypertrophy that can be observed using echocardiography analysis. The wall thickness of the left ventricle increases in the early hypertrophy state, followed by the gradual decline of cardiac function. A persistent overload pressure in aortic resistance can turn compensatory mechanisms into destructive processes that can reduce cardiac function. The changes in fractional shortening (FS) and ejection fraction (EF) were observed three weeks after the TAC procedure (before the treatments were initiated) and after the treatments were complete (at the end of the experiment).

A significant reduction in FS and EF occurs three weeks after the TAC procedure (based on the comparison between sham and both TAC groups). A follow-up measurement of FS and EF shows that XMU-MP-1 treatment can preserve cardiac function following TAC, whereas, the cardiac function in the vehicle group continues to deteriorate. Figure 3.11 reveals some representative images of 2-dimensional echocardiography of each group, in addition to the cardiac function with FS and EF as indicators. Echocardiography analysis was performed by two operators blinded to the treatment groups to minimise technical bias.

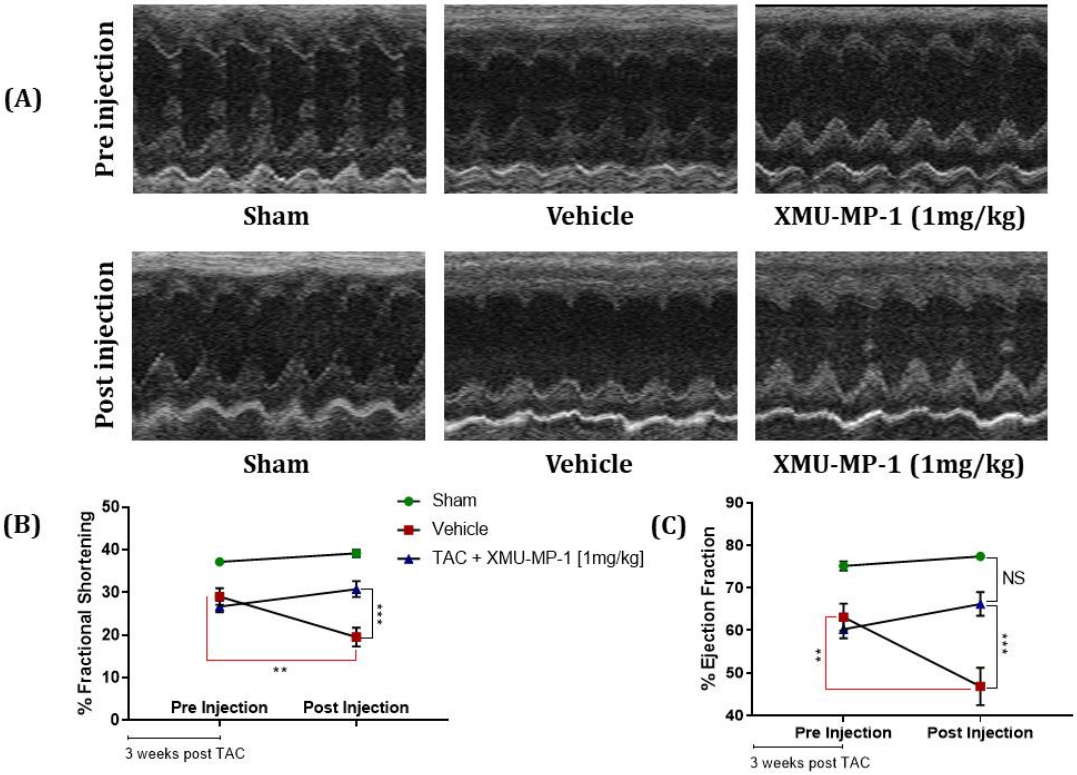

Figure 3.11 The comparison of echocardiography parameters showing the difference in the wall thickness and the cardiac function among groups. (A) Representative images from a short-axis angle (M-mode) of echocardiography show the thickness of the left ventricular wall, diastolic diameter and systolic diameter at three weeks after the TAC procedure (pre-injection) and five weeks after the TAC procedure (post-injection). (B) Within-group comparison of pre-injection and post-injection of FS in the vehicle groups is significantly different, showing a reduction at the end of the experiment. There is a significant difference in the FS after 10-day treatment amongst groups with the order of cardiac function from high to low as follows: sham (39.17 ± 0.86 %), XMU-MP-1 (30.79 ± 1.84 %), vehicle (19.51 ± 2.21 %), respectively. (C) There is a significant decrease of EF in the vehicle group (46.79 ± 4.41 %) at the end of the experiment that is statistically different from the sham group (77.42 ± 0.94 %) and XMU-MP-1 group (66.20 ± 2.78 %). Data (shown as mean ± SEM) were analysed using two-way ANOVA with Tukey's post-hoc test for multiple comparisons, *p<0.05, **p<0.01, ***p<0.001 and ****p<0.0001 indicate significant differences in results. NS: not significant. Sham n=5, vehicle n=10, XMU-MP-1 n=10.

3.4.6 The impacts of XMU-MP-1 treatment post-TAC surgery on cardiomyocyte size and the expression of hypertrophic markers

Hypertrophic responses as compensatory mechanisms of the TAC procedure bring some consequences in cardiomyocytes. As discussed above, cardiomyocyte enlargement is one of

the important aspects involved in cardiac remodelling. Hence, cardiomyocyte size needs to be quantified to evaluate whether Mst1/2 inhibition using XMU-MP-1 has anti hypertrophy activity. Haematoxylin and Eosin (H&E) staining on the histological heart sections was conducted, followed by cardiomyocyte circumference measurement. As presented in Figure 3.12, the average cardiomyocyte circumference in TAC groups is significantly higher compared to that of the sham group. My data demonstrate that the XMU-MP-1 treatment shows protection against TAC-induced cardiomyocyte enlargement.

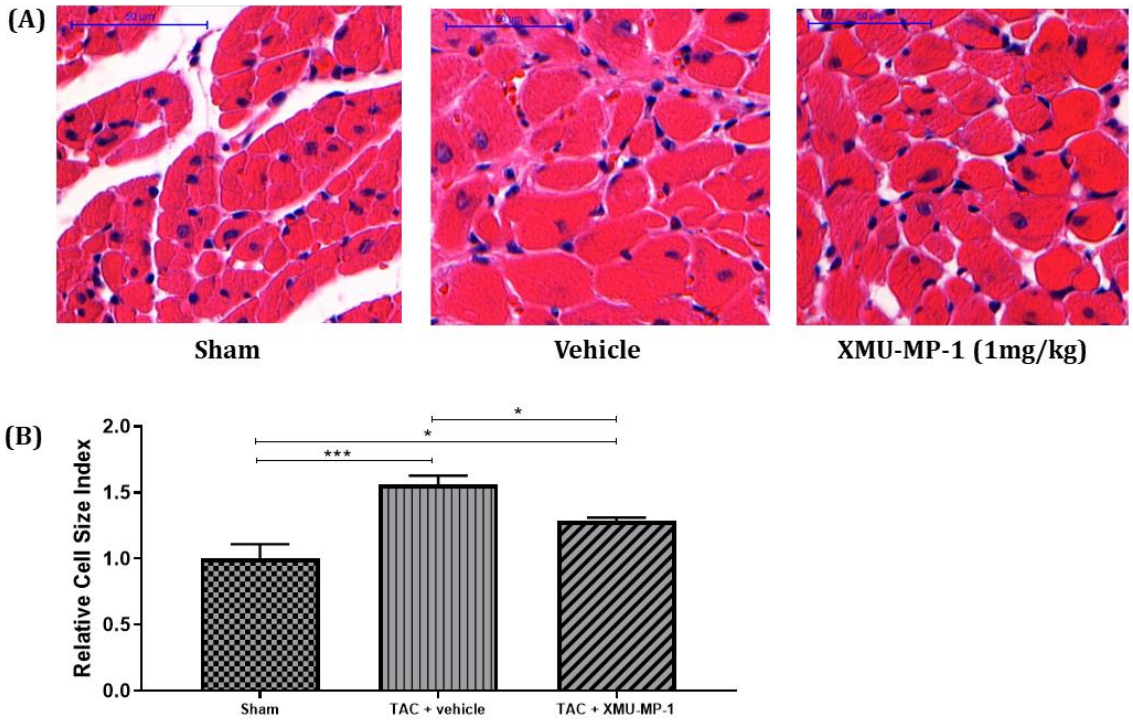

Figure 3.12 Analysis of cardiomyocyte size using H&E staining on the histological heart section. (A) Representative images from histological heart sections (stained with H&E) of the mice after the TAC procedure show a larger cell size in the vehicle group (1.56 ± 0.07)compared to the sham (1.00 ± 0.11) and XMU-MP-1 (1.29 ± 0.02) groups. (B) The cell size analysis suggests a significant increase in the vehicle group compared to the sham and XMU-MP-1 groups. XMU-MP-1 treatment significantly reduces cell size when compared to the vehicle group. Data (shown as mean ± SEM) were analysed using one-way ANOVA with Tukey's post-hoc test for multiple comparisons, *p<0.05, **p<0.01, ***p<0.001 and ****p<0.0001 indicate significant differences in results. Sham n=5, vehicle n=10, XMU-MP-1 n=10. More than 100 cardiomyocytes were analysed in each mouse. Scale bar = 100 μm.

Cell size analysis indicates that XMU-MP-1 treatment significantly inhibits cardiomyocyte hypertrophic growth and prevents cardiomyocyte enlargement. Therefore, assessments of the expression level of hypertrophy markers (ANP and BNP) using real-time quantitative polymerase chain reaction (RT-qPCR) were performed. Based on the transcript analysis of ANP and BNP mRNA using RT-qPCR, I found that the XMU-MP-1 treatment significantly reduced ANP and BNP levels compared to the vehicle group (Figure 3.13).

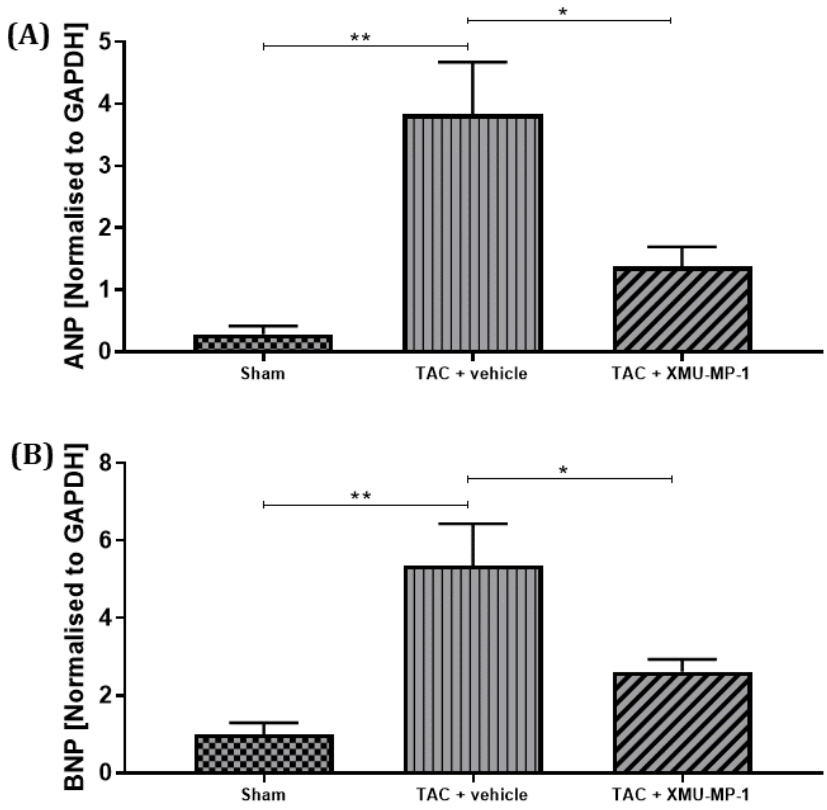

Figure 3.13 The transcript mRNA analysis of hypertrophy markers after the TAC procedure. (A) The analysis of the ANP mRNA transcript suggests that the vehicle group (3.83 ± 0.85) shows the highest ANP level when compared to the sham (1.00 ± 0.13) and XMU-MP-1 (1.38 ± 0.32) groups. (B) Based on the analysis of the BNP mRNA transcript, the TAC procedure significantly increases the BNP level (in the vehicle group (5.08 ± 1.01)) and XMU-MP-1 (2.64 ± 0.28). XMU-MP-1 treatment can suppress the increase in the BNP level up to less than two-fold compared to the sham group. Data (shown as mean ± SEM) were analysed using one-way ANOVA with Tukey's post-hoc test for multiple comparisons, *$p<0.05$ and **$p<0.01$ indicate significant differences in results. Sham n=5, vehicle n=10, XMU-MP-1 n=10.

Additionally, western blot experiments were conducted to determine whether ERK1/2 (extracellular signal-regulated kinase), a member of the mitogen-actvated protein kinase family involved in cardiac hypertrophy might be altered by XMU treatment.. My western blot analysis results suggest that there is no significant change in ERK1/2 expression among all treatment groups when analysed through the ratio of phosphorylated ERK1/2 to total ERK1/2 (Figure 3.14).

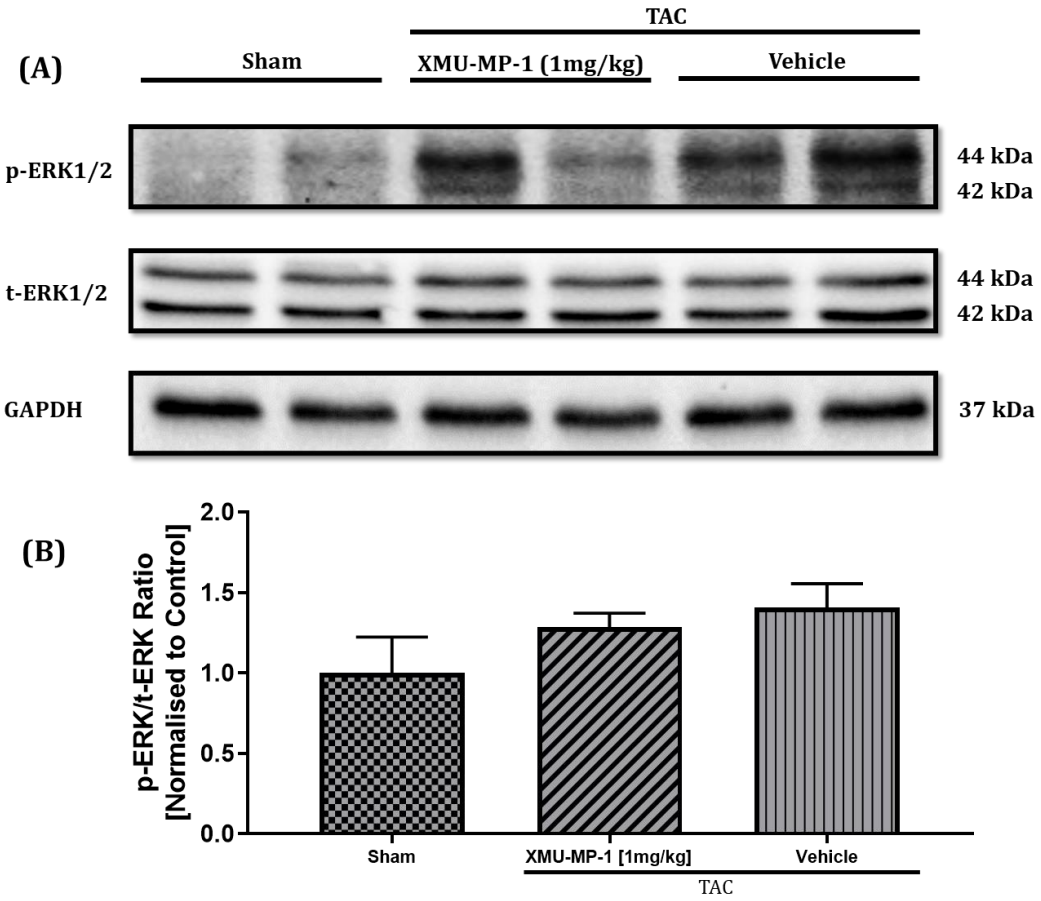

Figure 3.14 The expression of protein ERK1/2 is associated with the hypertrophy pathway. (A) Representative images of phosphorylated ERK1/2 (p-ERK1/2) and total ERK1/2 (t-ERK1/2) as well as GAPDH as a loading control. (B) Based on densitometry analysis, I found that there is no significant difference in the ratio of p-ERK1/2 to t-ERK1/2 expression among all groups. Data were analysed using one-way ANOVA (Sham n=5, vehicle n=5, XMU-MP-1 n=5).

3.4.7 Analysis of fibrosis level in mice treated with XMU-MP-1

The TAC procedure can trigger interstitial collagen deposition in the heart, which causes cardiac fibrosis. The formation of cardiac fibrosis increases ventricular-wall stiffness, loss of heart contractility and reduction in cardiac function. I performed Masson's Trichrome staining on the heart sections to assess the level of cardiac fibrosis. The blue colour appearing after the Masson's Trichrome staining indicates collagen deposition. Quantification of the interstitial fibrotic area percentage to total heart area ratio was used to compare the difference among groups. Based on my analysis, some scattered interstitial fibrotic areas were found on the heart sections of the mice that underwent the TAC procedure. Mice that underwent TAC surgery show a significant increase in the fibrotic area deposition in the interstitial space. Interestingly, I observed that in the XMU-MP-1 group, the level of interstitial fibrosis is significantly lower than that in the vehicle group (Figure 3.15).

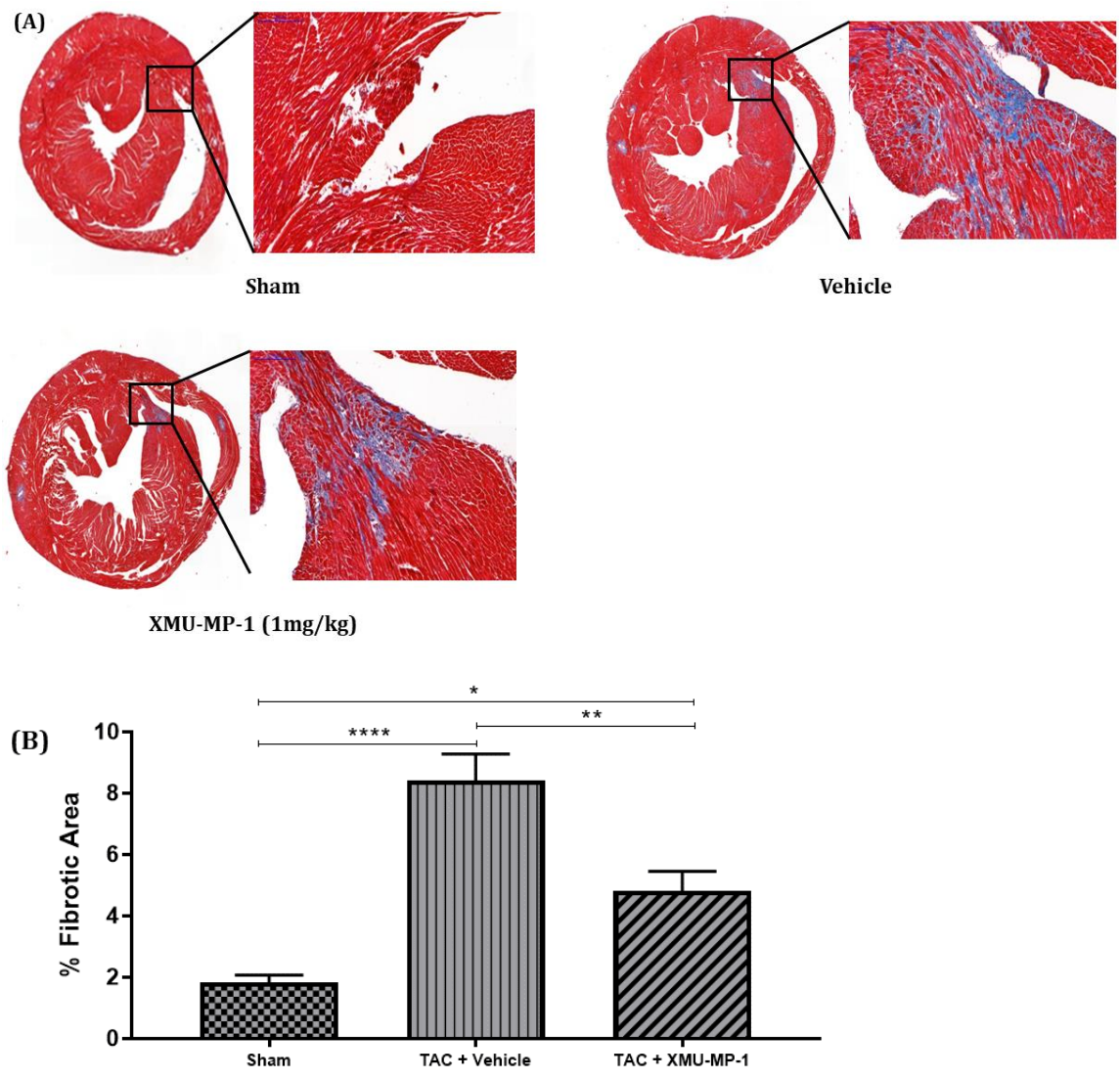

Figure 3.15 Deposition of the fibrotic area in the interstitial space of the heart sections in mice after TAC. (A) Representative images of Masson's Trichrome staining from histological heart sections of the mice following TAC. (B) The analysis of the fibrotic area shows that the TAC procedure increases the deposition of the fibrotic area. All treatment groups show a statistical difference with the order of fibrotic area from high to low as follows: sham (1.84 ± 0.22 %), XMU-MP-1 (4.81 ± 0.64 %) and vehicle (8.42 ± 0.87 %), respectively. Data (shown as mean ± SEM) were analysed using one-way ANOVA with Tukey's post-hoc test for multiple comparisons, *p<0.05, **p<0.01, and ****p<0.0001 indicate a statistical significance in results. Sham n=5, vehicle n=10, XMU-MP-1 n=10. Scale bar = 100 µm.

3.4.8 The effects of XMU-MP-1 treatment in cardiomyocyte apoptosis

Cardiomyocytes play a crucial role in sustaining cardiac function. Thus, excessive cardiomyocyte apoptosis is an important sign of reduced cardiac function. The TAC procedure induces cardiomyocyte apoptosis alongside cardiomyocyte hypertrophy. The TUNEL assay was applied to detect DNA fragmentation as an indication of cell apoptosis. Cardiomyocytes on the heart sections were stained using the anti-α-actinin antibody. As shown in Figure 3.16, the XMU-MP-1 treatment can suppress cardiomyocyte apoptosis compared to the vehicle group. Similar to the results of the fibrotic area analysis, the sham

group has the lowest level of cell apoptosis. The rate of positive TUNEL cells is quantified by dividing the number of cardiomyocytes with positive TUNEL signals (greenish-blue) by the total number of cardiomyocytes (blue in red) in each field of view.

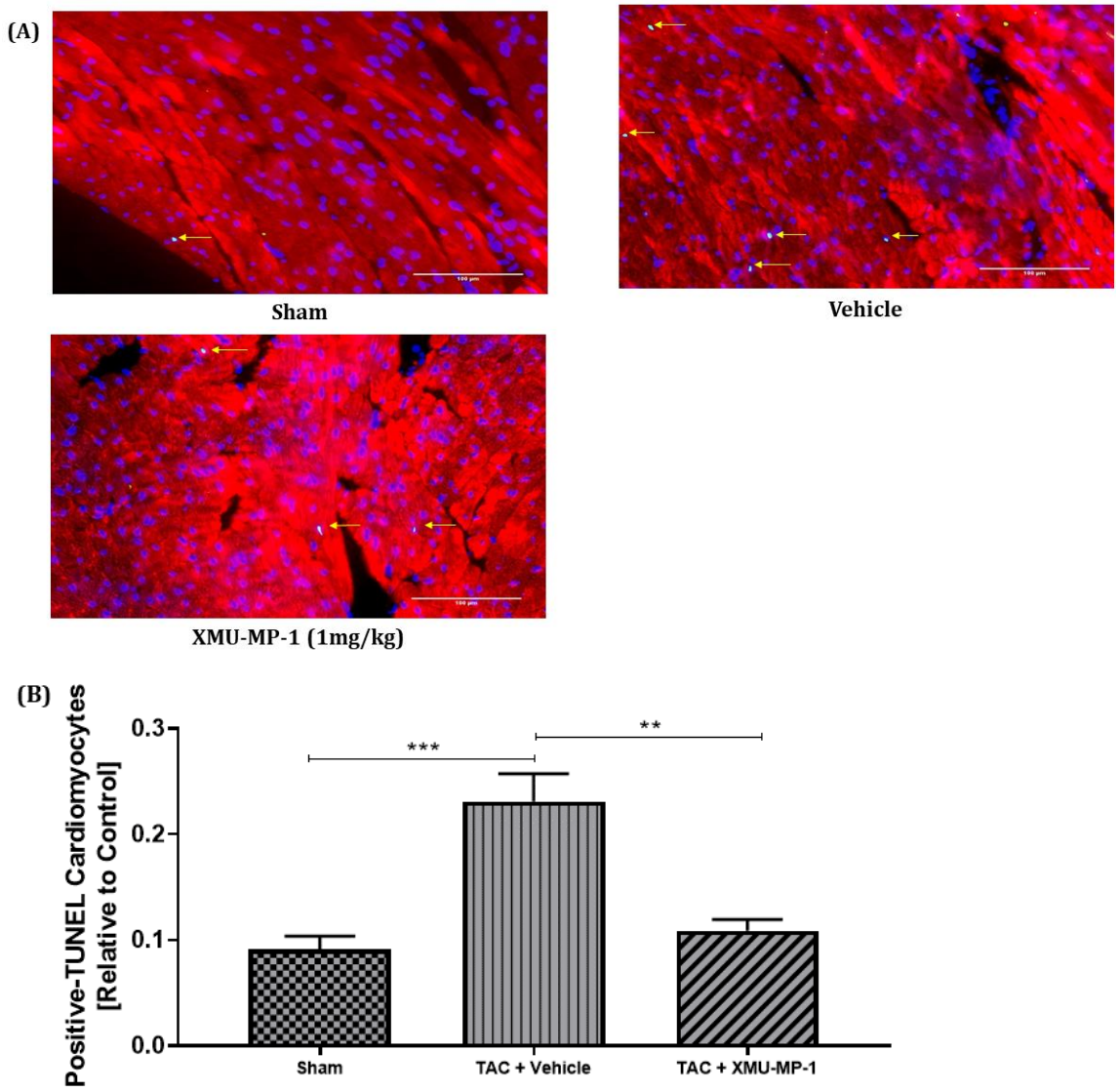

Figure 3.16 TUNEL staining on the heart sections in mice after TAC. (A) Representative images of TUNEL staining from histological heart sections after the TAC procedure. The overlay position of green and blue colour indicates positive TUNEL cells (shown by yellow arrows). (B) The apoptosis rate in cardiomyocytes is elevated after TAC (compared to sham (0.09 ± 0.01 %)). The rate of cardiomyocyte apoptosis in the XMU-MP-1 group (0.11 ± 0.01 %) is significantly lower than the vehicle group (0.23 ± 0.03 %). Data (shown as mean ± SEM) were analysed using one-way ANOVA with Tukey's post-hoc test for multiple comparisons, **p<0.01 and ***p<0.001 indicate significant differences in results. Sham n=5, vehicle n=10, XMU-MP-1 n=10. More than 1,000 cardiomyocytes were analysed in each mouse. Scale bar = 100 μm.

To confirm the TUNEL assay results, I conducted western blot experiments to check the protein involved in the apoptosis pathway (caspase-3). Densitometry analysis shows that there is a significant difference in caspase-3 activation following the TAC procedure. However, XMU-MP-1 treatment does not show any difference in suppressing the activation of caspase-3 when compared to the vehicle (Figure 3.17).

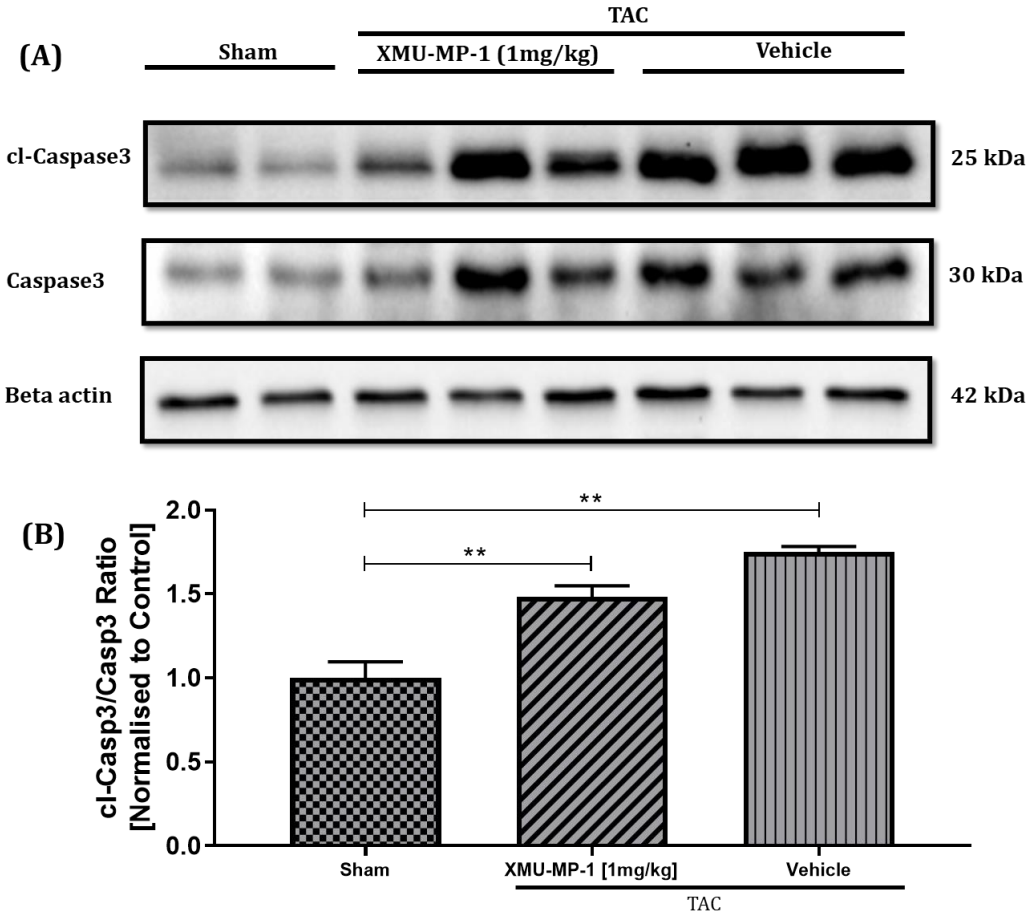

Figure 3.17 Densitometry analysis of caspase-3 protein in TAC model mice. (A) Representative images of cleaved-caspase-3 and caspase-3, together with beta-actin as a loading control. (B) My data suggest that five weeks after the TAC procedure, caspase-3 activation is increased. There is a small decrease but not statistically significant in caspase-3 activity in the XMU-MP-1 group compared to the vehicle group. Data were analysed using one-way ANOVA (Sham n=5, vehicle n=5, XMU-MP-1 n=5).

3.4.9 Cardiomyocyte proliferation associated with XMU-MP-1 treatment in TAC model mice

As shown before in this chapter, XMU-MP-1 has been proven to increase YAP activity and increase cardiomyocyte proliferation in the primary cell culture of NRCMs. Increasing cardiomyocyte proliferation is desirable in the pressure-overload condition because it means that new cardiomyocytes are available to help the heart in compensating the pressure-overload condition instead of forcing the existing cardiomyocytes to bear too much load. To determine the cardiomyocyte proliferation in TAC model mice, I performed Ki-67 staining on the heart sections to indicate the active cell cycle. Figure 3.18 shows that 1mg/kgBW of XMU-MP-1 treatment (every two days for ten days) does not significantly increase cardiomyocyte proliferation. Positive Ki-67 cells were observed based on the co-position of blue and green fluorescence signals in cardiomyocytes. The cell proliferation

rate was quantified by taking the ratio between positive Ki-67 cardiomyocytes and the total number of cardiomyocytes per field.

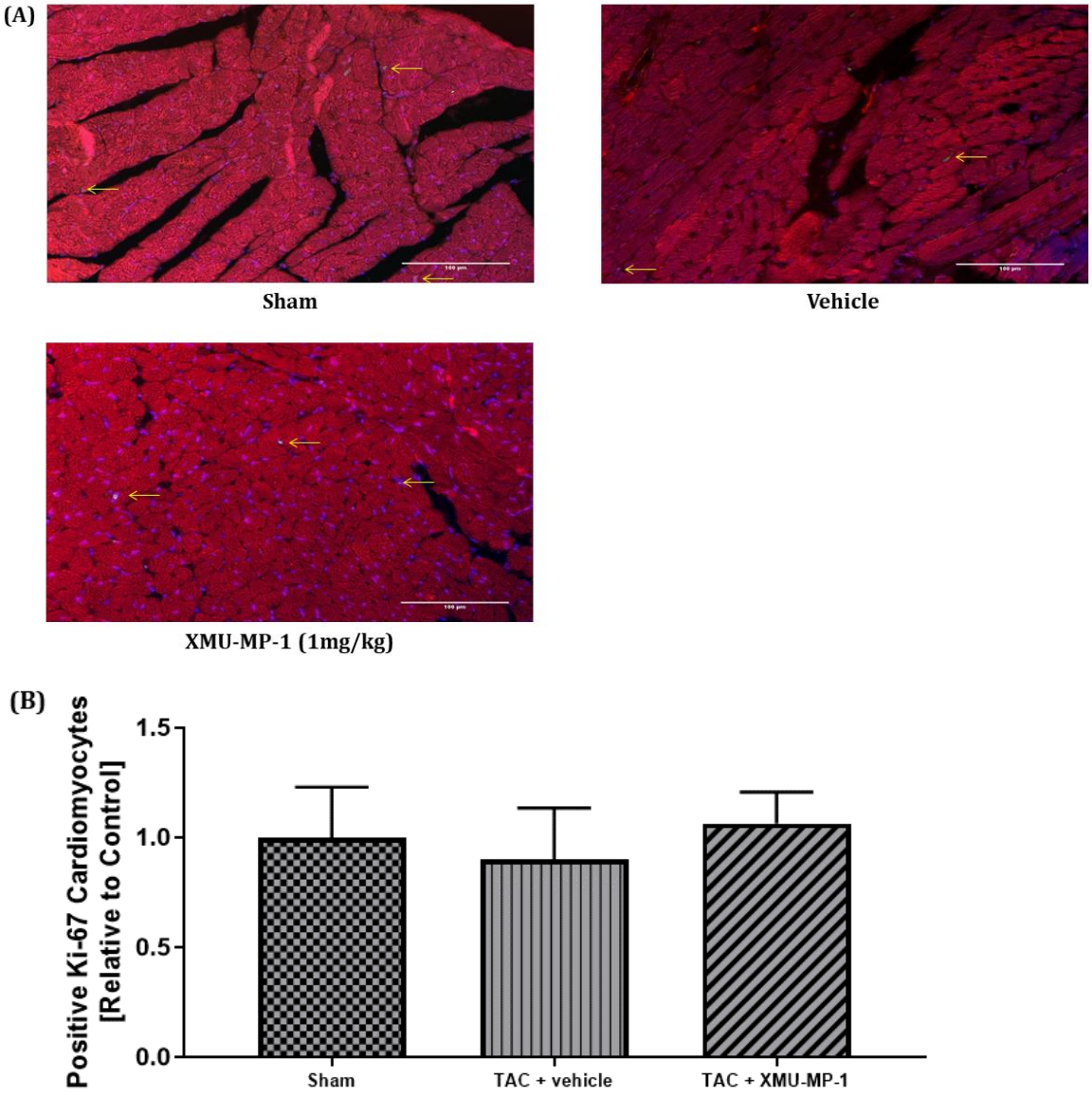

Figure 3.18 Cardiomyocyte proliferation rate as indicated using Ki-67 staining on the heart sections after TAC. (A) Representative images of Ki-67 staining from histological heart sections after the TAC procedure. The co-position of green and blue fluorescence signals indicates positive Ki-67 cells (shown by yellow arrows). (B) The cardiomyocyte proliferation rate is not significantly increased after XMU-MP-1 treatment after TAC. The rate of cardiomyocyte proliferation in the sham, vehicle and XMU-MP-1 treatment groups are 1.00 ± 0.22, 0.90 ± 0.23, 1.06 ± 0.14, respectively. Data (shown as mean ± SEM) were analysed using one-way ANOVA. Sham n=5, vehicle n=10, XMU-MP-1 n=10. More than 1,000 cardiomyocytes were analysed in each mouse. Scale bar = 100 μm.

3.4.10 Analysis of XMU-MP-1 effects on the liver and kidney

Non-specific targeted drug administration can have undesirable consequences called side effects. Moreover, XMU-MP-1 targets the Mst that is available in many organs. Hence, it is necessary to carry out a screening of possible side effects of the XMU-MP-1. In this study, I primarily examined two major organs (the kidney and the liver) that are important in the

pharmacokinetic processes of the drugs. The kidney is an organ responsible for excretion, and most of the drugs are eliminated through the kidney. The liver is an organ where drug metabolism mostly occurs. After the XMU-MP-1 treatment in TAC model mice, some assays were performed, such as Masson's Trichrome staining, serum alanine aminotransferase (ALT) assay, serum creatinine kinase assay and ki-67 staining to observe any side effects in both organs.

My data suggest that there is no significant change in the level of fibrosis (identified using Masson's Trichrome staining), serum ALT and serum creatinine between groups. The ALT test is one of the examination methods for checking liver function. Based on my results, I found that XMU-MP-1 administration five times every two days does not affect liver function. Similarly, creatinine level was used as a marker to assess kidney function. Additionally, 1 mg/kgBW XMU-MP-1 treatment does not alter the kidney function in TAC model mice when assessed using creatinine assay. The results of ALT and creatinine assays are shown in Figure 3.19, whereas Figure 3.20 and Figure 3.21 show the analysis of the fibrotic area in the liver and kidney.

As the XMU-MP-1 treatment modulates the Hippo pathway, one of the consequences is that the Hippo pathway core effector, YAP, becomes more active. The activation of YAP induces an increase in cell proliferation. Based on my *in vitro* data using neonatal rat cardiomyocytes, I found that XMU-MP-1 can increase cell cycle activity (identified using Ki-67 assay). Knowing that cardiomyocytes have a low regeneration capacity and that their proliferation is enhanced by XMU-MP-1 treatment (*in vitro*), there is a necessity to investigate the cell proliferation in other cells. Thus, cell proliferation on the liver and kidney sections was analysed. My results suggest that XMU-MP-1 treatment every alternate day for ten days significantly increases the cell cycle activity as indicated using Ki-67 in liver and kidney tissues (Figure 3.22 and Figure 3.23).

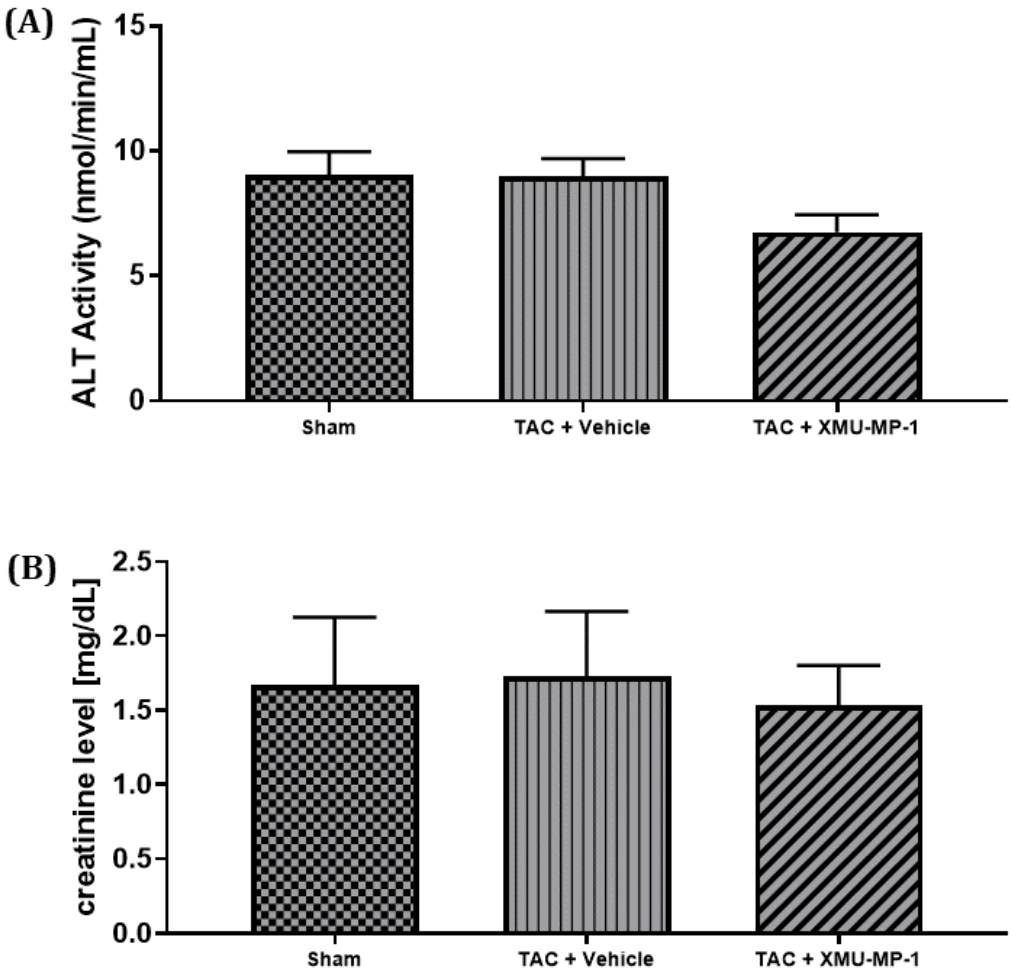

Figure 3.19 The analyses of serum ALT and creatinine levels. (A) There is no significant difference among sham (9.04 ± 0.93 nmol/min/mL), vehicle (8.98 ± 0.71 nmol/min/mL) and XMU-MP-1 (6.76 ± 0.68 nmol/min/mL) groups in terms of serum ALT level. (B) There is no significant difference in serum creatinine level either in sham (1.67 ± 0.46 mg/dL), vehicle (1.73 ± 0.44 mg/dL) and XMU-MP-1 (1.53 ± 0.27 mg/dL) groups. Data (shown as mean ± SEM) were analysed using one-way ANOVA. Sham n=5, vehicle n=10, XMU-MP-1 n=10.

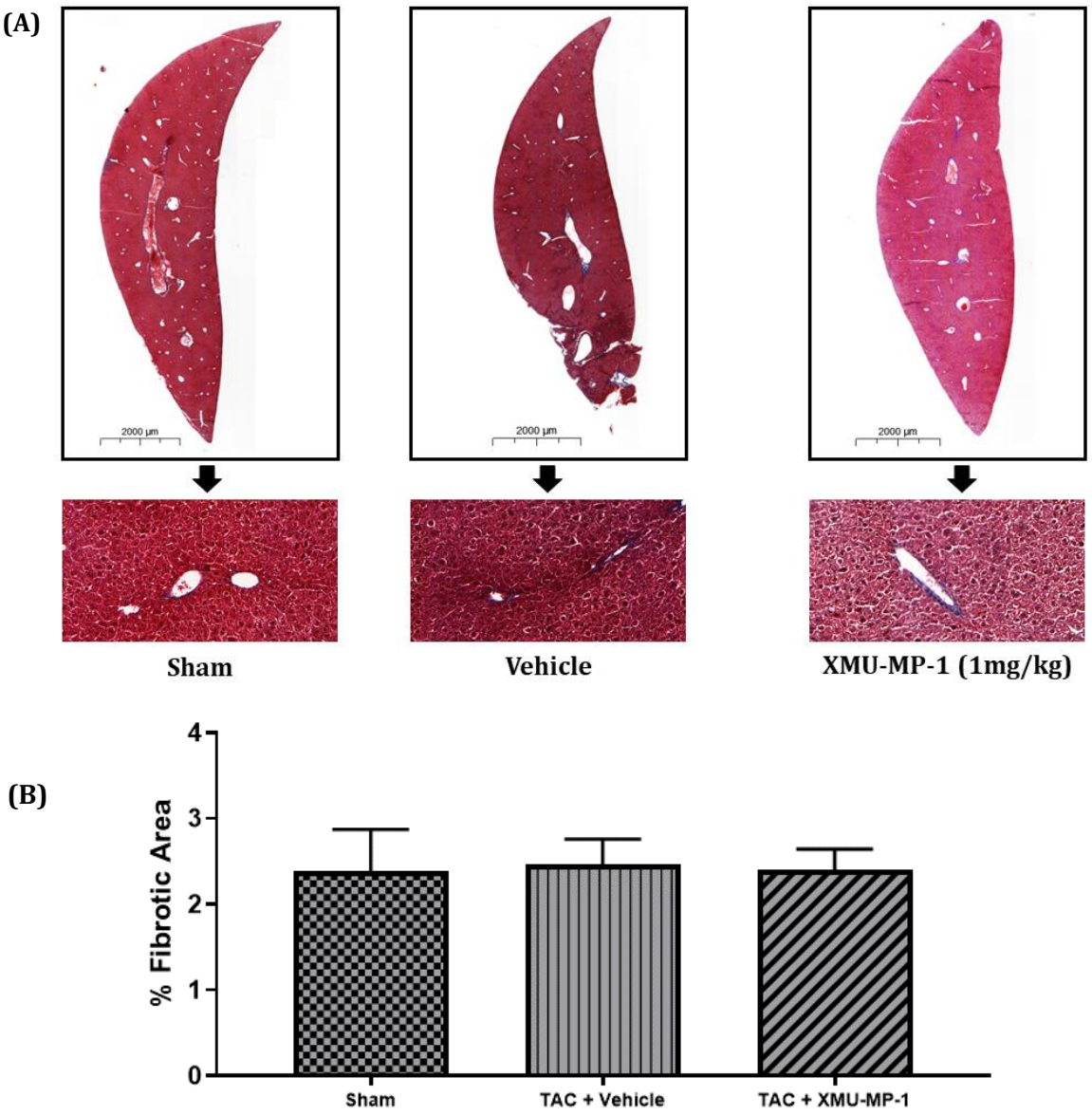

Figure 3.20 Fibrotic area in the liver identified using Masson's Trichrome. (A) There is no significant difference in the liver fibrosis in sham (2.39 ± 0.49 %), vehicle (2.47 ± 0.29 %) or XMU-MP-1 (2.41 ± 0.23 %) groups. Data (shown as mean ± SEM) were analysed using one-way ANOVA. Sham n=5, vehicle n=10, XMU-MP-1 n=10. Scale bar = 2000 µm.

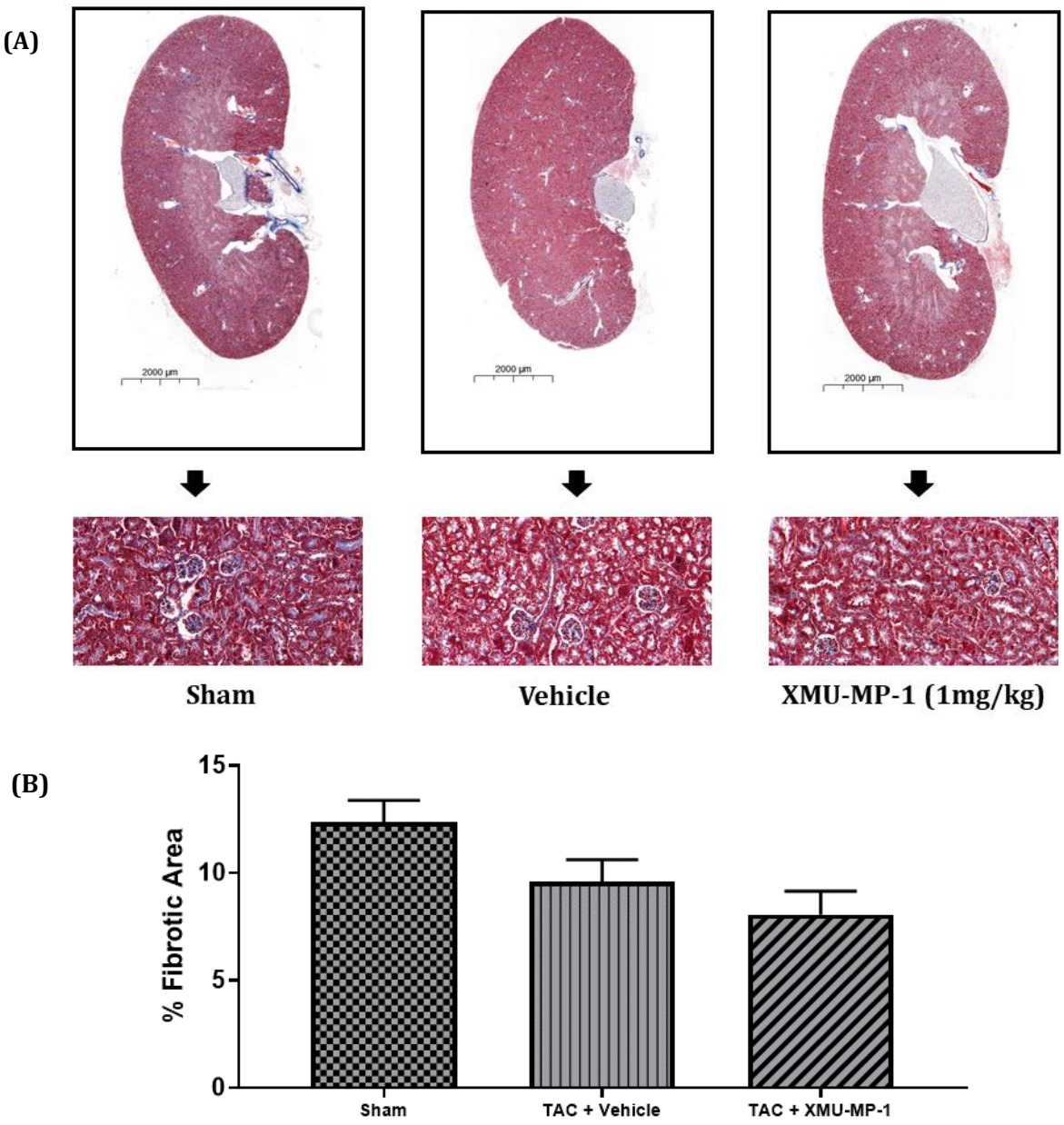

Figure 3.21 Fibrotic area in the kidney identified using Masson's Trichrome. (A) The analysis in the fibrotic area of the kidney suggests that the kidney fibrosis of sham (12.35 ± 1.03 %), vehicle (9.59 ± 1.02 %) and XMU-MP-1 (8.06 ± 1.09 %) groups is not significantly different. Data (shown as mean ± SEM) were analysed using one-way ANOVA. Sham n=5, vehicle n=10, XMU-MP-1 n=10. Scale bar = 2000 µm.

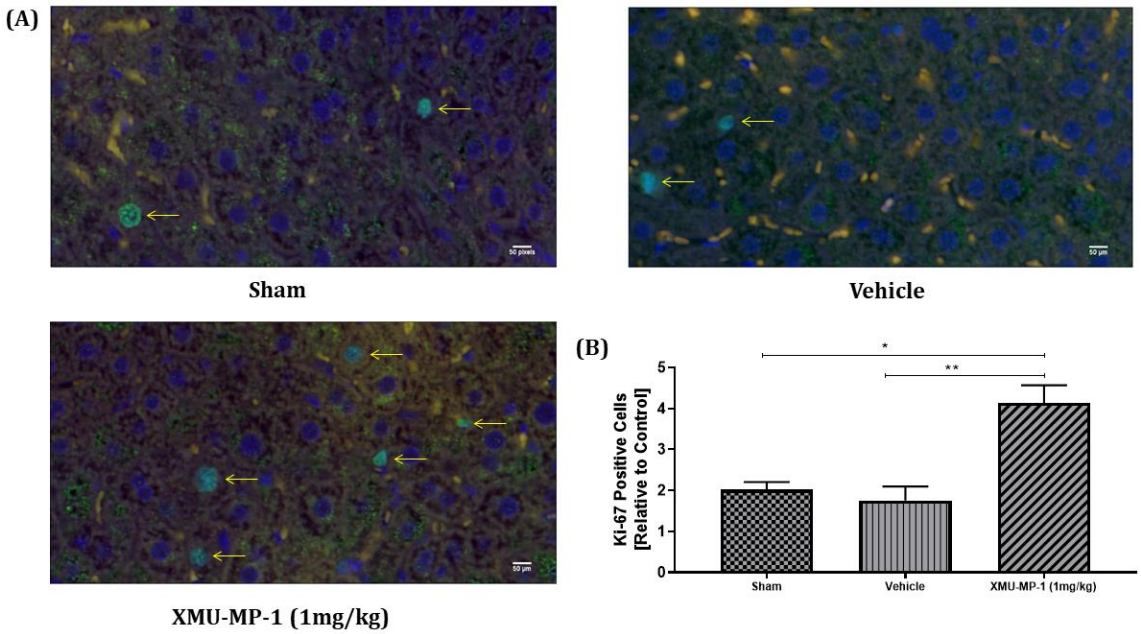

Figure 3.22 Ki-67 staining on the liver sections. (A) Representative images of Ki-67 staining from the histological section of the liver after the TAC procedure. The overlay position of green and blue colour indicates positive Ki-67 cells (shown by yellow arrows). (B) The level of cell proliferation is significantly higher in the XMU-MP-1 treatment group (4.13 ± 0.44 %) when compared to the sham (2.02 ± 0.19 %) and vehicle (1.75 ± 0.34 %) groups. Data (shown as mean ± SEM) were analysed using one-way ANOVA with Tukey's post-hoc test for multiple comparisons, *p<0.05 and **p<0.01 indicate significant differences in results. Sham n=5, vehicle n=10, XMU-MP-1 n=10. More than 1,000 cardiomyocytes were analysed in each mouse. Scale bar = 50 μm.

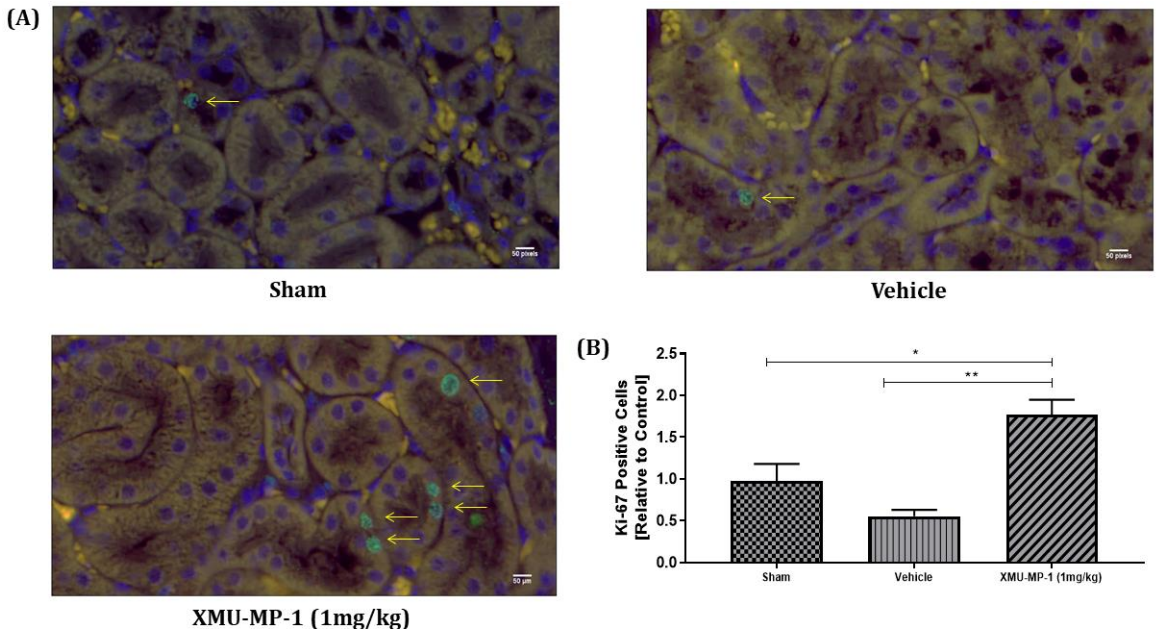

Figure 3.23 Ki-67 staining on the kidney sections in mice after TAC. (A) Representative images of Ki-67 staining from the histological section of the kidney. The overlay position of green and blue colour indicates positive Ki-67 cells (shown by yellow arrows). (B) The rate of Ki-67 positive cells is significantly increased after XMU-MP-1 treatment (1.77 ± 0.18 %) when compared to sham (0.98 ± 0.21 %) and vehicle (0.55 ± 0.08 %) groups. Data (shown as mean ± SEM) were analysed using one-way ANOVA with Tukey's post-hoc test for multiple comparisons, *p<0.05 and **p<0.01 indicate significant differences in results. Sham n=5, vehicle n=10, XMU-MP-1 n=10. More than 1,000 cardiomyocytes were analysed in each mouse. Scale bar = 50 µm.

3.5 Discussion

This chapter addresses the recognised disparity between the progression of adverse cardiac remodelling and the limitations of the pharmacological treatments currently available to prevent heart failure. The lack of pharmacological treatments that are used clinically in reversing cardiac remodelling exposes the need for finding new therapeutic approaches to inhibit the progression of heart failure. The Hippo pathway is one of the pathways involved in the mechanisms underlying the cardiac remodelling process. Given the strong association between the Hippo pathway and organ growth, the modulation of the Hippo pathway in the hypertrophic growth of the heart could be beneficial. The impact of pharmacological inhibition of the Hippo/Mst on the pathological hypertrophy of the heart is indeed fascinating to elaborate on because genetic modification of Mst1/2 of the Hippo pathway has been established to modulate adverse cardiac remodelling. The results of my investigation on XMU-MP-1 treatment in TAC model mice confirm the protective effects of Hippo/Mst inhibition in cardiac remodelling.

3.5.1 XMU-MP-1 induces NRCM proliferation

In 2016, Fuqin Fan and colleagues reported the role of XMU-MP-1 in inhibiting the Hippo kinases (Mst1 and Mst2) and promoting cell proliferation. Their study demonstrated that XMU-MP-1 treatment successfully enhances mouse cell liver proliferation based on Ki-67 and Bromodeoxyuridine (BrdU) stainings. An increase in cell proliferation after XMU-MP-1 treatment was also observed in human hepatocytes transplanted into the mouse liver (Fan et al., 2016).

Consistent with the findings of Fan et al. (2016) regarding the effects of XMU-MP-1 on cell proliferation, my results suggest that the cell proliferation rate is enhanced following XMU-MP-1 (1 and 3 μM) treatment in neonatal rat cardiomyocyte cultures. However, my data from Ki-67 staining on TAC model mice heart sections do not show any statistical difference in cardiomyocyte proliferation after 1 mg/kgBW of XMU-MP-1 treatment every other day for ten days. The possible explanation for this discrepancy is that adult cardiomyocytes have limited regeneration capability. In humans, cardiomyocyte production stops when the heart reaches adult size. Adult cardiomyocytes are mostly terminally differentiated and mitotically inactive. Nonetheless, cardiomyocyte cycle activity can still be measured at a very low level (Zhu et al., 2020). The Hippo pathway is one of the pathways that regulate cardiomyocyte proliferation, meaning that XMU-MP-1 targets the appropriate pathway. The lacking *in vivo* effects of XMU-MP-1 perhaps is a matter of optimisation insufficiency.

The inadequate effects of XMU-MP-1 in the *in vivo* experiment might be due to its inhibition on Mst1/2 not being enough to increase the expression of genes needed in adult cardiomyocyte proliferation. As a comparison, another chemical compound (TT-10) was reported to enhance cardiomyocyte proliferation and ameliorate cardiac function post-MI through direct activation of YAP-TEAD binding (Hara et al., 2018). Additionally, XMU-MP-1 at the dose regimentation I administered (1 mg/kgBW every alternate day for ten days) is possibly not adequate. I adapted the dose regimentation from the study of Fan et al. (1 mg/kgBW). However, due to my project license regulation for animal study, I am only allowed to inject the mice once per day and not more than five injections in total, which is different from the dosage administered by Fan et al. (1 mg/kgBW twice per day for 21 days).

The effects of XMU-MP-1 in cell proliferation were more convincing in my *in vitro* experiments using NRCM culture. Detected using a Ki-67 assay, XMU-MP-1 significantly increases cardiomyocyte proliferation at the dose of 1 and 3 μM. Interestingly, the effects of XMU-MP-1 in cardiomyocyte proliferation seem to decrease in a higher dose (5 μM). The reduction of the XMU-MP-1 effects in cardiomyocyte proliferation might be due to its toxicity, considering that my TUNEL and MTT assays in NRCMs show that 5 μM XMU-MP-1 has slightly higher apoptosis and less viability than the dose of 3μM.

The association between Mst and cardiomyocyte proliferation has been studied previously. The complex formed of Mst and a scaffolding protein (Sav) activates a tumour suppressor kinase (LATS). Consistently, the cardiac-specific knockout of Mst leads to dissociation of the Mst-Sav complex and LATS inactivation. As a consequence, cardiomyocyte proliferation is increased significantly (Heallen et al., 2011).

My results suggest that the inhibition of the Hippo/Mst using XMU-MP-1 promotes YAP activation significantly. YAP activation, attributed to XMU-MP-1 treatment, was detected using the GAL4-TEAD luciferase system, GFP-YAP immunofluorescence and western blot. The activation of YAP is strongly related to the increase in cardiomyocyte proliferation. A previous study revealed that YAP overexpression using an adenoviral vector enhanced fetal cardiomyocyte proliferation. The activation of YAP could also increase the fetal cardiomyocyte proliferation *in vivo* by promoting pro-proliferation genes, such as cyclins D1 and D2 (von Gise et al., 2012).

3.5.2 XMU-MP-1 reduces cardiomyocyte apoptosis

My experiments (both in NRCMs and TAC model mice) suggest that XMU-MP-1 can protect cardiomyocytes from apoptosis. To induce apoptosis in cardiomyocytes, I treated the cell with 200 μM of hydrogen peroxide for four hours. The dose and duration of hydrogen peroxide used in my experiments were based on the optimisation of its effect in inducing cell apoptosis and reducing cell viability.

Mst1/2 are vital regulators of apoptosis and cell death. When there is an apoptosis stimulus, Mst becomes a direct substrate of caspase and is activated through proteolytic cleavage (Lee et al., 1998). The Mst stimulation outcome is the activation of caspase-3 to execute apoptosis (Lee et al., 2001). Mst also plays a crucial role in cardiomyocyte survival and death in cellular stress conditions. Activated Mst1 during cardiac stress phosphorylates Beclin1, which then associates with Bcl-2. The complex of Beclin1 and Bcl-2 promotes protein aggregation and induces cardiomyocyte apoptosis. Additionally, the phosphorylation of Beclin1 by Mst1 results in the dissociation between Bcl-2 and Bax. Free Bax enters into the mitochondria and releases cytochrome-c, leading to cardiomyocyte apoptosis (Dhingra and Kirshenbaum, 2013). Furthermore, the cardiomyocyte-specific knockout of Mst1 in mice protects cardiomyocytes from apoptosis after Angiotensin II induction, accompanied by the reduction of cleaved caspase-3, Bax and phosphorylated JNK expressions (Cheng et al., 2019).

The role of Mst1/2 in cell apoptosis is also associated with their action on the Hippo effectors, YAP/TAZ. Mst1/2 activation will activate kinase cascade in the Hippo signalling

pathway and subsequently phosphorylate YAP/TAZ. The role of YAP/TAZ in gene transcription is diminished when they are phosphorylated. YAP activity directly affects the expression of mitochondria-associated genes such as Dynamin-related protein 1 (*Drp1*), Jun amino-terminal kinases (*Jnk*), extracellular signal-regulated kinase (*Erk*) and AMP-activated protein kinase (*Ampk*). Those genes are strongly associated with cell apoptosis and survival (Piccolo et al., 2014). YAP activation was reported to preserve cardiac function by inhibiting apoptosis induced by mitochondrial fission related to the mitogen-activated protein kinase (MAPK)–ERK pathway (Ma and Dong, 2019).

Consistent with previous studies associating Mst1/2 and apoptosis, my results show that Mst1/2 inhibition using XMU-MP-1 could inhibit cardiomyocyte apoptosis. The inhibition of apoptosis in cardiomyocytes is followed by less expression of cleaved caspase-3 (an apoptosis marker). My *in vivo* experiment also shows a reduction in cardiac fibrosis following XMU-MP-1 treatment. This result suggests that XMU-MP-1 successfully inhibits the involvement of Mst in cardiac stress. The effect of XMU-MP-1 in preventing cardiomyocyte apoptosis and cardiac fibrosis is possibly mediated by YAP activation. YAP is well-known as a potent regulator of cell survival. YAP was also reported to enhance cardiomyocyte survival and reduce cardiomyocyte apoptosis by upregulating Akt1. Supporting data from the study of Del Re et al. (2013) suggest that YAP deficiency results in the deterioration of cardiac injury in chronic MI (Del Re et al., 2013).

3.5.3 XMU-MP-1 related to cardiomyocyte hypertrophy

Increased cardiac workload promotes the pathological growth of the heart, including abnormal cardiomyocyte enlargement. Prolonged hypertrophic stimuli to the heart will cause ventricular wall thickening and ultimately result in heart failure (Tham et al., 2015). Therefore, treatment strategies in preventing adverse cardiac hypertrophy are needed.

The role of the Hippo pathway in cardiac hypertrophy has been discussed extensively. However, contracditory findings from previous studies make it difficult to assert whether Hippo pathway inhibition promotes or attenuates cardiac hypertrophy. Yang et al. revealed that downstream signals to the Hippo pathway cause YAP activation that induces cardiac hypertrophy via acceleration of miR-206 transcription and degradation of Foxp1 mRNA (Yang et al., 2015). Nonetheless, a study by Windmueller and Morrisey opposed the exclusive association between YAP and Foxp1 that was reported by Yang et al. They suggested that activation of both YAP and miR-206 results in cardiomyocyte enlargement, but YAP activation has other support mechanisms apart from Foxp1 effects, whereas miR-206 activation depends on Foxp1 activity (Windmueller and Morrisey, 2015). However, in

2011 Xin et al. demonstrated that YAP overexpression in mice resulted in an increase of cardiomyocyte proliferation and a decrease in cardiomyocyte size (Xin et al., 2011a).

Furthermore, the downregulation of the Hippo components (Sav and LATS1/2) enhances cardiomyocyte proliferation without affecting the size (Heallen et al., 2011). Another Hippo component, Mst1, was reported to induce cardiomyocyte apoptosis without any association with cardiomyocyte hypertrophy (Odashima et al., 2007; Yamamoto et al., 2003). Interestingly, a study by Zi et al. demonstrated a strong association between Mst2 and cardiomyocyte hypertrophy. Mst2 knockout results in the inhibition of cardiomyocyte hypertrophy, whereas hypertrophy is associated with Mst2 overexpression (Zi et al., 2014).

My data support the findings from previous studies by Xin et al., Odhasima et al., and Zi et al. My *in vitro* experiment using neonatal rat cardiomyocytes reveals the effect of XMU-MP-1 in inhibiting phenylephrine-induced hypertrophy. In my study, I used 50 μM of phenylephrine to induce cardiomyocyte hypertrophy. This dose was chosen after I conducted several optimisation experiments measuring BNP activity. Additionally, phenylephrine at the dose of 50 μM was also used in a study examining the role of ERK in cardiomyocyte hypertrophy (Yue et al., 2000). Based on my experiments, 24 hours treatment of 50 μM phenylephrine can induce BNP activity when determined using BNP-luciferase transporter. Besides, I observed an increase in cardiomyocyte size after 50 μM of phenylephrine treatment for 72 hours.

3.5.4 The relationship between XMU-MP-1 and adverse cardiac remodelling

As mentioned before, XMU-MP-1 can prevent cardiomyocytes from apoptosis and hypertrophy, along with increasing cardiomyocyte proliferation. Those qualities are essential in protecting the heart from mechanical stress-induced adverse cardiac remodelling. Cardiomyocyte death is a major incident that occurs during adverse cardiac remodelling. A significant loss of cardiomyocytes in the heart causes weakened cardiac contractility. Along with cardiomyocyte death, other conditions occurring during adverse cardiac remodelling, such as cardiac fibrosis and hypertrophy, contribute to cardiac function deterioration.

The effects of XMU-MP-1 in cardiomyocyte apoptosis, hypertrophy and proliferation have been explained above. Here I will discuss the relationship between the Hippo pathway and cardiac fibrosis. The evidence shows a strong association between Hippo component modulation and the development of cardiac fibrosis. For instance, downregulation of the Hippo effector, YAP, develops dilatation and fibrosis in the heart (Del Re et al., 2013). Also,

Mst1 over-expression in mice causes premature death with cardiac fibrosis (Yamamoto et al., 2003).

By and large, the Hippo system regulates cardiac fibrosis during adverse cardiac remodelling through its components, YAP and Mst1. Therefore, I found that it is necessary to determine the cardiac fibrosis level following XMU-MP-1 treatment in TAC model mice. And yet, my data suggest that XMU-MP-1 significantly suppresses the cardiac fibrosis level after TAC surgery compared to the mice that underwent TAC surgery treated with the vehicle. The combined effects of XMU-MP-1 in inhibiting Mst1 and activating YAP have a beneficial outcome in mice with pressure overload.

3.5.5 Effects of XMU-MP-1 treatment in the liver and kidney

As I administered XMU-MP-1 intraperitoneally without any specific-targeted delivery system, it is essential to screen the possible side effects of XMU-MP-1, primarily non-targeted organ effects. As mentioned above, I performed some assays to check the function of the liver and kidney. All the results were compared to the sham control as the healthy normal standard.

The level of ALT in the serum was determined to check the liver function because ALT is highly reproducible and more specific. ALT is usually used to predict hepatocellular injury (Kwo et al., 2017). Regardless of some doubts about the reliability of the creatinine level, the level of creatinine in serum was used to determine kidney function. This decision is based on the similarities in the mice used in terms of the average weight, strain and age. Hence, the individual variation was minimised. The serum creatinine level is still used to predict kidney abnormalities (Kellum et al., 2015).

My results in determining serum ALT and creatinine levels demonstrate that XMU-MP-1 does not affect liver and kidney function. Moreover, my experiments in analysing the liver and kidney fibrosis also do not show any significant difference between XMU-MP-1 treated mice compared to the sham and vehicle groups. However, when I performed Ki-67 staining on both the liver and kidney sections, I found an increase in cell proliferation in mice treated with XMU-MP-1. These findings confirm the previous study results that XMU-MP-1 treatment can increase hepatocyte proliferation (Fan et al., 2016).

The explanation about the difference in cardiomyocyte, hepatocyte and kidney cell proliferation is the distinctive sensitivity of the cells in responding to XMU-MP-1 effects. Moreover, cardiomyocytes are known to be cells with limited regeneration capacity, so they probably need more stimuli to induce their proliferation. Another explanation is due to the possible variation of the XMU-MP-1 distribution rate in those organs. In order to obtain

exact information, a comprehensive pharmacokinetic experiment needs to be done. My data on the kidney and liver proliferation rates suggest that we need to be aware of any possibility of cancer development in other organs.

3.6 Conclusion

The results of my study contribute to the justification of the association between the Hippo pathway and adverse cardiac remodelling. Knowing that current pharmacological therapies cannot fundamentally reverse cardiac remodelling, my data encourage a new way of inhibiting the progression of adverse cardiac remodelling through the inhibition of Mst1/2 of the Hippo pathway. I also provide some additional insights, such as using a chemical substance (XMU-MP-1) inhibiting the Mst1/2 can alleviate adverse cardiac remodelling and prevent cardiac hypertrophy and apoptosis. In conclusion, Mst1 and Mst2 of the Hippo pathway play essential roles in the progression of adverse cardiac remodelling, making them promising therapeutic targets.

CHAPTER 4

THE EFFECTS OF XMU-MP-1 TREATMENT ON MOUSE MODEL OF MYOCARDIAL INFARCTION

4.1 The theoretical overview and conceptual frameworks

Myocardial infarction (MI) is a type of acute heart disease that causes massive numbers of cardiomyocyte deaths. Cardiomyocyte death in myocardial infarction occurs as a result of an ischaemic condition due to coronary arterial occlusion that causes a deficiency of blood and oxygen supply into the heart (Saraste et al., 1997). The ischaemic condition will cause cell death, mainly due to necrosis and apoptosis. Otherwise, the limited capacity of adult cardiomyocytes in regeneration results in inadequacy for responding to extensive heart damage. A profound loss of cardiomyocytes induces cardiac dysfunction, which further provokes cardiac remodelling-induced heart failure, and ultimately, it can result in sudden death (Sutton and Sharpe, 2000).

The lack of blood supply into the heart during myocardial infarction can be reversed using reperfusion treatments. However, despite the valuable effects of reperfusion therapy in reducing infarct size and short-term death after an infarction attack, reperfusion injury is strongly related to the development of heart failure post-myocardial infarction. In the infarction area, most cells undergo irreversible destruction (Fliss and Gattinger, 1996). On the other hand, some cells in the border area go through biochemical changes to compensate for ischaemic conditions. The adapted processes include energy efficiency, ionic regulation, substrate utilisation and fluid haemostasis that make the cells viable (Piper et al., 1998). On the other hand, reperfusion therapy forces the cells to encounter immediate changes during reverse ischaemic conditions. The rapid changes inside the cells can trigger cell homeostasis disruption, which eventually results in cell necrosis (Maxwell and Lip, 1997).

It is useful to find new approaches to protect the heart against adverse cardiac remodelling post-myocardial infarction and heart failure progression. A crucial point in impeding heart failure progression is preserving cardiomyocyte viability, either reducing apoptosis or increasing regeneration. As previously described in Chapter 1 and Chapter 3, the Hippo pathway is involved in the regulation of cell proliferation and cell apoptosis. Hence, the modulation of the Hippo pathway is potentially beneficial for alleviating post-infarction cardiac remodelling. Moreover, previous studies have shown that Hippo pathway modulation exhibited favourable effects in myocardial infarction conditions, for example, the activation of the Hippo effector, YAP, is protective against myocardial infarction through enhancing cardiomyocyte survival (Shao et al., 2014). This chapter discusses the effects of a small molecule targeting the Hippo/Mst called XMU-MP-1 at the dose of 1 mg/kgBW in mice that underwent coronary artery ligation. I have two different approaches to investigate the effects of XMU-MP-1 in myocardial infarction, and they include the administration of XMU-MP-1 in both acute (XMU-MP-1 was administered straight after coronary artery

ligation) and sub-acute conditions (XMU-MP-1 treatment began three weeks after MI surgery). The projection role of XMU-MP-1 in the MI heart is outlined in Figure 4.1.

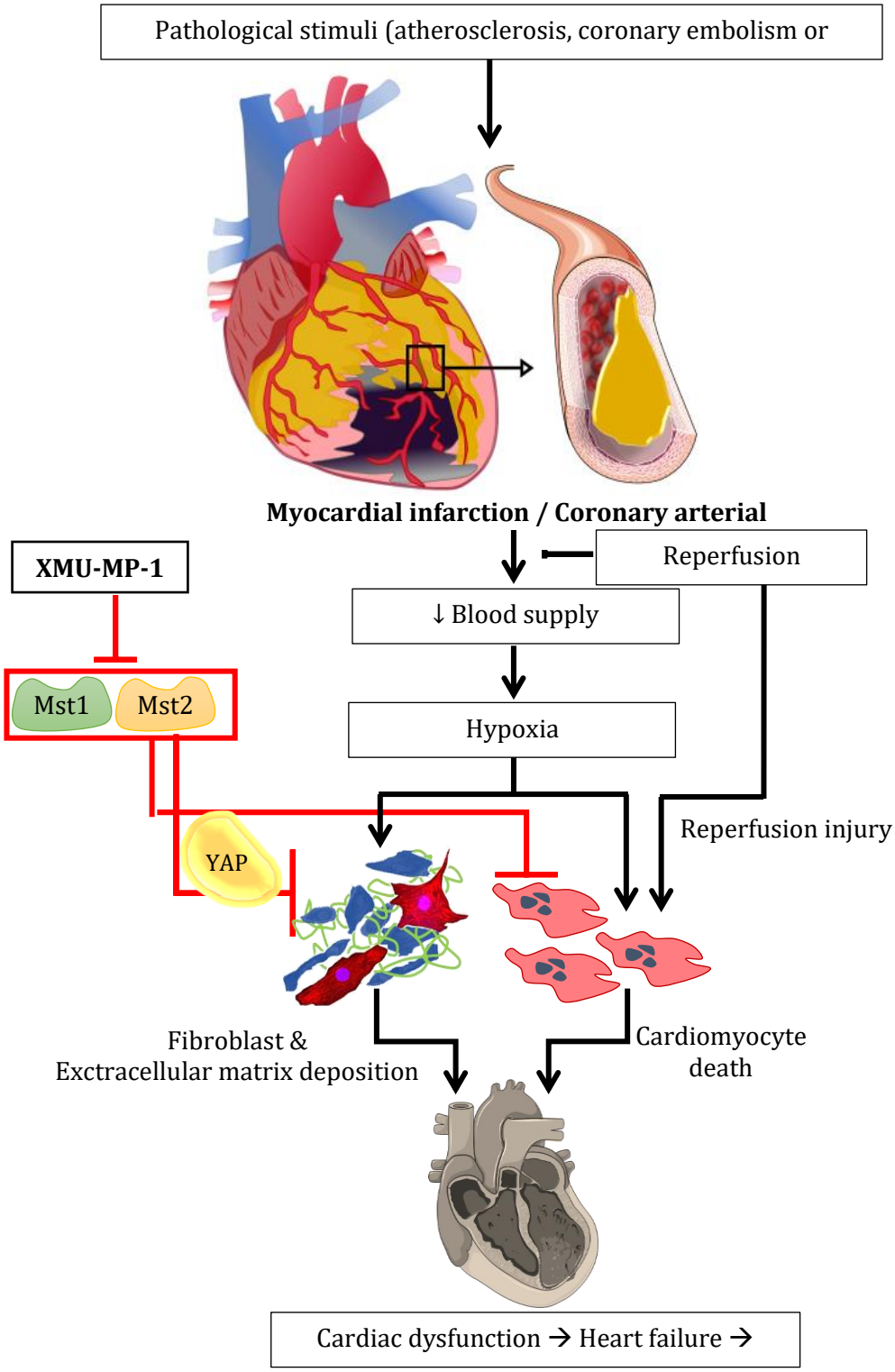

Figure 4.1 potential action of XMU-MP-1 in myocardial infarction. Pathological stimuli such as atherosclerosis, arterial embolism and thrombosis can obstruct the coronary artery of the heart. This blockage provokes myocardial infarction. Reperfusion therapies can reverse the ischaemic condition and restore blood supply. However, reperfusion injury might occur and induce cardiomyocyte death. XMU-MP-1 activates YAP, which potentially prevents heart failure by reducing cardiomyocyte death and cardiac fibrosis.

4.2 Aims

This chapter mainly focuses on the analysis of cardiac phenotypes of the mouse model of MI following XMU-MP-1 treatment. The specific objectives are as follows:

- To explore how XMU-MP-1 treatment amends survival and cardiac phenotypes of the mice in acute MI.
- To determine if XMU-MP-1 treatment is beneficial when given in sub-acute MI.

4.3 Hypotheses

I hypothesise that increased YAP activity via inhibition of Mst1/2 by XMU-MP-1 can enhance cardiomyocyte survival after MI surgery. Cardiomyocyte apoptosis might be attenuated through the blockade of Mst1 activity by XMU-MP-1 in MI model mice. Inhibition of Mst2 by XMU-MP-1 can suppress cardiomyocyte hypertrophy and prevent cardiac remodelling after MI surgery.

4.4 Results

In this chapter, I studied the effects of XMU-MP-1 in a different disease model, i.e., myocardial infarction. Based on the *in vitro* and *in vivo* experiments discussed in Chapter 3, antihypertrophic and antiapoptotic effects of XMU-MP-1 were identified in NRCMs and mouse models of pressure overload. Therefore, I decided to extend the application of XMU-MP-1 treatment in the MI model mice. I postulated that inhibition of the Hippo/Mst using XMU-MP-1 could alleviate the MI condition by inhibiting cardiomyocyte death. The dose regimentation of XMU-MP-1 applied in the MI model mice is the same as its regimentation in the TAC model mice (1 mg/kgBW, every other day within ten days). I conducted two sets of MI experiments with two different starting points of XMU-MP-1 treatment. The first MI experiment allocated the XMU-MP-1 treatment right after MI surgery. The idea of this design is to determine the effects of XMU-MP-1 in acute MI conditions. The second experimental design is delaying the XMU-MP-1 treatment after the acute phase in MI has been passed. In my second MI experiment, XMU-MP-1 treatment was administered three weeks after MI surgery. The sham group was set as the normal control. As a comparison, some MI model mice were also treated with the vehicle (50% DMSO + 50% water) to assure that the XMU-MP-1 solvent does not affect the results. The experimental designs of acute and sub-acute MI in this study are outlined in Figure 2.8 and Figure 2.9.

4.4.1 Investigation of XMU-MP-1 treatment following acute myocardial infarction modifies cardiac phenotypes

This experiment is relevant in demonstrating that massive cardiomyocyte death during MI can be alleviated by inhibiting the Hippo pathway. The role of XMU-MP-1 in inhibiting the Hippo/Mst can protect cardiomyocytes from apoptosis and necrosis after TAC. Therefore, XMU-MP-1 treatment potentially eases MI morbidity.

4.4.1.1 Overall survival at the end of acute MI experiment

As an acute pathological condition, MI attack has a high mortality rate. Overall survival in the MI experiment is an important outcome in evaluating the effectiveness of the treatments. In my acute MI experiment, mice that underwent MI surgery were treated with XMU-MP-1 at the end of the MI surgery up until ten days afterwards (when the experiment was concluded). Overall survival was evaluated at the end of the experiment to see if XMU-MP-1 can reduce the mortality rate after MI surgery. A Kaplan Meier curve and a Log-rank test were performed to compare overall survival among treatment groups.

Based on the overall survival analysis, there is no significant difference among the three groups, with a total of 20 mice used (see Figure 4.2). The rate of mortality both in the vehicle group and the XMU-MP-1 group is 28%. Two mice of the XMU-MP-1 group were found dead on day four after the MI surgery, whereas in the vehicle group, one mouse was found dead on day four after MI surgery and another one died the day after. Two mice were excluded from analyses because they died due to surgical complications (they did not recover after the surgical procedure).

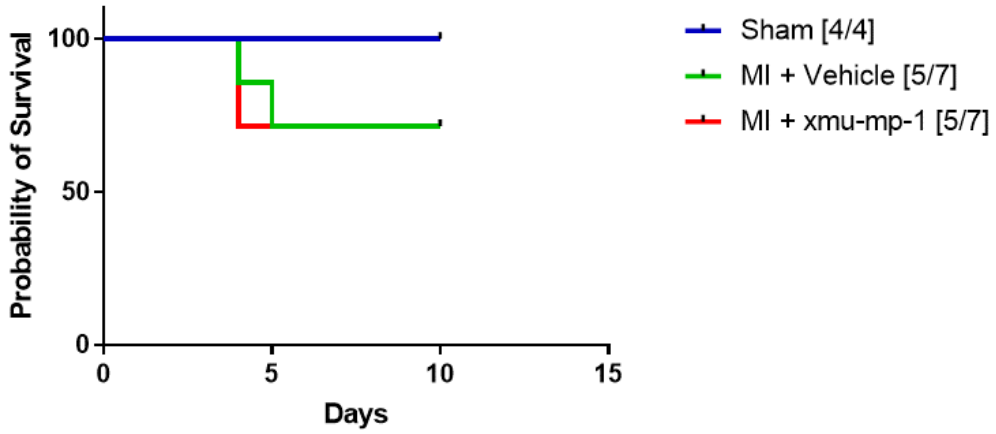

Figure 4.2 The Kaplan Meier survival curve of XMU-MP-1 treated mice following MI surgery compared to the vehicle and sham groups. There is no significant difference in overall survival observed from day 0 to day ten after MI surgery. All mice in the sham group survived up to the end of the experimental period. Two out of seven mice from each XMU-MP-1 and vehicle groups died between day four and day five after the MI surgery. Data were analysed using a Log-rank (Mantel-Cox) test. Sham n=4, vehicle n=7, XMU-MP-1 n=7.

4.4.1.2 Cardiac structure and function of acute MI model mice following XMU-MP-1 treatment

The ligation of the left anterior descending artery promotes an ischaemic condition in the heart that eventually results in heart failure. Right after the ligation in the left anterior descending artery, there is an impulse force of cell death and tissue inflammation, followed by the cardiac remodelling process. The left ventricular mass to body weight ratio, together with the diastolic and systolic diameters from echocardiography analysis were assessed to determine the extent of cardiac remodelling at the initial phase following MI. The echocardiography parameters are measured before and after treatments. Therefore, only mice that survived until the end of the experiment were analysed. Mice that died within the treatment period were excluded because mortality can be caused by other factors outside the treatments.

The left ventricular mass to body weight ratio is one of the echocardiography parameters that shows left ventricular dilatation. Based on my data (see Figure 4.3), there is a significant increase in the left ventricular mass to body weight ratio within ten days after MI surgery. However, no significant difference is observed between the XMU-MP-1 and vehicle groups.

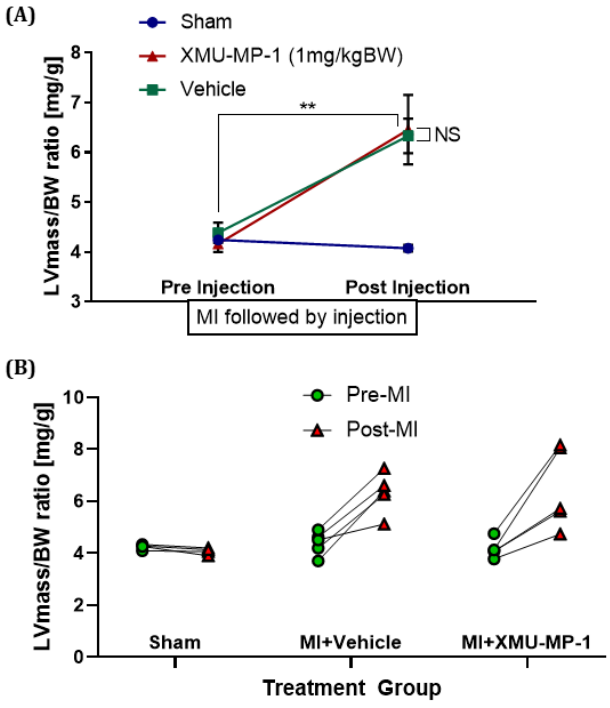

Figure 4.3 Left Ventricular mass to body weight ratio in mice, ten days following MI surgery. MI surgery distinctly enhances the ratio between left ventricular mass and body weight. A. A substantial increment of left ventricular mass to body weight ratio is observed in the vehicle (from 4.39 ± 0.21 before MI surgery to 6.33 ± 0.35 ten days following MI surgery) and XMU-MP-1 (from 4.16 ± 0.16 before MI surgery to 6.46 ± 0.69 ten days following MI surgery) groups. The sham mice show a steady value before (4.24 ± 0.05) and after (4.08 ± 0.07) MI surgery. There is no significant difference between the vehicle and XMU-MP-1 groups. B. Individual plot of LV mass to body weight ratio before and after MI surgery. Data are presented as mean ± SEM and analysed using two-way ANOVA with Tukey's post-hoc test for multiple comparisons. **p<0.01 indicates significant differences in results. NS: not significant. Sham n=4, vehicle n=5, XMU-MP-1 n=5.

Other echocardiography parameters that can exemplify the left ventricular dilatation are the systolic left ventricular internal diameter (sLVID) and diastolic left ventricular internal diameter (dLVID). Both sLVID and dLVID also can indicate cardiac function because they show left ventricular contractility. My results suggest that ten days after MI surgery, both sLVID and dLVID parameters are increased. The XMU-MP-1 treated mice show a higher left ventricular dilatation compared to the vehicle group. Nevertheless, the difference between the vehicle and XMU-MP-1 groups is not statistically significant (illustrated in Figure 4.4).

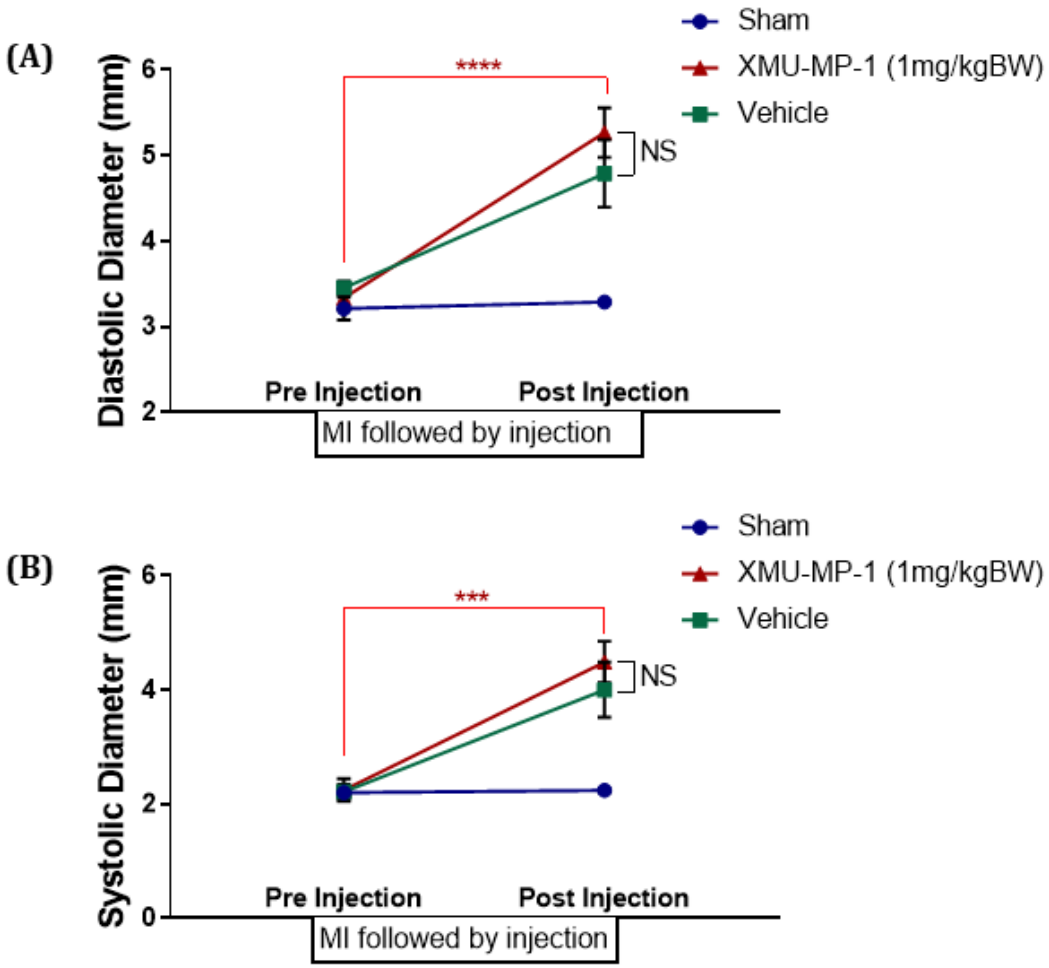

Figure 4.4 Left ventricular dimensions ten days post-MI. Both systolic and diastolic left ventricular diameters are significantly escalated on day ten after MI surgery. (A) The dLVID increases from about three mm at the baseline to approximately five mm on day ten after MI surgery. (B) The sLVID is increased around twice higher from the baseline. At the end of the experiment, the XMU-MP-1 group showed a small but not significant increase in sLVID (4.48 ± 0.19 mm in the XMU-MP-1 group compared to 4.00 ± 0.48 in the vehicle group) and dLVID (5.27 ± 0.29 mm in the XMU-MP-1 group and 4.79 ± 0.39 in the vehicle group). Data are presented as mean ± SEM and analysed using two-way ANOVA with Tukey's post-hoc test for multiple comparisons. ***p<0.001 and ****p<0.0001 indicate significant differences in results. NS: not significant. Sham n=4, vehicle n=5, XMU-MP-1 n=5.

Morphometric and echocardiographic parameters were measured to confirm if cardiac dilatation following the MI surgical procedure is affected by the treatments (see Table 4.1). Calculation of the heart weight to tibia length ratio is one of the morphometric variables used to examine the dilated heart. I found a small but not significant increase in the ratio between the heart weight and tibia length of the mice that underwent MI surgery compared to the sham group. However, there was no significant difference between the XMU-MP-1 and the vehicle groups.

Additionally, I analysed left ventricular posterior wall thickness (LVPW) both during diastole and systole (see Table 4.1). They are echocardiography parameters that can show if the dilated heart is accompanied by wall thinning. There was a small reduction in diastolic LVPW of mice that underwent MI surgery, but this was not statistically significant compared to the sham group. The systolic LVPW of XMU-MP-1 treated mice is thinner but not statistically significant than that in the vehicle-treated mice. The systolic LVPW of the sham group is significantly thicker than that in the XMU-MP-1 group ($P<0.01$) and vehicle group ($P<0.05$).

Table 4.1 Morphometric measurements ten days after MI surgery

Parameters	Treatment groups		
	Sham	Vehicle	XMU-MP-1
Heart weight (mg)	149.80 ± 4.09	172.00 ± 13.93	220.00 ± 43.24
Lung weight (mg)	154.30 ± 5.04	176.80 ± 23.93	190.00 ± 30.26
Body weight (g)	28.13 ± 0.82	29.26 ± 0.58	27.90 ± 0.59
Heart weight/Tibia Length (mg/mm)	0.73 ± 0.03	0.89 ± 0.07	1.03 ± 0.14
Diastolic LVPW (mm)	0.92 ± 0.03	0.85 ± 0.07	0.79 ± 0.05
Systolic LVPW (mm)	1.44 ± 0.02	1.20 ± 0.07	1.10 ± 0.04

Both cardiac structure and function are essential parameters that should be monitored in the condition of myocardial infarction. Ejection fraction (EF) and fractional shortening (FS) are echocardiography parameters that were used to determine cardiac function. I analysed the change in cardiac function before and ten days after MI surgery. The difference in cardiac function was assessed among and within treatment groups. I found that the EF and FS were reduced significantly after MI surgery when compared to the control sham. There was no significant difference in cardiac function parameters between the XMU-MP-1 and vehicle groups on day ten after MI surgery. However, the EF and FS values in the XMU-MP-1 group were less than the vehicle group but were not statistically significant (shown in Figure 4.5).

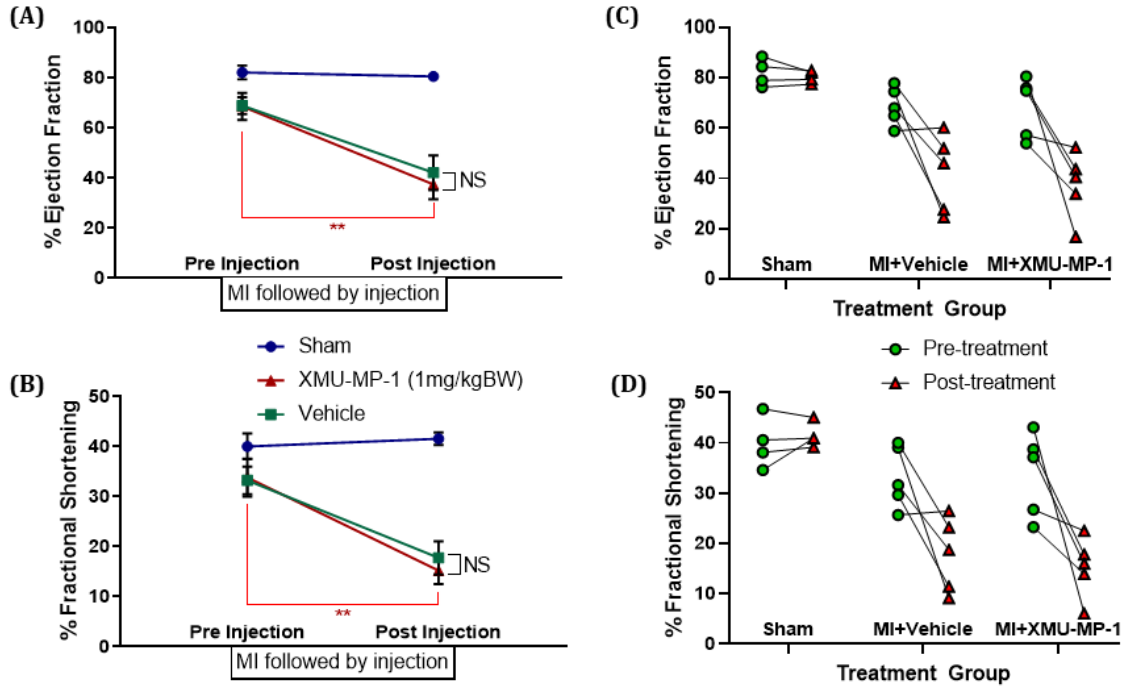

Figure 4.5 The assessment of ejection fraction and fractional shortening on day ten after MI surgery. Cardiac contractility, indicated by the EF and FS, is attenuated after the MI procedure. (A) The average EF value is decreased by around 40% from the baseline level after MI surgery (37.45 ± 5.96 % in the XMU-MP-1 group, 42.08 ± 6.91 % in the vehicle group and 78.43 ± 0.56 % in the sham group). (B) The FS reduction after the MI procedure is around 50% compared to the baseline level. The following are mean values of the FS: 15.21 ± 2.69 % in the XMU-MP-1 group, 17.73 ± 3.33 % in the vehicle group and 40.04 ± 0.52 % in the sham group. (C&D) Individual plots of EF and FS in the acute MI experiment. Data are presented as mean ± SEM and analysed using two-way ANOVA with Tukey's post-hoc test for multiple comparisons. **p<0.01 indicates significant differences in results. NS: not significant. Sham n=4, vehicle n=5, XMU-MP-1 n=5.

Following the EF and FS measurements, the correlation between both parameters and the concentration of cardiac Troponin I (cTnI) in plasma was further assessed. The cTnI value indicates the severity of MI as it is expressed in the myocardium and then released into the bloodstream. The correlation between Ef or FS and cTnI was analysed in all groups using the Spearman correlation test. The results show that EF and FS have a strong negative correlation with the cTnI value. Four out of five mice in the XMU-MP-1 group have EF values under the linear curve (Illustrated in Figure 4.6).

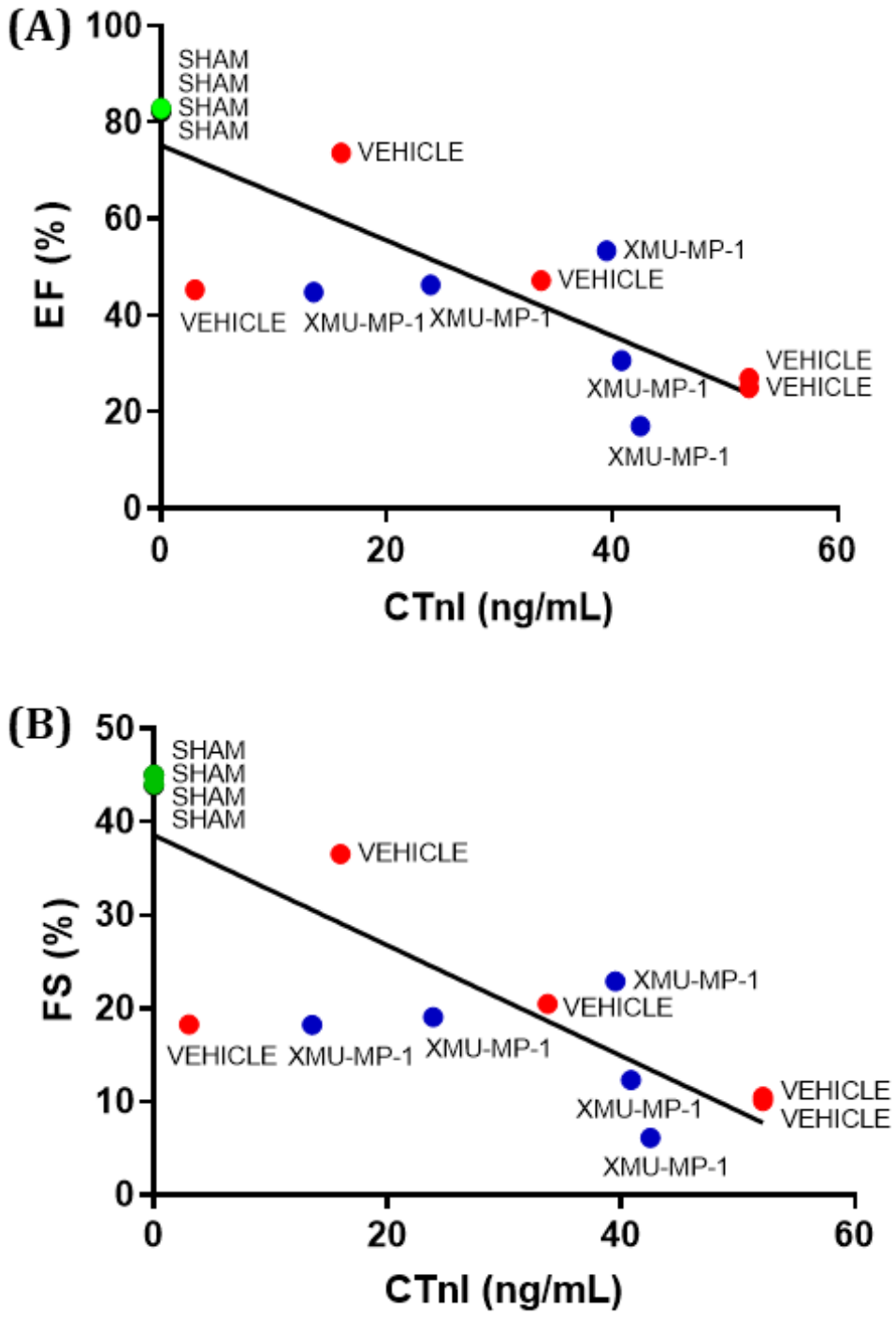

Figure 4.6 Correlation between cardiac function indicated by EF or FS and cTnI value ten days after MI. There is a strong correlation between cTnI values and EF (A) (r^2 = -0.8731, p = 0.0001) or FS (B) (r^2 = -0.8776, p < 0.0001) when all groups were analysed together. The negative correlation of cTnI values with EF or FS stipulates that the higher value of cTnI is related to the lower Ef or FS value. When the XMU-MP-1 and vehicle groups were analysed separately, there was no difference in the strength of the correlation between cTnI values and EF or FS. However, the slope of the linear curve in the vehicle group was slightly steeper than that in the XMU-MP-1 treatment group but not statistically significant. Sham n=4, vehicle n=5, XMU-MP-1 n=5.

4.4.1.3 The effects of XMU-MP-1 treatment on the infarct size in acute MI model mice

Infarct size is a vital determinant parameter that reveals the severity of the infarction attack in the heart. Masson's Trichrome staining was performed on the histological section of the heart to detect the infarct area. The heart was cut into at least six layers and each layer was sectioned and stained to calculate the infarct size. The infarct size was measured using a length-based calculation based on the ratio between the length of the infarcted segment and the left ventricular perimeter.

Representative images of the heart section in mice following MI surgery are shown in Figure 4.7.

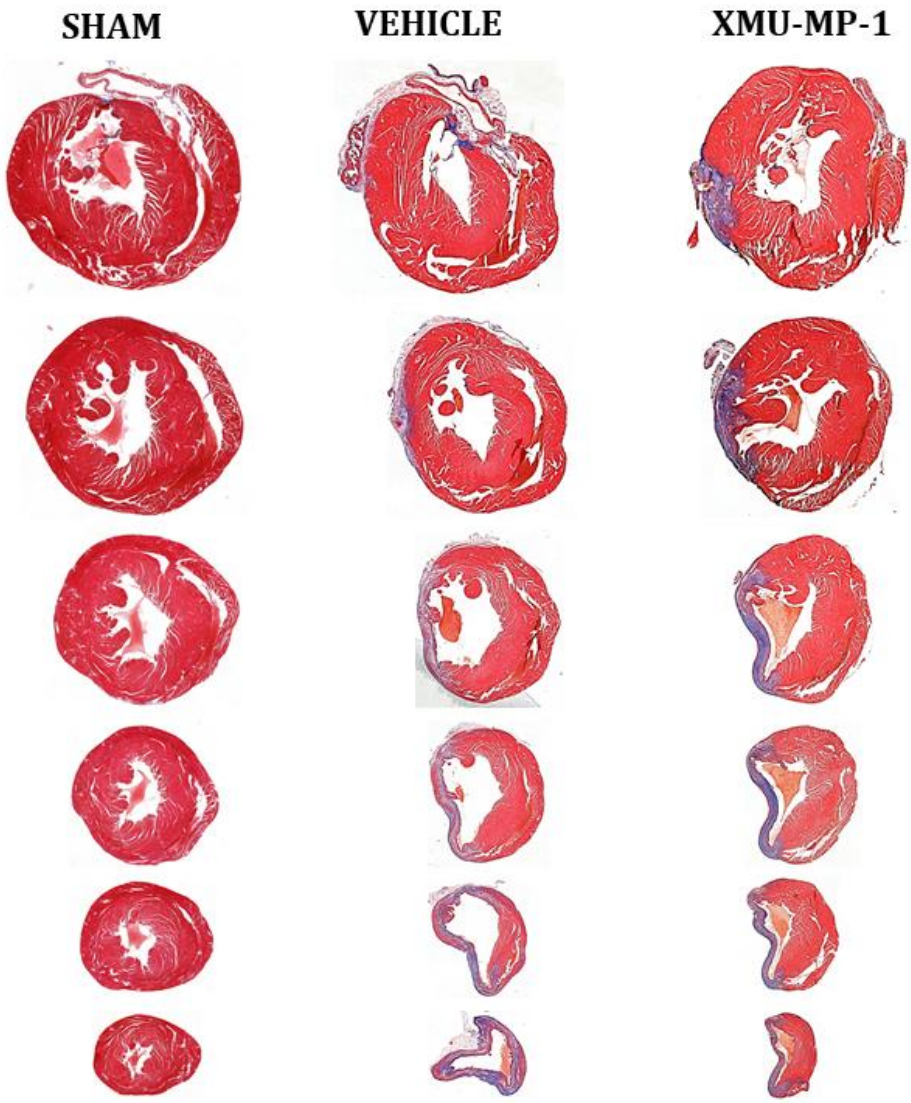

Figure 4.7 Histological section of the heart stained using Masson's Trichrome method. The paraffin-embedded heart was cut transversely into thin layers, each 5 µm thickness. The heart was separated into at least six levels with a 500 µm distance of each level, starting from the apex of the heart (level 1). The blue staining on the tissue section shows the infarct area.

Based on the infarct size analysis, I found that the XMU-MP-1 group has a bigger infarct size than the vehicle group, but this is not statistically significant (Figure 4.8 A). I also checked the correlation between the infarct size and cTnI level to assess if both parameters can better describe the phenotypes among groups. Additionally, another test was performed to determine the correlation between the infarct size and EF percentage (% EF).

My data suggest that there is a strong correlation between the infarct size and cTnI level. The group-related patterns show that the XMU-MP-1 group has consistently higher infarct size values for each cTnI value than the vehicle group (Figure 4.8 B). I also found a strong correlation between infarct size and % EF with consistent group-related patterns showing higher infarct size values for each % EF value in the XMU-MP-1 treated mice when compared to the vehicle group (Figure 4.8 C).

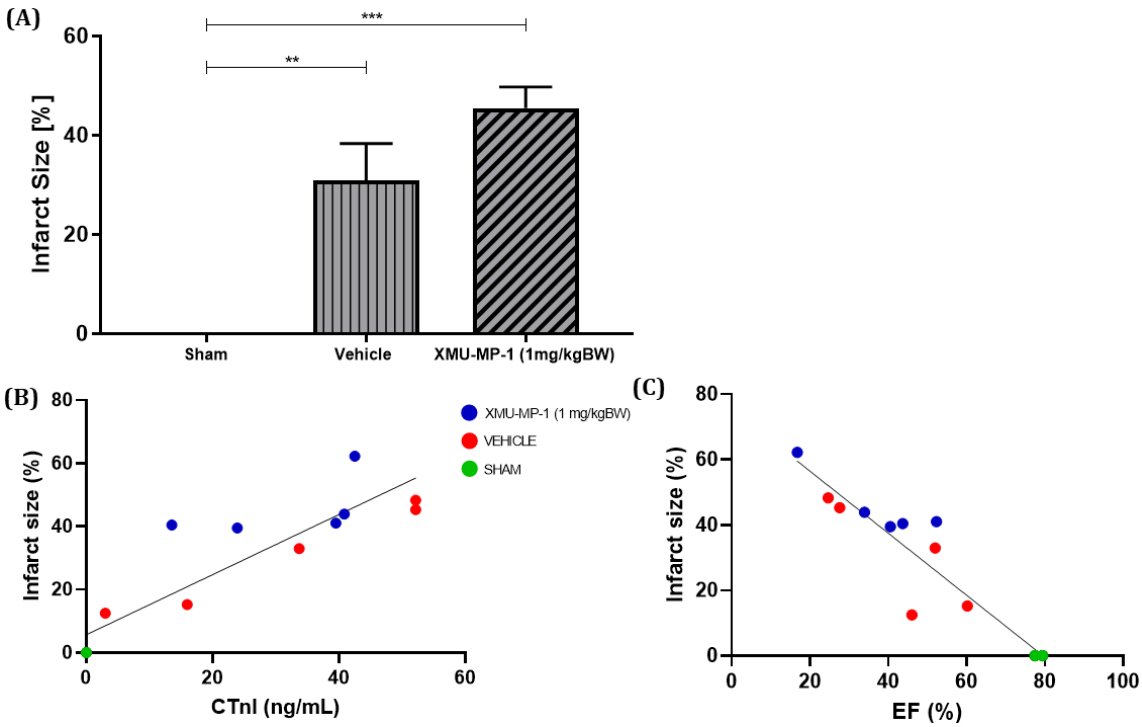

Figure 4.8 The Infarct size analyses in acute MI condition. The infarct size analysis shows that the MI procedure increases fibrosis deposition in the heart. (A) The order of the infarct size values, from the lowest to the highest, is the sham group (0%), the vehicle group (30.86 ± 7.41 %) and the XMU-MP-1 group (45.41 ± 4.27 %). (B) There is a strong correlation between the infarct size and cTnI values (r^2 = 0.8959, p = 0.0001). (C) The correlation between the infarct size and % EF values is strong (r^2 = -0.9233, p = 0.0001). Sham n=4, vehicle n=5, XMU-MP-1 n=5.

4.4.1.4 Analyses of cardiomyocyte hypertrophy, apoptosis and proliferation following XMU-MP-1 treatment in acute MI model mice

As mentioned above, the ischaemic condition in the MI heart changes the regulation of biochemical processes. The changes in post-MI biochemical processes provoke some responses, such as the increase in cardiomyocyte hypertrophy and apoptosis. Hence, I analysed the effects of XMU-MP-1 treatment in cardiomyocyte hypertrophy, apoptosis and proliferation post-MI.

The cross-sectional cardiomyocyte size of the heart sections was measured following H&E staining to characterise the cellular hypertrophy (see Figure 4.9). My analysis of cardiomyocyte size shows a significant increase in the cell size following MI surgery. However, there is no statistical difference in cell size between the XMU-MP-1 and vehicle groups both in the border area and remote area (as shown in Figure 4.10).

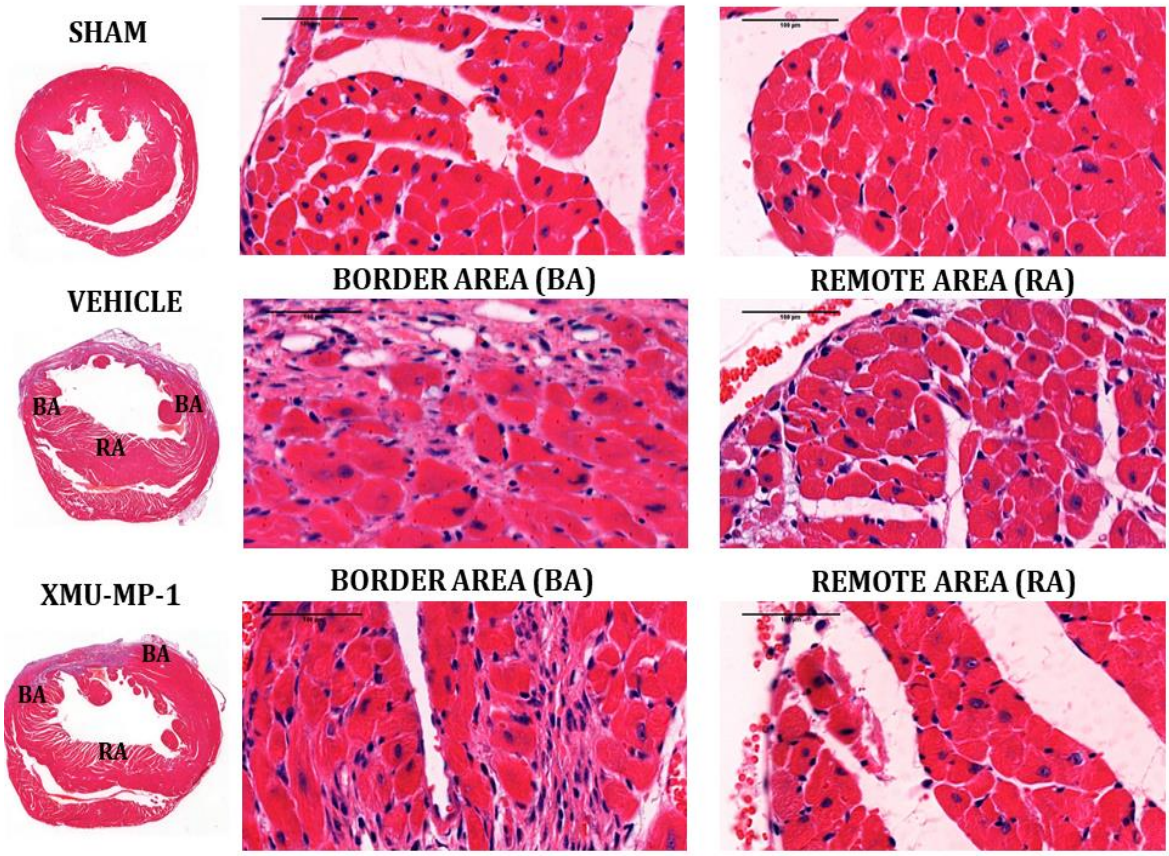

Figure 4.9 The histological section of the MI heart stained using Haematoxylin and Eosin. Transverse sections of the heart were stained using Haematoxylin and Eosin to analyse the cell size. In the MI heart section, cell size analysis was measured from two different regions: border area (BA) and remote area (RA). BA is the area close to the infarct site, whereas RA is the area remotely distant from the infarct site. More than 100 cardiomyocytes were analysed in each mouse. Scale bar = 100 μm.

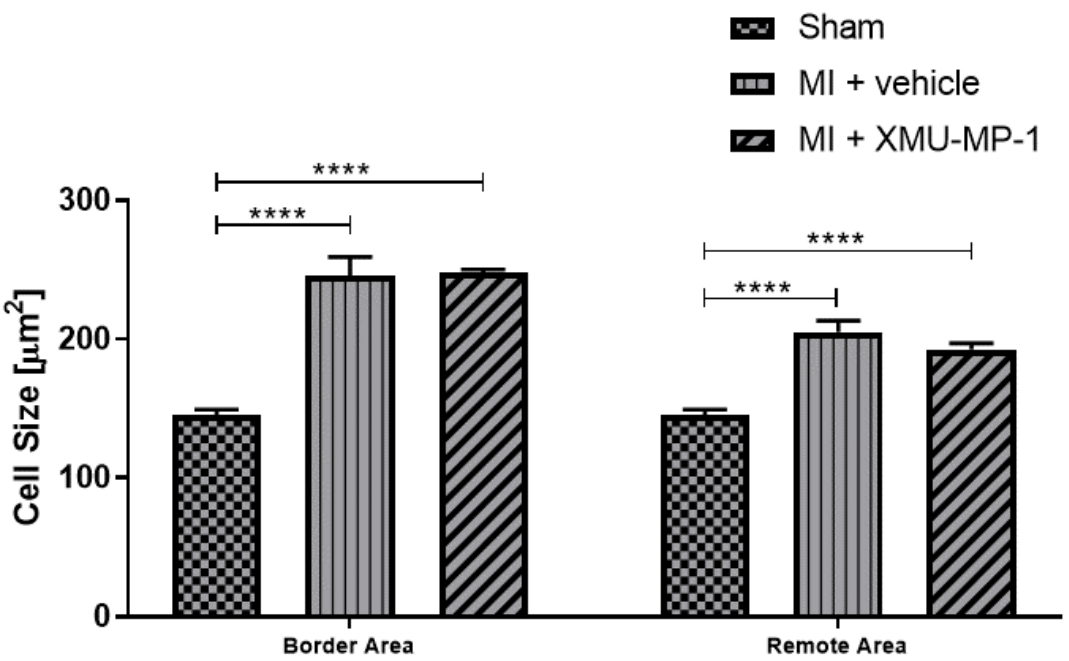

Figure 4.10 The analysis of cross-sectional cardiomyocyte size on day ten after MI surgery. The cardiomyocyte size analysis reveals a significant increase in mice that underwent MI surgery compared to the sham group (145.2 ± 4.04) both in the border and remote areas. There is no significant difference in the average cardiomyocyte size between the vehicle group (BA = 245.8 ± 13.23; RA = 205.2 ± 7.99) and the XMU-MP-1 group (BA = 248.1 ± 2.15; RA = 192.3 ± 4.58). Data (shown as mean ± SEM) were analysed using one-way ANOVA with Tukey's multiple comparison test, ****$p<0.0001$ indicates significant differences in results. Sham n=4, vehicle n=5, XMU-MP-1 n=5.

The number of cardiomyocyte deaths following MI is strongly related to the deterioration of cardiac function. The ability of the left ventricle to pump the blood is usually poor during cardiomyocyte loss. Hence, a TUNEL assay was performed on the heart sections to identify the level of dying cardiomyocytes after infarction. The TUNEL assay reveals fragmented DNA in the nuclei in the dying cells (green fluorescence). The ratio between positive TUNEL cardiomyocyte and total cardiomyocyte per field of view was determined. The sarcomeric protein alpha-actinin of cardiomyocytes was stained using the anti-α-actinin antibody. Figure 4.11 reveals the representative images of TUNEL staining on the heart section in the acute MI experiment.

The TUNEL analysis shows that the level of cardiomyocyte apoptosis rises after MI surgery. As illustrated in Figure 4.12, the cardiomyocyte apoptosis level in the area near the infarction site is higher than that in the remote region. The difference in cardiomyocyte apoptosis level between the vehicle and the XMU-MP-1 groups is not statistically significant in both the border and remote areas.

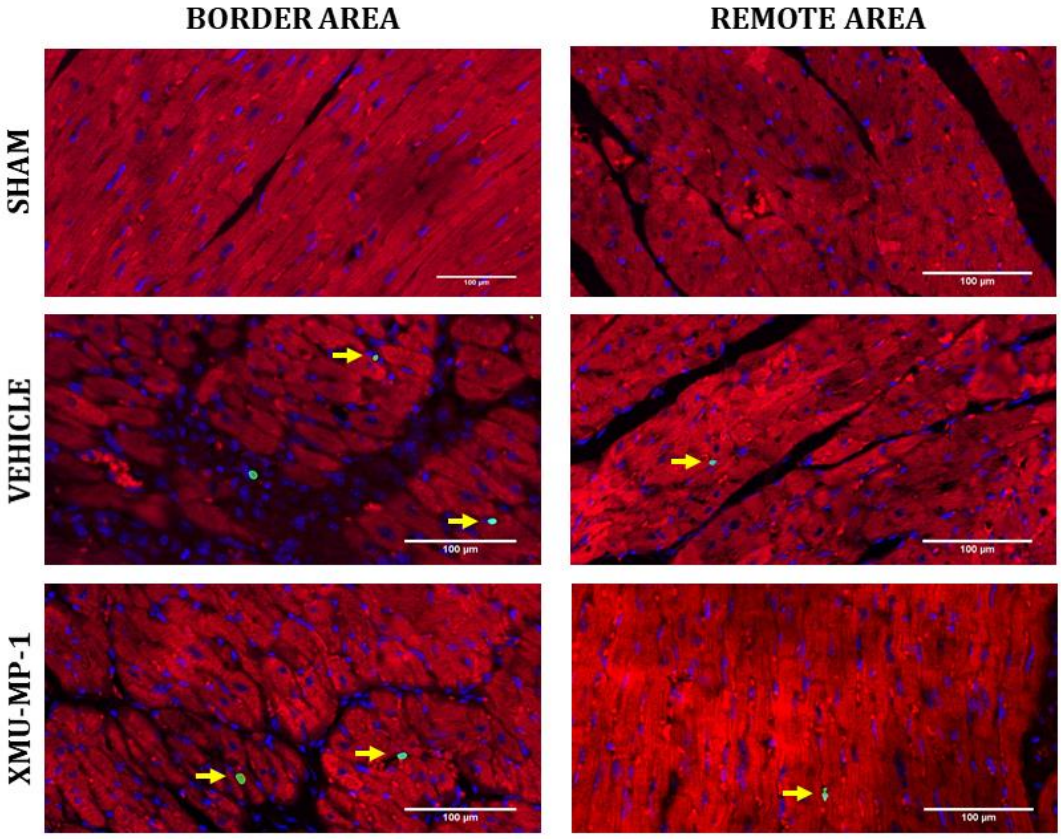

Figure 4.11 Representative images of TUNEL staining on the heart section ten days after MI surgery. TUNEL positive cardiomyocytes are indicated by co-localisation of green and blue fluorescences in the red area (α-actinin). Scale bar = 100 µm.

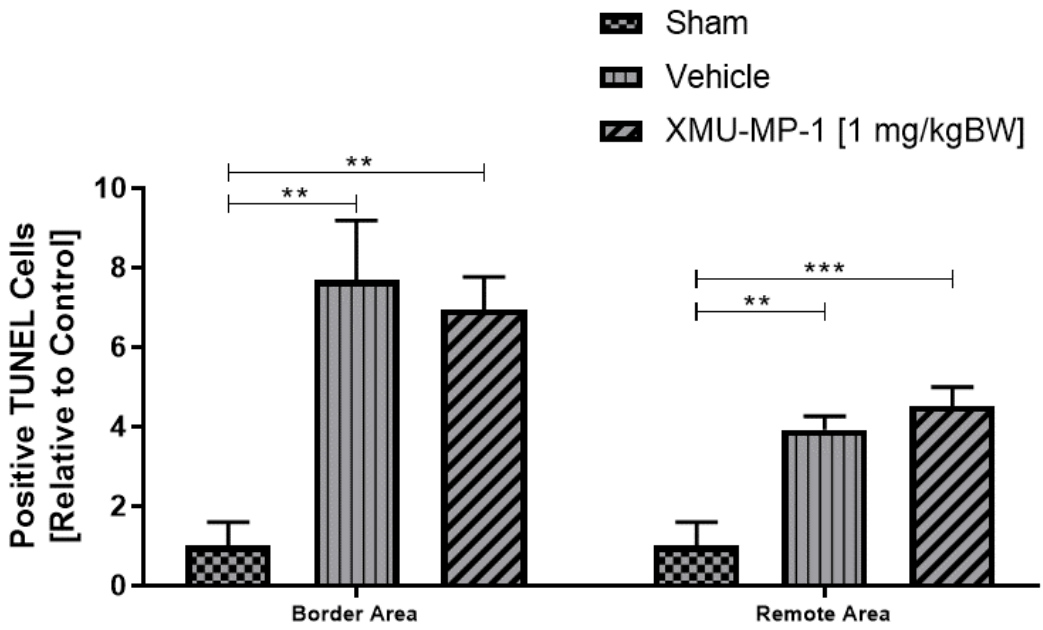

Figure 4.12 The analysis of TUNEL staining on the heart section on day ten after MI. Positive TUNEL rate augments more than six-fold after MI surgery compared to the sham group (7.68 ± 1.51 in the vehicle group and 6.95 ± 0.82 in the XMU-MP-1 group). The increment of positive TUNEL rate in the remote area after MI surgery is about four times when compared to the sham group (3.92 ± 0.34 in the vehicle group and 4.52 ± 0.48 in the XMU-MP-1 group). Data (shown as mean ± SEM) were analysed using two-way ANOVA with Tukey's multiple comparison test, **p<0.01 and ***p<0.001 indicate significant differences in results. Sham n=4, vehicle n=5, XMU-MP-1 n=5. More than 1,000 cardiomyocytes were analysed in each mouse.

As mentioned in Chapter 2, YAP activation through Mst1/2 inhibition can enhance proliferation in the NRCM culture. As cardiomyocytes have limited regeneration capacity, YAP activation could be potentially beneficial during pathological conditions, including MI. I postulated that YAP activation through Mst1/2 inhibition could promote cardiomyocyte proliferation. Hence, I subjected mice to MI surgery and treated them with 1 mg/kgBW XMU-MP-1 every other day for ten days and then assessed the cardiomyocyte proliferation at the end of the experiment.

Unfortunately, my *in vivo* experimental design in mimicking acute MI conditions failed to show any beneficial effects of XMU-MP-1 treatment in increasing cardiomyocyte proliferation. As shown in Figure 4.13, my analysis of cardiomyocyte proliferation suggests that there is no significant difference among all treatment groups.

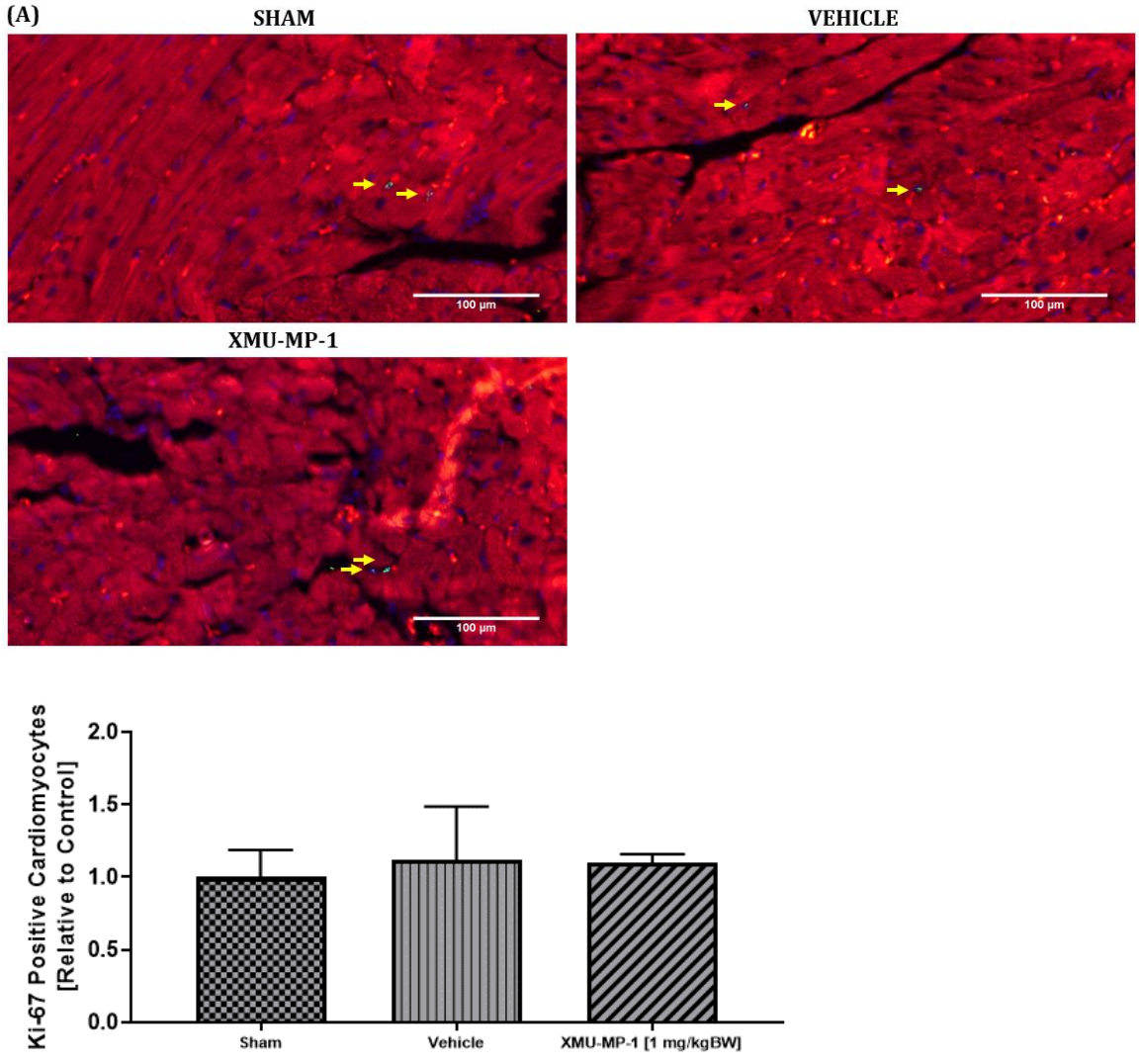

Figure 4.13 Ki-67 Analysis of the heart section in acute MI. (A) Representative images of Ki-67 staining on the heart sections. Positive Ki-67 cardiomyocytes are shown as greenish-blue fluorescence signals in the area stained by α-actinin (red). (B) The difference in the rate of Ki-67 positive cardiomyocytes is not statistically significant among all groups. Data (shown as mean ± SEM) were analysed using one-way ANOVA. Sham n=4, vehicle n=5, XMU-MP-1 n=5. More than 1,000 cardiomyocytes were analysed in each mouse. Scale bar = 100 µm.

4.4.2 Alteration in cardiac phenotypes after XMU-MP-1 treatment in sub-acute myocardial infarction

Considering that the XMU-MP-1 treatment is not more dominant than the vehicle group in my acute MI experiment, I decided to administer XMU-MP-1 in sub-acute MI conditions. The idea was that the XMU-MP-1 treatment was aimed to modulate the cardiac remodelling process after acute MI conditions have been passed. Similar to the TAC experiment, I started the XMU-MP-1 treatment three weeks after the MI surgical procedure.

4.4.2.1 Survival of sub-acute MI model mice after XMU-MP-1 treatment

As mentioned above, the survival rate is an important outcome to assess the effectiveness of the treatment after the surgical procedure. In the sub-acute MI experiment, I excluded all deaths before the treatments were started for survival analysis. I consider that all deaths that occurred before giving the treatments were not related to the purposes of this study. The overall survival among treatment groups was compared using a Kaplan Meier curve and a Log-rank test.

From a total of twenty mice that were assigned into three groups, fourteen mice were allowed for analyses. There were four mice in the sham group, five mice in the vehicle group and five mice in the XMU-MP-1 group. Six other mice died within 21 days following the surgical procedure and were thus excluded from analyses. As seen in Figure 4.14, survival analysis demonstrates that there is no significant difference in the overall survival of all groups. One out of five mice in the vehicle group died on day 25.

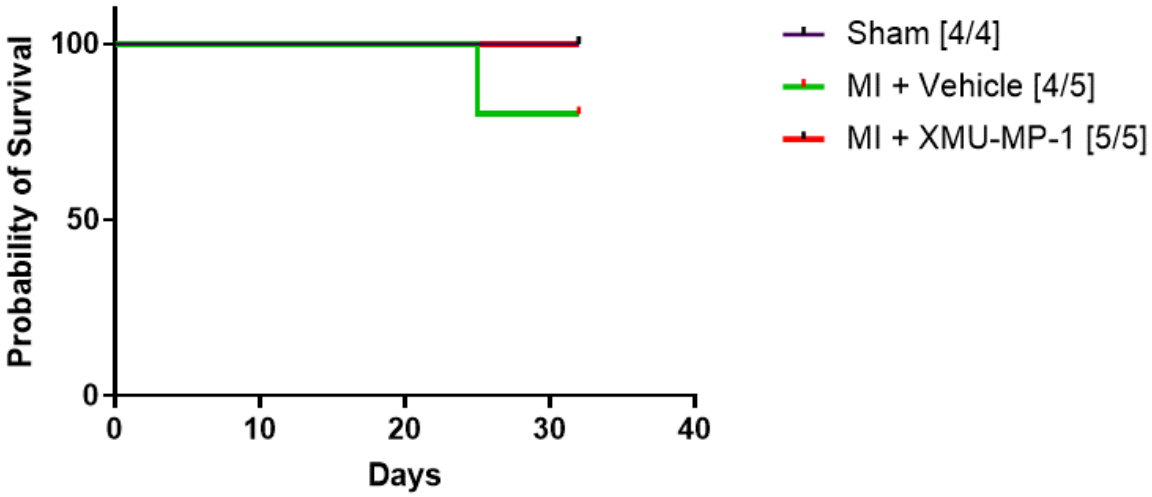

Figure 4.14 The Kaplan Meier survival curve in sub-acute MI conditions. There is no significant difference in overall survival in all groups. All mice in the sham and XMU-MP-1 groups survived up to the end of the experimental period. The survival rate in the vehicle group is 80%. Data were analysed using a Log-rank (Mantel-Cox) test. Sham n=4, vehicle n=5, XMU-MP-1 n=5.

4.4.2.2 Analyses of cardiac structure and function in sub-acute MI model mice treated with XMU-MP-1

The cardiac structure and function analyses were performed before and after the vehicle or XMU-MP-1 treatments were administered starting at three weeks after MI surgery. The assessment of cardiac function parameters was conducted using transthoracic echocardiography. One mouse in the vehicle group was found dead before the second echocardiography assessment was performed. The cardiac function of this mouse was not be able to measure at the end of the experiment, that could affect the comparison analysis between the XMU-MP-1 and the vehicle group. Hence, the cardiac function analysis at the end of the experiment was only applied to four out of five mice in the vehicle group.

The left ventricular mass to body weight ratio is a cardiac structure parameter that shows any changes in the size of the left ventricle as a sign of dilatation. This parameter is important to determine whether the treatment has an anti-hypertrophic effect or not. The ratio between left ventricular mass and body weight is escalated due to the MI procedure, as shown in the vehicle and XMU-MP-1 groups (Figure 4.15).

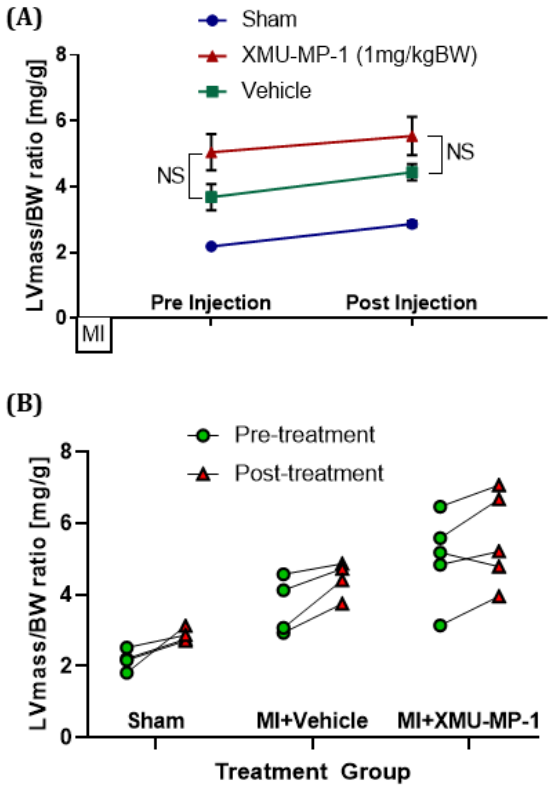

Figure 4.15 The left ventricular mass to body weight ratio in sub-acute MI conditions. A. There is a substantial increase without a statistical significance in the LV/BW ratio before and after the vehicle treatment (3.68 ± 0.39 mg/g and 4.44 ± 0.25 mg/g, respectively). The ratio of LV/BW is significantly increased after MI surgery in the XMU-MP-1 group (5.05 ± 0.55 mg/g pre-treatment and 5.54 ± 0.58 mg/g post-treatment). The sham group has a stable value of the LV/BW ratio (2.18 ± 0.15 at three weeks after MI and 2.87 ± 0.09 at five weeks after MI). B. Individual plot of LV mass to body weight ratio before and after treatment. Data are presented as mean ± SEM and analysed using two-way ANOVA with Tukey's post-hoc test for multiple comparisons. NS: not significant. Sham n=4, vehicle n=4, XMU-MP-1 n=5.

The cardiac structure changes can also be assessed using the measurement of left ventricular diameter either in the diastolic or systolic phase (dLVID or sLVID). There is no significant difference in dLVID or sLVID between the vehicle and XMU-MP-1 groups at the end of the experiment. However, when compared with the control, it is pronounced that the sham group has a smaller dLVID and sLVID. The within-group comparison does not show any significant difference in the dLVID or sLVID before and after the vehicle and XMU-MP-1 treatments were given (see Figure 4.16).

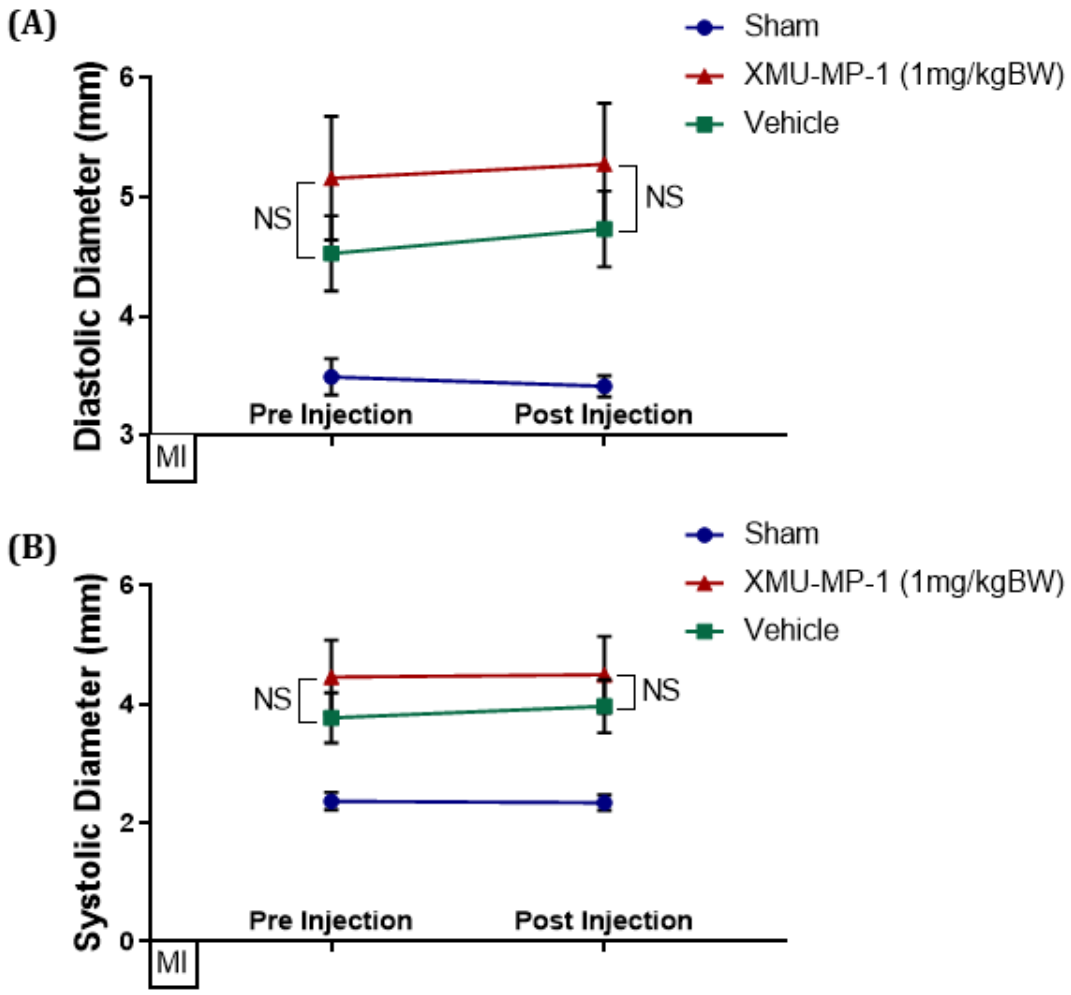

Figure 4.16 The diastolic and systolic diameters of the left ventricle in sub-acute MI. (A) The dLVID is expanded after MI. There is no significant difference in the dLVID within-group comparison: the vehicle group (4.53 ± 0.32 before treatment and 4.73 ± 0.32 after treatment) and the XMU-MP-1 group (5.16 ± 0.52 before treatment and 5.28 ± 0.51 after treatment). (B) The sLVID in the MI mice is almost twice as high as the sLVID of the sham group. The within-group comparison of sLVID does not show any significant change in the vehicle group (3.77 ± 0.42 before treatment and 3.97 ± 0.45 after treatment) and the XMU-MP-1 group (4.46 ± 0.62 before treatment and 4.49 ± 0.65 after treatment). Data are presented as mean ± SEM and analysed using two-way ANOVA with Tukey's post-hoc test for multiple comparisons. NS: not significant. Sham n=4, vehicle n=4, XMU-MP-1 n=5.

The morphometric measurement shows a small increase, but not a statistically significant one in the heart weight to the tibia length (HW/TL) ratio of the mice that underwent MI surgery compared to the sham group. The difference in HW/TL ratio is not statistically significant between the vehicle and XMU-MP-1 treatment groups. Other morphometric measurements can be seen in Table 4.2. No significant differences are observed in heart weight, lung weight, body weight, diastolic LVPW and systolic LVPW among the experimental groups.

Table 4.2 Morphometric measurements in sub-acute MI conditions.

Parameters	Treatment groups		
	Sham	Vehicle	XMU-MP-1
Heart weight (mg)	147.50 ± 6.29	180.00 ± 31.09	192.00 ± 18.81
Lung weight (mg)	147.60 ± 5.26	138.70 ± 5.45	231.70 ± 53.14
Body weight (g)	30.55 ± 0.95	29.70 ± 0.63	29.84 ± 0.61
Heart weight/Tibia Length (mg/mm)	0.72 ± 0.03	0.86 ± 0.15	0.91 ± 0.09
Diastolic LVPW (mm)	0.78 ± 0.02	0.66 ± 0.09	0.71 ± 0.06
Systolic LVPW (mm)	1.18 ± 0.07	0.96 ± 0.12	0.99 ± 0.11

In addition to the cardiac structure, I also assessed the cardiac function to determine the treatment effects in sub-acute MI conditions. Ejection fraction (EF) and fractional shortening (FS) are echocardiography parameters that were measured to determine cardiac function. Those parameters were assessed twice (before the treatment was started and at the end of the experiment). The comparison between EF and FS values was determined among and within experimental groups.

My analysis of cardiac function suggests that EF and FS values are decreased due to the MI procedure. At the end of the experiment, or in other words, five weeks after MI surgery, there is a small decrease of EF and FS values but not statistically significant in the vehicle group. The change of EF and FS values in the XMU-MP-1 group from three weeks to five weeks after MI surgery is insignificant. The illustration of both EF and FS analysis is shown in Figure 4.17.

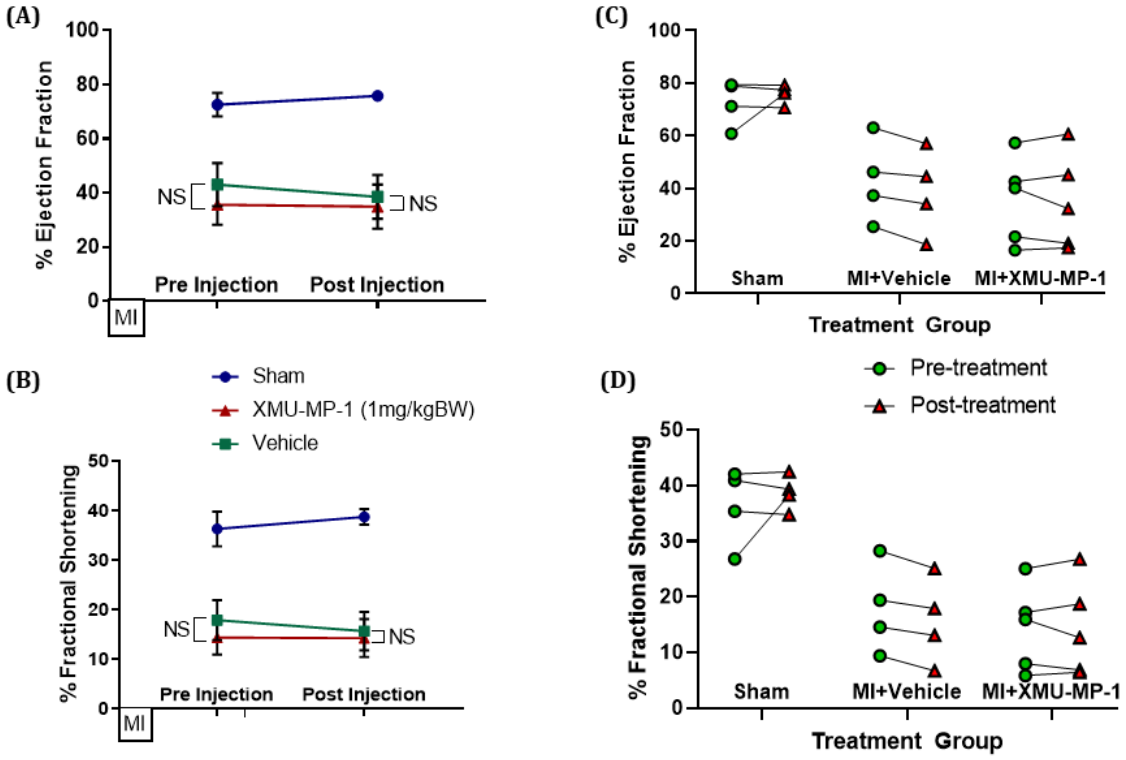

Figure 4.17 The assessment of cardiac function in sub-acute MI conditions. A&B. EF and FS values are significantly reduced by around 50% in the vehicle and XMU-MP-1 groups compared to the sham group at three weeks after MI surgery. The within-group comparison demonstrates that EF and FS change before and after treatment is not statistically significant in all experimental groups. C&D. Individual plots of EF and FS before and after treatment in the sub-acute MI experiment. Data are presented as mean ± SEM and analysed using two-way ANOVA with Tukey's post-hoc test for multiple comparisons. NS: not significant. Sham n=4, vehicle n=4, XMU-MP-1 n=5.

The correlation between EF or FS and cardiac Troponin I (cTnI) in plasma was determined using the Spearman correlation test. The correlation analysis shows the strength of dependence between EF or FS and cTnI value. The changes in the EF and FS values in the experimental groups are strongly related to the level of plasma cTnI. The correlation analysis suggests that EF and FS have a strong negative correlation with plasma cTnI values. Four out of five mice in the XMU-MP-1 group have EF values under the linear curve. Meanwhile, the EF values of the vehicle-treated mice are distributed evenly above and under the linear curve (see Figure 4.18).

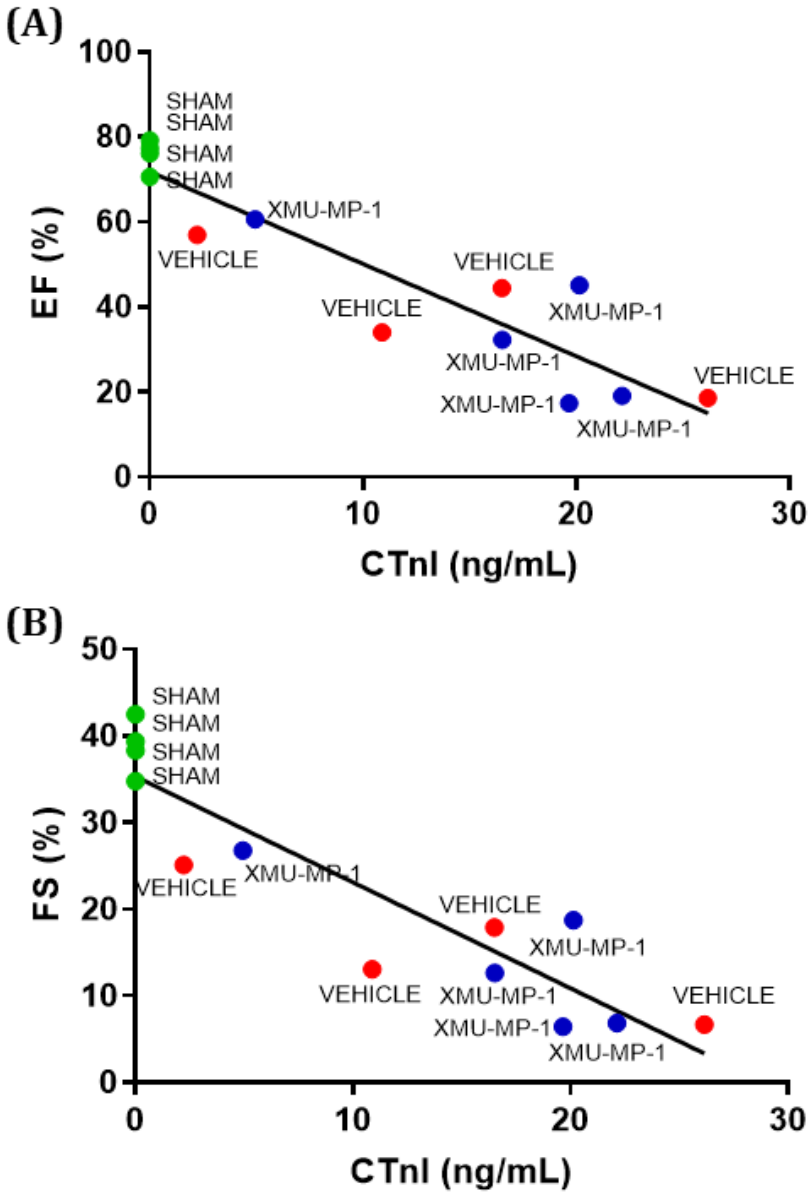

Figure 4.18 The correlation analysis of cardiac function and cTnI values in sub-acute MI. When all experimental groups were analysed, I found a strong correlation between cTnI values and EF (A) (r^2 = -0.8530, $p < 0.0001$) or FS (B) (r^2 = -0.8397, $p < 0.0001$). The negative correlation means that EF or FS are increased when cTnI values are reduced. There is no significant difference in the strength of the correlation between the XMU-MP-1 and vehicle groups when analysed separately. Sham n=4, vehicle n=5, XMU-MP-1 n=5.

4.5 Discussion

The most suitable strategy for treating myocardial infarction has yet to be determined because residual heart failure symptoms post-MI attack are still high. Despite novel inventions targeting long-term cardioprotective effects post-MI, their translation into clinical application is still limited.

Given that myocardial infarction induces severe inflammatory responses, cardioprotective therapy is essential for improving clinical outcomes post-MI. Initially, the inflammatory

response post-MI aims to remove damaged cell aggregates in the infarction area after pathological stimuli (Ong et al., 2018). Reperfusion therapy after an MI attack can exacerbate this inflammatory response mediated by toll-like receptor (TLR) to induce chemokine upregulation and cytokine synthesis (Fuentes et al., 2019).

Tian et al. demonstrated that the Hippo/Mst1 modulates the inflammatory response in MI conditions. Mst1 is upregulated in the hypoxic cardiomyocytes. Conversely, Mst1 knockdown suppresses the expression of inflammation factors and reactive oxygen species (ROS). The cardioprotective effect of Mst1 downregulation in the hypoxic condition is associated with the inhibition of the heme oxygenase-1 (HO-1) signalling pathway (Tian et al., 2020). HO-1 is a protein that is involved in oxidative stress generation and inflammation (Kapturczak et al., 2004). HO-1 contributes to the heme conversion into biliverdin and bilirubin that have antioxidant properties (Otterbein et al., 2003).

This chapter aimed to find another strategy to get a long-term cardioprotective outcome post-MI by targeting the Hippo/Mst using a chemical substance. The Hippo/Mst inhibitor, XMU-MP-1, was administered using the same dose as in the TAC model. 1 mg/kgBW of XMU-MP-1 was given every other day for ten days in the XMU-MP-1 group and an equal volume of DMSO was injected into mice in the vehicle (control) group. I conducted two different designs of XMU-MP-1 administration in the MI model. My first experimental design was administering XMU-MP-1 treatment straight after the MI surgery to examine the effects of XMU-MP-1 in the acute remodelling phase following MI. The second design was aimed to evaluate XMU-MP-1 effects in sub-acute MI conditions by giving XMU-MP-1 treatment three weeks after MI surgery. My experiments investigating the impact of XMU-MP-1 in acute MI and sub-acute MI do not show any beneficial outcomes in cardiac phenotypes. These results exclusively demonstrate the effects of XMU-MP-1 at the dose of 1 mg/kgBW that was given every other day for ten days as I did not apply other doses/treatment strategies.

4.5.1 The XMU-MP-1 treatment is not superior in improving clinical outcomes and cardiac function both in acute and sub-acute MI

In a different disease model, intracerebral haemorrhage (ICH), XMU-MP-1 treatment has been found to be effective in reducing neural cell death and inflammatory responses. However, there was no significant difference in the mortality rate among the experimental groups. In this study, XMU-MP-1 was administered in ICH model rats at a single dose of 1 mg/kgBW. Even though the effect of XMU-MP-1 on mortality rate is not assertive, the clinical behaviour was reported to be significantly improved (Zhang et al., 2019).

Similar to the results from the study by Zhang et al., my investigation of XMU-MP-1 effects in both acute and sub-acute MI conditions demonstrates that there is no significant difference in mortality rate among my experimental groups. Unlike the findings of Zhang et al., the clinical outcomes in both acute and sub-acute MI do not show any improvement of phenotypes following XMU-MP-1 treatment compared with the vehicle group. A direct comparison between my results and the findings of Zhang et al is not possible. because I used different disease models so that the biochemical signalling mechanisms related to the pathological stimuli are also different. Also, XMU-MP-1 dose regimentation in my experiment was limited to only five injections over a ten-day period as the project license only allows a maximum of five injections given. Nevertheless, it is valuable to evaluate the effects of XMU-MP-1 in severe pathological conditions using different regimentation and delivery systems.

The inhibition of the Hippo components has been reported to have beneficial impacts on MI conditions. Leach et al. revealed that sav deletion is effective in improving vascularisation in scar borders, reducing cardiac fibrosis and ameliorating cardiac function after MI (Leach et al., 2017). Wang and Song reported that Mst1 deletion decreases cardiac fibrosis and cardiomyocyte death after MI. They also found an association between Mst1 deletion and the reduction of mitochondrial fission (Wang and Song, 2018). Moreover, the Hippo pathway inhibition leads to YAP activation, which has been reported to have antiapoptosis and prosurvival activities. YAP overexpression was found to preserve cardiac function and increase the survival rate in the mouse model of MI (Lin et al., 2014).

Unlike data from Leatch et al. or Wang and Song, which reported the reparative effects of the Hippo pathway inactivation after MI (Leach et al., 2017; Wang and Song, 2018), my data could not affirm the beneficial effects of Mst1/2 inhibition using XMU-MP-1 in the MI experiments. In the acute and sub-acute MI experiments, I found that the XMU-MP-1 treated mice had no superiority in cardiac structure and cardiac function compared to the vehicle group. The discrepancy between my results and previous studies could be attributed to the different experimental designs. Both Leach et al. and Wang and Song used genetically modified animals to examine the effects of the Hippo component ablation in MI settings. On the other hand, my study used a pharmacological approach in inhibiting the Hippo/Mst. Presumably, the inhibition of XMU-MP-1 on the Mst1/2 is not an absolute selectivity making it possible to affect other substrates. XMU-MP-1 effects are not solely attributed to YAP activity because it can also interact with other kinases, such as aurora kinase A (AURKA) and phosphatidylinositol-4,5-biphosphate 3-kinase catalytic subunit gamma (PIK3CG) (Fan et al., 2016). Moreover, I only use one dose regimentation, which might not adequate in treating severe pathological stress mechanisms in MI. As a comparison, another small

molecule directly targeting YAP, TT-10, exhibited cardiac function amelioration associated with increased cardiomyocyte proliferation (Hara et al., 2018).

My analysis of the cardiac structure in the MI experiment, both in acute and sub-acute experimental designs, does not exhibit anti-hypertrophic effects of XMU-MP-1. The heart weight to tibia length ratio in the XMU-MP-1 is not significantly different from the vehicle group. Both XMU-MP-1 and vehicle groups showed an increased ratio of heart weight to tibia length. The analysis of diastolic and systolic diameters of the left ventricle also does not reveal any difference between the XMU-MP-1 and vehicle groups showing expanded left ventricular chambers. The administration of the same dose regimentation of XMU-MP-1, as in my TAC experiment, is not sufficient to protect the heart from dilatation post-MI.

Regarding the potential role of the Hippo/Mst inhibition in alleviating clinical outcomes after a MI attack, Mst1 is activated during oxidative stress. Mst1 activation promotes cell apoptosis through mitochondrial damage mediated by Bcl-xL phosphorylation. The suppression of Mst1 activity has been proven to protect the heart from pathological stimuli and prevent the cardiomyocytes from death and hypertrophy (Nakamura et al., 2016; Yamamoto et al., 2003). Interestingly, some studies marked the role of Mst1 associated with FOXO family members in different consequences (Lehtinen et al., 2006). Yuan et al. reported that Mst1 triggers FOXO-3 phosphorylation, which then dissociates FOXO-3 from 14-3-3 proteins. Excessive free FOXO-3 due to its dissociation from 14-3-3 proteins stimulates the translocation of FOXO-3 into the nuclei and induces cell death (Yuan et al., 2009). On the contrary, a recent paper published by Kim et al. revealed an essential role of Mst1 association with FOXO-1 in directing cell migration for sprouting angiogenesis into the hypoxic area. The existence of Mst1 in the endothelial cells is necessary for revascularisation in the hypoxic condition (Kim et al., 2019).

In summary, the inhibition of the Hippo/Mst1 in cardiomyocytes is useful to improve clinical outcomes after an MI attack. However, the effects of Mst1 inhibition in endothelial cells could inhibit revascularisation or angiogenesis after MI. These findings imply that XMU-MP-1 treatment in MI conditions could be beneficial when its action in endothelial cells is minimised, or other treatments are given to promote angiogenesis.

4.5.2 The correlation between infarct size and cTnI value or cardiac function in acute MI model mice

The infarct size analysis shows that the XMU-MP-1 treated mice had a larger infarct size compared to the vehicle but not statistically significant (see Figure 4.8). The MI procedure significantly increases cardiac fibrosis. Sham mice did not show any fibrotic area in the

heart. In contrast, mice in the vehicle and XMU-MP-1 groups exhibited transmural fibrotic areas in the left ventricle, as shown in Figure 4.7.

Further investigation would be needed to confirm whether XMU-MP-1 treatment is associated with less vascularisation after MI. An assessment that could be done is the determination of angiogenesis in the heart. An increase in the sprouting angiogenesis during compensatory processes after an MI attack is necessary to provide oxygen supply. Vascularisation in the infarction or border area could rescue more cardiomyocytes and suppress fibrosis development. Some immunofluorescence methods could be performed to detect the state of vascularisation, such as VE-cadherin, $CD31^+$ vessels and ERG^+ nuclei. VE-cadherin staining could detect endothelial junctions, CD31 staining could show vascular shapes, and ERG staining could present endothelial nuclei (Kim et al., 2019).

Another consideration is that the Hippo effector, YAP, has crosstalk mechanisms with various proteins that can affect vascularisation. A previous study by Kim et al. reported that YAP could increase endothelial cell proliferation, promote sprouting angiogenesis and enhance vascular barrier formation and maturation by activating the actin cytoskeleton and upregulation of MYC signalling (J. Kim et al., 2017). Additionally, Sakabe et al. revealed that phosphorylated-YAP was found to promote endothelial cell migration through the activation of the small GTPase CD42 (Sakabe et al., 2017).

After performing infarct size analysis, I assessed the correlation between infarct size and cTnI value, then compared the correlation among experimental groups. Based on my findings, four out of five mice in the vehicle group were distributed under the correlation curve of infarct size and cTnI value, while in the XMU-MP-1 group, three out of five mice were distributed above the curve (see Figure 4.8B). Differences in the distribution between the vehicle and XMU-MP-1 groups infer that at the same cTnI value, the infarct size in the vehicle group is less than that in the XMU-MP-1 group. In a similar manner, Figure 4.8C manifests a correlation between infarct size and EF, showing that the XMU-MP-1 group has a larger infarct size than the vehicle group for the same EF value. More works would be needed to elaborate on the underlying conditions attributed to these findings, such as molecular analyses for pathways known to be involved in the biochemical processes after MI.

4.5.3 XMU-MP-1 treatment in acute MI conditions is not sufficient to change cardiomyocyte hypertrophy, apoptosis and proliferation

Based on the analysis of cross-sectional cardiomyocyte circumference, I found that cardiomyocyte hypertrophy occurred after MI both in the XMU-MP-1 and vehicle groups.

Figure 4.10 shows that cardiomyocyte hypertrophy in the border area is more significant than that in the remote area. From my findings of the acute MI experiment, it can be inferred that 1 mg/kgBW XMU-MP-1 every two days is not effective in preventing cardiomyocyte hypertrophy following MI injury. Although I failed to show the effect of XMU-MP-1 in preventing cardiac hypertrophy in the acute MI experiment, my *in vitro* data and TAC experiment exhibit a promising anti-hypertrophic effect of XMU-MP-1. Mechanistically, the anti-hypertrophic effect of Mst inhibition is attributed to Mst2-Raf1-ERK crosstalks (Romano et al., 2014). The Hippo/Mst2 has been proven to have a cross-talk coordination with one of the Raf family members, Raf1 (O'Neill et al., 2004). Mst2 and Raf1 form a complex that activates the pro-hypertrophic Raf1-ERK1/2 pathway (Zi et al., 2014).

The analysis of cardiomyocyte apoptosis in the acute MI experiment exemplifies that the border area has a higher apoptosis level compared to the remote area. As shown in Figure 4.12, there is no significant difference in apoptosis level between the XMU-MP-1 and vehicle groups either in the border or remote area. Furthermore, cardiomyocyte proliferation analysis does not perceive any statistical significance among the experimental groups (see Figure 4.13). My data on cardiomyocyte apoptosis and proliferation in acute MI could not represent the association between the Hippo pathway inhibition and cell apoptosis and proliferation. Further investigation would be needed to elaborate on the comprehensive effects of XMU-MP-1 in cardiomyocyte apoptosis and proliferation. Different approaches, such as administering higher doses of XMU-MP-1 or continuous infusion using minipump after MI injury, are valuable to be done.

4.6 Conclusion

Regardless of acute or sub-acute MI conditions, 1 mg/kgBW of XMU-MP-1 treatment every other day for ten days is not sufficient to show any significant changes in terms of survival, cardiac structure and cardiac function. Besides, the results presented in this chapter are not conclusive to demonstrate the differences between XMU-MP-1 treatment and the vehicle in improving infarct size, cardiomyocyte hypertrophy, apoptosis and proliferation in acute MI.

CHAPTER 5

PHARMACOLOGICAL INHIBITION OF MST1/2 IN VASCULAR ENDOTHELIAL CELLS

5.1 The theoretical overview and conceptual framework

Whether angiogenesis is supportive or destructive for cardiovascular diseases remains debatable. The extent to which the changes in angiogenesis affect cardiovascular diseases is still the subject of much research and new therapeutic strategies are yet to be determined. This chapter reveals the relevant evidence in elaborating the association between the Hippo pathway and angiogenesis that has been briefly mentioned in the previous section.

Angiogenesis upregulation occurs during the adaptive phase of cardiac hypertrophy (Marcus et al., 1983). Vascular endothelial growth factor (VEGF) has a pivotal role in stimulating angiogenesis in the early phase of cardiac hypertrophy. The angiogenic process in cardiac hypertrophy is associated with the Akt pathway, which promotes VEGF production. Initially, stimulation of the Akt pathway in the early phase of cardiac hypertrophy development is related to preserved cardiac function (Shiojima et al., 2005). However, prolonged activation of the Akt pathway results in cardiac dysfunction and heart failure (Izumiya et al., 2006).

The association between the Hippo components and angiogenesis has been previously reported. A previous study proved that VEGF and vascular endothelial growth factor receptor (VEGFR) activate YAP activity by inhibiting the Hippo kinases. The regulation of the Hippo kinases (Mst and LATS) by VEGF is related to the effects of VEGF in the MAPK and PI3K signalling (Azad et al., 2018). Likewise, the Hippo effectors, YAP and TAZ, also contribute to VEGF-induced angiogenesis. The inhibition of YAP/TAZ activity was reported to suppress tube-like formation. TAZ was found to have more substantial effects on angiogenesis than YAP (Wang et al., 2017). Additionally, Choi et al. revealed that YAP upregulates angiopoietin-2 activity as a pro-angiogenic factor (Choi et al., 2015). LATS1/2 has been proven to phosphorylate angiomotin (AMOT). The phosphorylation of AMOT causes disruption of AMOT and the F-actin bond, which subsequently results in the reduction of endothelial cell migration and angiogenesis (Dai et al., 2013). Interestingly, Kim et al. reported that Mst1 promotes FoxO1 activity and facilitates sprouting angiogenesis by maintaining endothelial polarity in hypoxic conditions (Kim et al., 2019). The association between the Hippo pathway and angiogenesis regulation might depend on the angiogenesis cues. Hence, I sought to elaborate on the effects of XMU-MP-1 treatment in angiogenesis. The suggested effects of XMU-MP-1 in the endothelial cells are outlined in Figure 5.1.

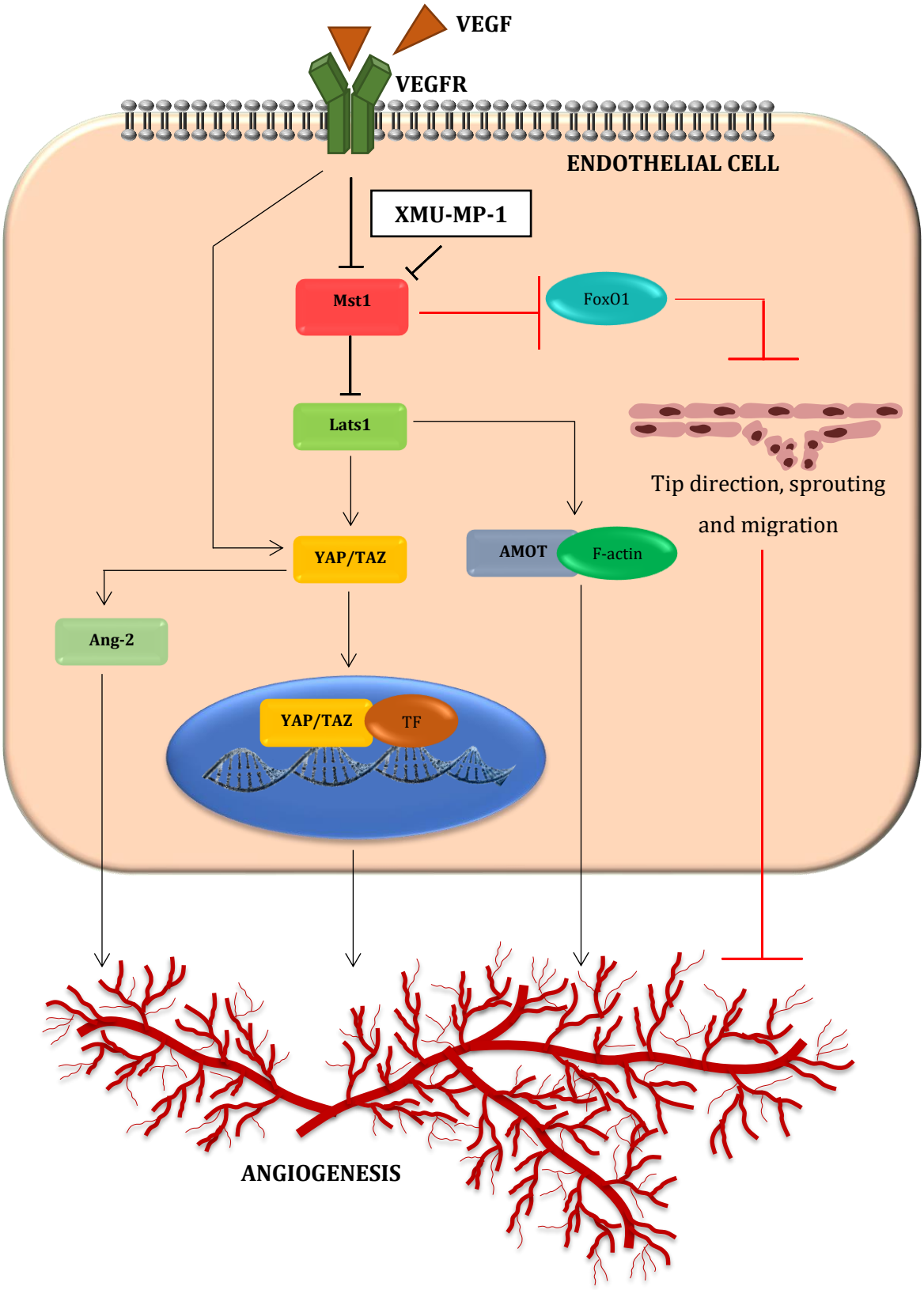

Figure 5.1 A suggested modelling framework of the role of XMU-MP-1 in angiogenesis. The inhibition of Mst1/2 using XMU-MP-1 should have similar consequences with VEGF in increasing angiogenesis (black arrows). The XMU-MP-1 treatment induces the angiogenic response attributed to YAP/TAZ activation, which results in Ang-2 activation and YAP/TAZ binding with transcription factors. XMU-MP-1 indirectly inhibits LATS1 and supports the binding between AMOT and F-actin, which also induces angiogenesis. Mst1 inhibition can also disrupt FoxO1-induced sprouting angiogenesis in hypoxic conditions (red arrows).

5.2 Aims

The main objective of this chapter is to evaluate the effects of the pharmacological inhibition of the Hippo pathway using XMU-MP-1 in human umbilical vein endothelial cells (HUVECs). Specific aims are as follows:

- To investigate the effects of XMU-MP-1 treatment on HUVEC proliferation and migration.
- To evaluate whether XMU-MP-1 treatment affects the angiogenic capacity of HUVECs using *in vitro* assays.
- To analyse the signalling pathways modulated by the Hippo pathway inhibitor, XMU-MP-1, in HUVECs.

5.3 Hypotheses

I propose that the extent to which XMU-MP-1 induces or inhibits angiogenesis is determined by the interaction between XMU-MP-1 and the Hippo kinases. HUVEC proliferation and migration can be enhanced by XMU-MP-1 through its inhibition on Mst1, which activates YAP/TAZ.

5.4 Results

This chapter sought to assess the phenotypes of cultured human umbilical vein endothelial cells (HUVECs) following treatment with XMU-MP-1. In the experiments, HUVECs were assigned into four groups, i.e., the control group (HUVECs treated with DMSO) or HUVECs treated with 1 μM, 3 μM and 5 μM of XMU-MP-1. The duration of treatment was dependent on the experimental design.

5.4.1 The effects of XMU-MP-1 on HUVEC viability

HUVEC viability was assessed to check if XMU-MP-1 at the designated doses has the potency to increase HUVEC viability using MTT and alamarBlue® assays. In the MTT assay, HUVEC viability was assessed after 24-hour treatment. Meanwhile, HUVECs were treated for eight days and the assay was conducted every other day in the alamarBlue® experiment. Repeated sample measurements are applicable in the alamarBlue® experiment because it is a non-toxic and non-invasive method.

My data on MTT assay suggests that there is no statistical significance in cell viability between the control group and XMU-MP-1 groups. However, as seen in Figure 5.2, there is a small reduction in HUVEC viability when they were treated with XMU-MP-1.

Additionally, the alamarBlue® assay shows a significant decline in HUVEC viability in the XMU-MP-1 treatment groups beginning from day four of treatment. HUVEC viability continued to decrease with prolonged XMU-MP-1 treatment duration (as shown in Figure 5.3).

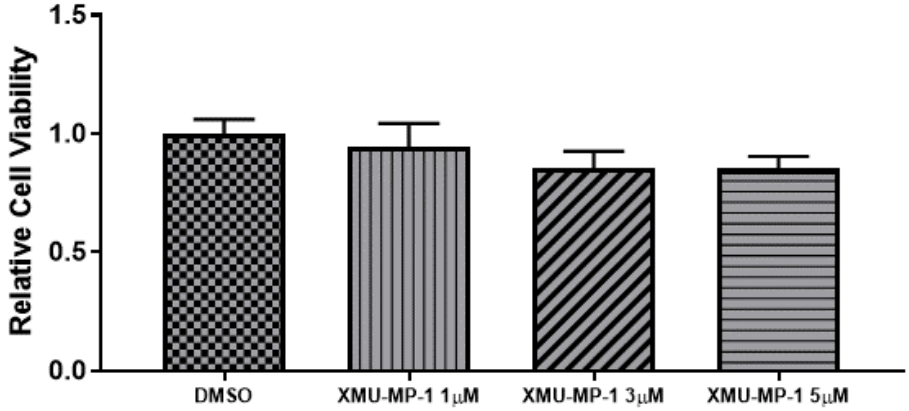

Figure 5.2 HUVEC viability assessed using MTT assay. There is a small decrease but not statistically significant in HUVEC viability when treated with XMU-MP-1 for 24 hours. Data presentation is in a relative unit compared to the control group. Data (shown as mean ± SEM) were analysed using one-way ANOVA. The number of independent experiments = 4.

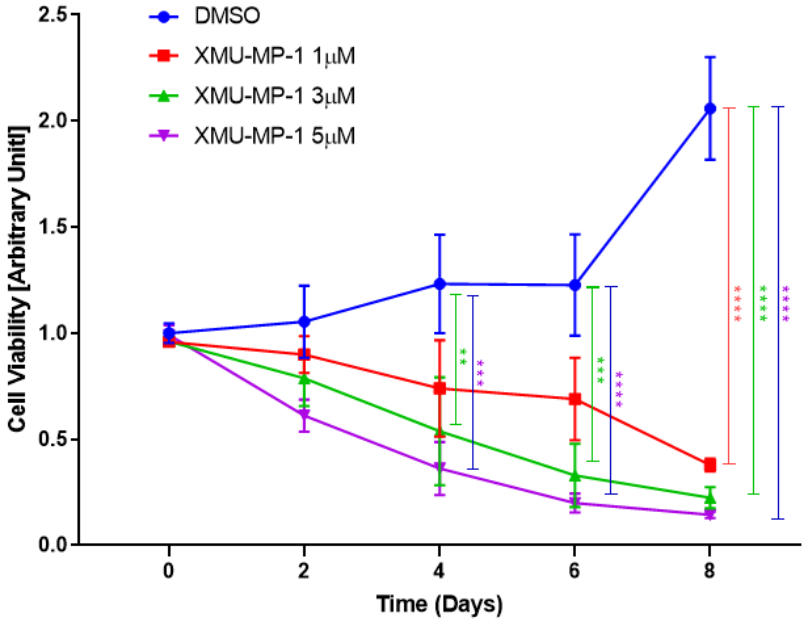

Figure 5.3 Analysis of HUVEC viability following XMU-MP-1 treatment using the alamarBlue® assay. HUVEC viability started to decline after two days of XMU-MP-1 treatment. A significant reduction in HUVEC viability was observed after four days of XMU-MP-1 treatment and persisted through the eight days. The decline in HUVEC viability occurred in a dose-dependent manner of XMU-MP-1 treatment. Data (shown as mean ± SEM) were analysed using two-way ANOVA followed by Tukey's multiple comparison test. **p<0.01, ***p<0.001 and ****p<0.0001 indicate significant differences in results. The number of independent experiments = 3.

5.4.2 The effects of XMU-MP-1 treatment on HUVEC proliferation

As mentioned before, the Hippo pathway is associated with cell proliferation. I sought to determine HUVEC proliferation in response to XMU-MP-1 treatment. I analysed the expression of proliferation markers, such as Ki-67 and Phospho Histone H3 (pH-H3), to assess the cell proliferation rate. HUVECs were treated with either DMSO or XMU-MP-1 (1 μM, 3 μM or 5 μM) for 24 hours, followed by fixation and immunofluorescence staining.

In the analysis of Ki-67 expression, I did not find a significant change in the level of Ki-67-positive cells following XMU-MP-1 treatment. I found a small decrease but not statistically significant in HUVEC proliferation when compared to the control group (Figure 5.4). On the other hand, the pH-H3 expression analysis demonstrated a substantial reduction in HUVEC proliferation in the XMU-MP-1 treatment at the dose of 3 μM and 5 μM (Figure 5.5).

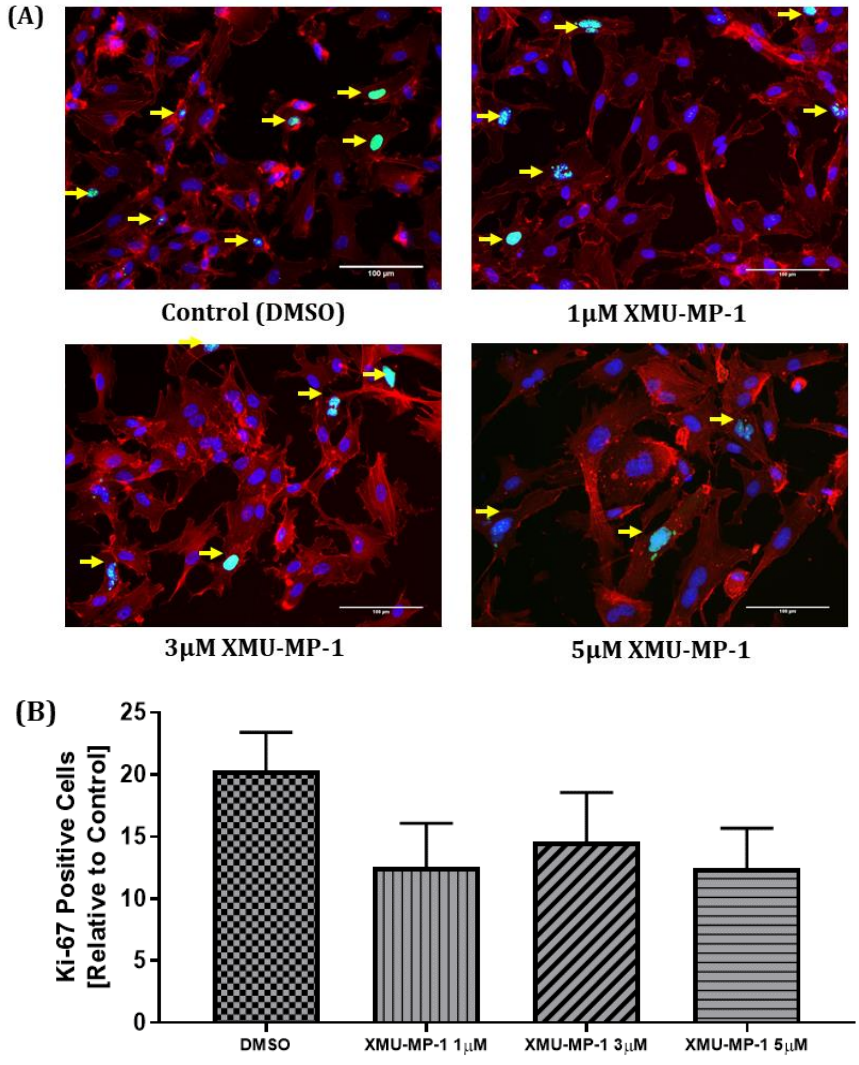

Figure 5.4 Ki-67 analysis in HUVECs. (A) Representative images of Ki-67 staining in HUVECs. Green fluorescence in the nuclei indicates positive Ki-67 cells (shown by yellow arrows). (B) Ki-67 rates in both control and XMU-MP-1 groups show a small decrease but not statistically significant in XMU-MP-1 treatment. Data (shown as mean ± SEM) were analysed using one-way ANOVA. The number of independent experiments = 5. (in total more than 2,000 HUVECs each groups were analysed). Scale bar = 100 μm.

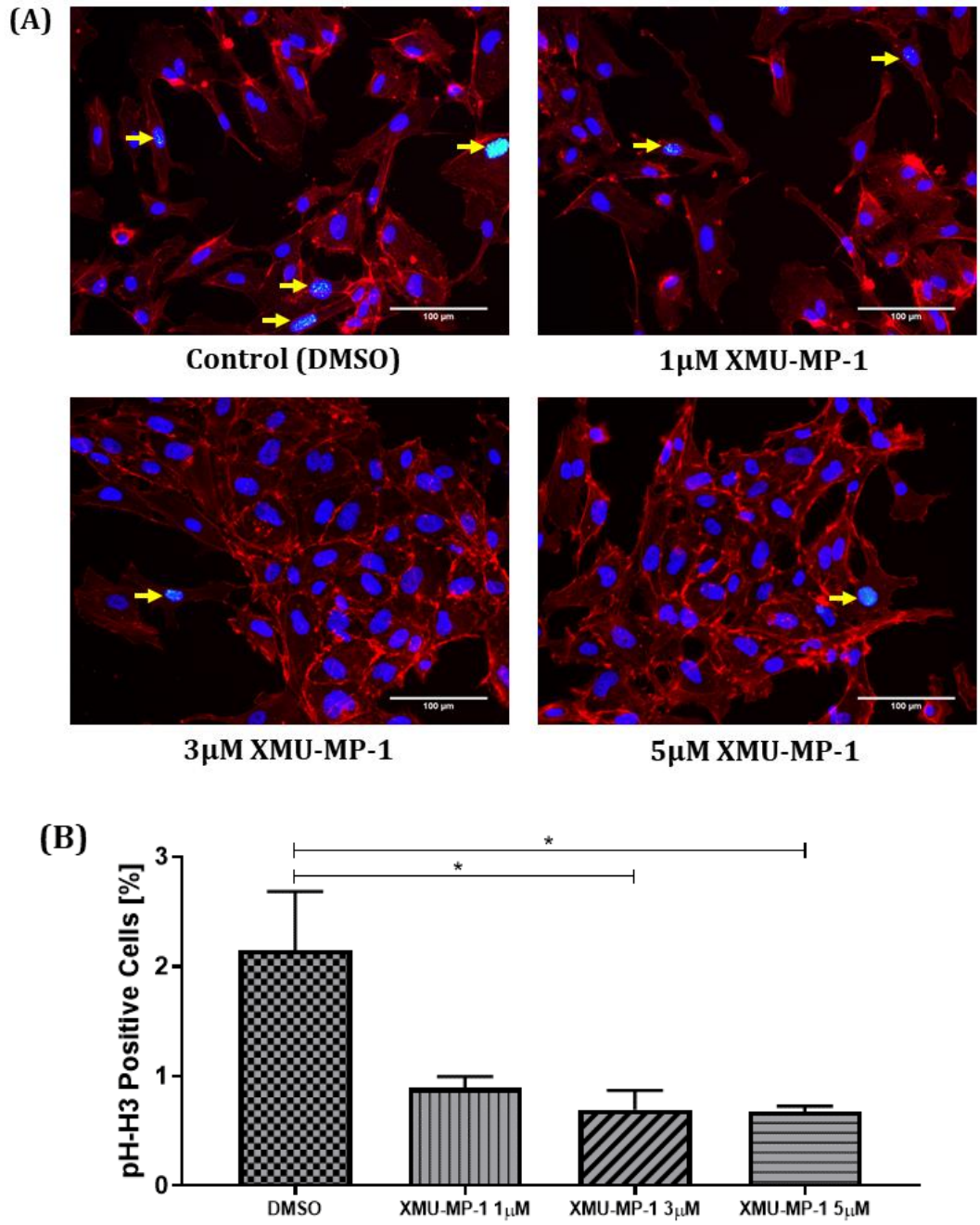

Figure 5.5 HUVEC proliferation determined using phospho-histone H3 (pH-H3) immunofluorescence. (A) Representative images of pH-H3 immunofluorescence staining in HUVECs. Green fluorescence in the nuclei indicates positive mitotic cells (shown by yellow arrows). (B) There is a significant reduction of pH-H3 positive rates in XMU-MP-1 groups at the dose of 3 μM (0.69 ± 0.18 %) and 5 μM (0.68 ± 0.05) compared to the control group (2.15 ± 0.53 %). The dose of 1 μM of XMU-MP-1 (0.89 ± 0.11) shows a reduction in pH-H3 rates, which is not statistically significant. Data (shown as mean ± SEM) were analysed using one-way ANOVA followed by Tukey's multiple comparison test. *$p<0.05$ indicates significant differences in the results. The number of independent experiments = 3. (more than 2,000 HUVECs were analysed). Scale bar = 100 μm.

5.4.3 The effects of XMU-MP-1 on *in vitro* angiogenesis assays

I conducted two different assays to examine *in vitro* angiogenesis using Matrigel and co-culture methods. A Matrigel assay can show the tubule-like formation from seeded HUVECs on a gel basement membrane matrix. The treatment (XMU-MP-1 or DMSO) was added to the seeding medium. The cells were kept in the incubator for 24 hours before they were examined under the microscope. Two cell types were used in the organotypic co-culture assay, i.e., HUVECs and human dermal fibroblasts (HDFs). HUVECs were seeded on top of HDFs that have been seeded on the culture flask one day before. After that, the cells were treated with XMU-MP-1 or DMSO. The administration of the treatments was every other day for thirteen days, followed by staining the cells for CD31 to observe capillary-like structures.

Based on my results on the Matrigel assay, there was an increase in the number of tubule-like structures in the cells treated with XMU-MP-1, but the changes are not statistically significant (Figure 5.6 A&B)

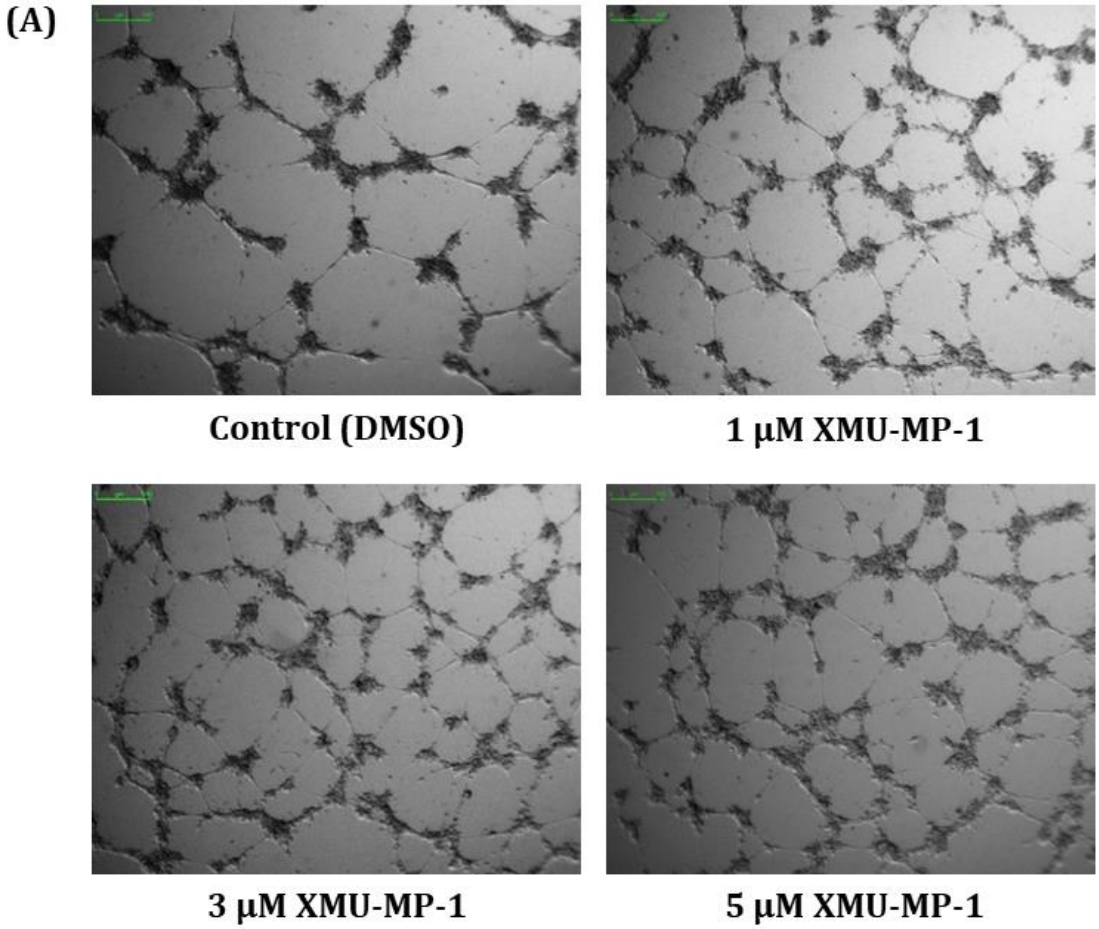

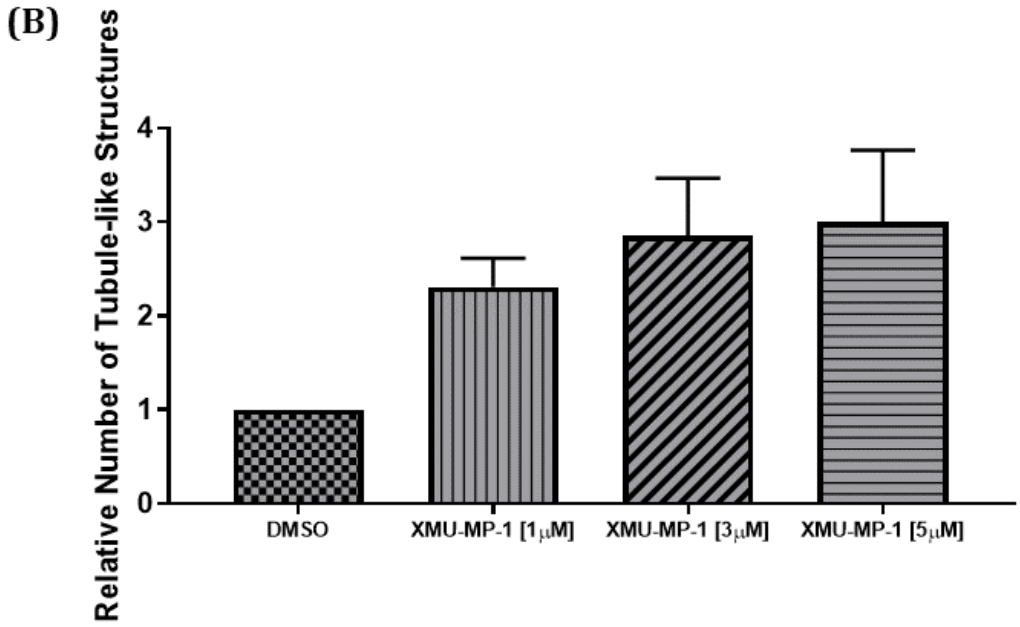

Figure 5.6 The analysis of tubule-like structures using a Matrigel assay. (A) Representative images of tubule-like structures in different treatment groups. (B) There is an increase in the number of tubule-like structures following XMU-MP-1 treatment, but this is not statistically significant. Data (shown as mean ± SEM) were analysed using one-way ANOVA. The number of independent experiments =5. Scale bar = 4 μm.

Interestingly, based on the organotypic co-culture experiment, I found a substantial reduction in the capillary-like structures in the cells treated with XMU-MP-1 (Figure 5.7 reveals the representative images of HUVEC tubule formation in co-culture assay). However, I could not analyse the statistical significance because I only conducted two independent experiments for this assay. Figure 5.8 shows the quantification of some parameters, such as the number of branches, numbers of junctions and the length of tubules, that indicate the level of tubule formation.

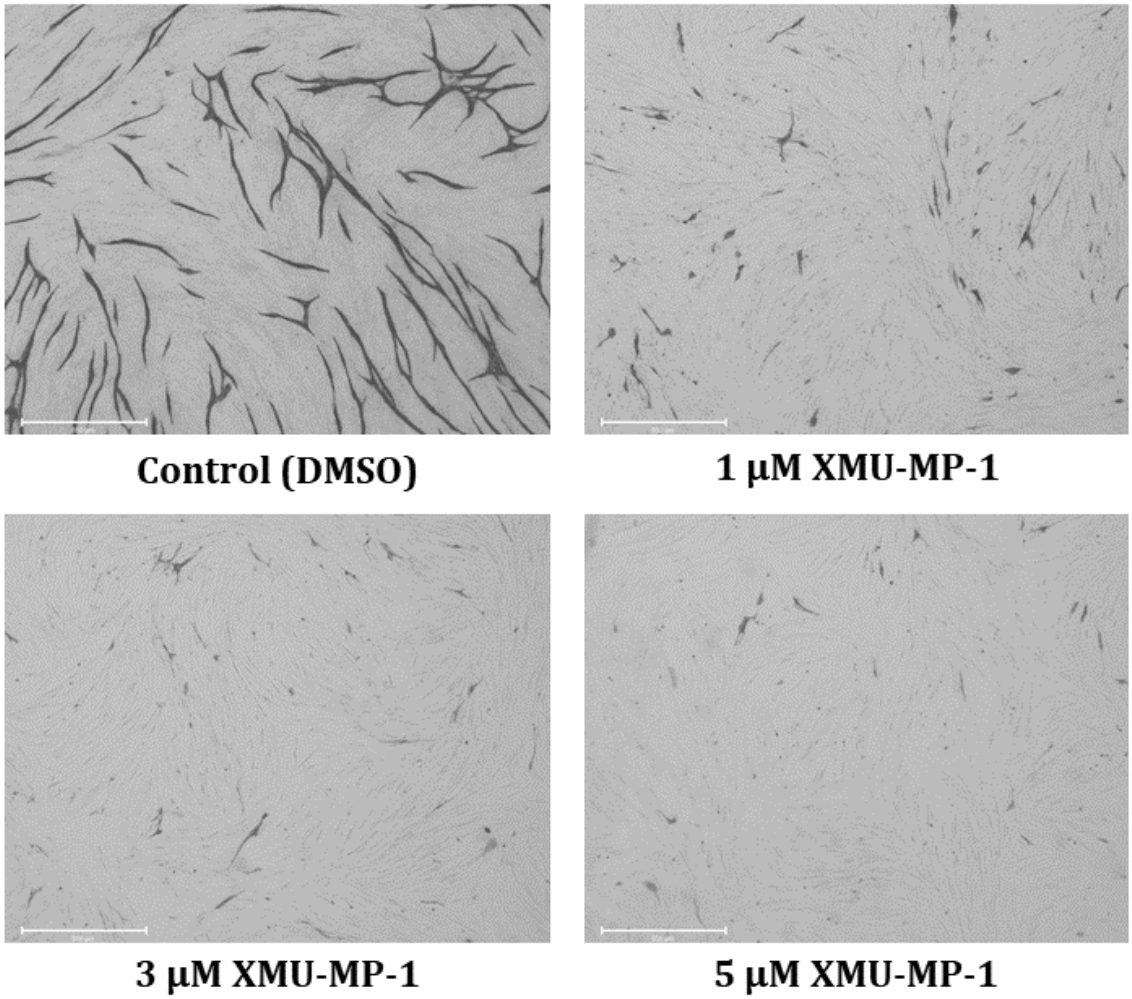

Figure 5.7 Tubule formation of HUVEC co-culture with human dermal fibroblasts with different treatments. The images represent how HUVECs can form tubules in the normal condition indicated by the connection between cells that form lining shapes with branches and junctions. These images were taken at the end of the co-culture experiment (day thirteen). The formation of tubules is almost absent in HUVECs treated with XMU-MP-1 at the given doses. Scale bar = 650 µm.

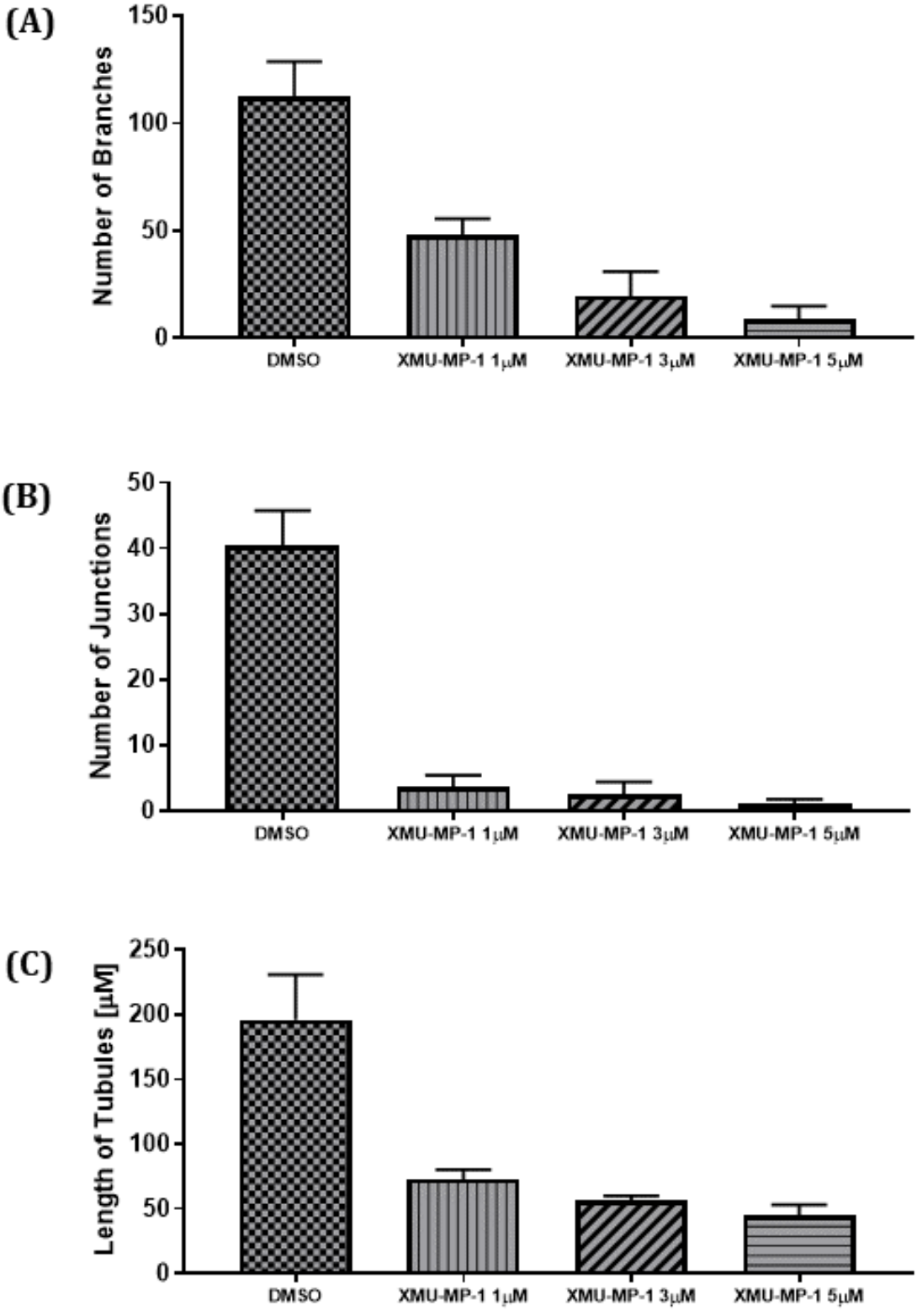

Figure 5.8 The quantification of the branch and junction numbers and tubule length based on the co-culture assay. All three angiogenesis parameters based on a co-culture assay reveal a similar trend showing that XMU-MP-1 treatments at the dose of 1 μM, 3 μM and 5 μM reduce the number of branches, the number of junctions and the length of tubules. The reduction of angiogenesis parameters seems to be dose-independent, showing the least levels in the highest dose of XMU-MP-1. Data (shown as mean ± SEM) were analysed using one-way ANOVA. The number of independent experiments =2.

5.4.4 HUVEC migration in response to XMU-MP-1 treatment

Endothelial cell migration is an essential aspect of the formation of new blood vessels. The migratory process allows endothelial cells to move and support sprout formation as one of the first steps of the angiogenesis process. To determine the association between XMU-MP-1 treatment and HUVEC migration, I performed the scratch-test assay. After seeding HUVECs on the 96-well plate, the wells were scratched using a sterile 96-pin wound maker. After the cells were washed using PBS, I changed the medium and added the treatments (DMSO, 1 μM XMU-MP-1, 3 μM XMU-MP-1 or 5 μM XMU-MP-1). The cells were monitored for 24 hours and captured every six hours using the Essen IncuCyte ZOOM system. As shown in Figure 5.9, my data on HUVEC migration demonstrates that there is no significant difference in the percentage of the migrated area between XMU-MP-1 treatment and the control group (treated with DMSO). Figure 5.10 shows HUVEC migration in each group every six hours.

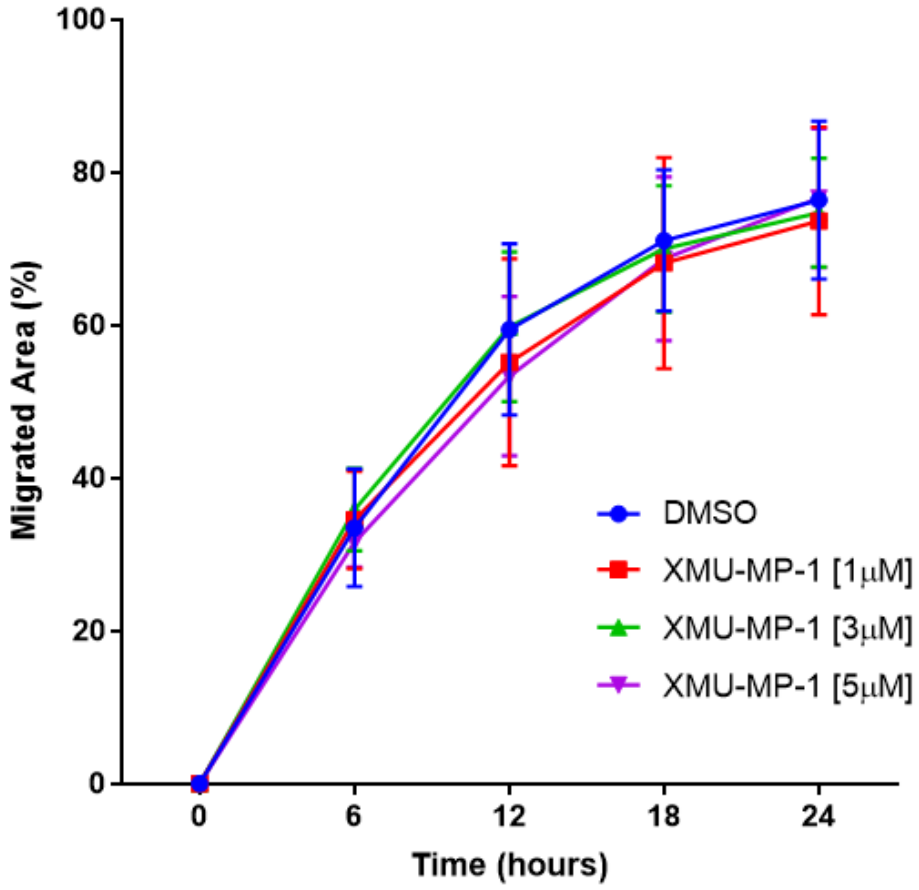

Figure 5.9 The analysis of HUVEC migratory capability. No statistical difference can be observed in the migrated area within 24 hours after different treatments. The average percentage of migration after 24 hours in all treatment groups is around 80%. Data (shown as mean ± SEM) were analysed using two-way ANOVA followed by Tukey's multiple comparison test. The number of independent experiments = 3. The number of HUVECs seeded on the plate for the scratch-test assay was 30,000 cells per well.

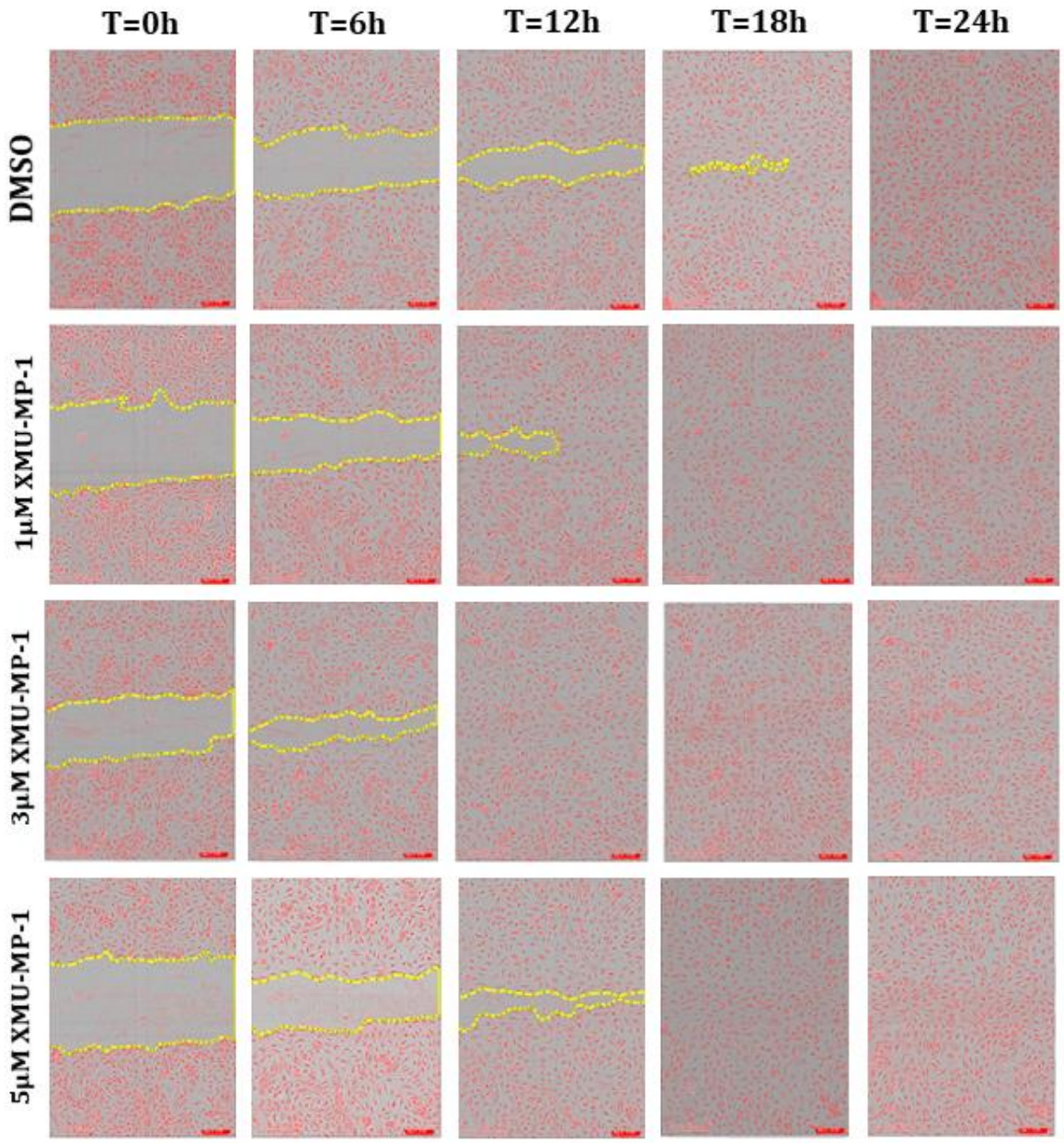

Figure 5.10 Representative images of the scratch-test assay. The images show an initial state of the well right after the scratch (T=0h) and the following six hours (T=6h), 12 hours (T=12h), 18 hours (T=18h) and 24 hours (T=24h), respectively. The red area illustrates the cell confluence; the grey area shows the scratch wound; the yellow lines are the wound edges. Scale bar = 100 μm.

5.4.5 Analysis of signalling pathways in HUVECs following XMU-MP-1 treatment

Western blot analysis was performed to determine the expression of proteins that were estimated to be involved in the mechanisms of how XMU-MP-1 affects angiogenesis. HUVECs were treated with either DMSO or XMU-MP-1 (1 μM, 3 μM or 5 μM) for one-hour prior to protein extraction. The relative expression of phosphorylated MOB1 to total MOB1 was determined to affirm the effect of XMU-MP-1 in the Hippo pathway in HUVECs. Figure 5.11 shows that the ratio between phosphorylated MOB1 and total MOB1 is reduced in

HUVECs treated with XMU-MP-1, even though this is not statistically significant. The number of independent experiments is possibly needed to get a statistical significance.

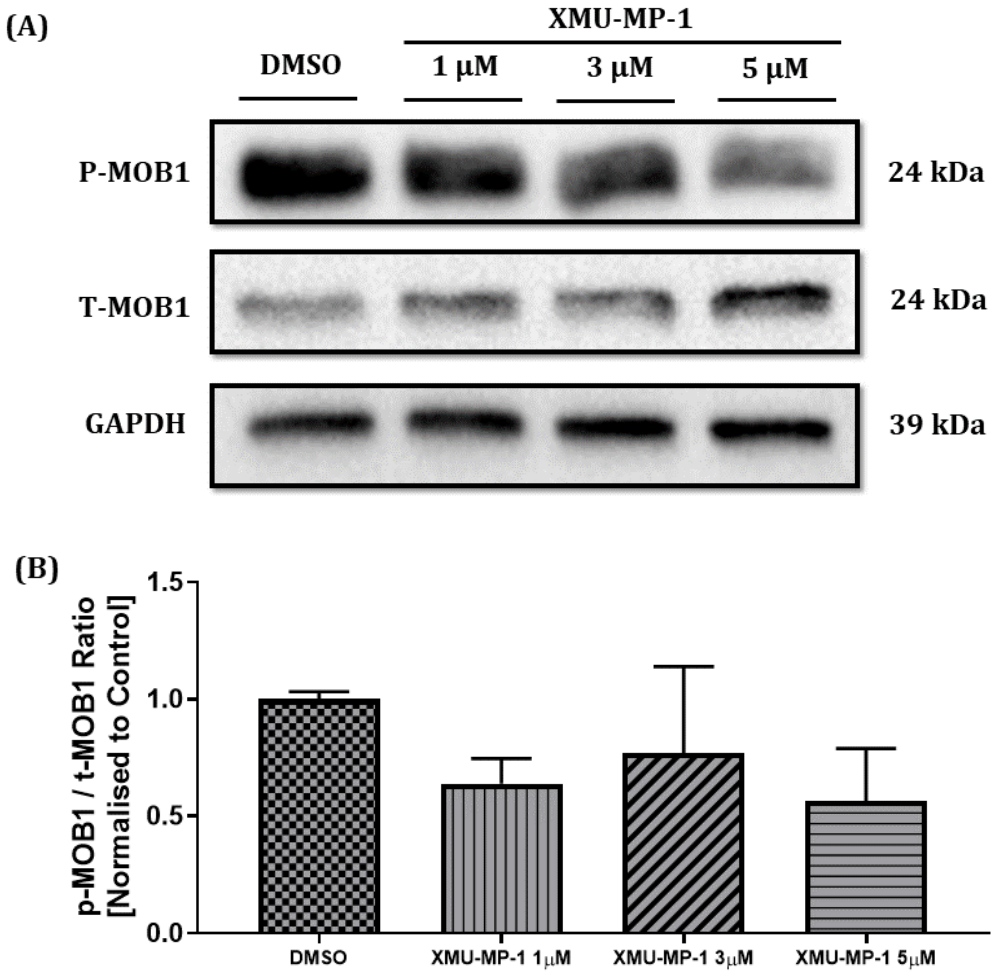

Figure 5.11 Protein analysis of the p-MOB1 to t-MOB1 ratio in HUVECs. (A) Representative bands of p-MOB1, t-MOB1 and GAPDH as a loading control. (B) Based on densitometry analysis, XMU-MP-1 treatments reduce the p-MOB1 to t-MOB1 ratio in HUVECs, but this is not statistically significant. Data were analysed using one-way ANOVA. N = 3 of independent experiments.

The inhibition of the Hippo/Mst could affect its crosstalk with the mitogen-activated protein kinase (MAPK) pathway. P38 MAPK plays an essential role in regulating angiogenesis mediated by VEGF. The inhibition of P38 MAPK is associated with the stimulation of VEGF-induced vasculogenesis and angiogenesis (Azad et al., 2018). To identify the change in P38 MAPK activity attributed to XMU-MP-1 treatment, an analysis of the ratio between phosphorylated P38 MAPK and total P38 MAPK was performed. However, there is no statistical significance observed in the ratio of phosphorylated P38 MAPK (p-P38 MAPK) to P38 MAPK in HUVECs treated with XMU-MP-1 (Figure 5.12). In the future, it is needed to treat HUVECs with VEGF too to get a pronounced increase in p-P38 MAPK.

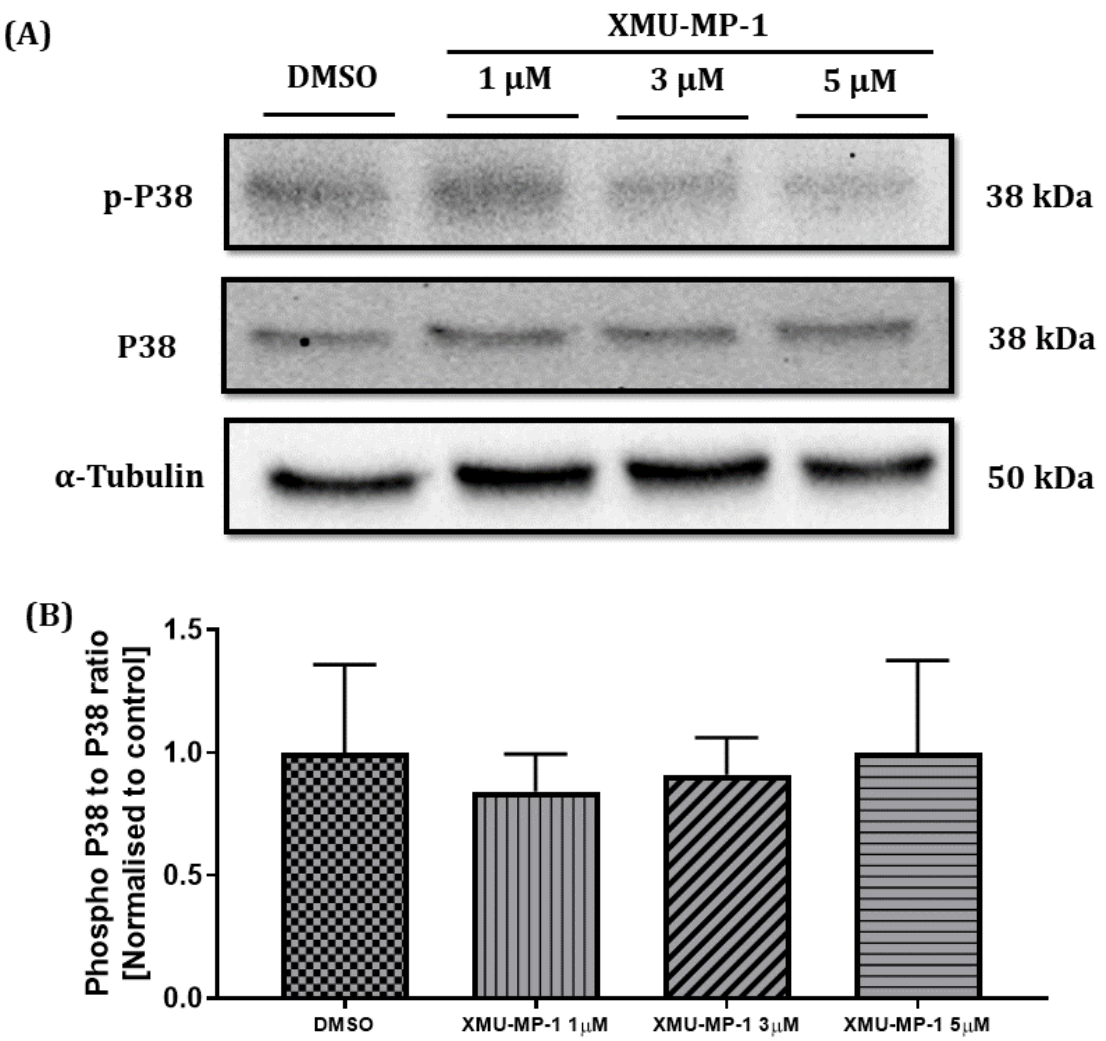

Figure 5.12 Western blotting of phosphorylated P38 MAPK and P38 MAPK in HUVECs. (A) Representative images of p-P38 and t-P38 compared to α-tubulin as a loading control. (B) The densitometry analysis suggests that XMU-MP-1 at the dose of 1 and 3 μM slightly reduces the activity of P38 MAPK, indicated by a small decrease in the p-P38 to t-P38 ratio. However, the reduction is not statistically different. Data were analysed using one-way ANOVA. N = 3 of independent experiments.

Apart from P38 MAPK, extracellular signal-regulated kinase (ERK)/MAPK also regulates angiogenesis by inducing endothelial cell proliferation, migration and tube formation. The effects of XMU-MP-1 on ERK1/2 activity were assessed to elaborate the possible mechanisms on how XMU-MP-1 causes changes in endothelial phenotypes (Azad et al., 2018). The activity of ERK1/2 was determined by measuring the ratio of phosphorylated ERK1/2 to total ERK1/2 from the western blot experiment. I found that there is no statistical difference between the control group and the dose of 1 μM and 3 μM of XMU-MP-1 treatment (Figure 5.13). The decrease of phosphorylated ERK1/2 expression is not distinct, which might be due to lacking VEGF stimulation. In the future, VEGF should be given together with other treatments.

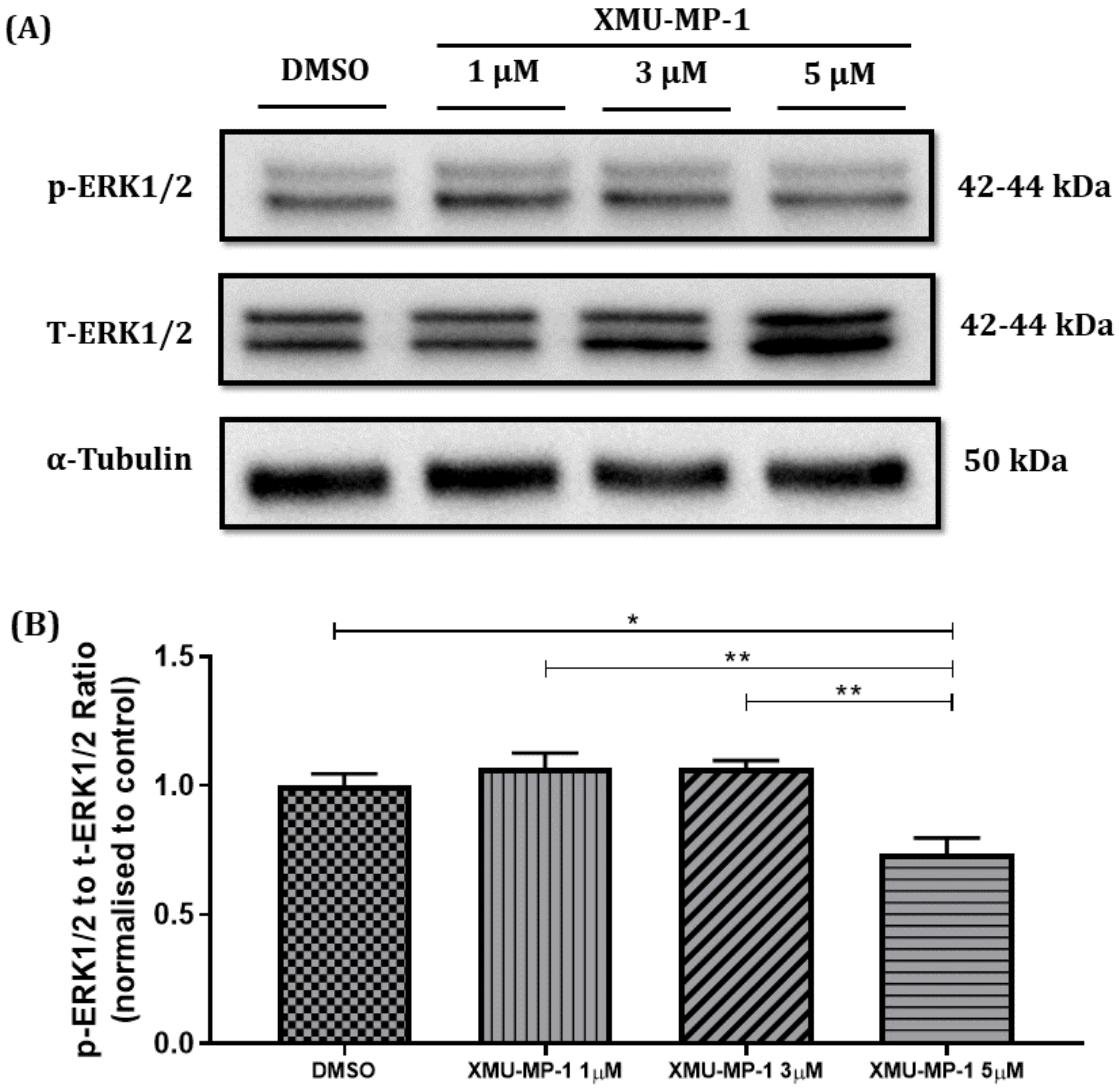

Figure 5.13 The analysis of ERK1/2 activity using the western blot experiment in HUVECs. (A) Representative images of p-ERK1/2 and t-ERK1/2 bands in HUVECs. (B) The densitometry analysis shows a significant reduction in the p–ERK1/2 to t-ERK1/2 ratio in HUVECs treated with 5 μM of XMU-MP-1 when compared to the control group and other XMU-MP-1 treatment groups (1μM and 3 μM). Data were analysed using one-way ANOVA followed by Tukey's multiple comparison test. *p<0.05 and **p<0.01 indicate significant differences in results. N = 3 of independent experiments.

As mentioned in the introduction, the activation of Mst1 during hypoxic conditions is required to promote FoxO1 activation. The role of FoxO1 is crucial in endothelial cell migration and sprouting-capacity. Additionally, FoxO1 is also essential in regulating endothelial cell morphology because it induces endothelial cell elongation, which is independent of VEGF intervention. I sought to verify whether XMU-MP-1 affects the endothelial phenotypes through its acting on FoxO1. The western blot data reveal that XMU-MP-1 treatment dose-dependently reduces the total FoxO1 protein expression in HUVECs (Figure 5.14). In the future, I plan to do a western blot with HUVEC samples to determine the expression of the phosphorylated FoxO1 to know the details of the interaction between XMU-MP-1 and FoxO1.

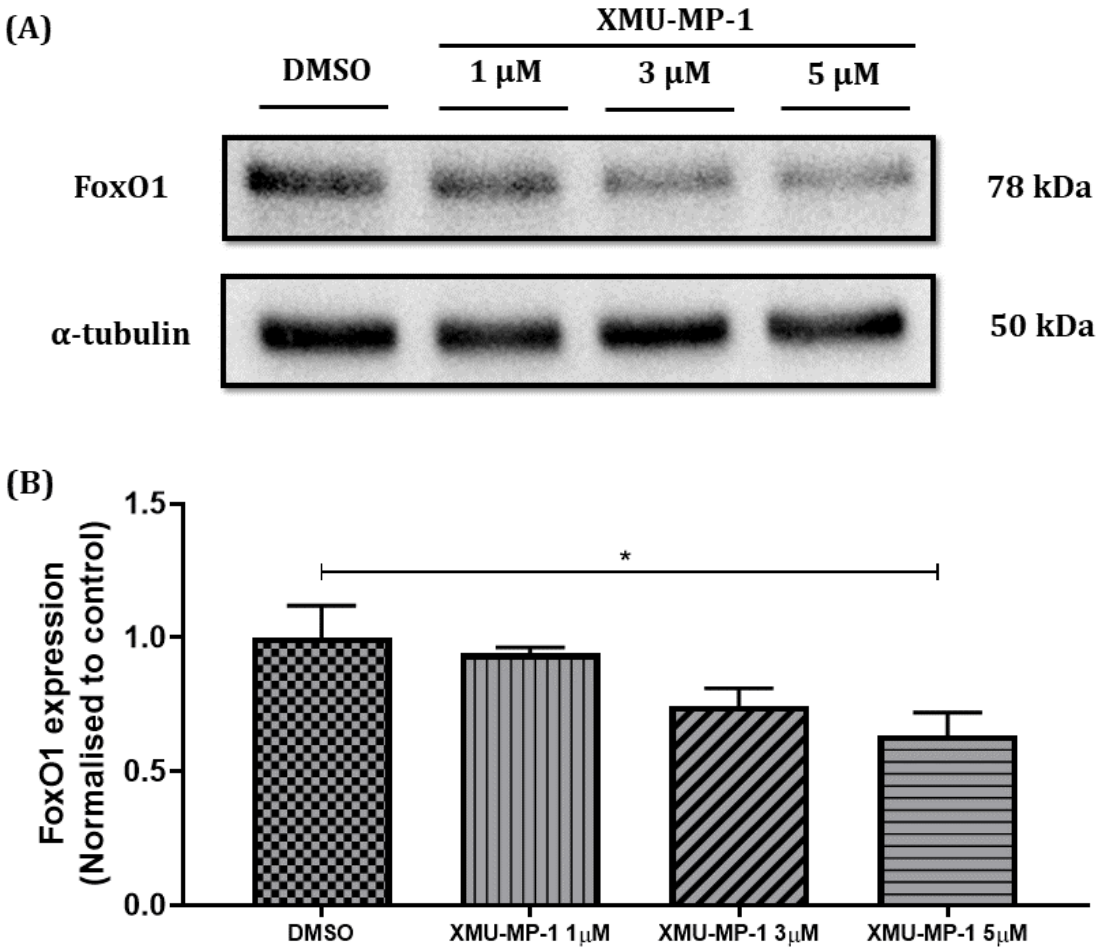

Figure 5.14 Protein levels of FoxO1 in HUVECs with different treatments. (A) Representative bands of FoxO1 protein and α-tubulin as a loading control. (B) My densitometry analysis suggests that XMU-MP-1 treatment dose-dependently reduces FoxO1 expression in HUVECs. Data were analysed using one-way ANOVA followed by Tukey's multiple comparison test. N = 4 of independent experiments.

Additionally, the effects of XMU-MP-1 on YAP activity were determined using the GAL4-UAS luciferase reporter system. I found that XMU-MP-1 at higher doses (3 and 5 μM) significantly increases YAP activity in HUVECs (Figure 5.15). This finding supports the western blot results on MOB1 protein, showing that the inhibition on MOB1 phosphorylation is followed by the activation of the Hippo effector, YAP. Taken together, XMU-MP-1 demonstrates its inhibition on the canonical Hippo pathway.

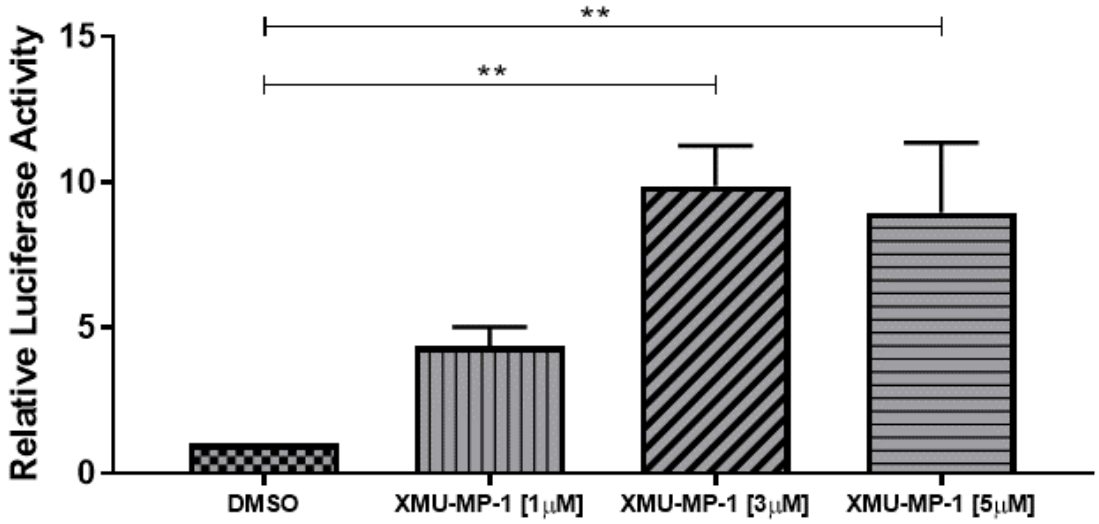

Figure 5.15 Following XMU-MP-1 treatment, YAP activity is significantly increased in HUVECs. Determination of YAP activity utilising a luciferase reporter system shows a significant increase at the higher dose of XMU-MP-1 (3 and 5 μM) following 24-hour treatment. Data were analysed using one-way ANOVA with Tukey's post-hoc test for multiple comparisons, **p<0.01 indicates significant differences in results. N = 5 of independent experiments.

5.5 Discussion

Novel therapeutic development that is involved in the angiogenic process is a potential strategy to treat cardiovascular diseases. The formation of new blood vessels from pre-existing vessels is known as angiogenesis. The angiogenesis process is frequently associated with pathways, such as PI3K-Akt, mTOR and Notch. Interestingly, there were some debates from previous studies regarding the association between angiogenesis and the Hippo pathway. Here I sought to add some data regarding the relationship between the Hippo/Mst and angiogenesis using a novel Mst1/2 inhibitor, XMU-MP-1. This chapter explains how XMU-MP-1 treatment affects HUVEC phenotypes.

5.5.1 XMU-MP-1 treatment alters endothelial cell viability

Endothelial cell viability is an important feature of angiogenesis. During the angiogenesis process, endothelial cell viability is determined by the balance between pro-angiogenic and anti-angiogenic cues. The way in which endothelial cell viability is altered by XMU-MP-1 treatment can be an indication of whether it is pro-angiogenic or anti-angiogenic.

Based on the analysis of cell viability using the MTT and alamarBlue® assays, XMU-MP-1 does not affect cell viability within 24 to 48 hours. However, the alamarBlue® assay suggests that prolonged XMU-MP-1 treatment might be toxic because it significantly reduces HUVEC viability if given for more than four days.

The toxicity of prolonged treatment of XMU-MP-1 in HUVECs was not observed in neonatal rat cardiomyocytes (NRCMs). However, the MTT assay in NRCMs following 24-hour treatment of XMU-MP-1 and 4-hour induction of H_2O_2 demonstrates a significant increase in cell viability compared to NRCMs treated with DMSO and H_2O_2. The opposite findings of the effects of XMU-MP-1 in cardiomyocyte viability might be associated with a difference in specific cell responsiveness. The effects of XMU-MP-1 in HUVECs have not been reported before. Accordingly, further elaboration of the XMU-MP-1 treatment in HUVECs is needed to comprehend the XMU-MP-1 mechanisms of action. Some explanatory reasons that could be considered are the possibilities of non-canonical effects of XMU-MP-1 in other pathways and inappropriate doses of XMU-MP-1 that affect HUVEC viability.

Fan et al. reported that XMU-MP-1 at the dose of 1 μM inhibits Mst3/4 (Mst3 IC_{50} = 44.8 nM; Mst4 IC_{50} = 27.3 nM) to a lesser degree than its inhibition of Mst1/2 (Mst1 IC_{50} = 9.8 nM; Mst2 IC_{50} = 18.2 nM) (Fan et al., 2016). The inhibition of XMU-MP-1 on Mst3/4 could be related to its effects on endothelial cells. Mst4 was reported to have a function in activating the ezrin-radixin-moesin (ERM) protein family that downregulates Rho, which ultimately promotes endothelial barrier function (Thompson and Sahai, 2015; Zheng et al., 2010). The inhibition of XMU-MP-1 on Mst4 might disrupt the endothelial barrier function. Based on the IC_{50} properties of XMU-MP-1, it is necessary to note that the effects of XMU-MP-1 on Mst4 might depend on the dose. However, the association between Mst4 inhibition and HUVEC viability needs to be further elaborated.

In addition to the inhibition on Mst kinases, XMU-MP-1 also inhibits other kinases, such as some of the tyrosine-protein kinases ABL1, aurora kinase A (AURKA), aurora kinase B (AURKB), Janus kinase 1 (JAK1), the mitogen-activated protein kinase kinase kinase (MAP3K) family, phosphatidylinositol 3-kinases (PIK3) and Serine/threonine-protein kinase (TAOK) family (Fan et al., 2016). The effects of XMU-MP-1 are not solely based on its activity on Mst1/2 because XMU-MP-1 can also interact with other kinases that might have some actions that affect cell viability.

5.5.2 The impacts of XMU-MP-1 in endothelial cell proliferation

A sprouting angiogenesis process needs the integration of some sequential events, including endothelial cell proliferation and migration. The Hippo pathway is strongly associated with cell proliferation. Accordingly, I carried out Ki-67 and Phospho Histone H3 (pH-H3) stainings to determine HUVEC proliferation. Both experiments exhibited a similar trend in HUVEC proliferation, showing that XMU-MP-1 treatment reduced HUVEC proliferation. A significant reduction in HUVEC proliferation was observed in XMU-MP-1 treatment at the dose of 3 and 5 μM when detected using the pH-H3 antibody.

Previous studies could explain the intriguing findings pertaining to HUVEC proliferation following XMU-MP-1 treatment. It has been reported that the Hippo pathway and CD44 work together to regulate endothelial cell proliferation. YAP/TAZ deletion results in the reduction of endothelial cell proliferation. Nuclear YAP/TAZ is essential for endothelial cell proliferation (Azad et al., 2019). Interestingly, the existence of YAP/TAZ in the cytoplasm is vital for endothelial cell migration. The balance between cytoplasmic and nuclear YAP/TAZ in endothelial cells is vital for regulating endothelial cell proliferation and migration during angiogenesis (Sakabe et al., 2017). XMU-MP-1 promotes YAP/TAZ localisation in the nucleus and hence disrupts the balance of YAP/TAZ levels in the nucleus and cytoplasms. HUVEC migration might be affected by XMU-MP-1 because it disturbs cytoplasmic YAP/TAZ function. However, it remains unclear how XMU-MP-1 reduces HUVEC proliferation, but it might be due to decreased HUVEC viability. In my experiments, increased YAP activity was not accompanied by an increase in HUVEC proliferation. Furthermore, I also observed an unprecedented change in the nuclear shape of endothelial cells treated with XMU-MP-1. The nuclei were not rounded and seemed to be in the mitotic phase but not fully separated. Further investigation is needed to determine the impact of the change in HUVEC nuclear shape on the proliferation and also the association between XMU-MP-1 treatment and the nuclear shape of HUVECs.

Another possible reason that might be attributed to the effects of XMU-MP-1 in HUVEC proliferation is the evidence that XMU-MP-1 has other substrates apart from the Hippo/Mst. XMU-MP-1 was reported to inhibit mitogen-activated protein kinase kinase kinase (MAP3K2 and MAP3K3) of the RAS/MAPK pathway (IC50 are 79.6 and 38.4 nM, respectively)(Fan et al., 2016). Both MAP3K2 and MAP3K3 have an essential function in endothelial cells. They stimulate MEK, which then activates ERK5 and induces endothelial cell proliferation (Nguyen et al., 2017). Eventually, the explanation of my results pertaining to the reduction of endothelial cell proliferation following XMU-MP-1 treatment might be due to a combination of XMU-MP-1 effects on the canonical Hippo pathway and the alternative pathway, RAS/MAPK.

5.5.3 XMU-MP-1 does not have a significant effect on the migration capacity of HUVECs

Endothelial cell chemotactic-migration and proliferation predominate the process of tubule formation in sprouting angiogenesis. Endothelial cells usually migrate towards pro-angiogenic cues. When healing some pathological cardiovascular conditions, neovascularisation is needed and it is vital to facilitate endothelial cell migratory capacity.

To ascertain whether XMU-MP-1 facilitates or ceases endothelial cell migration, I evaluated HUVEC migratory capacity using the scratch-test assay. The migration of the cells was monitored over a 24-hour period after scratching the surface of the plates. Essentially, the scratch makes a gap on the endothelial cells that were evenly spread out on the plates. The endothelial cells normally migrate towards the gap and cover the scratch. My data on the scratch-test assay do not exhibit any statistical difference in migration capacity among all treatment groups when compared to the control. The reason why I did not observe a significant difference in HUVEC migration might be due to the time point assessment. As described above, HUVEC viability assessed using alamarBlue® is not significantly changed over the 24-hour treatment of XMU-MP-1. A significant reduction in HUVEC viability was observed after four days of XMU-MP-1 treatment. Unfortunately, I could not observe cell migration for more than 24 hours because the scratch has been fully covered by the cells.

In the study by Sakabe et al. (2017), cytoplasmic YAP and TAZ regulate endothelial cell migration during angiogenesis through their control of the Rho family GTPase CDC42 activity. The ablation of YAP and TAZ results in the reduction of endothelial cell proliferation, branch-point and tip cell numbers. Interestingly, reduced YAP/TAZ phosphorylation by deleting LATS1 exhibited a decrease in the vascular area and tip cell numbers but is accompanied by an increment in branch-point number (Sakabe et al., 2017). This evidence might be considered to relate the effects of XMU-MP-1 on HUVEC migration because XMU-MP-1 inhibits Mst1/2 activities and ultimately increases YAP/TAZ phosphorylation. Further experiments, such as the transwell migration assay, using a greater dose range of XMU-MP-1 or seeding fewer endothelial cells, are needed to assess the effects of XMU-MP-1 on endothelial cell migration.

5.5.4 How XMU-MP-1 affects angiogenesis parameters in HUVECs

Angiogenesis can be determined using *in vitro* experiments. *In vitro* angiogenesis can be assessed using Matrigel and co-culture assays that visualise tube formation from seeded endothelial cells.

In this study, I examined the effects of XMU-MP-1 on *in vitro* angiogenesis using Matrigel and co-culture assays. In the Matrigel assay, I assessed *in vitro* angiogenesis following a 24-hour treatment of XMU-MP-1. Whereas in the co-culture assay, I determined *in vitro* angiogenesis following long-term treatment with XMU-MP-1 (thirteen days).

There is a non-significant increase in tubule-like formation in XMU-MP-1 treatment groups compared to the control group when assessed using a Matrigel assay. Intriguingly, based on an organotypic co-culture assay, prolonged XMU-MP-1 treatment reduced *in vitro*

angiogenesis. The discrepancy between Matrigel and organotypic co-culture results is possibly due to the different systems applied in both experiments. The Matrigel assay employed a basement membrane-like system to mimic the body's condition in which endothelial cells are surrounded by the extracellular matrix (ECM). A single cell type was used in the Matrigel assay. Thus it does not represent the real body condition. On the other hand, organotypic co-culture used two different types of cells, i.e., HUVECs and HDFs. In the organotypic co-culture system, HDFs provide a single-cell basement membrane for depicting the *in vivo* angiogenesis process. The distinct effects of XMU-MP-1 in HUVECs might be influenced by different angiogenesis signalling pathways involved in the Matrigel and organotypic co-culture assays. Additionally, the effects of XMU-MP-1 on HDFs have not been elucidated, but they might impact the angiogenesis process in the organotypic co-culture assay.

Sakabe et al. (2017) and Azad et al. (2018) mentioned that YAP and TAZ regulate angiogenesis in a dose-dependent manner. It is essential to maintain the balance of YAP/TAZ levels in the cytoplasms and nucleus (Azad et al., 2018; Sakabe et al., 2017). Based on the YAP luciferase analysis, XMU-MP-1 significantly enhances the interaction between YAP and TEAD, which indicates an increase in YAP translocation into the nuclei. Extensive migration of YAP from the cytoplasm into the nuclei can affect angiogenesis by inhibiting endothelial cell migration. Moreover, the non-canonical effects of XMU-MP-1 at a higher dose can affect endothelial cell viability by disrupting the endothelial barrier function through its inhibition on Mst4 (Thompson and Sahai, 2015). Conclusively, the XMU-MP-1 doses that I used to treat HUVECs might be too high. Further investigation is needed to determine the appropriate dose of XMU-MP-1 to enhance angiogenesis.

5.5.5 The effects of XMU-MP-1 in proteins involved in the angiogenesis pathway

The expression of phosphorylated MOB1 relative to total MOB1 is slightly decreased in endothelial cells that were treated with XMU-MP-1. As expected, XMU-MP-1 treatment results in YAP activation in endothelial cells showing its action in inhibiting the Hippo pathway. This confirmation can be considered as an explanation for my results regarding the changes in endothelial cell phenotypes associated with YAP/TAZ activity.

The MAPK pathway is strongly associated with the angiogenesis process. The inhibition of P38 MAPK has been revealed to induce VEGF-induced angiogenesis, whereas its activation reduces endothelial cell survival via c-Jun kinase (JNK) stimulation (Issbrücker et al., 2003). On the other hand, ERK1/2 MAPK is known to contribute to preserving endothelial cell survival and promoting angiogenesis (Mavria et al., 2006). In this study, I examined the expression of proteins in the MAPK pathway, which is also involved in the angiogenesis

process. My western blot analysis suggests that the effects of XMU-MP-1 on P38 and ERK1/2 MAPK activities are not statistically significant. Even though XMU-MP-1 shows significant effects on YAP activity in a dose-dependent manner, the effects of XMU-MP-1 on MAPK proteins are not pronounced. Further investigation using additional VEGF exposure and a greater range of the XMU-MP-1 dose is needed to explain the effect of XMU-MP-1 in angiogenesis.

Additionally, I also performed a western blot analysis on the FoxO1 protein to ascertain if XMU-MP-1 has other alternative pathways to affect angiogenesis. FoxO1 is a transcription factor that is essential in controlling the responsiveness of endothelial cells towards VEGFA as one of the pro-angiogenic cues (Furuyama et al., 2004; Jeon et al., 2018). Moreover, FoxO1 activity is essential in promoting sprouting angiogenesis and the activity of FoxO1 is induced by Mst1 in hypoxic conditions (Kim et al., 2019). My analysis reveals that the expression of FoxO1 in HUVECs is decreased in a dose-dependent manner by XMU-MP-1 and significantly reduced at a higher dose (5 μM). This finding supports the effects of XMU-MP-1 in changing endothelial cell phenotypes and angiogenesis. However, further studies are needed to elucidate the mechanisms underlying the effects of XMU-MP-1 in HUVECs.

5.6 Conclusion

In summary, my study adds to some insights about the effects of Hippo/Mst inhibition in endothelial cell phenotypes and angiogenesis. The canonical effects of XMU-MP-1 on the Hippo pathway influence angiogenesis in a dose-dependent manner. High-dose XMU-MP-1 (3 or 5 μM) and prolonged treatment of XMU-MP-1 are considered toxic to endothelial cells. XMU-MP-1 may also have some impacts on endothelial cells through its non-canonical effects. Further investigations, including *in vivo* experiments, are needed to get more information about the impacts of XMU-MP-1 on endothelial cells and the angiogenesis process.

CHAPTER 6

STUDIES ON A NOVEL MST2 INHIBITOR - MRT137

6.1 The theoretical overview and conceptual framework

This chapter encompasses a preliminary study on a new selective Mst2 inhibitor named MRT00056137, which will be referred to as MRT137 thereafter. MRT137 was identified as an Mst2 inhibitor by LifeArc during their kinase inhibitor screening project. LifeArc and our laboratory have established a collaboration for studying the effects of treatment with MRT137 in cardiomyocytes. LifeArc kindly supplied the compound, but due to the restriction in the MTA, they only provided us with the following information: i) molecular weight of MRT137 (Mr = 485.58); ii) the IC_{50} value for the Mst2 kinase inhibition is 0.0025 μM, which is equal to 2.5 nM. The IC_{50} value of MRT137 to Mst2 is lower than that in XMU-MP-1 (18.2 nM), meaning that MRT137 may inhibit Mst2 to a greater degree than XMU-MP-1. Unfortunately, there was no information on MRT137 molecular structure and whether MRT137 inhibits other Mst2 isoforms. It is interesting to examine whether a different degree of inhibition of the Hippo/Mst2 can affect cardiomyocyte phenotypes. Therefore, this chapter focuses on studying the effects of MRT137 in cardiomyocyte phenotypes (*in vitro*).

Considering that Mst2 is expressed in the heart, together with the fact that it interacts with Raf-1, there is a chance that Mst2 might affect cardiomyocyte survival. Raf-1 has a strong impact on the pro-apoptotic function of Mst2. The binding between Raf-1 and Mst2 results in the inhibition of Mst2 activity in promoting apoptosis (O'Neill and Kolch, 2005). Interestingly, Raf-1 itself has a crucial role in cardiac hypertrophy. When Raf-1 and Mst2 interaction is dissociated, Raf-1 activates MEK, which then stimulates ERK to induce a pro-hypertrophic transcription factor, GATA4 (Tham et al., 2015). The interaction between Mst2 and Raf-1 in hypertrophic response has not been widely explained. However, in a study by Zi et al. (2014), the role of Mst2 in cardiac hypertrophy was revealed. Global knockout of Mst2 significantly reduced TAC-induced cardiac hypertrophy in mice (Zi et al., 2014).

Raf-1 and Ras association domain family 1 isoform A (RASSF1A) play a crucial role in the crosstalk between Mst2 and ERK pathways. Both Raf-1 and RASSF1A are competing for binding with Mst2. RASSF1A and Mst2 complex results in Raf-1 and Mst2 binding disruption, which then promotes Raf-1-MEK binding and induces ERK activities. The RASSF1A-Mst2 binding also promotes Mst2 activity in inducing apoptosis. Interestingly, another Hippo kinase, LATS1, contributes to the Mst2 and ERK crosstalk. The downregulation of LATS1 results in dull feedback to Raf-1 and switches on the Raf-1 and MEK complex (Romano et al., 2014). Unfortunately, Romano et al. did not explain the effects of Mst2 downregulation in the Mst2 and ERK crosstalk mediated by Raf-1.

The role of Mst2 in the hypertrophy process was reported by Zi et al. in 2014. The systemic ablation of Mst2 protects the cardiomyocytes from hypertrophy in the pressure overload

condition. Interestingly, systemic deletion of Mst2 in mice does not affect cardiomyocyte proliferation (Zi et al., 2014). From the perspective of elaborating strategies to prevent cardiac hypertrophy with the least undesirable cell proliferation, the specific inhibition of Mst2 appears to be a potential approach. In this study, I conducted experiments to test the effects of Mst2 selective inhibition using MRT137 in the hypertrophy response and other cardiomyocyte phenotypes regarding the changes in the Hippo components. Figure 6.1 outlines the estimation of MRT137 effects in the hypertrophy pathway.

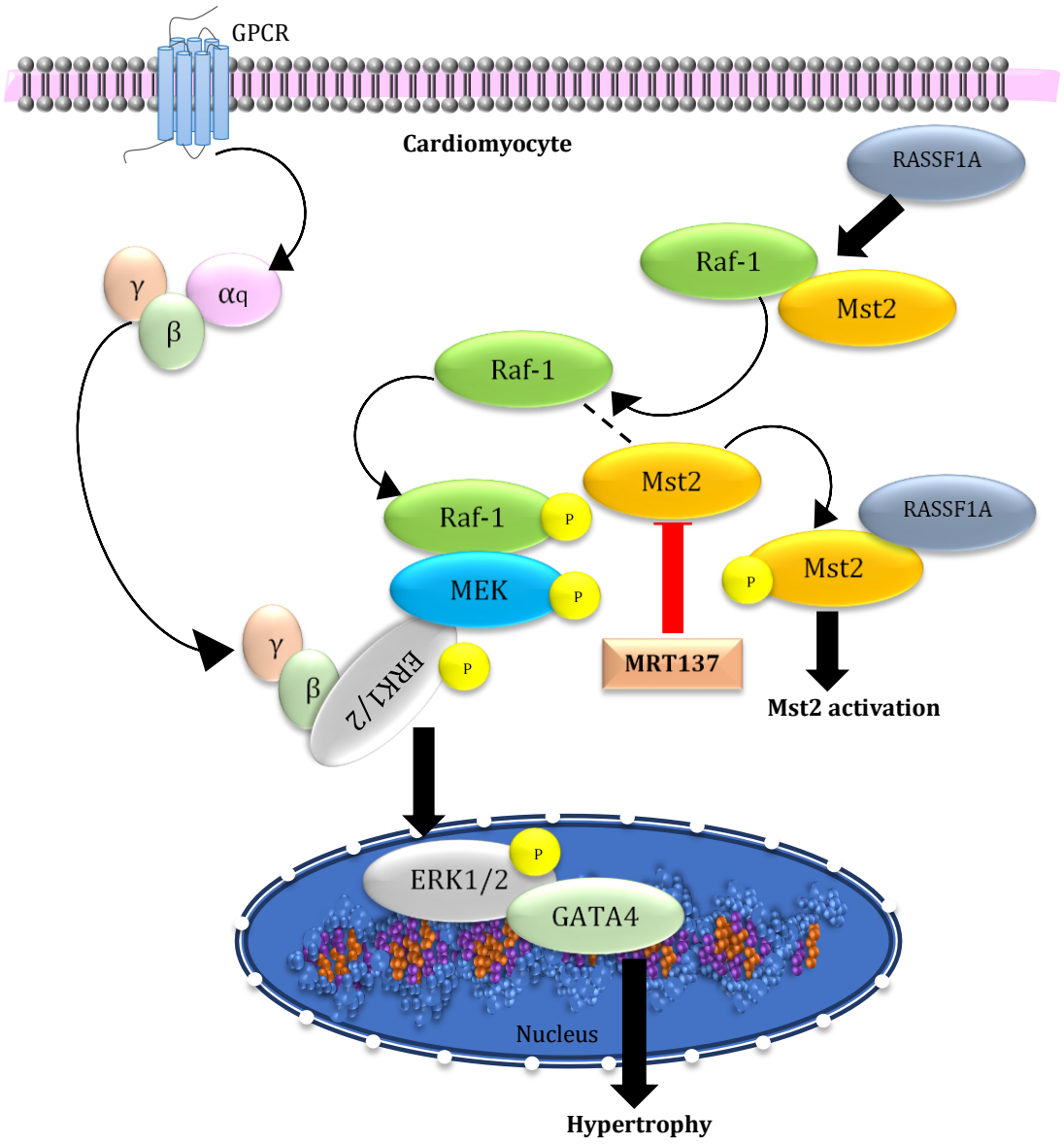

Figure 6.1 The crosstalk between the Hippo/Mst2 and ERK in the hypertrophy pathway. Raf-1 binding with Mst2 inhibits Mst2 activity. RASSF1A competes with Raf-1 to bind with Mst2. When RASSF1A disrupts the Mst2-Raf-1 complex, Mst2 will bind with RASSF1A and render in Mst2 activation. Raf-1, which detaches from Mst2, will interact with MEK and promote ERK1/2 activation. Active ERK1/2 will enter the nucleus and activate transcription factors and genes involved in hypertrophy. MRT137 strongly inhibits Mst2 activation. I postulated that the inhibition of Mst2 activity would induce Mst2-Raf-1 complex formation and reduce ERK1/2 activation.

6.2 Aims

This chapter principally investigates the role of Mst2 inhibition using a novel Mst2 inhibitor, MRT137, in neonatal cardiomyocyte phenotypes. Specific aims are as follows:

- To evaluate whether MRT137 affects YAP activity.
- To investigate whether inhibition of Mst2 using MRT137 affects cardiomyocyte hypertrophic response.
- To examine if inhibition of Mst2 using MRT137 alters cardiomyocyte proliferation.
- To determine if MRT137 increases survival and viability in cardiomyocytes.
- To characterise signalling pathways that might be altered by the Mst2 inhibition using MRT137.

6.3 Hypotheses

I suggest that pharmacological inhibition of Mst2 using MRT137 will help protect cardiomyocytes against pathological hypertrophy and enhance cardiomyocyte survival.

6.4 Results

This chapter describes cardiomyocyte phenotypes following Mst2 inhibition by MRT137. Three different doses of MRT137, 1 μM, 3 μM and 5 μM, were administered to the cultured neonatal rat cardiomyocytes. MRT137 was dissolved in DMSO. Hence, cardiomyocytes treated with an equal volume of DMSO were set as the control group. The duration of treatments depends on the types of experiments.

6.4.1 The analysis of YAP activity following MRT137 treatment

Mst2 is an upstream modulator of the Hippo pathway. YAP activity was assessed using the YAP luciferase and YAP translocation assay using a GFP-YAP reporter to confirm if Mst2 inhibition by MRT137 activates the Hippo pathway. Data from both YAP luciferase and YAP translocation assays show that YAP translocation into the nucleus is not significantly affected, but YAP activity is significantly increased by MRT137 treatment at the dose of 1μM (Figure 6.2).

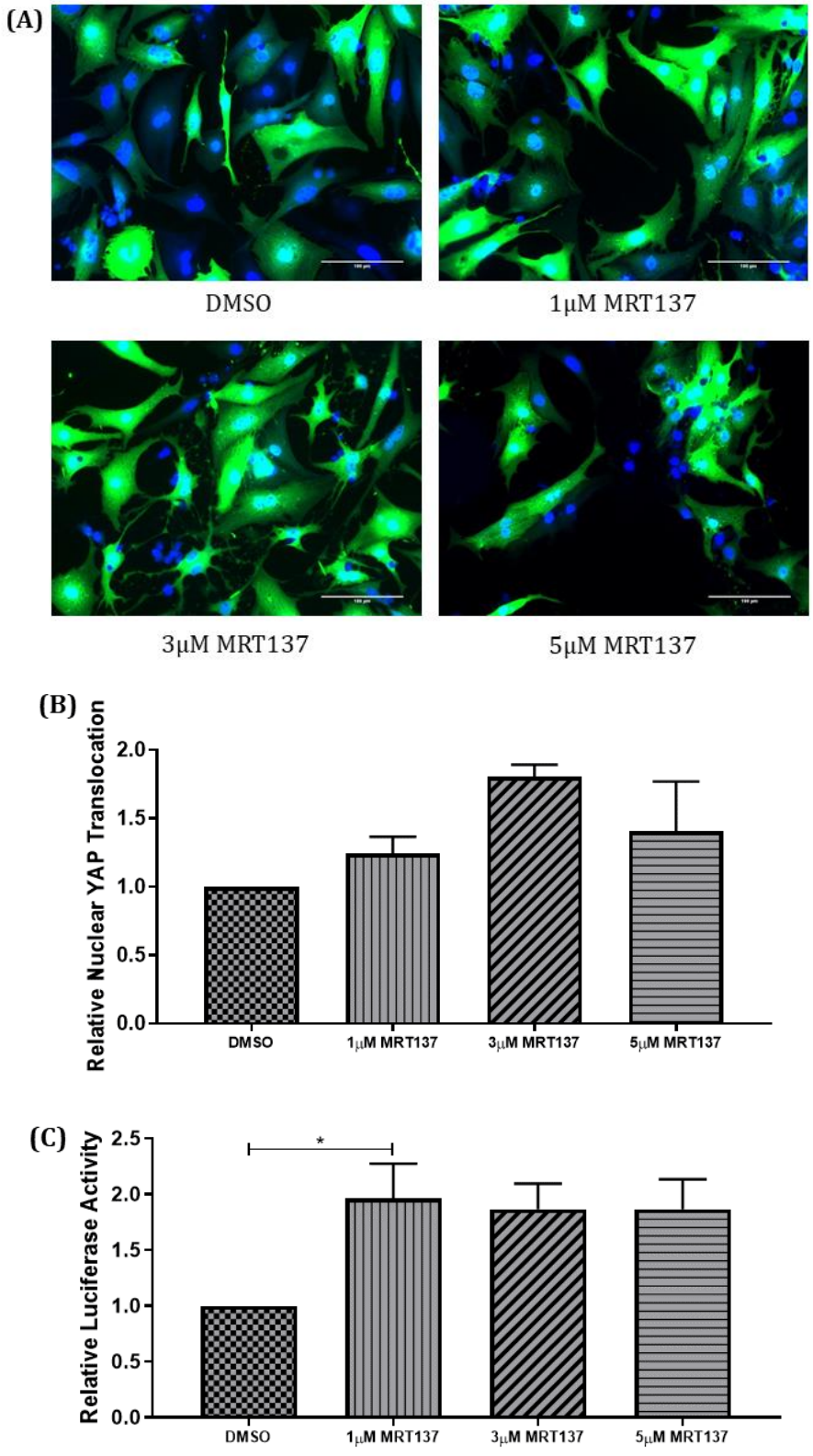

Figure 6.2 The analysis of YAP activity in NRCMs following MRT137 treatment. (A) Representative images of YAP translocation assay in NRCMs following MRT137 treatment. The green fluorescence signal shows the location of YAP in the cells. (B) YAP translocation into the nucleus is increased following MRT137 treatment, but this is not statistically significant. More translocation of YAP into the nucleus indicates more active YAP in the cells. (C) YAP luciferase assay suggests that MRT137 enhances YAP activity. The statistical significance was observed in the MRT137 group at the dose of 1 μM. Data (shown as mean ± SEM) were analysed using one-way ANOVA with Tukey's post-hoc test for multiple comparisons, *$p<0.05$ indicates significant differences in results. The number of independent experiments = 3. The number of NRCMs seeded were 250,000 for both assays and more than 1,000 NRCMs were analysed in the YAP translocation assay. Scale bar = 100 μm.

6.4.2 Characterisation of cardiac hypertrophy markers in response to MRT137 treatment

As discussed in the introduction, Mst2 has a pivotal role in the crosstalk between the Hippo and ERK pathways. The crosstalk lets the Mst2 interfere in the hypertrophy process through modulation of ERK activity. The effects of MRT137 in phenylephrine-induced cardiomyocyte hypertrophy were examined using a BNP luciferase assay and cell size measurement.

BNP expression (a marker of cardiomyocyte hypertrophy) was determined using the BNP luciferase assay. Data shown in Figure 6.3 suggests that there is a reduction of BNP luciferase activity in the MRT137 treatment groups, but this is not statistically significant. The results show the potency of MRT137 in inhibiting the hypertrophy process.

The results of the BNP luciferase assay were confirmed by cell size measurement. NRCMs were treated with 50 μM of phenylephrine to induce hypertrophy for 72 hours. The treatment of DMSO or MRT137 was given concomitantly with phenylephrine. NRCMs were stained using the anti-α-actinin antibody to make the cell shape visible. The analysis of cell size reveals that MRT137 at the dose of 3 and 5 μM significantly protects the cardiomyocytes from phenylephrine-induced hypertrophy (Figure 6.4).

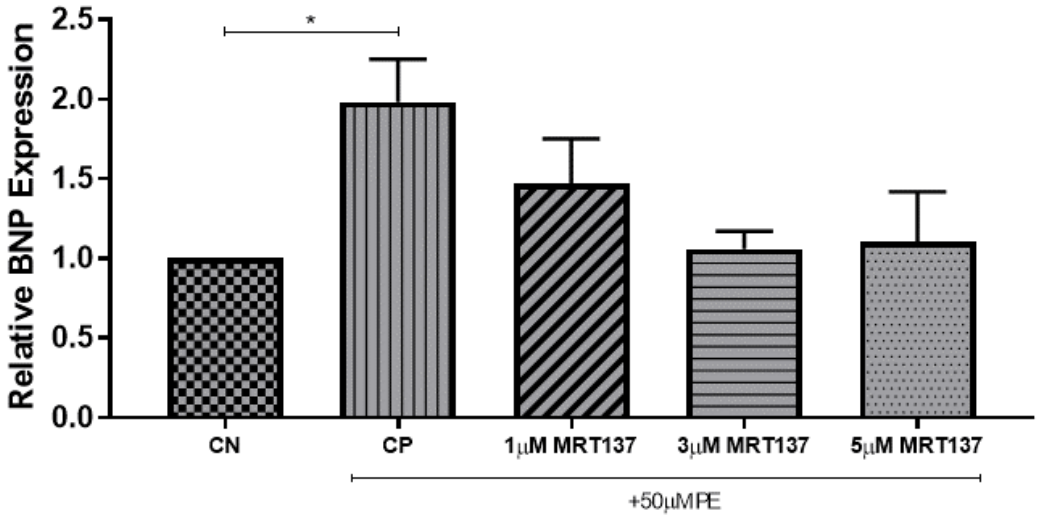

Figure 6.3 the analysis of BNP luciferase assay in NRCMs following MRT137 treatment. The exposure of 50 μM phenylephrine for 14 hours significantly escalates BNP activity by almost twice as much as the negative control (CP = 1.98 ± 0.27). A small reduction but not statistically significant of BNP reporter activity is shown in the MRT137 treatment groups (1 μM = 1.47 ± 0.28; 3 μM = 1.06 ± 0.11; 5 μM = 1.11 ± 0.31). Data (shown as mean ± SEM) were analysed using one-way ANOVA with Tukey's post-hoc test for multiple comparisons, *$p<0.05$ indicates significant differences in results. The number of independent experiments = 6. The number of NRCMs seeded = 250,000 for the BNP luciferase assay.

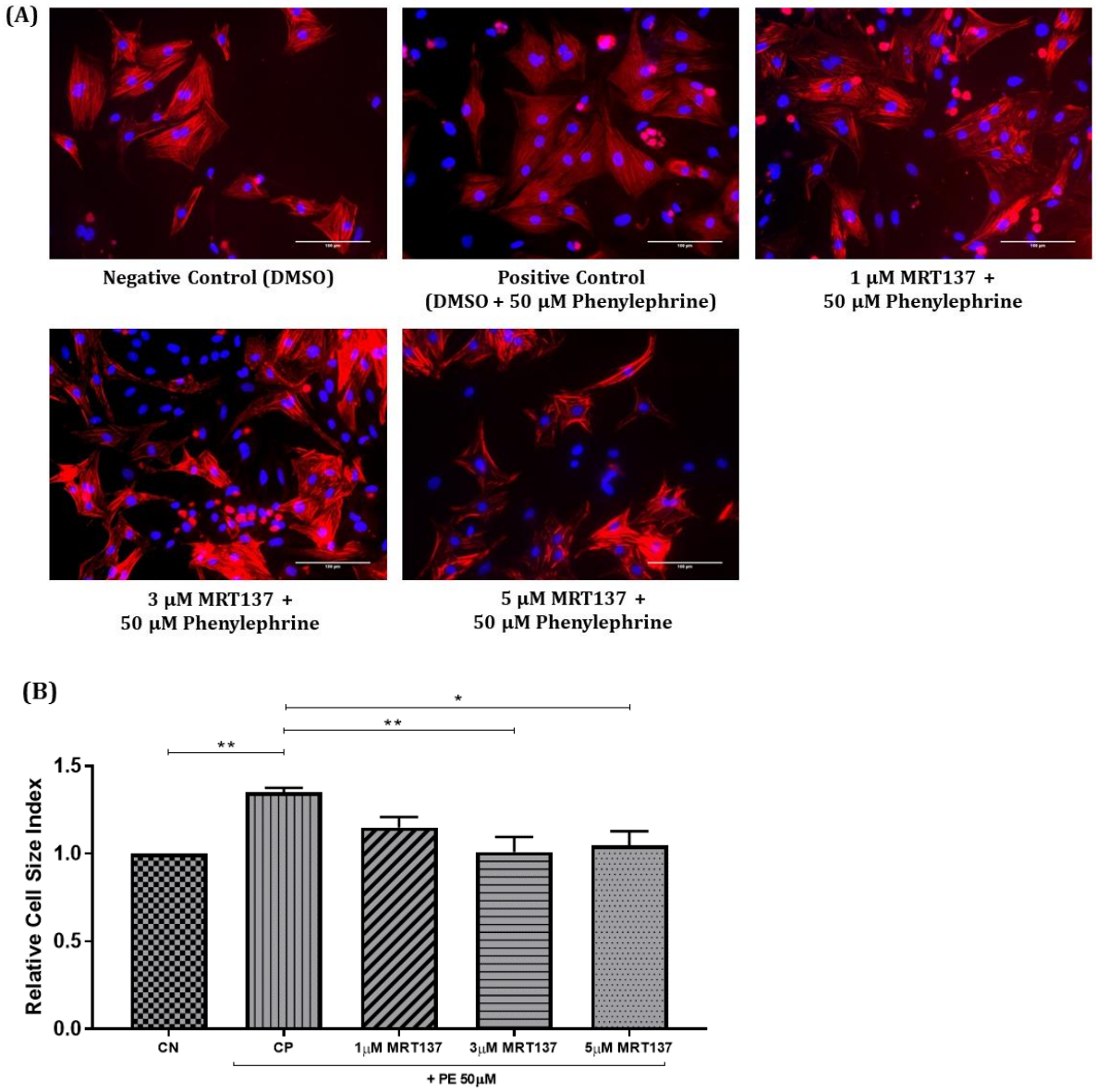

Figure 6.4 The cardiomyocyte size analysis following MRT137 treatment. (A) Representative images of cardiomyocytes immunofluorescence stained using the anti-α-actinin antibody. (B) The 72-hour exposure of 50 µM phenylephrine significantly causes cardiomyocyte enlargement (CP = 1.35 ± 0.03). MRT137 at the dose of 3 and 5 µM shows a significant decrease in cell size (1.01 ± 0,09 and 1.05 ± 0,08, respectively). 1 µM MRT137 displays a small decrease but not a statistically significant one (1.15 ± 0.06). Data (shown as mean ± SEM) were analysed using one-way ANOVA with Tukey's post-hoc test for multiple comparisons, *p<0.05 and **p<0.01 indicate significant differences in results. The number of independent experiments = 4. More than 100 cardiomyocytes were analysed in each independent experiment for cell size analysis. Scale bar = 100 µm.

6.4.3 The effects of MRT137 treatment in cardiomyocyte proliferation

Both Mst1 and Mst2 reduce YAP activation in the canonical Hippo pathway. The downregulation of YAP activity will result in the reduction of cell proliferation. However, the systemic ablation of Mst2 does not affect cardiomyocyte proliferation (Zi et al., 2014). Thus, as a selective Mst2 inhibitor, MRT137 is expected to produce weaker effects in

inducing cell proliferation. The role of MRT137 in cell proliferation was assessed using the analysis of cell proliferation markers: the phospho-Histone H3 (pH-H3) and Ki-67.

Cardiomyocyte proliferation analysis demonstrated that MRT137 enhances cell proliferation, as indicated by more positive cells with the pH-H3 staining in the MRT137 group when compared to the control group. An increase in cardiomyocyte proliferation is observed at the dose of 1 and 3 μM of MRT137 but not at 5 μM (Figure 6.5).

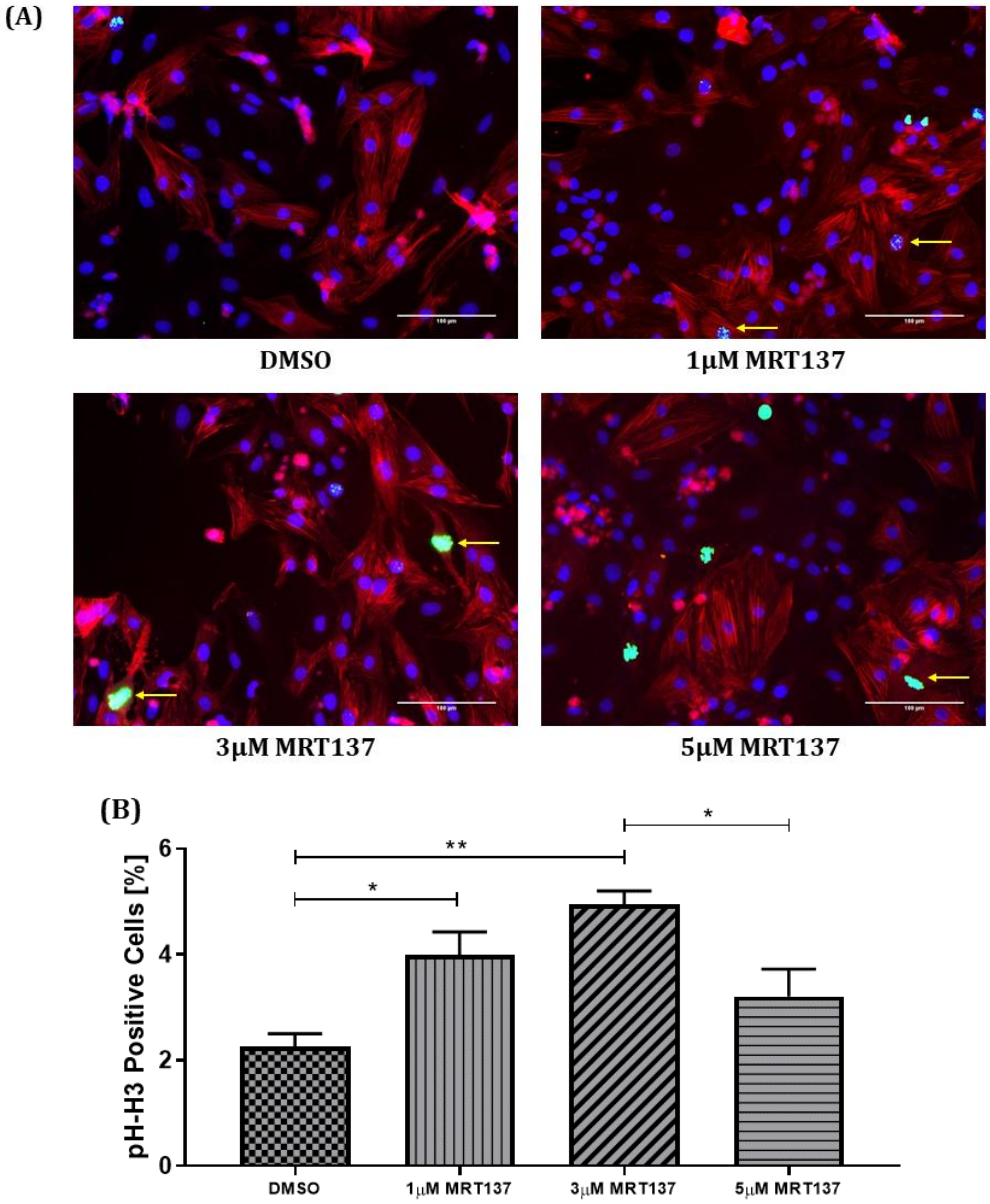

Figure 6.5 The analysis of mitotic cardiomyocytes following MRT137 treatment. (A) Representative images of pH-H3 staining in neonatal cardiomyocytes following MRT137 treatment. The co-localisation of red, blue and green fluorescence signals indicates positive mitotic cardiomyocytes (shown by yellow arrows). (B) MRT137 at the dose of 1 and 3 μM shows a significant increase in the mitotic cardiomyocyte rate (3.98 ± 0.43 % and 4.95 ± 0.25 %, respectively) when compared to the control group (2.27 ± 0.24 %). 5 μM of MRT137 shows a significant decrease in cardiomyocyte proliferation (3.21 ± 0,52 %) compared to other doses of MRT137. The decrease might be caused by MRT137 toxicity. Data (shown as mean ± SEM) were analysed using one-way ANOVA with Tukey's post-hoc test for multiple comparisons, *$p<0.05$ and **$p<0.01$ indicate significant differences in results. The number of independent experiments = 3 (more than 1,000 cardiomyocytes were analysed in each independent experiment). Scale bar = 100 μm.

The analysis of the Ki-67 expression also confirms that MRT137 significantly enhances cardiomyocyte proliferation significantly. The analysis of Ki-67 expression in Figure 6.6 indicates that MRT137 at a lower dose (1 μM) enhances cardiomyocyte proliferation approximately two-fold compared to the control group. At higher doses of MRT137 (3 and 5 μM), the cardiomyocyte proliferation is higher than that in the control group but is less than that in 1 μM of MRT137. As one might expect, MRT137 at higher doses can affect other kinases or proteins that compensate for the effects of MRT137 on cardiomyocyte proliferation.

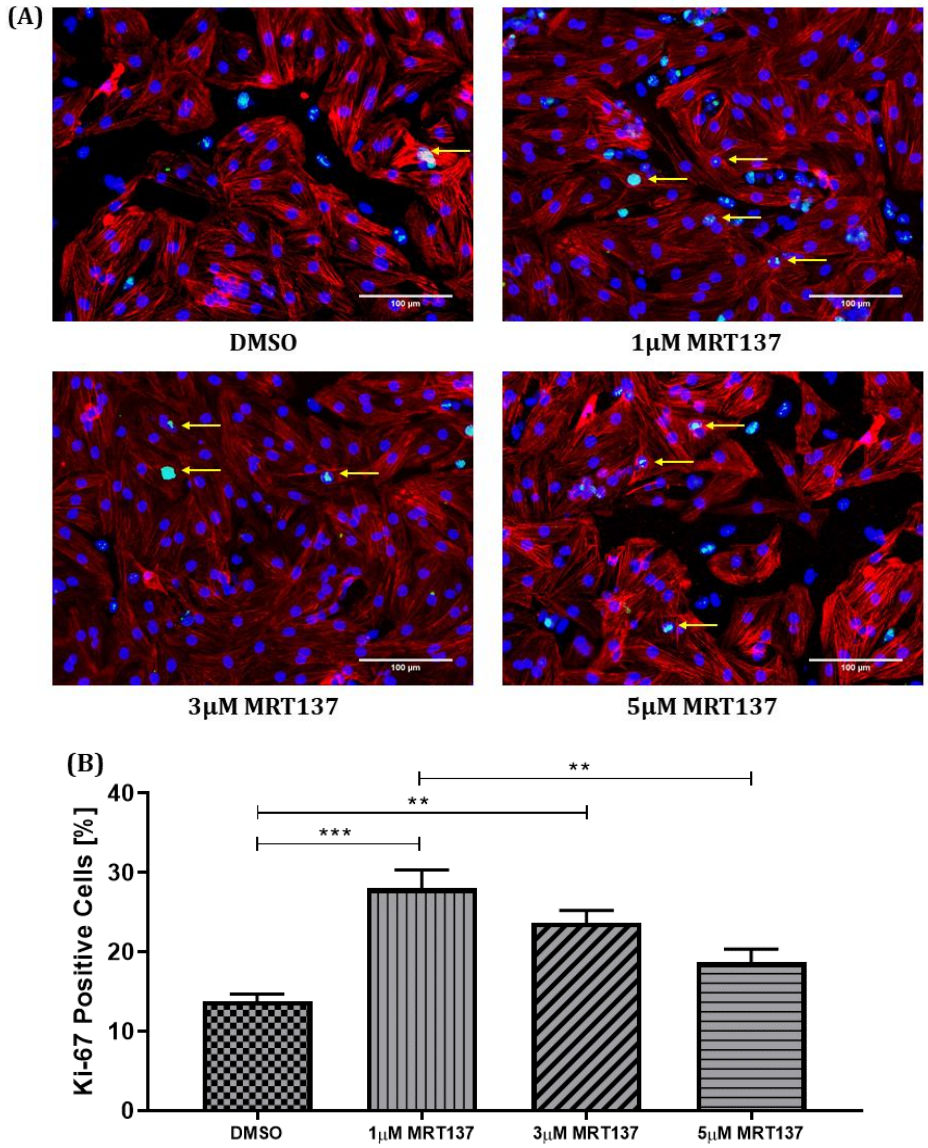

Figure 6.6 Ki-67 analysis in cardiomyocytes following MRT137 treatment. (A) Representative images of Ki-67 staining. The co-localisation of red, blue and green fluorescence signals indicates positive Ki-67 cells (shown by yellow arrows). (B) A significant increase in cardiomyocyte proliferation was observed in the MRT137 treatment groups at the dose of 1 μM (28.04 ± 2.31 %), 3 μM (23.73 ± 1.73 %) and 5 μM (18.69 ± 1.67 %) compared to the control group (13.81 ± 0.92 %). The proliferation rate is decreased dose-dependently in the mRT137 groups. This is probably due to its toxicity in higher doses. Data (shown as mean ± SEM) were analysed using one-way ANOVA with Tukey's post-hoc test for multiple comparisons, **p<0.01 and ***p<0.001 indicate significant differences in results. The number of independent experiments = 4 (more than 1,000 cardiomyocytes were analysed in each independent experiment). Scale bar = 100 μm.

6.4.4 Cardiomyocyte viability associated with MRT137 treatment

As mentioned in the introduction, Mst2 is involved in apoptosis modulation through its regulation of YAP activity and interaction with Raf-1/RASSF1A. Therefore, MRT137 may enhance cardiomyocyte viability following pathological stimulation, such as oxidative stress. To address this question, I performed experiments using 100 μM H_2O_2 as an oxidative stress inducer. The cardiomyocyte viability was identified using the MTT assay. Briefly, H_2O_2 was administered together with the treatments (either MRT137 or DMSO) for four hours. At the end of the incubation period, MTT solution was added onto the medium until purple crystals appeared. The purple crystals were dissolved in the solubilisation solution, then the absorbance of the solution was measured at 570 nm. Data on the MTT assay demonstrate that MRT137 does not significantly increase cardiomyocyte viability. Despite its statistical insignificance, cardiomyocyte viability in the MRT137 treatment groups is higher than that in the positive control group (Figure 6.7).

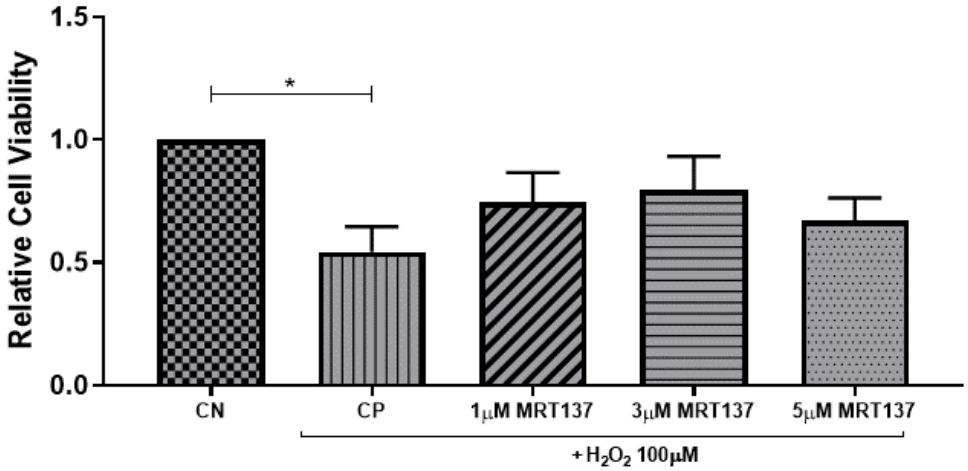

Figure 6.7 The MTT analysis in cardiomyocytes following 100 μM H_2O_2 and MRT137 treatment. The 4-hour exposure of 100 μM H_2O_2 significantly decreases cell viability (CP = 0.54 ± 0.10). The MRT137 treatment at any dose shows a small increase in cell viability but not statistically significant. Data (shown as mean ± SEM) were analysed using one-way ANOVA with Tukey's post-hoc test for multiple comparisons, *p<0.05 indicates significant differences in results. The number of independent experiments = 4. The number of NRCMs seeded = 250,000 for MTT assay.

6.4.5 Molecular changes in Cardiomyocytes following MRT137 treatment

As previously mentioned, Mst2 firmly controls some signalling pathways, including the Hippo and ERK pathways. The modulation of Mst2 activity by MRT137 brings some changes in the expression of proteins involved in both pathways. The changes of some proteins closely related to Mst2 were determined using a western blot analysis.

As a potent Mst2 inhibitor, MRT137 does not seem to alter the expression of either Mst1/2 phosphorylation or total Mst1/2. However, the levels of phosphorylated-MOB1 and phosphorylated-LATS1 are substantially decreased in the MRT137 group at the dose of 5

μM. The reduction in the phosphorylated LATS1 is not accompanied by the changes in the levels of total LATS1 and LATS2. To clarify that Mst2 inhibition by MRT137 results in the modulation of the Hippo pathway, the level of active YAP was assessed. MRT137 provides an increase in active YAP expression (Figure 6.8).

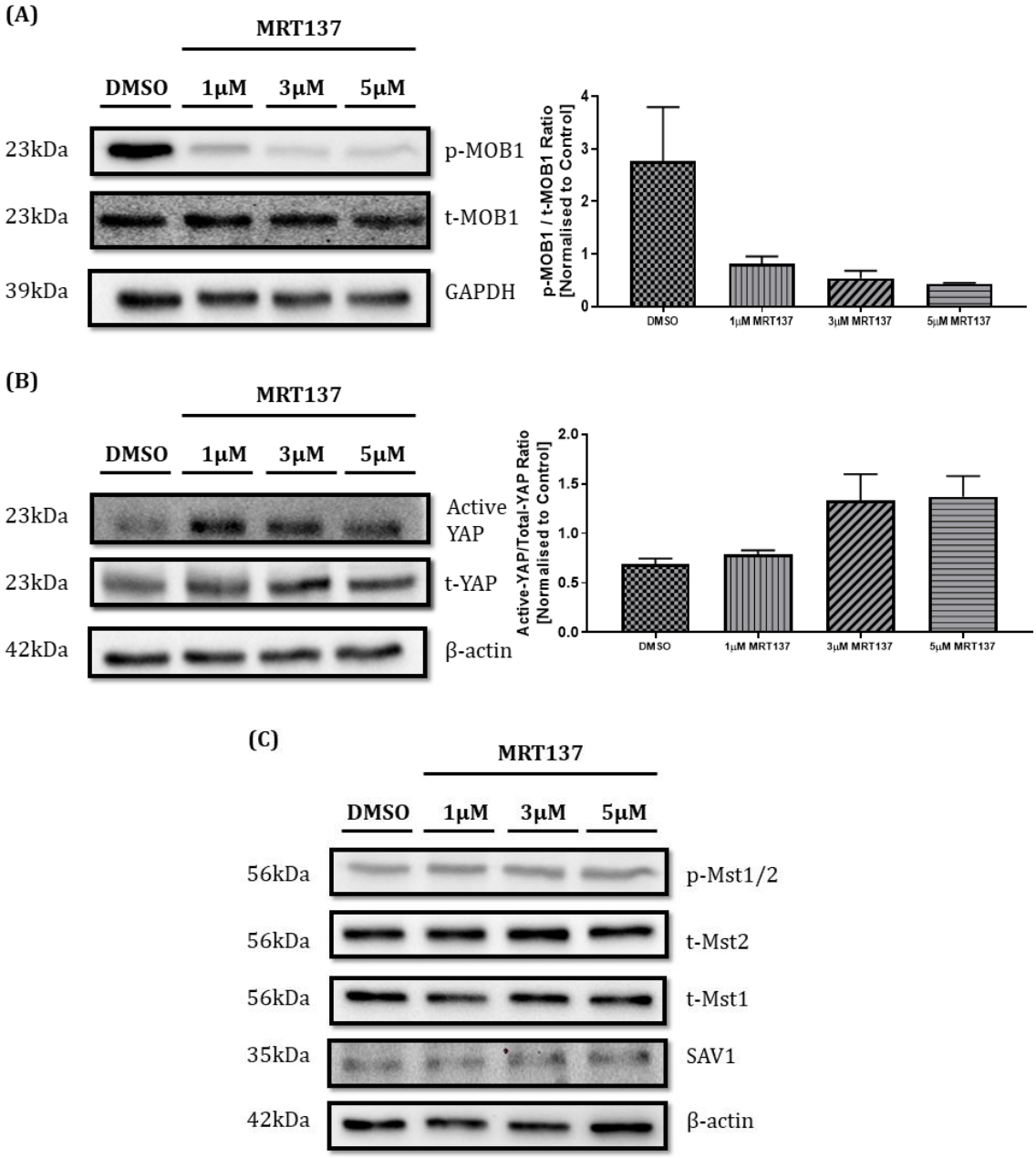

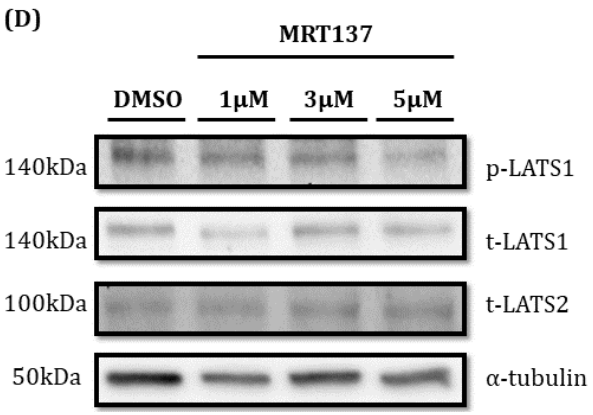

Figure 6.8 Protein levels of the canonical Hippo components in cardiomyocytes treated with MRT137. (A) The level of phosphorylated MOB1 is decreased in the MRT137 groups. (B) The expression of active YAP is enhanced after MRT137 treatment. (C) There are no changes in the levels of phosphorylated Mst1/2, total Mst1, total Mst2 and SAV1. (D) The level of phosphorylated LATS1 is reduced after 5 μM of MRT137 treatment. MRT137 does not alter the expression of total LATS1 and total LATS2.

MRT137 was identified as a selective Mst2 inhibitor by LifeArc. To assess if MRT137 works on Mst2 rather than Mst1, MRT137 was introduced into the cardiomyocytes after the siRNA-mediated knockdown of either Mst1 or Mst2. The expressions of the Hippo canonical components were determined using a western blot analysis. After Mst2 deletion, MRT137 does not affect the expression of active YAP. Conversely, in Mst1 deletion, the expression of active YAP is observed at an increased rate. The ratio of phosphorylated LATS1 to total LATS1 remains unchanged following MRT137 treatment in both Mst1 and Mst2 deletion. Similarly, the total YAP level is also unaffected by MRT137 in both cases (Figure 6.9).

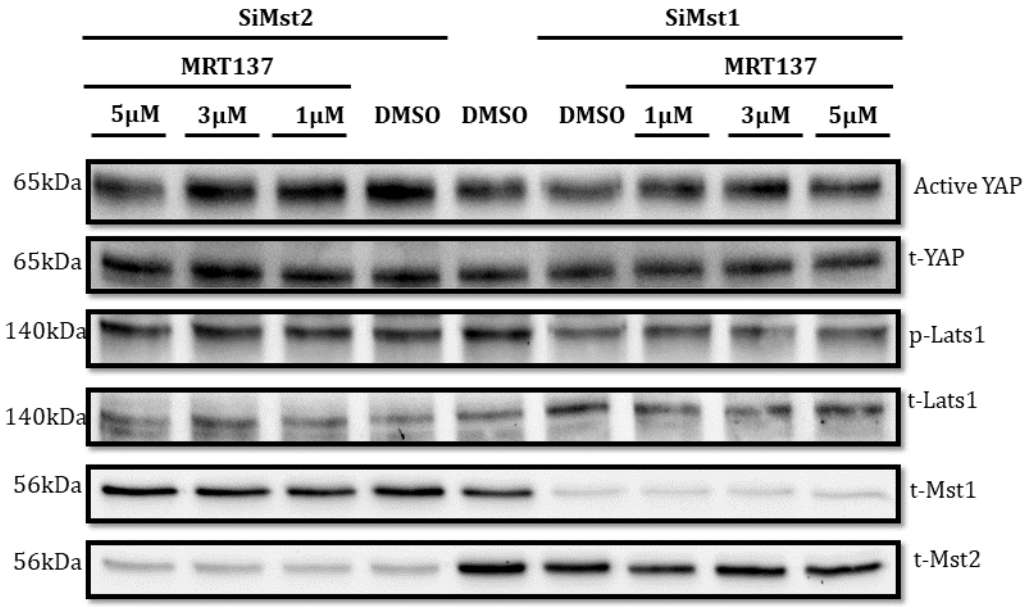

Figure 6.9 The western blot analysis of the Hippo component expression following siRNA-mediated knockdown of Mst1 and Mst2 and MRT137 treatment in neonatal rat cardiomyocytes. The effects of MRT137 is diminished in the Mst2 knockdown. MRT137 increases the level of active YAP after Mst1 knockdown. However, MRT137 does not change the total YAP, phosphorylated LATS1 and total LATS1 levels after either Mst1 or Mst2 knockdown.

The western blot analysis shows that MRT137 downregulates the ERK pathway by decreasing the phosphorylated ERK1/2 level (Figure 6.10). The reduction in the ratio of phosphorylated ERK1/2 to total ERK1/2 follows a dose-dependent pattern with the highest dose of MRT137 giving the biggest blockade on the ERK pathway.

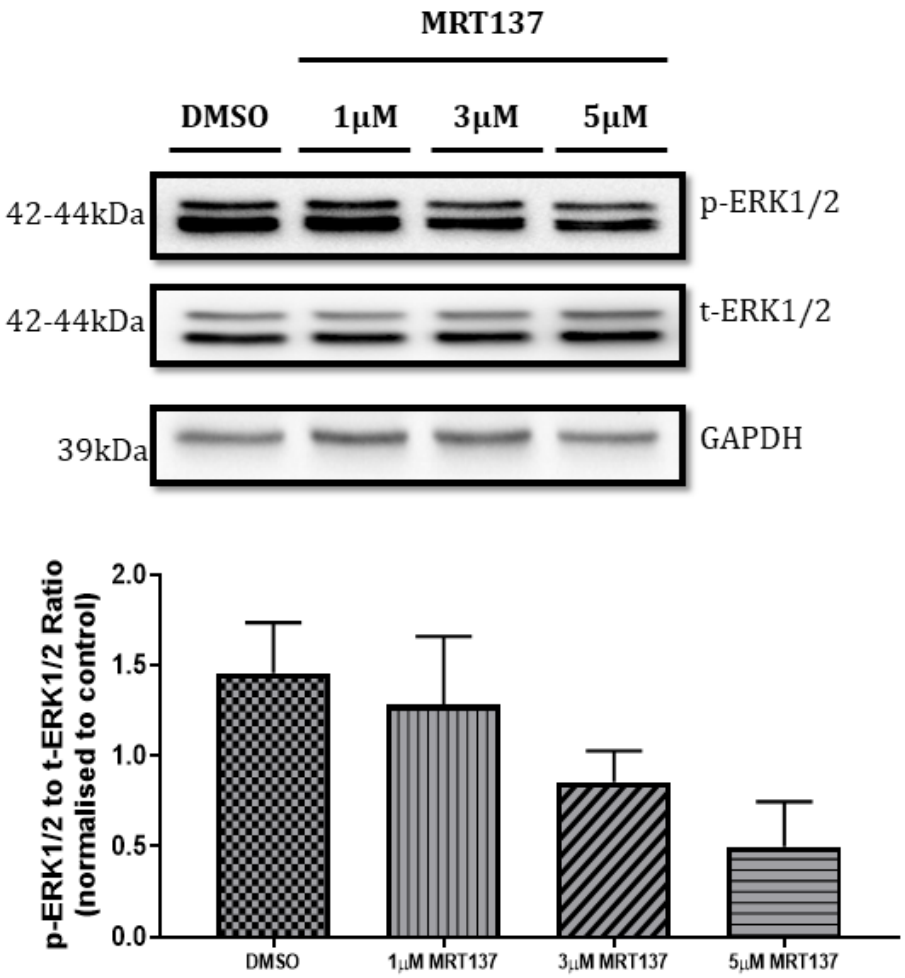

Figure 6.10 Densitometry quantification of phosphorylated ERK1/2 to total ERK1/2 ratio in response to MRT137 treatment. There is a dose-dependent reduction of phosphorylated ERK1/2 to total ERK1/2 ratio following MRT137 treatment, but the difference is not statistically significant.

6.5 Discussion

The selectivity of the Hippo pathway inhibitor is vital because a complete blockade of the Hippo components can result in uncontrolled cell proliferation, which eventually leads to cancer development. Inhibition of both Mst1 and Mst2 renders an intense activation of the Hippo effectors, YAP and TAZ, which ultimately induce cell proliferation and prevent cell apoptosis. Robust activation of YAP and TAZ creates risks of cancer development (Nallet-Staub et al., 2014). Hence, one of the alternative strategies in targeting the Hippo/Mst for therapeutic purposes is using a selective isoform inhibitor.

Mst2 is a conserved cell apoptosis regulator that can play a role both in the Hippo and ERK pathways. Global deletion of Mst2 has demonstrated a significant reduction in cardiomyocyte apoptosis following pressure overload. Moreover, Mst2 has been associated with cardiac hypertrophy. The systemic ablation of Mst2 results in a less hypertrophic heart. Moreover, the Mst2 level is increased after pressure overload (Zi et al., 2014). Therefore, direct therapeutic inhibition of Mst2 emerges to be valuable in protecting the heart from hypertrophy. This chapter highlights the effects of a novel Mst2 inhibitor, MRT137, in cultured cardiomyocytes regarding hypertrophy and apoptosis.

6.5.1 MRT137 inhibits phenylephrine-induced hypertrophy in NRCMs

Cardiac hypertrophy occurs due to an augmentation of cardiomyocyte numbers, enlargement of cardiomyocytes, or both. However, in adverse cardiac hypertrophy that is caused by pathological stimuli, an increase in cardiomyocyte size is more dominant to change the shape, the structure and the function of the heart. Some pathways are reported to be involved in the development of adverse cardiac remodelling. The MEK/ERK pathway is one of the pathways that contribute to cardiac hypertrophy. The MEK/ERK pathway activation in the hypertrophy progression is closely related to Raf-1 kinase activity. The mechanism of how Raf-1 induces cardiac hypertrophy is attributed to YAP activation (Yu et al., 2015).

Interestingly, the role of Raf-1 in controlling the MEK/ERK pathway can be disrupted by the Hippo/Mst2. Interaction between Mst2 and Raf-1 results in the disruption of the Raf-MEK connection and causes inhibition of ERK activity (Romano et al., 2014). A study by Zi et al. further explained how Mst2 modulates Raf-1 in cardiomyocytes. Mst2 was proven to regulate Raf-1-ERK activity through the contribution of phosphatase 2A (PP2A). Mst2 modulates Raf-1 by increasing Raf-1 phosphorylation, followed by ERK activation. An inactive form of Mst2 was reported to lose the ability of Mst2 in inducing Raf-1 phosphorylation. Hence, Mst2 inactivation can reduce ERK activity (Zi et al., 2014). Kilili and Kyriasis also explained the impact of Mst2 in the Raf-1/ERK interaction. They revealed that the Mst2 ablation results in the inactivation of the catalytic subunit of PP2A and the reduction of Raf-1 phosphorylation (Kilili and Kyriakis, 2010).

My data suggest that MRT137 protects cardiomyocytes from phenylephrine-induced hypertrophy. Anti-hypertrophic action of MRT137 was indicated by the lesser BNP activity and reduced cardiomyocyte size in the MRT137 treatment groups. The possible mechanism of how MRT137 inhibits cardiomyocyte hypertrophy is attributed to the inhibition of the ERK pathway through its modulation in Raf-1 phosphorylation. MRT137 shows a reduction in the phosphorylated ERK expression when identified using a western blot experiment.

Further investigation is needed to get a determined mechanism of action of how MRT137 prevents hypertrophy. Moreover, the role of MRT137 in protecting cardiomyocytes from hypertrophy needs to be tested using *in vivo* experiments.

6.5.2 MRT137 increases cardiomyocyte proliferation

In the canonical Hippo pathway, YAP and TAZ are the main downstream effectors that can induce cell proliferation. Mst1 and Mst2 act as major upstream regulators of the Hippo pathway that eventually inhibit YAP and TAZ activities (Avruch et al., 2012). The inhibition of both Mst isoforms results in YAP and TAZ activation, which then promotes gene expression that contributes to cell proliferation (Lee et al., 2008).

There are several concerns about the association between Mst2 and cell proliferation. A previous study demonstrated that the genetic ablation of Mst2 is not associated with an increase in cardiomyocyte proliferation (Zi et al., 2014). Another study stated that the interaction between Mst2 and Raf-1 is attributed to pro-proliferative activity. Through its interaction with Raf-1, Mst2 controls the Hippo and ERK pathways by intruding on the effects of Raf-1 in regulating ERK activity (Feng et al., 2017). The alteration of Raf-1 control to the ERK pathway can also affect cell proliferation (O'Neill et al., 2004). Nonetheless, whether pharmacological inhibition of Mst2 affects cardiomyocyte proliferation has not been fully elucidated. In this chapter, I performed analyses to assess pH-H3 and Ki-67 expression to test the impact of a novel Mst2 inhibitor, MRT137, on cardiomyocyte proliferation.

Based on the analysis of pH-H3 and Ki-67 immunofluorescence, MRT137 treatment significantly promotes cardiomyocyte proliferation. An increment in cell proliferation following MRT137 treatment can be attributed to increased YAP activation, as indicated by YAP-luciferase and YAP nuclear translocation analyses. As mentioned previously, Mst2 inhibition could affect the activation of ERK by Raf-1. Mst2 inhibition using MRT137 could also affect ERK activity, which influences the cell proliferation process. Based on the western blot analysis, MRT137 induces the activation of YAP but also inhibits ERK activity. Considering the western blot analyses, MRT137 more likely induces cell proliferation through its impact on the canonical Hippo pathway. The exact mechanisms of how MRT137 promotes YAP activation need to be investigated thoroughly. As a chemical compound, MRT137 possibly interacts with other kinases and proteins that can contribute to YAP activation.

6.5.3 Cardiomyocyte viability is enhanced following MRT137 treatment

Mst2 is known as an apoptosis modulator. In the canonical Hippo pathway, Mst2 phosphorylates LATS1 with the help of WW45 (Galan and Avruch, 2016). The phosphorylation of LATS1 causes the accumulation of YAP in the cytoplasm, which ultimately results in YAP proteasomal degradation. YAP is a transcription co-activator that is essential in the production of anti-apoptotic genes. The degradation of YAP results in increased apoptosis and reduced viability (Oka et al., 2008). Either way, YAP activation was proven to enhance cardiomyocyte survival following myocardial infarction (Del Re et al., 2013). Mst2 may regulate apoptosis through other pathways. The interaction between Mst2 and Raf-1 is associated with anti-apoptosis action (Romano et al., 2014). On the other hand, RASSF1A is known as a Raf-1 competitor for the Mst2 substrate. Excessive levels of RASSF1A cause dissociation of the Mst2 and Raf-1 bond and induces apoptosis (O'Neill et al., 2004).

The MTT assay shows that MRT137 does not significantly augment cardiomyocyte viability after H_2O_2 exposure. However, a small increase in cardiomyocyte viability was observed in the MRT137 groups when compared to the control group. The rise in cardiomyocyte viability in MRT137 groups might be due to the activation of YAP. YAP activation following MRT137 treatment was indicated using the western blot analysis. More elaboration on the effects of MRT137 in cell apoptosis is required to get a better understanding of the association between Mst2 and cell apoptosis.

6.6 Conclusion

Overall, data in this chapter show that MRT137 significantly increases YAP activity through the inhibition of the Hippo kinase, Mst2. MRT137 also exhibits an anti-hypertrophic action following phenylephrine-induced cardiomyocyte hypertrophy. The pro-proliferative effects of MRT137 might be associated with YAP activation. These findings suggest that MRT137 could become a prospective cardiac remodelling treatment. Further investigation is needed to support the effects of MRT137 in reversing cardiac remodelling.

CHAPTER 7

GENERAL DISCUSSION AND CONCLUSIONS

7.1 Overview and result summary

Despite extensive studies on cardiovascular diseases, heart failure remains one of the leading causes of morbidity and mortality worldwide. Heart failure is the manifestation of progressive adverse cardiac remodelling, which first occurs as an adaptation process of the heart in response to pathological stimuli. Since the regulation of this process involves the alteration of signalling pathways in various cell types, it will eventually affect cardiac structure and function in the long-term.

The Hippo pathway is an evolutionarily conserved regulator of cell apoptosis and cell proliferation that is involved in organ size control during embryonic development. During heart development in the fetus, the Hippo pathway is inactive. The Hippo pathway consists of kinase cascades that inhibit YAP/TAZ activity when they are upregulated. YAP/TAZ works extensively to allow cardiomyocyte proliferation during this phase. The activation of the Hippo pathway occurs after birth and YAP activity is gradually reduced. In this phase, the heart growth is mostly due to the enlargement of cardiomyocyte size. The Hippo pathway activation opposes cardiomyocyte regeneration capacity (Zhou et al., 2015). The Hippo pathway consists of several kinases and scaffolding proteins. These kinases and scaffolding proteins are phosphorylated during the activation of the Hippo pathway. The phosphorylation of the Hippo kinases and scaffolding proteins induces the Hippo effector's (YAP/TAZ) degradation through their phosphorylation. On the other hand, the inhibition of the Hippo kinases and scaffolding proteins results in excessive YAP/TAZ activity and uncontrolled cell proliferation (Heallen et al., 2011).

In general, the Hippo pathway is also associated with malignancy as the inhibition of this pathway could induce tumour formation. However, in degenerative diseases, the Hippo pathway could be a potential therapeutic target. In cardiovascular diseases, the inhibition of the Hippo components retrieves the regenerative capacity of cardiomyocytes. Cardiac-specific inducible knockout of sav following myocardial infarction protects the heart from heart failure progression (Leach et al., 2017). Global knockout of Mst2 has been proven to protect the heart from cardiac hypertrophy in pressure overload (Zi et al., 2014). Otherwise, a preserved cardiac function and an increase in cardiac regeneration are also achieved when YAP is activated following myocardial infarction (Del Re et al., 2013; Xin et al., 2013). Given the Hippo pathway's modulation in cardiac regeneration, there is a promising opportunity for pharmacological approaches targeting the Hippo pathway to mend cardiovascular diseases.

Therapeutic approaches to help impede the progression of heart failure become a challenging research topic. This PhD project began with the idea of the importance of the Hippo pathway in a living organism. The key objective of this PhD project was to determine

the effects of pharmacological inhibition of the members of the Hippo pathway, Mst1/2, in reversing cardiac remodelling. I hypothesised that inhibiting Mst1/2 using chemical compounds helps protect the heart from developing adverse cardiac remodelling under pathological conditions.

This PhD study reveals the protective effects of Mst inhibition in cardiomyocyte hypertrophy induced by phenylephrine exposure or transverse aortic constriction. My data suggest that the pharmacological inhibition of Mst1/2 protects cardiomyocytes from apoptosis and potentially enhances proliferation. Interestingly, in my *in vivo* experiment using the TAC surgical procedure, mice treated with XMU-MP-1 exhibited an improvement in cardiac function, which was not apparent in the control mice. The mechanisms on how XMU-MP-1 improved cardiac function in mice with TAC might be due to apoptosis and fibrosis inhibition. On the other hand, the findings of my experiment using HUVECs showed that Mst1/2 inhibition by XMU-MP-1 could reduce angiogenesis. Overall, the inhibition of both Mst1 and Mst2 using pharmacological agents potentially alleviates adverse cardiac remodelling. Additionally, my colleagues and I also glimpsed a potential effect of XMU-MP-1 to alleviate glucose tolerance in streptozotocin-induced diabetes (Faizah et al., 2020). More comprehensive studies are needed to determine the best pharmacological agent suitable for translation into clinical studies. Figure 7.1 highlights the summary of the findings in this PhD

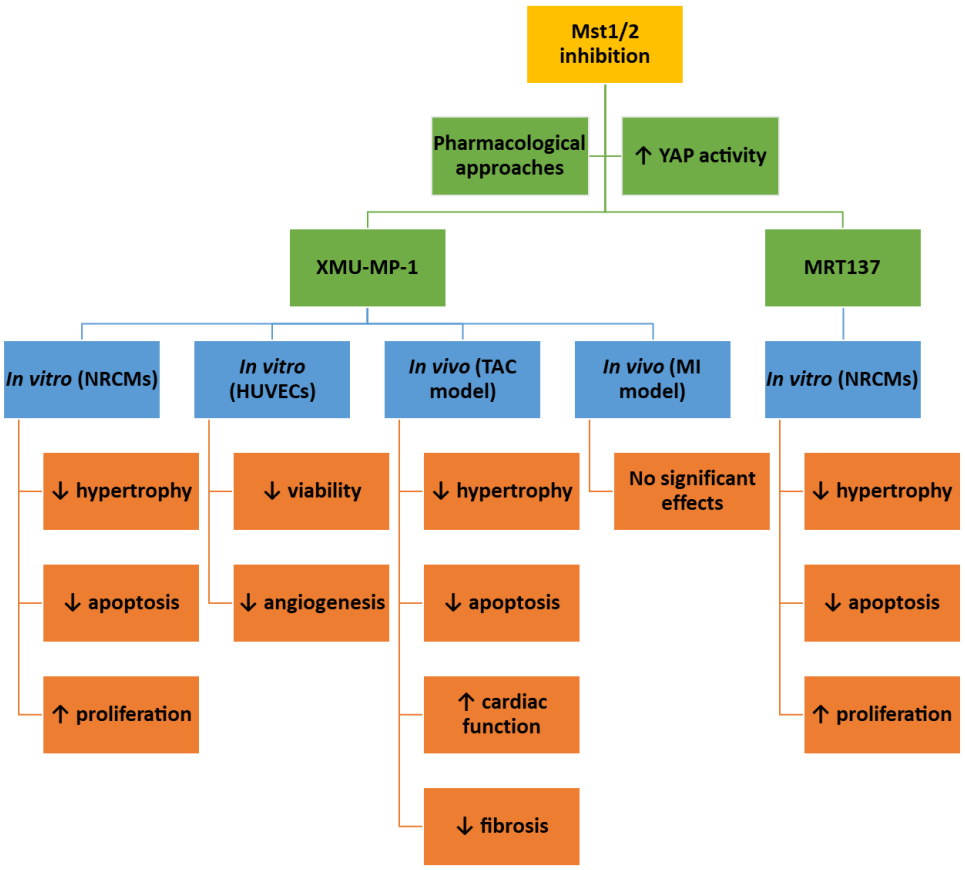

Figure 7.1 The summary of the main findings related to the inhibition of Mst1/2 of the Hippo pathway using pharmacological approaches in cardiac remodelling parameters.

7.2 Discussion and study implications

This study will be appraised in a comprehensive perspective by depicting its implications in the Hippo pathway records. Since the first invention of a tumour suppressor gene, *Warts*, in 1995, some studies have been conducted to elucidate a pathway involved in controlling organ growth (Justice et al., 1995). Another tumour suppressor gene named *Hpo* is revealed to encode The Hippo kinases, Mst1 and Mst2, in humans. Following the Hippo pathway's research evolution, other core components of the Hippo pathway were found (Harvey et al., 2003; Jia et al., 2003). In 2005, some more core components of the Hippo pathway were identified. The first component found in 2005 was Mats or later known as the homologue of MOB1 in the *Drosophila.* Mats showed an ability to bind with Warts, followed by Warts phosphorylation (Wei et al., 2007). In the same year, Huang et al. identified the downstream effectors of the Hippo pathway, later known as YAP and TAZ (Huang et al., 2005). The Hippo pathway's elucidation is still evolving to determine its regulators and related pathways. G-protein-coupled receptors (GPCR), Rho-kinase (ROCK), VGLL4 and Nemo-like kinase (NLK) are some regulators of the Hippo pathway as they can affect YAP activity. The Hippo pathway regulation in controlling organ development requires the integration of other extracellular and intracellular cues (Kim and Jho, 2018). A timeline of the Hippo component identification is revealed in Figure 7.2.

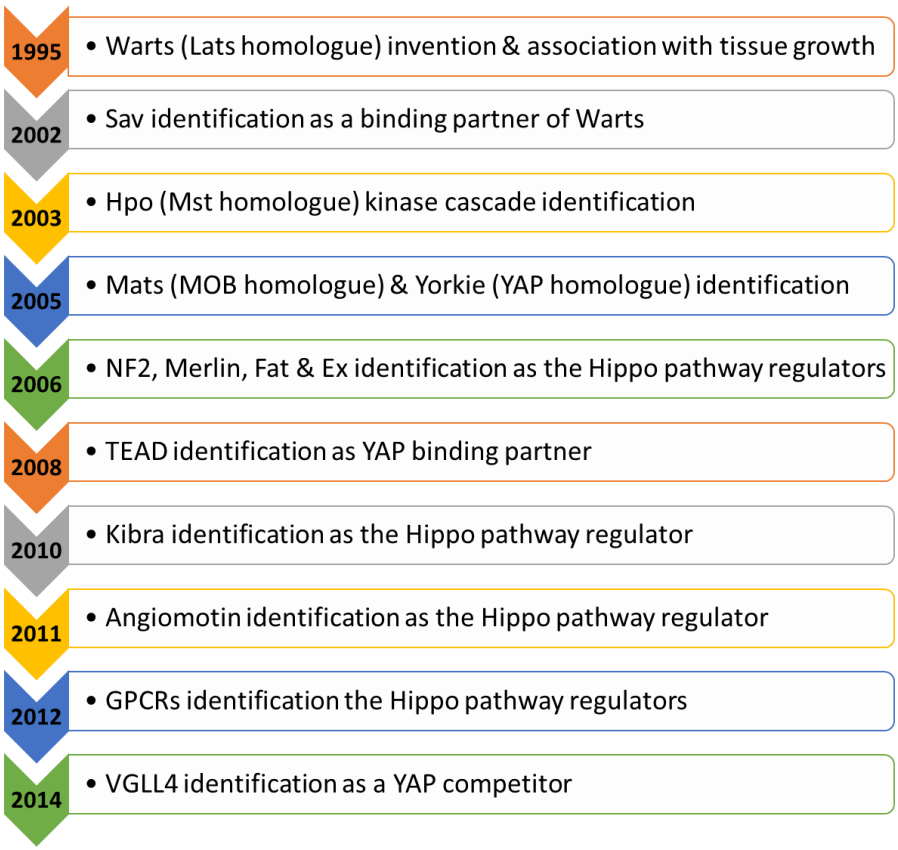

Figure 7.2 A timeline of the Hippo component identification

Drug development targeting the Hippo pathway can be used in different disease settings. Downregulation of the Hippo pathway is beneficial in degenerative diseases. On the other hand, drugs that upregulate the pathway are useful for malignancy diseases. Some studies have found strategies for activating the Hippo core components and inhibiting YAP/TAZ using chemical agents against malignancy. Mst1/2 and LATS1/2 are the Hippo core components that could be activated by chemical agents to impede malignancy. Chemical agents that showed some degree of Mst1/2 activation are C19, staurosporine and okadaic acid. Meanwhile, an antidiabetic drug, metformin, was proven to activate LATS1/2. The degradation of LATS1/2 can be prevented using chemical agents, such as clomipramine, Heclin, BI-107F7 and BI-107F9 (Nakatani et al., 2017).

On the other hand, malignancy can be impeded by blocking YAP/TAZ activity. Ivermectin, statins, and zoledronic acid are some small molecules that are stated as YAP inhibitors. Besides, Verteporfin (VP) and Protoporphyrin IX (PPIX) were identified to disrupt YAP and TEAD interaction (Woodard et al., 2017). VP is a promising drug for malignancy as it has shown moderate inhibition on the YAP activity and inhibition in cell proliferation and cell viability. Super-TDU is a peptide that mimics VGLL4 and disrupts the interaction between YAP and TEAD (Nakatani et al., 2017).

Given the role of the Hippo Pathway in repairing organ damage, the Hippo pathway has emerged as an attractive therapeutic target to induce regeneration. As mentioned in the introduction, Mst is one of the Hippo core components that becomes a therapeutic target to improve tissue regeneration. A chemical compound, 9E1, was reported to inhibit Mst1 based on kinase assays, but its effect on YAP activity has not been elucidated (Anand et al., 2009). Another Mst inhibitor is XMU-MP-1, which shows beneficial effects in liver regeneration (Fan et al., 2016). YAP as a Hippo effector is also a potent target for chemical compounds. For instance, a small molecule called TT-10 that activates YAP has been proven to induce cardiomyocyte proliferation and improve cardiac function post-myocardial infarction (Hara et al., 2018). Another update is the discovery of a reversible LATS kinase inhibitor called TRULI, which has been proven to be safe and potent to induce cardiomyocyte proliferation (Kastan et al., 2020).

Other chemical compounds also potentially modulate the Hippo pathway indirectly. Dobutamine and epinephrine are GPCR inhibitors that can inhibit LATS phosphorylation indirectly. Other compounds that inhibit LATS phosphorylation are Y27632, as an RHO-ROCK inhibitor, and jasplakinolide as an F-actin stabiliser (Dey et al., 2020). Some compounds such as auranofin, metformin and XAV939 act as YAP inhibitors indirectly by inhibiting AMOT. Other chemical agents, such as neratinib (irreversible pan-HER tyrosine

kinase inhibitor) and dasatinib (Scr family kinase inhibitor), have been used clinically to treat malignancy. Meanwhile, latrunculin (F-actin inhibitor) is used to increase Lats phosphorylation and prevent YAP nuclear localisation (Nakatani et al., 2017).

Both Mst1 and Mst2 kinases are involved in the apoptotic pathway. Proapoptotic stimuli activate Mst1 and Mst2 through loop phosphorylation on multiple sites and also on their cleavage sites for caspase 3. Mst1 and Mst2 over-expression is also associated with the stimulation of apoptosis through p-53 and JNK pathways. Alternatively, the activation of Mst1 and Mst2 during apoptosis can be mediated by Rassf1A (Avruch et al., 2012). Given the strong relationship between Mst and apoptosis, targeting Mst rather than direct modulation of YAP/TAZ using chemical agents is preferable in degenerative disease settings because it has less risk of malignancy but still prevents damaged tissues. Thus, it is worth trying to continue elaborating this PhD study in the future to find the optimum treatment in cardiovascular diseases using Mst inhibitors. Putting this PhD study into the current scientific evolution of the Hippo pathway, this study is categorised as a pre-translational study direct-targeting of the Hippo core components in degenerative disease.

There are some challenges regarding drug development targeting the Hippo pathway. Therefore, drugs targeting the Hippo pathway make very little progress, especially when new drugs come into the translational process. The most difficult part is to find effective drug treatments with the least toxicity and adverse effects. New drug candidates targeting the Hippo pathway that pass the translational process are very few, and they are mostly drugs against malignancy. However, the development of drug candidates targeting the Hippo pathway in degenerative diseases is still promising because drug delivery systems are now advanced enough to optimise the effectiveness of the drug and minimise off-target effects.

7.3 Research limitations

Due to the restrictions in the project license, XMU-MP-1 treatment in animal models was not ideal. The administration of XMU-MP-1 was every other day, which could make a big gap in the level of the drug in the blood. Maintaining a stable drug level in the blood is important to optimise the effectiveness of the drug. This limitation could affect the results of this study. The difference in drug level in the blood might explain the lesser significance of XMU-MP-1 treatment in the MI model mice because MI is more severe compared to pressure overload. Furthermore, the restriction in the project license also affects the duration of XMU-MP-1 treatment. Five times intraperitoneal injection of XMU-MP-1 is considered as a short-term treatment. Hence, it does not really reflect the real application

of the drug in the clinical settings, particularly in treating pressure overload conditions, which need to be treated on a long-term basis.

Five injections of 1 mg/kgBW of XMU-MP-1 as the dose regimentation in the *in vivo* experiments is possibly inadequate. Further clarification using a wider range of XMU-MP-1 doses might give more apprehension about the effectiveness and toxicity of XMU-MP-1. Therefore, further investigations are required to ameliorate the understanding of XMU-MP-1 effects on cardiovascular diseases.

7.4 Future directions

Upon considering the Hippo pathway as a therapeutic target, safety concerns must be addressed. It is yet to be evaluated if pharmacological inhibition of the Mst1 or Mst2 has more benefits rather than risks. The characterisation of the on and off-target toxicities is particularly needed for both XMU-MP-1 and MRT137 before addressing clinical settings.

This study has highlighted the effectiveness of XMU-MP-1 in preventing cardiac hypertrophy based on the *in vitro* experiments and *in vivo* study using pressure overload model mice. Therefore, the next step is to evaluate the on and off-target toxicities if the drug is administered on a long-term basis. A comprehensive evaluation throughout target and non-target organs is essential for testing the toxicity of long-term XMU-MP-1 treatment.

Furthermore, some modifications in XMU-MP-1 administration are worth assessing. For instance, using specific-targeted or extended-release delivery systems can give a greater understanding of the effectiveness of XMU-MP-1. Additionally, a pharmacokinetic experiment needs to be performed to clarify the fate of XMU-MP-1 in living organisms.

The next stage in evaluating MRT137 effects is to translate the results of *in vitro* experiments into *in vivo* experiments in disease models. Toxicity screening of MRT137 can be performed using novel technologies such as micropatterned culture and micro-physiological systems.

7.5 Overall conclusions

Pharmacological therapy targeting the Hippo pathway potentially bridges a distinct gap between the cardiac remodelling process and its treatments. This study demonstrates that Mst1/2 could be therapeutic targets in reversing cardiac remodelling by preventing hypertrophy, reducing apoptosis and possibly increasing cardiomyocyte proliferation. Translating the pharmacological therapies targeting the Hippo pathway into the clinical setting of degenerative disease is very challenging. However, given the development of

drugs targeting the Hippo pathway in malignancy diseases, the possibility to address the challenge in degenerative diseases becomes widely opened.

REFERENCES

Alaa, A. M., Bolton, T., Di Angelantonio, E., Rudd, J. H., & van der Schaar, M. (2019). Cardiovascular disease risk prediction using automated machine learning: A prospective study of 423,604 UK Biobank participants. *PloS one, 14*(5), e0213653.

Ambrosy, A. P., Fonarow, G. C., Butler, J., Chioncel, O., Greene, S. J., Vaduganathan, M., Nodari, S., Lam, C. S., Sato, N., & Shah, A. N. (2014). The global health and economic burden of hospitalizations for heart failure: lessons learned from hospitalized heart failure registries. *Journal of the American College of Cardiology, 63*(12), 1123-1133.

An, Y., Kang, Q., Zhao, Y., Hu, X., & Li, N. (2013). Lats2 modulates adipocyte proliferation and differentiation via hippo signaling. *PloS one, 8*(8), e72042.

Anand, R., Maksimoska, J., Pagano, N., Wong, E. Y., Gimotty, P. A., Diamond, S. L., Meggers, E., & Marmorstein, R. (2009). Toward the development of a potent and selective organoruthenium mammalian sterile 20 kinase inhibitor. *Journal of medicinal chemistry, 52*(6), 1602-1611.

Ardestani, A., Lupse, B., & Maedler, K. (2018). Hippo signaling: key emerging pathway in cellular and whole-body metabolism. *Trends in Endocrinology & Metabolism, 29*(7), 492-509.

Ardestani, A., Paroni, F., Azizi, Z., Kaur, S., Khobragade, V., Yuan, T., Frogne, T., Tao, W., Oberholzer, J., & Pattou, F. (2014). MST1 is a key regulator of beta cell apoptosis and dysfunction in diabetes. *Nature medicine, 20*(4), 385-397.

Avruch, J., Zhou, D., Fitamant, J., Bardeesy, N., Mou, F., & Barrufet, L. R. (2012). Protein kinases of the Hippo pathway: regulation and substrates. Seminars in cell & developmental biology,

Azad, T., Ghahremani, M., & Yang, X. (2019). The role of YAP and TAZ in angiogenesis and vascular mimicry. *Cells, 8*(5), 407.

Azad, T., Van Rensburg, H. J., Lightbody, E., Neveu, B., Champagne, A., Ghaffari, A., Kay, V., Hao, Y., Shen, H., & Yeung, B. (2018). A LATS biosensor screen identifies VEGFR as a regulator of the Hippo pathway in angiogenesis. *Nature communications, 9*(1), 1-15.

Balling, L., Thomsen, J. H., Wolsk, E., Hassager, C., Boesgaard, S., Goldsmith, S., & Gustafsson, F. (2016). Treatment with the V1a/V2-Vasopressin Receptor Antagonist Conivaptan Increases Cardiac Output During Exercise in Patients with Advanced Heart Failure. *Journal of the American College of Cardiology, 67*(13S), 1319-1319.

Basu, D., Lettan, R., Damodaran, K., Strellec, S., Reyes-Mugica, M., & Rebbaa, A. (2014). Identification, mechanism of action, and antitumor activity of a small molecule inhibitor of hippo, TGF-β, and Wnt signaling pathways. *Molecular cancer therapeutics, 13*(6), 1457-1467.

Basu, S., Totty, N. F., Irwin, M. S., Sudol, M., & Downward, J. (2003). Akt phosphorylates the Yes-associated protein, YAP, to induce interaction with 14-3-3 and attenuation of p73-mediated apoptosis. *Molecular cell, 11*(1), 11-23.

Bernardo, B. C., Weeks, K. L., Pretorius, L., & McMullen, J. R. (2010). Molecular distinction between physiological and pathological cardiac hypertrophy: experimental findings and therapeutic strategies. *Pharmacology & therapeutics, 128*(1), 191-227.

Beverdam, A., Claxton, C., Zhang, X., James, G., Harvey, K. F., & Key, B. (2013). Yap controls stem/progenitor cell proliferation in the mouse postnatal epidermis. *Journal of Investigative Dermatology, 133*(6), 1497-1505.

Bhatnagar, P., Wickramasinghe, K., Wilkins, E., & Townsend, N. (2016). Trends in the epidemiology of cardiovascular disease in the UK. *Heart, 102*(24), 1945-1952.

Biala, A. K., & Kirshenbaum, L. A. (2014). The interplay between cell death signaling pathways in the heart. *Trends in cardiovascular medicine, 24*(8), 325-331.

Camargo, F. D., Gokhale, S., Johnnidis, J. B., Fu, D., Bell, G. W., Jaenisch, R., & Brummelkamp, T. R. (2007). YAP1 increases organ size and expands undifferentiated progenitor cells. *Current biology, 17*(23), 2054-2060.

Cao, X., Pfaff, S. L., & Gage, F. H. (2008). YAP regulates neural progenitor cell number via the TEA domain transcription factor. *Genes & development, 22*(23), 3320-3334.

Chen, H., Levine, Y. C., Golan, D. E., Michel, T., & Lin, A. J. (2008). Atrial natriuretic peptide-initiated cGMP pathways regulate vasodilator-stimulated phosphoprotein phosphorylation and angiogenesis in vascular endothelium. *Journal of Biological Chemistry, 283*(7), 4439-4447.

Chen, J., Wu, J., Li, L., Zou, Y. Z., Zhu, D. L., & Gao, P. J. (2011). Effect of an acute mechanical stimulus on aortic structure in the transverse aortic constriction mouse model. *Clinical and Experimental Pharmacology and Physiology, 38*(9), 570-576.

Chen, T. H., Chen, C. Y., Wen, H. C., Chang, C. C., Wang, H. D., Chuu, C. P., & Chang, C. H. (2017). YAP promotes myogenic differentiation via the MEK5-ERK5 pathway. *The FASEB Journal, 31*(7), 2963-2972.

Cheng, Z., Zhang, M., Hu, J., Lin, J., Feng, X., Wang, S., Wang, T., Gao, E., Wang, H., & Sun, D. (2019). Cardiac-specific Mst1 deficiency inhibits ROS-mediated JNK signalling to alleviate Ang II-induced cardiomyocyte apoptosis. *Journal of cellular and molecular medicine, 23*(1), 543-555.

Choi, H.-J., Zhang, H., Park, H., Choi, K.-S., Lee, H.-W., Agrawal, V., Kim, Y.-M., & Kwon, Y.-G. (2015). Yes-associated protein regulates endothelial cell contact-mediated expression of angiopoietin-2. *Nature communications, 6*(1), 1-14.

Chung, C., Kim, T., Kim, M., Kim, M., Song, H., Kim, T.-S., Seo, E., Lee, S.-H., Kim, H., & Kim, S. K. (2013). Hippo-Foxa2 signaling pathway plays a role in peripheral lung maturation

and surfactant homeostasis. *Proceedings of the National Academy of Sciences, 110*(19), 7732-7737.

Cicero, A. F. G., Cosentino, E. R., Kuwabara, M., Degli Esposti, D., & Borghi, C. (2019). Effects of allopurinol and febuxostat on cardiovascular mortality in elderly heart failure patients. *Internal and emergency medicine, 14*(6), 949-956.

Codelia, V. A., Sun, G., & Irvine, K. D. (2014). Regulation of YAP by mechanical strain through Jnk and Hippo signaling. *Current biology, 24*(17), 2012-2017.

Cohn, J. N., Ferrari, R., & Sharpe, N. (2000). Cardiac remodeling—concepts and clinical implications: a consensus paper from an international forum on cardiac remodeling. *Journal of the American College of Cardiology, 35*(3), 569-582.

Cohn, J. N., Ferrari, R., Sharpe, N., & Remodeling, a. I. F. o. C. (2000). Cardiac remodeling—concepts and clinical implications: a consensus paper from an international forum on cardiac remodeling. *Journal of the American College of Cardiology, 35*(3), 569-582.

Comín-Colet, J., Manito, N., Segovia-Cubero, J., Delgado, J., García Pinilla, J. M., Almenar, L., Crespo-Leiro, M. G., Sionis, A., Blasco, T., & Pascual-Figal, D. (2018). Efficacy and safety of intermittent intravenous outpatient administration of levosimendan in patients with advanced heart failure: the LION-HEART multicentre randomised trial. *European journal of heart failure, 20*(7), 1128-1136.

Dai, X., She, P., Chi, F., Feng, Y., Liu, H., Jin, D., Zhao, Y., Guo, X., Jiang, D., & Guan, K.-L. (2013). Phosphorylation of angiomotin by Lats1/2 kinases inhibits F-actin binding, cell migration, and angiogenesis. *Journal of Biological Chemistry, 288*(47), 34041-34051.

Danchin, N., Puymirat, E., Steg, P. G., Goldstein, P., Schiele, F., Belle, L., Cottin, Y., Fajadet, J., Khalife, K., & Coste, P. (2014). Five-Year Survival in Patients With ST-Segment–Elevation Myocardial Infarction According to Modalities of Reperfusion Therapy: The French Registry on Acute ST-Elevation and Non–ST-Elevation Myocardial Infarction (FAST-MI) 2005 Cohort. *Circulation, 129*(16), 1629-1636.

Del Re, D. P., Matsuda, T., Zhai, P., Gao, S., Clark, G. J., Van Der Weyden, L., & Sadoshima, J. (2010). Proapoptotic Rassf1A/Mst1 signaling in cardiac fibroblasts is protective against pressure overload in mice. *The Journal of clinical investigation, 120*(10), 3555-3567.

Del Re, D. P., Matsuda, T., Zhai, P., Maejima, Y., Jain, M. R., Liu, T., Li, H., Hsu, C.-P., & Sadoshima, J. (2014). Mst1 promotes cardiac myocyte apoptosis through phosphorylation and inhibition of Bcl-xL. *Molecular cell, 54*(4), 639-650.

Del Re, D. P., Yang, Y., Nakano, N., Cho, J., Zhai, P., Yamamoto, T., Zhang, N., Yabuta, N., Nojima, H., & Pan, D. (2013). Yes-associated protein isoform 1 (Yap1) promotes cardiomyocyte survival and growth to protect against myocardial ischemic injury. *Journal of Biological Chemistry, 288*(6), 3977-3988.

Dey, A., Varelas, X., & Guan, K.-L. (2020). Targeting the Hippo pathway in cancer, fibrosis, wound healing and regenerative medicine. *Nature Reviews Drug Discovery, 19*(7), 480-494.

Dhingra, R., & Kirshenbaum, L. A. (2013). Mst-1 switches between cardiac cell life and death. *Nature medicine, 19*(11), 1367-1368.

Dong, J., Feldmann, G., Huang, J., Wu, S., Zhang, N., Comerford, S. A., Gayyed, M. F., Anders, R. A., Maitra, A., & Pan, D. (2007). Elucidation of a universal size-control mechanism in Drosophila and mammals. *Cell, 130*(6), 1120-1133.

Dzau, V. J., Antman, E. M., Black, H. R., Hayes, D. L., Manson, J. E., Plutzky, J., Popma, J. J., & Stevenson, W. (2006). The cardiovascular disease continuum validated: clinical evidence of improved patient outcomes: part I: Pathophysiology and clinical trial evidence (risk factors through stable coronary artery disease). *Circulation, 114*(25), 2850-2870.

Ellison, D. H., & Felker, G. M. (2017). Diuretic treatment in heart failure. *New England Journal of Medicine, 377*(20), 1964-1975.

Engberding, N., Spiekermann, S., Schaefer, A., Heineke, A., Wiencke, A., Müller, M., Fuchs, M., Hilfiker-Kleiner, D., Hornig, B., & Drexler, H. (2004). Allopurinol attenuates left ventricular remodeling and dysfunction after experimental myocardial infarction: a new action for an old drug? *Circulation, 110*(15), 2175-2179.

Faizah, Z., Amanda, B., Ashari, F. Y., Triastuti, E., Oxtoby, R., Rahaju, A. S., Aziz, M. A., Lusida, M. I., & Oceandy, D. (2020). Treatment with Mammalian Ste-20-like Kinase 1/2 (MST1/2) Inhibitor XMU-MP-1 Improves Glucose Tolerance in Streptozotocin-Induced Diabetes Mice. *Molecules, 25*(19), 4381.

Fan, F., He, Z., Kong, L.-L., Chen, Q., Yuan, Q., Zhang, S., Ye, J., Liu, H., Sun, X., & Geng, J. (2016). Pharmacological targeting of kinases MST1 and MST2 augments tissue repair and regeneration. *Science translational medicine, 8*(352), 352ra108-352ra108.

Farah, A., & Barbagelata, A. (2017). Unmet goals in the treatment of Acute Myocardial Infarction. *F1000Research, 6*.

Felker, G. M., Mentz, R. J., Cole, R. T., Adams, K. F., Egnaczyk, G. F., Fiuzat, M., Patel, C. B., Echols, M., Khouri, M. G., & Tauras, J. M. (2017). Efficacy and safety of tolvaptan in patients hospitalized with acute heart failure. *Journal of the American College of Cardiology, 69*(11), 1399-1406.

Feng, R., Gong, J., Wu, L., Wang, L., Zhang, B., Liang, G., Zheng, H., & Xiao, H. (2017). MAPK and Hippo signaling pathways crosstalk via the RAF-1/MST-2 interaction in malignant melanoma. *Oncology reports, 38*(2), 1199-1205.

Fliss, H., & Gattinger, D. (1996). Apoptosis in ischemic and reperfused rat myocardium. *Circulation research, 79*(5), 949-956.

Fu, V., Plouffe, S. W., & Guan, K.-L. (2017). The Hippo pathway in organ development, homeostasis, and regeneration. *Current opinion in cell biology, 49*, 99-107.

Fuentes, E., Moore-Carrasco, R., de Andrade Paes, A. M., & Trostchansky, A. (2019). Role of platelet activation and oxidative stress in the evolution of myocardial infarction. *Journal of cardiovascular pharmacology and therapeutics, 24*(6), 509-520.

Furuyama, T., Kitayama, K., Shimoda, Y., Ogawa, M., Sone, K., Yoshida-Araki, K., Hisatsune, H., Nishikawa, S.-i., Nakayama, K., & Nakayama, K. (2004). Abnormal angiogenesis in Foxo1 (Fkhr)-deficient mice. *Journal of Biological Chemistry, 279*(33), 34741-34749.

Galan, J. A., & Avruch, J. (2016). MST1/MST2 protein kinases: regulation and physiologic roles. *Biochemistry, 55*(39), 5507-5519.

Gibbons, G. H. (1997). Endothelial function as a determinant of vascular function and structure: a new therapeutic target. *The American journal of cardiology, 79*(5), 3-8.

Greenberg, B., Quinones, M. A., Koilpillai, C., Limacher, M., Shindler, D., Benedict, C., & Shelton, B. (1995). Effects of long-term enalapril therapy on cardiac structure and function in patients with left ventricular dysfunction: results of the SOLVD echocardiography substudy. *Circulation, 91*(10), 2573-2581.

Hara, H., Takeda, N., Kondo, M., Kubota, M., Saito, T., Maruyama, J., Fujiwara, T., Maemura, S., Ito, M., & Naito, A. T. (2018). Discovery of a small molecule to increase cardiomyocytes and protect the heart after ischemic injury. *JACC: Basic to Translational Science, 3*(5), 639-653.

Harvey, K. F., Pfleger, C. M., & Hariharan, I. K. (2003). The Drosophila Mst ortholog, hippo, restricts growth and cell proliferation and promotes apoptosis. *Cell, 114*(4), 457-467.

He, J., Bao, Q., Yan, M., Liang, J., Zhu, Y., Wang, C., & Ai, D. (2018). The role of Hippo/yes-associated protein signalling in vascular remodelling associated with cardiovascular disease. *British journal of pharmacology, 175*(8), 1354-1361.

Heallen, T., Morikawa, Y., Leach, J., Tao, G., Willerson, J. T., Johnson, R. L., & Martin, J. F. (2013). Hippo signaling impedes adult heart regeneration. *Development, 140*(23), 4683-4690.

Heallen, T., Zhang, M., Wang, J., Bonilla-Claudio, M., Klysik, E., Johnson, R. L., & Martin, J. F. (2011). Hippo pathway inhibits Wnt signaling to restrain cardiomyocyte proliferation and heart size. *Science, 332*(6028), 458-461.

Heineke, J., & Molkentin, J. D. (2006). Regulation of cardiac hypertrophy by intracellular signalling pathways. *Nature reviews Molecular cell biology, 7*(8), 589-600.

Heineke, J., Ruetten, H., Willenbockel, C., Gross, S. C., Naguib, M., Schaefer, A., Kempf, T., Hilfiker-Kleiner, D., Caroni, P., & Kraft, T. (2005). Attenuation of cardiac remodeling after myocardial infarction by muscle LIM protein-calcineurin signaling at the

sarcomeric Z-disc. *Proceedings of the National Academy of Sciences, 102*(5), 1655-1660.

Heo, K.-S., Fujiwara, K., & Abe, J.-i. (2014). Shear stress and atherosclerosis. *Molecules and cells, 37*(6), 435.

Heusch, G., Libby, P., Gersh, B., Yellon, D., Böhm, M., Lopaschuk, G., & Opie, L. (2014). Cardiovascular remodelling in coronary artery disease and heart failure. *The lancet, 383*(9932), 1933-1943.

Hong, J.-H., Hwang, E. S., McManus, M. T., Amsterdam, A., Tian, Y., Kalmukova, R., Mueller, E., Benjamin, T., Spiegelman, B. M., & Sharp, P. A. (2005). TAZ, a transcriptional modulator of mesenchymal stem cell differentiation. *Science, 309*(5737), 1074-1078.

Huang, H., Wu, W., Zhang, L., & Liu, X.-Y. (2013). Drosophila ste-20 family protein kinase, hippo, modulates fat cell proliferation. *PloS one, 8*(4), e61740.

Huang, J., Wu, S., Barrera, J., Matthews, K., & Pan, D. (2005). The Hippo signaling pathway coordinately regulates cell proliferation and apoptosis by inactivating Yorkie, the Drosophila Homolog of YAP. *Cell, 122*(3), 421-434.

Huang, L., Li, S., Dai, Q., Zhang, A., Yu, Q., Du, W., Zhao, P., Mo, Y., Xu, K., & Chen, S. (2020). Astrocytic Yes-associated protein attenuates cerebral ischemia-induced brain injury by regulating signal transducer and activator of transcription 3 signaling. *Experimental Neurology, 333*, 113431.

Issbrücker, K., Martin, H. H., Hippenstiel, S., Springmann, G., Voswinckel, R., Gaumann, A., Breier, G., Drexler, H. C., Suttorp, N., & Clauss, M. (2003). p38 MAP kinase—a molecular switch between VEGF-induced angiogenesis and vascular hyperpermeability. *The FASEB Journal, 17*(2), 262-264.

Izumiya, Y., Shiojima, I., Sato, K., Sawyer, D. B., Colucci, W. S., & Walsh, K. (2006). Vascular endothelial growth factor blockade promotes the transition from compensatory cardiac hypertrophy to failure in response to pressure overload. *Hypertension, 47*(5), 887-893.

Jagannathan, R., Patel, S. A., Ali, M. K., & Narayan, K. V. (2019). Global updates on cardiovascular disease mortality trends and attribution of traditional risk factors. *Current diabetes reports, 19*(7), 44.

Jeon, H. H., Yu, Q., Lu, Y., Spencer, E., Lu, C., Milovanova, T., Yang, Y., Zhang, C., Stepanchenko, O., & Vafa, R. P. (2018). FOXO1 regulates VEGFA expression and promotes angiogenesis in healing wounds. *The Journal of pathology, 245*(3), 258-264.

Jia, J., Zhang, W., Wang, B., Trinko, R., & Jiang, J. (2003). The Drosophila Ste20 family kinase dMST functions as a tumor suppressor by restricting cell proliferation and promoting apoptosis. *Genes & development, 17*(20), 2514-2519.

Johnson, R., & Halder, G. (2014). The two faces of Hippo: targeting the Hippo pathway for regenerative medicine and cancer treatment. *Nature Reviews Drug Discovery, 13*(1), 63-79.

Juan, W. C., & Hong, W. (2016). Targeting the hippo signaling pathway for tissue regeneration and cancer therapy. *Genes, 7*(9), 55.

Justice, R. W., Zilian, O., Woods, D. F., Noll, M., & Bryant, P. J. (1995). The Drosophila tumor suppressor gene warts encodes a homolog of human myotonic dystrophy kinase and is required for the control of cell shape and proliferation. *Genes & development, 9*(5), 534-546.

Kapturczak, M. H., Wasserfall, C., Brusko, T., Campbell-Thompson, M., Ellis, T. M., Atkinson, M. A., & Agarwal, A. (2004). Heme oxygenase-1 modulates early inflammatory responses: evidence from the heme oxygenase-1-deficient mouse. *The American journal of pathology, 165*(3), 1045-1053.

Kastan, N., Gnedeva, K., Alisch, T., Petelski, A., Huggins, D., Chiaravalli, J., Aharanov, A., Shakked, A., Tzahor, E., & Nagiel, A. (2020). Small-molecule inhibition of Lats kinases promotes Yap-dependent proliferation in postmitotic mammalian tissues. *bioRxiv*.

Kawano, Y., Nakae, J., Watanabe, N., Fujisaka, S., Iskandar, K., Sekioka, R., Hayashi, Y., Tobe, K., Kasuga, M., & Noda, T. (2012). Loss of Pdk1-Foxo1 signaling in myeloid cells predisposes to adipose tissue inflammation and insulin resistance. *Diabetes, 61*(8), 1935-1948.

Kellum, J. A., Sileanu, F. E., Murugan, R., Lucko, N., Shaw, A. D., & Clermont, G. (2015). Classifying AKI by urine output versus serum creatinine level. *Journal of the American Society of Nephrology, 26*(9), 2231-2238.

Kilili, G. K., & Kyriakis, J. M. (2010). Mammalian Ste20-like kinase (Mst2) indirectly supports Raf-1/ERK pathway activity via maintenance of protein phosphatase-2A catalytic subunit levels and consequent suppression of inhibitory Raf-1 phosphorylation. *Journal of Biological Chemistry, 285*(20), 15076-15087.

Kim, J., Kim, Y. H., Kim, J., Bae, H., Lee, D.-H., Kim, K. H., Hong, S. P., Jang, S. P., Kubota, Y., & Kwon, Y.-G. (2017). YAP/TAZ regulates sprouting angiogenesis and vascular barrier maturation. *The Journal of clinical investigation, 127*(9), 3441-3461.

Kim, N.-G., Koh, E., Chen, X., & Gumbiner, B. M. (2011). E-cadherin mediates contact inhibition of proliferation through Hippo signaling-pathway components. *Proceedings of the National Academy of Sciences, 108*(29), 11930-11935.

Kim, W., & Jho, E.-h. (2018). The history and regulatory mechanism of the Hippo pathway. *BMB reports, 51*(3), 106.

Kim, W., Khan, S. K., Gvozdenovic-Jeremic, J., Kim, Y., Dahlman, J., Kim, H., Park, O., Ishitani, T., Jho, E.-h., & Gao, B. (2017). Hippo signaling interactions with Wnt/β-catenin and Notch signaling repress liver tumorigenesis. *The Journal of clinical investigation, 127*(1), 137-152.

Kim, Y. H., Choi, J., Yang, M. J., Hong, S. P., Lee, C.-k., Kubota, Y., Lim, D.-S., & Koh, G. Y. (2019). A MST1–FOXO1 cascade establishes endothelial tip cell polarity and facilitates sprouting angiogenesis. *Nature communications, 10*(1), 1-17.

Kivelä, R., Bry, M., Robciuc, M. R., Räsänen, M., Taavitsainen, M., Silvola, J. M., Saraste, A., Hulmi, J. J., Anisimov, A., & Mäyränpää, M. I. (2014). VEGF-B-induced vascular growth leads to metabolic reprogramming and ischemia resistance in the heart. *EMBO molecular medicine, 6*(3), 307-321.

Knöll, R., Hoshijima, M., Hoffman, H. M., Person, V., Lorenzen-Schmidt, I., Bang, M.-L., Hayashi, T., Shiga, N., Yasukawa, H., & Schaper, W. (2002). The cardiac mechanical stretch sensor machinery involves a Z disc complex that is defective in a subset of human dilated cardiomyopathy. *Cell, 111*(7), 943-955.

Konstam, M. A., Rousseau, M. F., Kronenberg, M. W., Udelson, J. E., Melin, J., Stewart, D., Dolan, N., Edens, T. R., Ahn, S., & Kinan, D. (1992). Effects of the angiotensin converting enzyme inhibitor enalapril on the long-term progression of left ventricular dysfunction in patients with heart failure. SOLVD Investigators. *Circulation, 86*(2), 431-438.

Krum, H., & Teerlink, J. R. (2011). Medical therapy for chronic heart failure. *The lancet, 378*(9792), 713-721.

Kuhn, M. (2012). Endothelial actions of atrial and B-type natriuretic peptides. *British journal of pharmacology, 166*(2), 522-531.

Kwo, P. Y., Cohen, S. M., & Lim, J. K. (2017). ACG clinical guideline: evaluation of abnormal liver chemistries. *American Journal of Gastroenterology, 112*(1), 18-35.

Landmesser, U., Bahlmann, F., Mueller, M., Spiekermann, S., Kirchhoff, N., Schulz, S., Manes, C., Fischer, D., de Groot, K., & Fliser, D. (2005). Simvastatin versus ezetimibe: pleiotropic and lipid-lowering effects on endothelial function in humans. *Circulation, 111*(18), 2356-2363.

Landmesser, U., Engberding, N., Bahlmann, F. H., Schaefer, A., Wiencke, A., Heineke, A., Spiekermann, S., Hilfiker-Kleiner, D., Templin, C., & Kotlarz, D. (2004). Statin-induced improvement of endothelial progenitor cell mobilization, myocardial neovascularization, left ventricular function, and survival after experimental myocardial infarction requires endothelial nitric oxide synthase. *Circulation, 110*(14), 1933-1939.

Lara-Castillo, N., Zandi, S., Nakao, S., Ito, Y., Noda, K., She, H., Ahmed, M., Frimmel, S., Ablonczy, Z., & Hafezi-Moghadam, A. (2009). Atrial natriuretic peptide reduces vascular leakage and choroidal neovascularization. *The American journal of pathology, 175*(6), 2343-2350.

Lázár, E., Sadek, H. A., & Bergmann, O. (2017). Cardiomyocyte renewal in the human heart: insights from the fall-out. *European heart journal, 38*(30), 2333-2342.

Leach, J. P., Heallen, T., Zhang, M., Rahmani, M., Morikawa, Y., Hill, M. C., Segura, A., Willerson, J. T., & Martin, J. F. (2017). Hippo pathway deficiency reverses systolic heart failure after infarction. *Nature, 550*(7675), 260-264.

Lee, J. H., Kim, T. S., Yang, T. H., Koo, B. K., Oh, S. P., Lee, K. P., Oh, H. J., Lee, S. H., Kong, Y. Y., & Kim, J. M. (2008). A crucial role of WW45 in developing epithelial tissues in the mouse. *The EMBO journal, 27*(8), 1231-1242.

Lee, K.-K., Murakawa, M., Nishida, E., Tsubuki, S., Kawashima, S.-i., Sakamaki, K., & Yonehara, S. (1998). Proteolytic activation of MST/Krs, STE20-related protein kinase, by caspase during apoptosis. *Oncogene, 16*(23), 3029-3037.

Lee, K.-K., Ohyama, T., Yajima, N., Tsubuki, S., & Yonehara, S. (2001). MST, a physiological caspase substrate, highly sensitizes apoptosis both upstream and downstream of caspase activation. *Journal of Biological Chemistry, 276*(22), 19276-19285.

Lee, K.-P., Lee, J.-H., Kim, T.-S., Kim, T.-H., Park, H.-D., Byun, J.-S., Kim, M.-C., Jeong, W.-I., Calvisi, D. F., & Kim, J.-M. (2010). The Hippo–Salvador pathway restrains hepatic oval cell proliferation, liver size, and liver tumorigenesis. *Proceedings of the National Academy of Sciences, 107*(18), 8248-8253.

Lehtinen, M. K., Yuan, Z., Boag, P. R., Yang, Y., Villén, J., Becker, E. B., DiBacco, S., de la Iglesia, N., Gygi, S., & Blackwell, T. K. (2006). A conserved MST-FOXO signaling pathway mediates oxidative-stress responses and extends life span. *Cell, 125*(5), 987-1001.

Lehtiö, L., Chi, N. W., & Krauss, S. (2013). Tankyrases as drug targets. *The FEBS journal, 280*(15), 3576-3593.

Levine, B., & Kroemer, G. (2008). Autophagy in the pathogenesis of disease. *Cell, 132*(1), 27-42.

Li, Y., Zhou, H., Li, F., Chan, S. W., Lin, Z., Wei, Z., Yang, Z., Guo, F., Lim, C. J., & Xing, W. (2015). Angiomotin binding-induced activation of Merlin/NF2 in the Hippo pathway. *Cell research, 25*(7), 801-817.

Lin, J., Huo, R., Wang, L., Zhou, Z., Sun, Y., Shen, B., Wang, R., & Li, N. (2012). A novel anti-Cyr61 antibody inhibits breast cancer growth and metastasis in vivo. *Cancer Immunology, Immunotherapy, 61*(5), 677-687.

Lin, Z., von Gise, A., Zhou, P., Gu, F., Ma, Q., Jiang, J., Yau, A. L., Buck, J. N., Gouin, K. A., & van Gorp, P. R. (2014). Cardiac-specific YAP activation improves cardiac function and survival in an experimental murine MI model. *Circulation research, 115*(3), 354-363.

Liu-Chittenden, Y., Huang, B., Shim, J. S., Chen, Q., Lee, S.-J., Anders, R. A., Liu, J. O., & Pan, D. (2012). Genetic and pharmacological disruption of the TEAD–YAP complex suppresses the oncogenic activity of YAP. *Genes & development, 26*(12), 1300-1305.

Ma, S., & Dong, Z. (2019). Melatonin Attenuates Cardiac Reperfusion Stress by Improving OPA1-Related Mitochondrial Fusion in a Yap–Hippo Pathway–Dependent Manner. *Journal of cardiovascular pharmacology, 73*(1), 27.

Ma, S., Meng, Z., Chen, R., & Guan, K.-L. (2019). The Hippo pathway: biology and pathophysiology. *Annual review of biochemistry, 88*, 577-604.

Ma, X., Liu, H., Foyil, S. R., Godar, R. J., Weinheimer, C. J., Hill, J. A., & Diwan, A. (2012). Impaired autophagosome clearance contributes to cardiomyocyte death in ischemia/reperfusion injury. *Circulation, 125*(25), 3170-3181.

Maejima, Y., Isobe, M., & Sadoshima, J. (2016). Regulation of autophagy by Beclin 1 in the heart. *Journal of Molecular and Cellular Cardiology, 95*, 19-25.

Mahmood, S. S., Levy, D., Vasan, R. S., & Wang, T. J. (2014). The Framingham Heart Study and the epidemiology of cardiovascular disease: a historical perspective. *The lancet, 383*(9921), 999-1008.

Makita, R., Uchijima, Y., Nishiyama, K., Amano, T., Chen, Q., Takeuchi, T., Mitani, A., Nagase, T., Yatomi, Y., & Aburatani, H. (2008). Multiple renal cysts, urinary concentration defects, and pulmonary emphysematous changes in mice lacking TAZ. *American Journal of Physiology-Renal Physiology, 294*(3), F542-F553.

Mao, B., Gao, Y., Bai, Y., & Yuan, Z. (2015). Hippo signaling in stress response and homeostasis maintenance. *Acta Biochim Biophys Sin, 47*(1), 2-9.

Marcus, M. L., Koyanagi, S., Harrison, D. G., Doty, D. B., Hiratzka, L. F., & Eastham, C. L. (1983). Abnormalities in the coronary circulation that occur as a consequence of cardiac hypertrophy. *The American journal of medicine, 75*(3), 62-66.

Massagué, J. (2012). TGFβ signalling in context. *Nature reviews Molecular cell biology, 13*(10), 616-630.

Matsuda, T., Zhai, P., Sciarretta, S., Zhang, Y., Jeong, J. I., Ikeda, S., Park, J., Hsu, C.-P., Tian, B., & Pan, D. (2016). NF2 activates Hippo signaling and promotes ischemia/reperfusion injury in the heart. *Circulation research, 119*(5), 596-606.

Matsui, Y., Nakano, N., Shao, D., Gao, S., Luo, W., Hong, C., Zhai, P., Holle, E., Yu, X., & Yabuta, N. (2008). Lats2 is a negative regulator of myocyte size in the heart. *Circulation research, 103*(11), 1309-1318.

Matsui, Y., Takagi, H., Qu, X., Abdellatif, M., Sakoda, H., Asano, T., Levine, B., & Sadoshima, J. (2007). Distinct roles of autophagy in the heart during ischemia and reperfusion: roles of AMP-activated protein kinase and Beclin 1 in mediating autophagy. *Circulation research, 100*(6), 914-922.

Mavria, G., Vercoulen, Y., Yeo, M., Paterson, H., Karasarides, M., Marais, R., Bird, D., & Marshall, C. J. (2006). ERK-MAPK signaling opposes Rho-kinase to promote endothelial cell survival and sprouting during angiogenesis. *Cancer cell, 9*(1), 33-44.

Maxwell, S. R., & Lip, G. Y. (1997). Reperfusion injury: a review of the pathophysiology, clinical manifestations and therapeutic options. *International journal of cardiology, 58*(2), 95-117.

Meininger, G. A., & Hill, M. A. (2020). Frontiers in Vascular Physiology Grand Challenges in Vascular Physiology. *Frontiers in Physiology, 11*.

Mitani, A., Nagase, T., Fukuchi, K., Aburatani, H., Makita, R., & Kurihara, H. (2009). Transcriptional coactivator with PDZ-binding motif is essential for normal alveolarization in mice. *American journal of respiratory and critical care medicine, 180*(4), 326-338.

Miyagawa, S., & Sawa, Y. (2018). Building a new strategy for treating heart failure using Induced Pluripotent Stem Cells. *Journal of cardiology, 72*(6), 445-448.

Nakagawa, T., Shimizu, S., Watanabe, T., Yamaguchi, O., Otsu, K., Yamagata, H., Inohara, H., Kubo, T., & Tsujimoto, Y. (2005). Cyclophilin D-dependent mitochondrial permeability transition regulates some necrotic but not apoptotic cell death. *Nature, 434*(7033), 652-658.

Nakajima, H., Yamamoto, K., Agarwala, S., Terai, K., Fukui, H., Fukuhara, S., Ando, K., Miyazaki, T., Yokota, Y., & Schmelzer, E. (2017). Flow-dependent endothelial YAP regulation contributes to vessel maintenance. *Developmental cell, 40*(6), 523-536. e526.

Nakamura, M., & Sadoshima, J. (2018). Mechanisms of physiological and pathological cardiac hypertrophy. *Nature Reviews Cardiology, 15*(7), 387-407.

Nakamura, M., Zhai, P., Del Re, D. P., Maejima, Y., & Sadoshima, J. (2016). Mst1-mediated phosphorylation of Bcl-xL is required for myocardial reperfusion injury. *JCI insight, 1*(5).

Nakatani, K., Maehama, T., Nishio, M., Goto, H., Kato, W., Omori, H., Miyachi, Y., Togashi, H., Shimono, Y., & Suzuki, A. (2017). Targeting the Hippo signalling pathway for cancer treatment. *The Journal of Biochemistry, 161*(3), 237-244.

Nallet-Staub, F., Marsaud, V., Li, L., Gilbert, C., Dodier, S., Bataille, V., Sudol, M., Herlyn, M., & Mauviel, A. (2014). Pro-invasive activity of the Hippo pathway effectors YAP and TAZ in cutaneous melanoma. *Journal of Investigative Dermatology, 134*(1), 123-132.

Neesse, A., Frese, K. K., Bapiro, T. E., Nakagawa, T., Sternlicht, M. D., Seeley, T. W., Pilarsky, C., Jodrell, D. I., Spong, S. M., & Tuveson, D. A. (2013). CTGF antagonism with mAb FG-3019 enhances chemotherapy response without increasing drug delivery in murine ductal pancreas cancer. *Proceedings of the National Academy of Sciences, 110*(30), 12325-12330.

Neto-Silva, R. M., de Beco, S., & Johnston, L. A. (2010). Evidence for a growth-stabilizing regulatory feedback mechanism between Myc and Yorkie, the Drosophila homolog of Yap. *Developmental cell, 19*(4), 507-520.

Nguyen, H.-L., Boon, L. M., & Vikkula, M. (2017). Vascular Anomalies: Vascular Anomalies Caused by Abnormal Signaling within Endothelial Cells: Targets for Novel Therapies. Seminars in interventional radiology,

Nishio, M., Hamada, K., Kawahara, K., Sasaki, M., Noguchi, F., Chiba, S., Mizuno, K., Suzuki, S. O., Dong, Y., & Tokuda, M. (2012). Cancer susceptibility and embryonic lethality in Mob1a/1b double-mutant mice. *The Journal of clinical investigation, 122*(12), 4505-4518.

Nolo, R., Morrison, C. M., Tao, C., Zhang, X., & Halder, G. (2006). The bantam microRNA is a target of the hippo tumor-suppressor pathway. *Current biology, 16*(19), 1895-1904.

O'Neill, E., Rushworth, L., Baccarini, M., & Kolch, W. (2004). Role of the kinase MST2 in suppression of apoptosis by the proto-oncogene product Raf-1. *Science, 306*(5705), 2267-2270.

O'Neill, E., & Kolch, W. (2005). Taming the Hippo: Raf-1 controls apoptosis by suppressing MST2/Hippo. *Cell Cycle, 4*(3), 365-367.

Oceandy, D., Cartwright, E. J., & Neyses, L. (2009). Ras-Association domain family member 1A (RASSF1A)—Where the heart and cancer meet. *Trends in cardiovascular medicine, 19*(8), 262-267.

Oceandy, D., Pickard, A., Prehar, S., Zi, M., Mohamed, T. M., Stanley, P. J., Baudoin-Stanley, F., Nadif, R., Tommasi, S., & Pfeifer, G. P. (2009). CLINICAL PERSPECTIVE. *Circulation, 120*(7), 607-616.

Odashima, M., Usui, S., Takagi, H., Hong, C., Liu, J., Yokota, M., & Sadoshima, J. (2007). Inhibition of endogenous Mst1 prevents apoptosis and cardiac dysfunction without affecting cardiac hypertrophy after myocardial infarction. *Circulation research, 100*(9), 1344-1352.

Oka, T., Mazack, V., & Sudol, M. (2008). Mst2 and Lats kinases regulate apoptotic function of Yes kinase-associated protein (YAP). *Journal of Biological Chemistry, 283*(41), 27534-27546.

Okuyama, M., Jiang, W., Yang, L., Javidan, A., Thiagarajan, D., & Subramanian, V. (2019). Pharmacological Inhibition of Hippo-YAP Signaling Attenuates Angiotensin II-induced Ascending Aortic Aneurysms in Male LDL Receptor Deficient Mice. *Arteriosclerosis, Thrombosis, and Vascular Biology, 39*(Suppl_1), A652-A652.

Ong, S.-B., Hernández-Reséndiz, S., Crespo-Avilan, G. E., Mukhametshina, R. T., Kwek, X.-Y., Cabrera-Fuentes, H. A., & Hausenloy, D. J. (2018). Inflammation following acute myocardial infarction: multiple players, dynamic roles, and novel therapeutic opportunities. *Pharmacology & therapeutics, 186*, 73-87.

Otterbein, L. E., Soares, M. P., Yamashita, K., & Bach, F. H. (2003). Heme oxygenase-1: unleashing the protective properties of heme. *Trends in immunology, 24*(8), 449-455.

Packer, M., Bristow, M. R., Cohn, J. N., Colucci, W. S., Fowler, M. B., Gilbert, E. M., & Shusterman, N. H. (1996). The effect of carvedilol on morbidity and mortality in

patients with chronic heart failure. *New England Journal of Medicine, 334*(21), 1349-1355.

Parrish, J. Z., Emoto, K., Jan, L. Y., & Jan, Y. N. (2007). Polycomb genes interact with the tumor suppressor genes hippo and warts in the maintenance of Drosophila sensory neuron dendrites. *Genes & development, 21*(8), 956-972.

Pedram, A., Razandi, M., & Levin, E. R. (2001). Natriuretic peptides suppress vascular endothelial cell growth factor signaling to angiogenesis. *Endocrinology, 142*(4), 1578-1586.

Piccolo, S., Dupont, S., & Cordenonsi, M. (2014). The biology of YAP/TAZ: hippo signaling and beyond. *Physiological reviews*.

Piper, H., Garcña-Dorado, D., & Ovize, M. (1998). A fresh look at reperfusion injury. *Cardiovascular research, 38*(2), 291-300.

Pobbati, A. V., Han, X., Hung, A. W., Weiguang, S., Huda, N., Chen, G.-Y., Kang, C., Chia, C. S. B., Luo, X., & Hong, W. (2015). Targeting the central pocket in human transcription factor TEAD as a potential cancer therapeutic strategy. *Structure, 23*(11), 2076-2086.

Ramjee, V., Li, D., Manderfield, L. J., Liu, F., Engleka, K. A., Aghajanian, H., Rodell, C. B., Lu, W., Ho, V., & Wang, T. (2017). Epicardial YAP/TAZ orchestrate an immunosuppressive response following myocardial infarction. *The Journal of clinical investigation, 127*(3), 899-911.

Reginensi, A., Scott, R. P., Gregorieff, A., Bagherie-Lachidan, M., Chung, C., Lim, D.-S., Pawson, T., Wrana, J., & McNeill, H. (2013). Yap-and Cdc42-dependent nephrogenesis and morphogenesis during mouse kidney development. *PLoS Genet, 9*(3), e1003380.

Rockman, H. A., Ross, R. S., Harris, A. N., Knowlton, K. U., Steinhelper, M. E., Field, L. J., Ross, J., & Chien, K. R. (1991). Segregation of atrial-specific and inducible expression of an atrial natriuretic factor transgene in an in vivo murine model of cardiac hypertrophy. *Proceedings of the National Academy of Sciences, 88*(18), 8277-8281.

Romano, D., Nguyen, L. K., Matallanas, D., Halasz, M., Doherty, C., Kholodenko, B. N., & Kolch, W. (2014). Protein interaction switches coordinate Raf-1 and MST2/Hippo signalling. *Nature cell biology, 16*(7), 673-684.

Rosenbluh, J., Nijhawan, D., Cox, A. G., Li, X., Neal, J. T., Schafer, E. J., Zack, T. I., Wang, X., Tsherniak, A., & Schinzel, A. C. (2012). β-Catenin-driven cancers require a YAP1 transcriptional complex for survival and tumorigenesis. *Cell, 151*(7), 1457-1473.

Ross, R. S., & Borg, T. K. (2001). Integrins and the myocardium. *Circulation research, 88*(11), 1112-1119.

Sakabe, M., Fan, J., Odaka, Y., Liu, N., Hassan, A., Duan, X., Stump, P., Byerly, L., Donaldson, M., & Hao, J. (2017). YAP/TAZ-CDC42 signaling regulates vascular tip cell migration. *Proceedings of the National Academy of Sciences, 114*(41), 10918-10923.

Samak, M., Fatullayev, J., Sabashnikov, A., Zeriouh, M., Schmack, B., Farag, M., Popov, A.-F., Dohmen, P. M., Choi, Y.-H., & Wahlers, T. (2016). Cardiac hypertrophy: an introduction to molecular and cellular basis. *Medical science monitor basic research, 22*, 75.

Saraste, A., Pulkki, K., Kallajoki, M., Henriksen, K., Parvinen, M., & Voipio-Pulkki, L.-M. (1997). Apoptosis in human acute myocardial infarction. *Circulation, 95*(2), 320-323.

Schlegelmilch, K., Mohseni, M., Kirak, O., Pruszak, J., Rodriguez, J. R., Zhou, D., Kreger, B. T., Vasioukhin, V., Avruch, J., & Brummelkamp, T. R. (2011). Yap1 acts downstream of α-catenin to control epidermal proliferation. *Cell, 144*(5), 782-795.

Schwartzman, M., Reginensi, A., Wong, J. S., Basgen, J. M., Meliambro, K., Nicholas, S. B., D'Agati, V., McNeill, H., & Campbell, K. N. (2016). Podocyte-specific deletion of Yes-associated protein causes FSGS and progressive renal failure. *Journal of the American Society of Nephrology, 27*(1), 216-226.

Shao, D., Zhai, P., Del Re, D. P., Sciarretta, S., Yabuta, N., Nojima, H., Lim, D.-S., Pan, D., & Sadoshima, J. (2014). A functional interaction between Hippo-YAP signalling and FoxO1 mediates the oxidative stress response. *Nature communications, 5*(1), 1-10.

Shiojima, I., Sato, K., Izumiya, Y., Schiekofer, S., Ito, M., Liao, R., Colucci, W. S., & Walsh, K. (2005). Disruption of coordinated cardiac hypertrophy and angiogenesis contributes to the transition to heart failure. *The Journal of clinical investigation, 115*(8), 2108-2118.

Shmilovich, H., Ben-Shoshan, J., Tal, R., Afek, A., Barshack, I., Maysel-Auslander, S., Harats, D., Keren, G., & George, J. (2009). B-type natriuretic peptide enhances vasculogenesis by promoting number and functional properties of early endothelial progenitor cells. *Tissue Engineering Part A, 15*(9), 2741-2749.

Singh, M. K., & Mia, M. M. (2019). The Hippo signaling pathway in cardiac development and diseases. *Frontiers in Cell and Developmental Biology, 7*, 211.

Sorrentino, G., Ruggeri, N., Specchia, V., Cordenonsi, M., Mano, M., Dupont, S., Manfrin, A., Ingallina, E., Sommaggio, R., & Piazza, S. (2014). Metabolic control of YAP and TAZ by the mevalonate pathway. *Nature cell biology, 16*(4), 357-366.

St John, M. A., Tao, W., Fei, X., Fukumoto, R., Carcangiu, M. L., Brownstein, D. G., Parlow, A. F., McGrath, J., & Xu, T. (1999). Mice deficient of Lats1 develop soft-tissue sarcomas, ovarian tumours and pituitary dysfunction. *Nature genetics, 21*(2), 182-186.

Stull, L. B., Leppo, M. K., Szweda, L., Gao, W. D., & Marbán, E. (2004). Chronic treatment with allopurinol boosts survival and cardiac contractility in murine postischemic cardiomyopathy. *Circulation research, 95*(10), 1005-1011.

Sutton, M. G. S. J., & Sharpe, N. (2000). Left ventricular remodeling after myocardial infarction: pathophysiology and therapy. *Circulation, 101*(25), 2981-2988.

Talman, V., & Kivelä, R. (2018). Cardiomyocyte—endothelial cell interactions in cardiac remodeling and regeneration. *Frontiers in cardiovascular medicine, 5*, 101.

Tham, Y. K., Bernardo, B. C., Ooi, J. Y., Weeks, K. L., & McMullen, J. R. (2015). Pathophysiology of cardiac hypertrophy and heart failure: signaling pathways and novel therapeutic targets. *Archives of toxicology, 89*(9), 1401-1438.

Thompson, B. J., & Sahai, E. (2015). MST kinases in development and disease. *Journal of Cell Biology, 210*(6), 871-882.

Tian, W., Yu, J., Tomchick, D. R., Pan, D., & Luo, X. (2010). Structural and functional analysis of the YAP-binding domain of human TEAD2. *Proceedings of the National Academy of Sciences, 107*(16), 7293-7298.

Tian, Y., Song, H., Jin, D., Hu, N., & Sun, L. (2020). MST1-Hippo pathway regulates inflammation response following myocardial infarction through inhibiting HO-1 signaling pathway. *Journal of Receptors and Signal Transduction, 40*(3), 231-236.

Tirziu, D., Chorianopoulos, E., Moodie, K. L., Palac, R. T., Zhuang, Z. W., Tjwa, M., Roncal, C., Eriksson, U., Fu, Q., & Elfenbein, A. (2007). Myocardial hypertrophy in the absence of external stimuli is induced by angiogenesis in mice. *The Journal of clinical investigation, 117*(11), 3188-3197.

Truett, J., Cornfield, J., & Kannel, W. (1967). A multivariate analysis of the risk of coronary heart disease in Framingham. *Journal of chronic diseases, 20*(7), 511-524.

Verghese, S., Bedi, S., & Kango-Singh, M. (2012). Hippo signalling controls Dronc activity to regulate organ size in Drosophila. *Cell Death & Differentiation, 19*(10), 1664-1676.

von Gise, A., Lin, Z., Schlegelmilch, K., Honor, L. B., Pan, G. M., Buck, J. N., Ma, Q., Ishiwata, T., Zhou, B., & Camargo, F. D. (2012). YAP1, the nuclear target of Hippo signaling, stimulates heart growth through cardiomyocyte proliferation but not hypertrophy. *Proceedings of the National Academy of Sciences, 109*(7), 2394-2399.

Wada, K.-I., Itoga, K., Okano, T., Yonemura, S., & Sasaki, H. (2011). Hippo pathway regulation by cell morphology and stress fibers. *Development, 138*(18), 3907-3914.

Walsh, K., & Shiojima, I. (2007). Cardiac growth and angiogenesis coordinated by intertissue interactions. *The Journal of clinical investigation, 117*(11), 3176-3179.

Wang, J., Liu, S., Heallen, T., & Martin, J. F. (2018). The Hippo pathway in the heart: pivotal roles in development, disease, and regeneration. *Nature Reviews Cardiology, 15*(11), 672-684.

Wang, K.-C., Yeh, Y.-T., Nguyen, P., Limqueco, E., Lopez, J., Thorossian, S., Guan, K.-L., Li, Y.-S. J., & Chien, S. (2016). Flow-dependent YAP/TAZ activities regulate endothelial phenotypes and atherosclerosis. *Proceedings of the National Academy of Sciences, 113*(41), 11525-11530.

Wang, L., Luo, J.-Y., Li, B., Tian, X. Y., Chen, L.-J., Huang, Y., Liu, J., Deng, D., Lau, C. W., & Wan, S. (2016). Integrin-YAP/TAZ-JNK cascade mediates atheroprotective effect of unidirectional shear flow. *Nature, 540*(7634), 579-582.

Wang, P., Mao, B., Luo, W., Wei, B., Jiang, W., Liu, D., Song, L., Ji, G., Yang, Z., & Lai, Y.-Q. (2014). The alteration of Hippo/YAP signaling in the development of hypertrophic cardiomyopathy. *Basic research in cardiology, 109*(5), 435.

Wang, T., Zhang, L., Hu, J., Duan, Y., Zhang, M., Lin, J., Man, W., Pan, X., Jiang, Z., & Zhang, G. (2016). Mst1 participates in the atherosclerosis progression through macrophage autophagy inhibition and macrophage apoptosis enhancement. *Journal of Molecular and Cellular Cardiology, 98*, 108-116.

Wang, W., Li, N., Li, X., Tran, M. K., Han, X., & Chen, J. (2015). Tankyrase inhibitors target YAP by stabilizing angiomotin family proteins. *Cell reports, 13*(3), 524-532.

Wang, X., & Song, Q. (2018). Mst1 regulates post-infarction cardiac injury through the JNK-Drp1-mitochondrial fission pathway. *Cellular & Molecular Biology Letters, 23*(1), 21.

Wang, X., Valls, A. F., Schermann, G., Shen, Y., Moya, I. M., Castro, L., Urban, S., Solecki, G. M., Winkler, F., & Riedemann, L. (2017). YAP/TAZ orchestrate VEGF signaling during developmental angiogenesis. *Developmental cell, 42*(5), 462-478. e467.

Wei, B., Dui, W., Liu, D., Xing, Y., Yuan, Z., & Ji, G. (2013). MST1, a key player, in enhancing fast skeletal muscle atrophy. *BMC biology, 11*(1), 1-13.

Wei, X., Shimizu, T., & Lai, Z. C. (2007). Mob as tumor suppressor is activated by Hippo kinase for growth inhibition in Drosophila. *The EMBO journal, 26*(7), 1772-1781.

Wilkinson, D. S., & Hansen, M. (2015). LC3 is a novel substrate for the mammalian Hippo kinases, STK3/STK4. *Autophagy, 11*(5), 856-857.

Willecke, M., Hamaratoglu, F., Sansores-Garcia, L., Tao, C., & Halder, G. (2008). Boundaries of Dachsous Cadherin activity modulate the Hippo signaling pathway to induce cell proliferation. *Proceedings of the National Academy of Sciences, 105*(39), 14897-14902.

Wilson, P. W., D'Agostino, R. B., Levy, D., Belanger, A. M., Silbershatz, H., & Kannel, W. B. (1998). Prediction of coronary heart disease using risk factor categories. *Circulation, 97*(18), 1837-1847.

Windmueller, R., & Morrisey, E. E. (2015). Hippo and cardiac hypertrophy: A complex interaction. *Circulation research, 117*(10), 832-834.

Wollert, K. C., & Drexler, H. (2005). Clinical applications of stem cells for the heart. *Circulation research, 96*(2), 151-163.

Woodard, G. A., Yang, Y.-L., You, L., & Jablons, D. M. (2017). Drug development against the hippo pathway in mesothelioma. *Translational Lung Cancer Research, 6*(3), 335.

Wu, Q.-Q., Xiao, Y., Yuan, Y., Ma, Z.-G., Liao, H.-H., Liu, C., Zhu, J.-X., Yang, Z., Deng, W., & Tang, Q.-z. (2017). Mechanisms contributing to cardiac remodelling. *Clinical Science, 131*(18), 2319-2345.

Wu, S., Liu, Y., Zheng, Y., Dong, J., & Pan, D. (2008). The TEAD/TEF family protein Scalloped mediates transcriptional output of the Hippo growth-regulatory pathway. *Developmental cell, 14*(3), 388-398.

Wu, Z., & Guan, K.-L. (2020). Hippo Signaling in Embryogenesis and Development. *Trends in Biochemical Sciences*.

Xin, M., Kim, Y., Sutherland, L. B., Murakami, M., Qi, X., McAnally, J., Porrello, E. R., Mahmoud, A. I., Tan, W., & Shelton, J. M. (2013). Hippo pathway effector Yap promotes cardiac regeneration. *Proceedings of the National Academy of Sciences, 110*(34), 13839-13844.

Xin, M., Kim, Y., Sutherland, L. B., Qi, X., McAnally, J., Schwartz, R. J., Richardson, J. A., Bassel-Duby, R., & Olson, E. N. (2011a). Regulation of insulin-like growth factor signaling by Yap governs cardiomyocyte proliferation and embryonic heart size. *Sci. Signal., 4*(196), ra70-ra70.

Xin, M., Kim, Y., Sutherland, L. B., Qi, X., McAnally, J., Schwartz, R. J., Richardson, J. A., Bassel-Duby, R., & Olson, E. N. (2011b). Regulation of insulin-like growth factor signaling by Yap governs cardiomyocyte proliferation and embryonic heart size. *Science signaling, 4*(196), ra70-ra70.

Xu, T., Ding, W., Ji, X., Ao, X., Liu, Y., Yu, W., & Wang, J. (2019). Oxidative stress in cell death and cardiovascular diseases. *Oxidative medicine and cellular longevity, 2019*.

Yamamoto, S., Yang, G., Zablocki, D., Liu, J., Hong, C., Kim, S.-J., Soler, S., Odashima, M., Thaisz, J., & Yehia, G. (2003). Activation of Mst1 causes dilated cardiomyopathy by stimulating apoptosis without compensatory ventricular myocyte hypertrophy. *The Journal of clinical investigation, 111*(10), 1463-1474.

Yang, Y., Del Re, D. P., Nakano, N., Sciarretta, S., Zhai, P., Park, J., Sayed, D., Shirakabe, A., Matsushima, S., & Park, Y. (2015). miR-206 mediates YAP-induced cardiac hypertrophy and survival. *Circulation research, 117*(10), 891-904.

Yu, F.-X., & Guan, K.-L. (2013). The Hippo pathway: regulators and regulations. *Genes & development, 27*(4), 355-371.

Yu, F.-X., Zhao, B., Panupinthu, N., Jewell, J. L., Lian, I., Wang, L. H., Zhao, J., Yuan, H., Tumaneng, K., & Li, H. (2012). Regulation of the Hippo-YAP pathway by G-protein-coupled receptor signaling. *Cell, 150*(4), 780-791.

Yu, J., Poulton, J., Huang, Y.-C., & Deng, W.-M. (2008). The hippo pathway promotes Notch signaling in regulation of cell differentiation, proliferation, and oocyte polarity. *PloS one, 3*(3), e1761.

Yu, J., Zheng, Y., Dong, J., Klusza, S., Deng, W.-M., & Pan, D. (2010). Kibra functions as a tumor suppressor protein that regulates Hippo signaling in conjunction with Merlin and Expanded. *Developmental cell, 18*(2), 288-299.

Yu, L., Daniels, J. P., Wu, H., & Wolf, M. J. (2015). Cardiac hypertrophy induced by active Raf depends on Yorkie-mediated transcription. *Science signaling, 8*(362), ra13-ra13.

Yuan, Z., Lehtinen, M. K., Merlo, P., Villén, J., Gygi, S., & Bonni, A. (2009). Regulation of neuronal cell death by MST1-FOXO1 signaling. *Journal of Biological Chemistry, 284*(17), 11285-11292.

Yue, T.-L., Gu, J.-L., Wang, C., Reith, A. D., Lee, J. C., Mirabile, R. C., Kreutz, R., Wang, Y., Maleeff, B., & Parsons, A. A. (2000). Extracellular signal-regulated kinase plays an essential role in hypertrophic agonists, endothelin-1 and phenylephrine-induced cardiomyocyte hypertrophy. *Journal of Biological Chemistry, 275*(48), 37895-37901.

Zhang, P., Wang, T., Zhang, D., Zhang, Z., Yuan, S., Zhang, J., Cao, J., Li, H., Li, X., & Shen, H. (2019). Exploration of MST1-mediated secondary brain injury induced by intracerebral hemorrhage in rats via hippo signaling pathway. *Translational stroke research, 10*(6), 729-743.

Zhao, B., Tumaneng, K., & Guan, K.-L. (2011). The Hippo pathway in organ size control, tissue regeneration and stem cell self-renewal. *Nature cell biology, 13*(8), 877-883.

Zhao, B., Ye, X., Yu, J., Li, L., Li, W., Li, S., Yu, J., Lin, J. D., Wang, C.-Y., & Chinnaiyan, A. M. (2008). TEAD mediates YAP-dependent gene induction and growth control. *Genes & development, 22*(14), 1962-1971.

Zhao, R., Fallon, T. R., Saladi, S. V., Pardo-Saganta, A., Villoria, J., Mou, H., Vinarsky, V., Gonzalez-Celeiro, M., Nunna, N., & Hariri, L. P. (2014). Yap tunes airway epithelial size and architecture by regulating the identity, maintenance, and self-renewal of stem cells. *Developmental cell, 30*(2), 151-165.

Zhe-Wei, S., Li-Sha, G., & Yue-Chun, L. (2018). The role of necroptosis in cardiovascular disease. *Frontiers in pharmacology, 9*, 721.

Zheng, X., Xu, C., Di Lorenzo, A., Kleaveland, B., Zou, Z., Seiler, C., Chen, M., Cheng, L., Xiao, J., & He, J. (2010). CCM3 signaling through sterile 20–like kinases plays an essential role during zebrafish cardiovascular development and cerebral cavernous malformations. *The Journal of clinical investigation, 120*(8), 2795-2804.

Zhou, D., Conrad, C., Xia, F., Park, J.-S., Payer, B., Yin, Y., Lauwers, G. Y., Thasler, W., Lee, J. T., & Avruch, J. (2009). Mst1 and Mst2 maintain hepatocyte quiescence and suppress hepatocellular carcinoma development through inactivation of the Yap1 oncogene. *Cancer cell, 16*(5), 425-438.

Zhou, Q., Li, L., Zhao, B., & Guan, K.-L. (2015). The hippo pathway in heart development, regeneration, and diseases. *Circulation research, 116*(8), 1431-1447.

Zhu, F., Meng, Q., Yu, Y., Shao, L., & Shen, Z. (2020). Adult cardiomyocyte proliferation: a new insight for myocardial infarction therapy. *Journal of Cardiovascular Translational Research*, 1-10.

Zhu, H., Tannous, P., Johnstone, J. L., Kong, Y., Shelton, J. M., Richardson, J. A., Le, V., Levine, B., Rothermel, B. A., & Hill, J. A. (2007). Cardiac autophagy is a maladaptive response to hemodynamic stress. *The Journal of clinical investigation, 117*(7), 1782-1793.

Zi, M., Maqsood, A., Prehar, S., Mohamed, T. M., Abou-Leisa, R., Robertson, A., Cartwright, E. J., Ray, S. G., Oh, S., & Lim, D.-S. (2014). The mammalian Ste20-like kinase 2 (Mst2) modulates stress-induced cardiac hypertrophy. *Journal of Biological Chemistry, 289*(35), 24275-24288.